ON HYDROELASTIC PLUG VALVE VIBRATION

ON HYDROELASTIC PLUG VALVE VIBRATION

by

WILLIAM M. D'NETTO, B.ENG.

A Thesis

Submitted to the School of Graduate Studies

in Partial Fulfilment of the Requirements

for the Degree

Master of Engineering

McMaster University

October 1982

MASTER OF ENGINEERING (1982) McMASTER UNIVERSITY
Mechanical Engineering Hamilton, Ontario

TITLE: On Hydroelastic Plug Valve Vibration

AUTHOR: William Mark D'Netto, B.Eng. (McMaster University)

SUPERVISOR: Professor D. S. Weaver

NUMBER OF PAGES: xii, 206

Abstract

The research reported in this thesis concentrated on experimentally investigating and theoretically modelling self-excited valve vibrations. In particular the jet-flow inertia mechanism has been studied. Experimentally, this has been achieved by allowing water to discharge from a constant head tank into a pipeline through a simple plug valve. The plug valve was restrained so that axial vibrations of the plug valve could occur. Using this equipment the conditions for which the valve was stable and unstable was obtained. Further experimental investigation using a Laser Doppler Anemometer allowed for recording of instantaneous fluid discharge during the valve limit cycles. In addition the records of the instantaneous pressure difference and valve opening allowed for instantaneous discharge coefficient calculations. Although no trends in these instantaneous discharge coefficients were apparent, these particular experiments allowed for improved modelling of the valve vibration.

Dimensionless nonlinear differential equations were derived to describe general flow control devices. A stability analysis of these differential equations showed that at large fluid inertias that the instability that arises is one of divergence, hence a quasistatic stability analysis is valid. Numerical integration of the differential equations of motion

was used to predict limit cycles as well as valve stability.

The divergence formula derived for large fluid inertia was found to coincide with the corresponding experimental results. Other predictions were found to generally agree with experimental results. Discrepancies which did arise were attributed to waterhammer. Hence the theory derived was concluded to be fundamentally correct. Recommendations for further research include inclusion of waterhammer in the model and investigation of local flow effects.

ACKNOWLEDGEMENTS

The author would like to express his sincere appreciation to his supervisor, Dr. D. S. Weaver, for advice, encouragement, and interest shown in the creation of this thesis.

The loan of equipment from Dr. B. Latto and Dr. J. H. T. Wade is gratefully acknowledged.

The financial support of the Natural Sciences and Engineering Research Council and McMaster University is also acknowledged.

The author wishes to thank Ms. BettyAnne Bedell for her excellent typing of this thesis.

The author wishes to thank his parents for their understanding and encouragement throughout this thesis.

The author also appreciates the effort and loving support of his fiancee, Jannette Dryburgh, to whom this thesis is dedicated.

TABLE OF CONTENTS

LIST OF FIGURES

CHAPTER 1

INTRODUCTION

1.1 Introduction

A valve is a device for controlling fluid flow through a pipe. There are many operating conditions to be considered when selecting a valve. Consideration has to be given to the type of fluid, whether it be air, water, a corrosive chemical, a slurry or a radioactive material. Operating temperatures can vary from those of cryogenic applications to higher temperatures such as when liquid metal is the fluid controlled. Operating pressures can vary from near vacuum to high pressure applications. Leakage requirements must also be considered. These may be very strict or, if the loss of fluid is of minor importance or easily recovered, these may be very generous.

Actuation methods are also important. Three typical actuation methods are: manual, pneumatic and electrical control. The controlling signals may be part of a process operation, which may respond to pressure, temperature or other signals received. Valve actuation may also occur as a result of a pressure difference acting directly on the valve as in the case of relief valves.

1.2 Instability of Valves

Most valves will vibrate under certain conditions. Generally, these vibrations occur when the valves are operating

at small openings. Possible consequences of such vibrations are undesirable pressure fluctuations and seat failure [1]. It is therefore important for designers to understand the vibration mechanisms and how to avoid these vibrations.

1.3 Plug Valves

Figure 1.1 shows a schematic of a simple plug valve which is used in the experimentation reported in this thesis. Such a configuration provides a relatively simple relation between flow area and valve lift. This fits well with the assumptions generally made for valves operating at small openings, that is to say for the region of interest, the flow area is approximately a linear function of valve displacement.

Figure 1.2 shows two typical configurations to which the results for the plug valve modelled in this thesis might be applied.

Predictions as to the values of initial openings, stiffnesses and static heads required to make a particular valve vibrate can be made using the formulation derived by Ziada [3] in conjunction with a computer program or the stability threshold suggested by Kolkman [4]. Weaver [5] in his review paper shows that a simple formulation of Kolkman's stability threshold can be derived for a valve with a long connecting pipe.

1.4 Purpose of Research

The purpose of the research reported in this thesis is to improve our understanding of the dynamic discharge character-

istics of a plug valve. In this way, the theoretical model developed by Weaver and Ziada [6] may be refined and better predictions for stability limits, as well as limit cycle amplitudes and frequencies may be obtained.

In this thesis, the reader will find the research reported in several sections. The background material in Chapter 2 outlines work already done by other researchers which is relevant to valve vibrations. In the ensuing chapters, there is a description of the apparatus and procedure used in the experimentation performed for this thesis. The results of the experiments are then presented with recommendations for refinement of the model developed by Weaver and Ziada. These refinements are implemented in Chapter 6 and the predictions of this model are compared to the experimental results as well as to the predictions of the original model. Further analysis of the refined model reveals that a simple expression can be derived for the upper stability boundary, provided there is large fluid inertia and a tank upstream of the valve. This analysis is presented in Chapter 6, along with a quasistatic stability analysis. Finally, conclusions are drawn along with recommendations for further research.

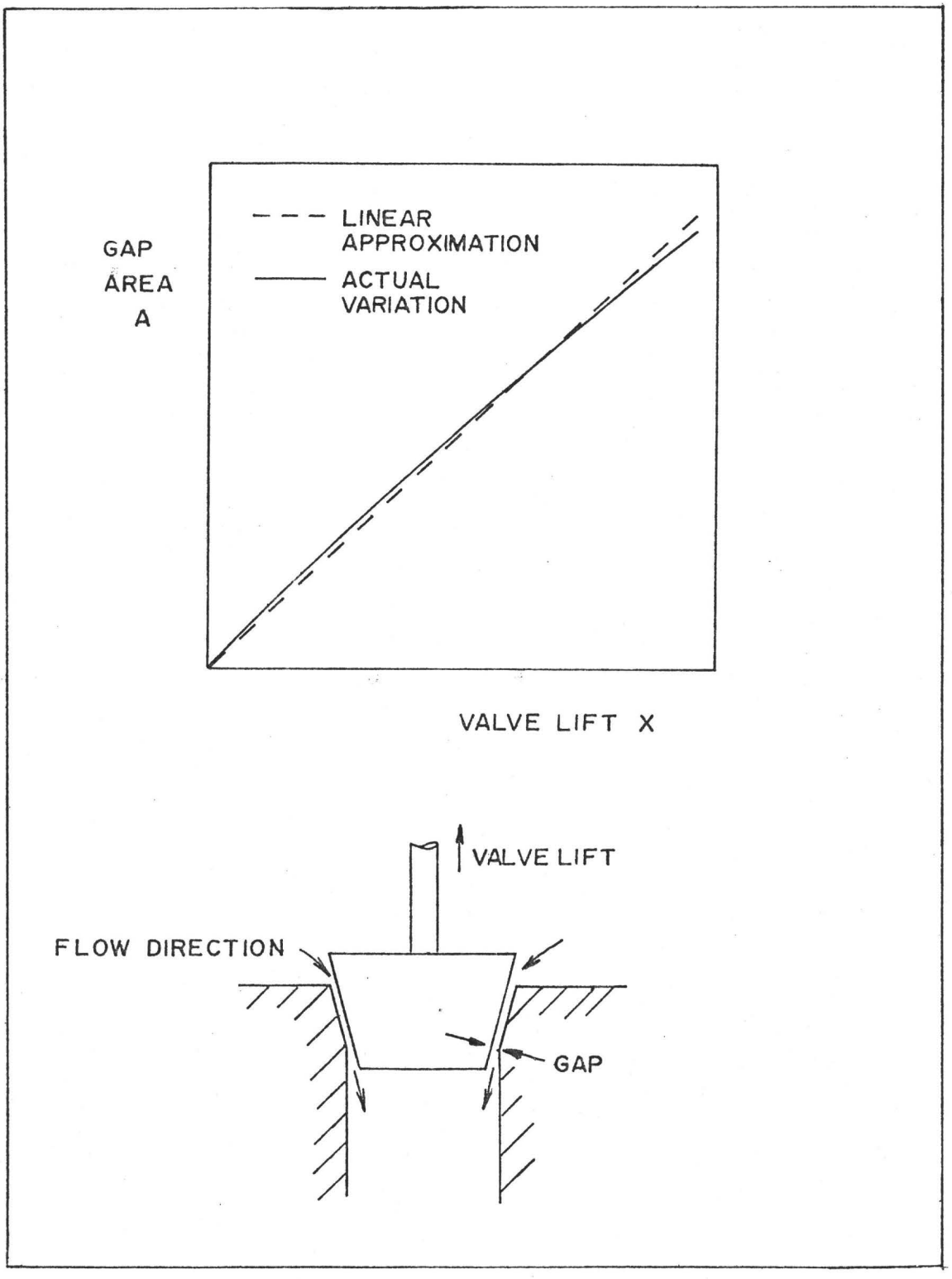

Fig. 1.1 Simple plug valve.

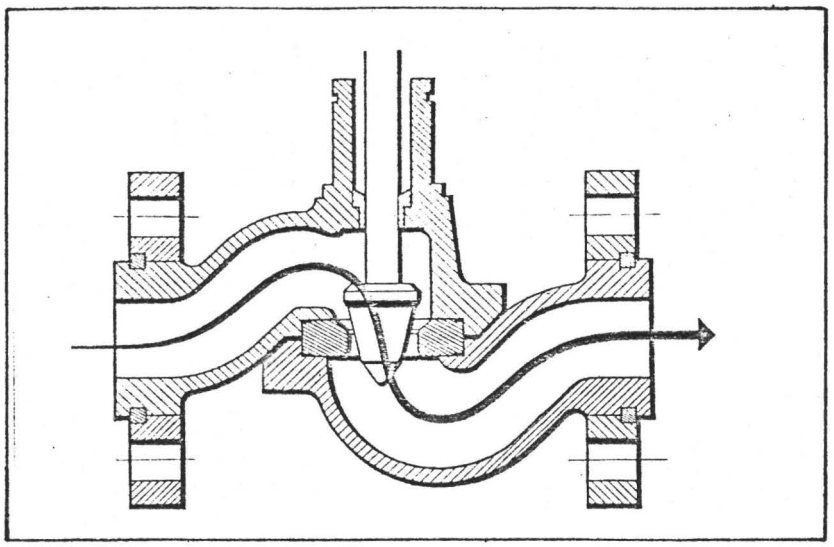

(a)

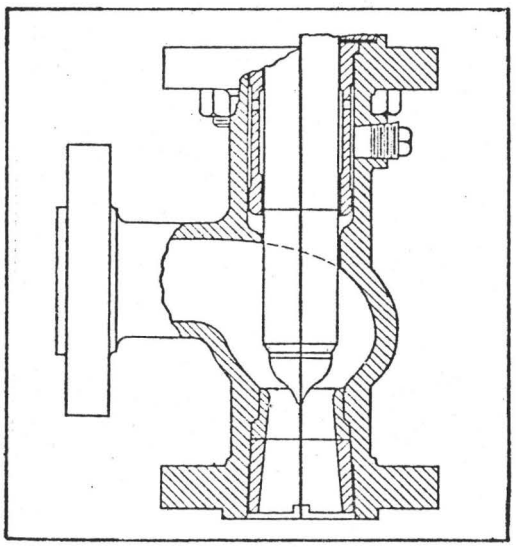

(b)

Figure 1.2 Examples of typical valves using plug valve configuration Ref. [2].

CHAPTER 2

BASIC CONCEPTS OF FLOW INDUCED STRUCTURAL VIBRATIONS

2.1 Introduction

As technology improves, performance demands increase. These increased demands may come in the form of higher efficiency, lower factors of safety, higher flowrates and higher material strengths. The net result for a structure which is required to withstand loading from a fluid is a less stiff structure exposed to high flow velocities and pressure differences.

One example of a less stiff structure exposed to higher flowrates is the evolution of the monoplane from the biplane. Previously unknown instabilities occurred which resulted in the flexible monoplane wings breaking off. These problems led to the development of the field of aeroelasticity. Aeroelasticity is defined by Fung [7] as the study of the effect of aerodynamic forces on elastic bodies. Flutter is characterized as the interaction of aerodynamic, elastic and inertia forces. Such a problem is one of dynamic aeroelastic instability. Divergence, or static buckling, occurs when a problem of this type has zero frequency, i.e. a non-oscillatory instability. In these cases, the inertia effects may be neglected in the analysis, and the phenomenon is termed static aeroelastic instability [7].

Buffeting is usually thought of as the elastic response of the structure to the fluid flow. The forces that cause the response are not greatly affected by the motion of the body.

Hydroelasticity can be defined in terms similar to aeroelasticity, except, of course, now the working fluid is water and hydrodynamic forces are present instead of aerodynamic ones. There are three important differences between the study of aeroelasticity and hydroelasticity. In aeroelasticity the added mass is usually negligible whereas in hydroelasticity this is not so. In fact, it is possible for the added mass to exceed the mass of the structure itself. Additionally, in hydroelastic problems the possibilities of cavitation and of a free surface exist. These two phenomena have no counterparts in aeroelasticity.

Hydroelasticity, like aeroelasticity can be divided into two classes of problems. Dynamic hydroelasticity is the interaction of hydrodynamic, elastic and inertial forces. Static hydroelasticity can be analyzed considering hydrodynamic and elastic forces only.

2.2 Classification of Flow-Induced Vibrations

Wherever fluids with high flow velocities impinge upon structures, there is a possibility of a flow-induced vibration problem. These problems can be divided into three classes: forced vibrations, self-controlled vibrations and self-excited vibrations.

In forced vibrations, the fluid forces can be considered to be unaffected by the response of the structure. An example of such a problem would be turbulent buffeting of a body. To ensure low amplitudes of vibration, it is necessary to determine the power spectrum of the flow affecting the structure. The structure may then be stiffened or damping added until vibration levels are in a range considered acceptable. In modelling such a problem, a rigid model is sufficient to determine the fluid forces.

Self-controlled vibrations may be characterized in the following manner. In the absence of structural motion, periodicity exists in the flow. When the flow velocity changes the periodicity of the flow changes. As the frequency of periodicity in the flow approaches that of the structure, resonance occurs. The amplitude of vibration may become large enough to dominate the fluid mechanics and control flow periodicity. To minimize response one of two approaches can be used. Mismatching the fluid and structural frequencies is one way. Another method is to change the flow path in such a way as to destroy flow periodicity. A rigid model can be used to describe fluid structure interaction before resonance occurs. However, a flexible model must be used when the deflections expected are large enough to control the fluid mechanics.

In self-excited vibrations the fluid forces depend on structural displacement. These problems are either one of static stability or dynamic stability and a flexible model is

required to study these phenomena. It should be noted that stiffening or adding damping to the structure may aggravate a self-excited vibration problem.

Summarizing, there are three basic classes of flow-induced vibrations, each of which has its own characteristic requirements for modelling, either mathematically or using a physical scale model.

2.3 Vibration of Valves

Weaver [5] has classified excitation mechanisms for valves operating at small openings into three categories: turbulence, acoustic resonance and the jet-flow inertia mechanism.

Turbulent excitation results in random excitation loads acting on the valve. These loads may be increased by tortuous flow paths upstream of the valve gap. This phenomenon is a typical example of a forced vibration as outlined in Section 2.2 of this thesis.

Acoustic resonance has been studied for several valve configurations: poppet valves [8], spool valves [9], [10], [11] and plug valves [12], connected to various piping systems. Instability in poppet valves has been found to be possible in both flow directions [8], that is either when the flow tends to open or to close the valve. In the case of spool valves flow in the wrong direction results in instability. Ainsworth [9] and Ezekiel [10] have shown that even if the flow is in the right direction that instability may still result. Further

analysis of spool valve instability is reported in [11] which is very cumbersome due to flow characteristics of the valve, conduit dynamics and application of stability theory. Thomann [12] analyzed and performed experiments for a simple plug valve, his results indicated frequencies of oscillations which were within ten percent of the natural frequency of the valve. These frequencies were either higher or lower than the natural frequency depending on whether the flow tended to open or close the plug valve respectively.

The term jet-flow inertia mechanism needs some explanation. Weaver [5] explains this mechanism in terms of the necessary existence of a high velocity coherent flow through the valve orifice. If the valve is perturbed the jet pulses, this results in forces on the valve changing. Fluid inertia causes hysteresis in these forces. It is this hysteresis which is responsible for feeding energy into the structure. (Hence this is a typical self-excited vibration). Abelev and Dolnikov [13] and Lyssenko and Chepajkin [14] have cited this mechanism as the cause of vibrations in leaf gates and seals. In both cases, the mathematical models proposed can be shown to reduce to negatively damped simple harmonic oscillators. In addition, both of their proposed mechanisms relied on variable discharge coefficients to explain the nature of the vibrations. There is at present no justification for using a variable discharge coefficient. Furthermore, the fact that the limit cycle oscillations usually do not coincide with the structural

natural frequency suggests that the mechanism of excitation is not simply negative damping.

Kolkman [4] has produced a stability predictor which does not depend upon a variable discharge coefficient. This model has been applied to a wide variety of flow control devices. Using this model it can be shown that a plug valve cannot undergo axial vibrations of the jet-flow inertia mechanism if the flow tends to open the plug valve. The stability criterion determined by Kolkman consists essentially of two parts. Firstly, there is a relationship between a rigidity coefficient and a mass coefficient. This defines the region where a plug valve with no mechanical damping would be stable. Secondly, if the rigidity and mass coefficients do not conform to the required relationship, a minimum mechanical damping is required to stabilize the system. Further examination of this damping reveals for long pipes, that the minimum required damping becomes proportional to the pipe length. This casts doubts on the usefulness of trying to eliminate valve vibrations by increasing damping.

Weaver et al. [15] have performed experiments which indicated that adding damping to a vibration prone valve results in the problem becoming worse, rather than eliminating the vibration. Their experiments also showed that increased stiffness resulted in a lower frequency. This trend cannot be explained by the negatively damped simple harmonic oscillator theories [13], [14] of the jet-flow inertia mechanism.

Weaver and Ziada [6] have derived a nonlinear mathematical model for the jet-flow inertia mechanism. This model has significant advantages over those proposed by Kolkman, Lyssenko and Chepajkin, and Dolhikov and Abelev. The nonlinear model does not require a variable discharge coefficient to explain the instability. Direct comparison of model predictions and actual vibrations are possible by integrating the equations of motion numerically. Hence it can be immediately established whether the physical phenomenon is correctly modelled. The physical effects of varying stiffness and initial opening as reported by Weaver et al. [15] are in agreement with the theoretical predictions of the model. Furthermore, the nonlinear model does not require the existence of an equilibrium position when simulating the vibrations. Such an equilibrium position is necessary to get a stability predictor from the linear models [4], [13], [14]. This is significant because this equilibrium position does not always exist or, at least, is unknown.

Weaver and Ziada [6] have indicated that their model has some minor discrepancies which they attributed to unsteady flow phenomena. Only Weaver and Adubi [1] have attempted to determine experimentally the flow changes through a cycle of valve vibration. The work recommended by Weaver and Ziada [6] is to measure the dynamic discharge characteristics so that the nonlinear model may be refined.

2.4 Added Mass Theory

When a body is accelerated in a frictionless fluid, the surrounding fluid must also be accelerated. The additional force required to accelerate fluid can be accounted for in terms of an 'added', 'virtual' or 'hydrodynamic' mass [16] such that,

$$F = (M + M') \frac{d^2x}{dt^2} \tag{2.1}$$

where F is the accelerating force, M is the mass of the body, M' is the added mass and $\frac{d^2x}{dt^2}$ is the acceleration. Added mass is usually negligible in air, however it's effects must be considered in water.

For simple cases, theoretical calculation of the added mass of a body submerged in quiescent fluid is possible. Lamb [17] has demonstrated that this can be done by integration of the potential flow field, followed by calculation of the kinetic energy associated with the movement of the fluid due to the body. Fritz [18] has used this method to calculate added mass, and includes in his paper a table summarizing added masses for some simple configurations. Some of the formulas in Fritz's paper [18] indicate that distance from a rigid boundary is important in determining added mass. Weaver [16] states that the depth of submergence and proximity of a rigid surface can result in significant variation of added mass.

The frequency and amplitude of a body oscillating also affect added mass. Logvinovich and Savchenko [19] through

experimentation have shown for vibrations greater than about five percent of the characteristic length of a body, that added mass becomes amplitude and frequency dependent. Their results show that increasing either the amplitude or frequency results in a greater added mass. Chandrasekaran et al. [20] have performed experiments which indicate otherwise. Hence it is unclear as to how frequency and amplitude affect added mass. Other factors which will be important in determining added mass are cavitation and wake effects.

2.5 Effects of Unsteady Flow

Frequently, prediction of the dynamic characteristics of a flow are made using steady-state properties. For instance, static discharge coefficients have been used to predict the flowrate of a fluid under unsteady conditions. However, there are effects outlined by McCloy [21] which can give rise to a difference between the actual unsteady flow and that flow predicted assuming quasisteady flow. These effects can be classified as those due to fluid inertia, those due to changes in discharge coefficients and those due to changes in friction losses.

When a flow is unsteady, a certain portion of the total pressure drop is required to accelerate or decelerate the flow. This inertial effect results in a delay in flowrate establishment. In the case of oscillating flow, this time lag can result in attenuation of the flowrate amplitude. McCloy [21] has shown that, due to nonlinearity of this system, the mean

flowrate will also change as a function of frequency.

The dynamic discharge coefficient can also be different from the steady-state one. Daily et al. [22] have shown for water flowing through orifices that certain changes in discharge coefficient occur. When the flow is accelerating the discharge coefficient increases, while in decelerating flow, the discharge coefficient decreases. McCloy and McGuigan [23] have concluded that their results for poppet valves are in agreement with those obtained by Daily et al. [22]. The McCloy and McGuigan [23] experiments were for oscillatory flow superimposed upon a mean flow and they concluded that there was a reduction in the mean discharge coefficient measured over the cycle. A part of this reduction was attributed to inertia effects. However, they also concluded that the mean dynamic discharge coefficient through the cycle was reduced.

Experiments performed by Alpay [24] shows that a general reduction in dynamic discharge coefficient as either the frequency or amplitude of a spool valve motion increased. However, at very low frequencies, inertia effects resulted in a higher dynamic discharge coefficient than the steady state one.

Daily et al. [22] have shown that turbulent losses are affected by the rate of change of flowrate. They concluded that small changes in frictional resistance resulted from unsteadiness in the flow. Accelerating flow resulted in slightly higher losses while decelerating flow resulted in slightly

lower losses.

It is clear that unsteady flow will influence the discharge characteristics of a vibrating valve. During the closing portion of the valve limit cycle the flow is decelerating while it is accelerating during the opening part of the cycle. These effects are expected to be frequency dependent. Thus, especially at higher frequencies, the use of static discharge characteristics throughout the valve cycle is unlikely to be a good approximation.

CHAPTER 3

EXPERIMENTAL APPARATUS

3.1 Introduction

The experimental apparatus described in this chapter is divided into two categories, namely, hydraulic equipment and instrumentation. The hydraulic equipment section describes the path of the fluid through the system and defines which parameters are fixed, which parameters are varied only to predetermined values and which parameters can be varied continuously. Enough information is provided in the section on hydraulic equipment so that all of the dimensionless parameters described by Weaver and Ziada [6] may be determined except for the discharge coefficient, the contraction coefficient, added mass and damping which are determined experimentally.

The instrumentation section describes the devices used for measuring plug valve displacement, pressure difference and instantaneous discharge, the location of measuring points and the location of the measuring equipment. The performance specifications prescribed for the instrumentation by each manufacturer is also examined.

3.2 Hydraulic Equipment

Figure 3.1 illustrates the constant head tank upstream of the plug valve. Water enters this tank through a

hose connected to the building water supply. Water may leave the tank in one of two ways, either through the overflow which is used to maintain a constant head or alternatively through the plug valve (Figure 3.2). After passing through the valve the water enters the downstream pipeline. The configurations of the downstream pipeline used during experimentation are shown in Figure 3.3. Notice the inverted U-section at the downstream end of the pipeline. The purpose of this U-section is to ensure that the pipeline remains full of water during the experiments. This is necessary because the model of Weaver and Ziada [6] is derived for flow in a completely filled closed conduit. The vertical distance from the surface of the water in the tank to the bottom of the pipe in the inverted U-section is 0.635 m. This quantity represents the static head available to drive flow through the valve-pipeline system.

The equipment was designed to allow for variation of three important vibration parameters, fluid inertia, valve plug restraint stiffness and initial no load valve opening.

The fluid inertia is changed by unscrewing the inverted U-section, removing or adding pipe lengths as desired and then reconnecting the inverted U-section.

The initial opening can be varied continuously by loosening the bolted connection joining the traversing section to the angle iron support shown in Figure 3.4, sliding the traversing section up or down as desired and then retightening

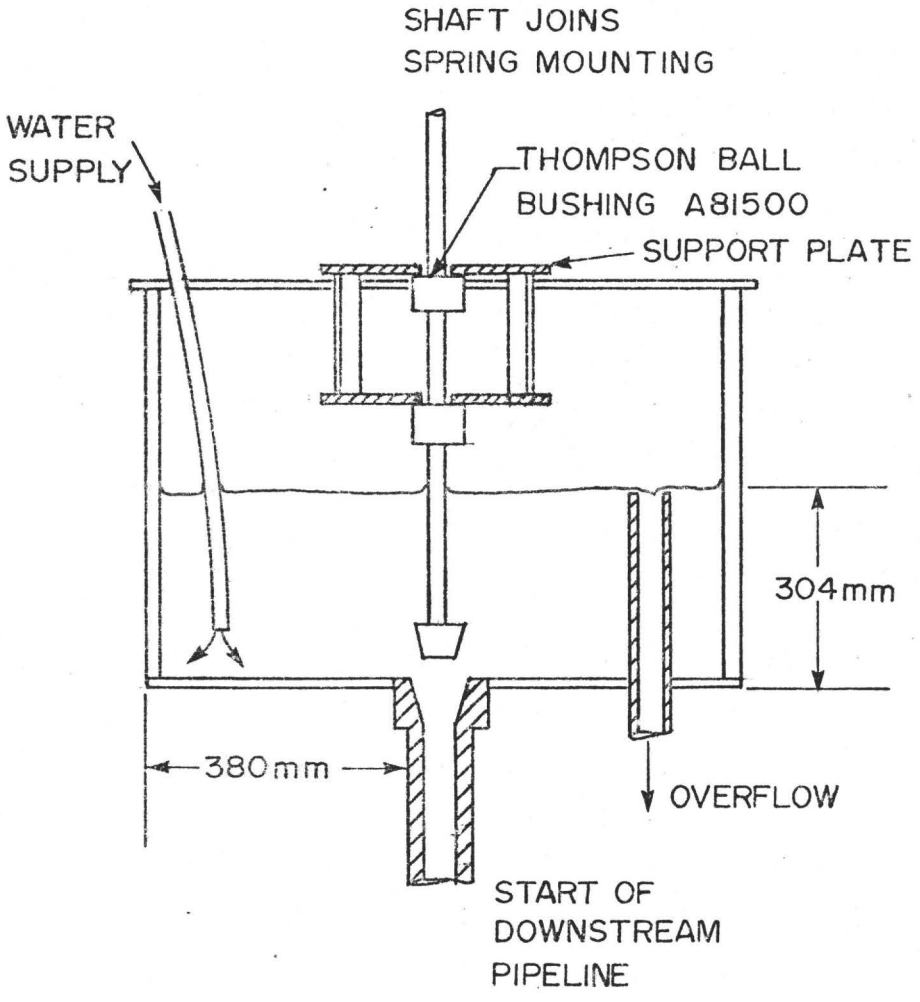

Figure 3.1 Constant head tank

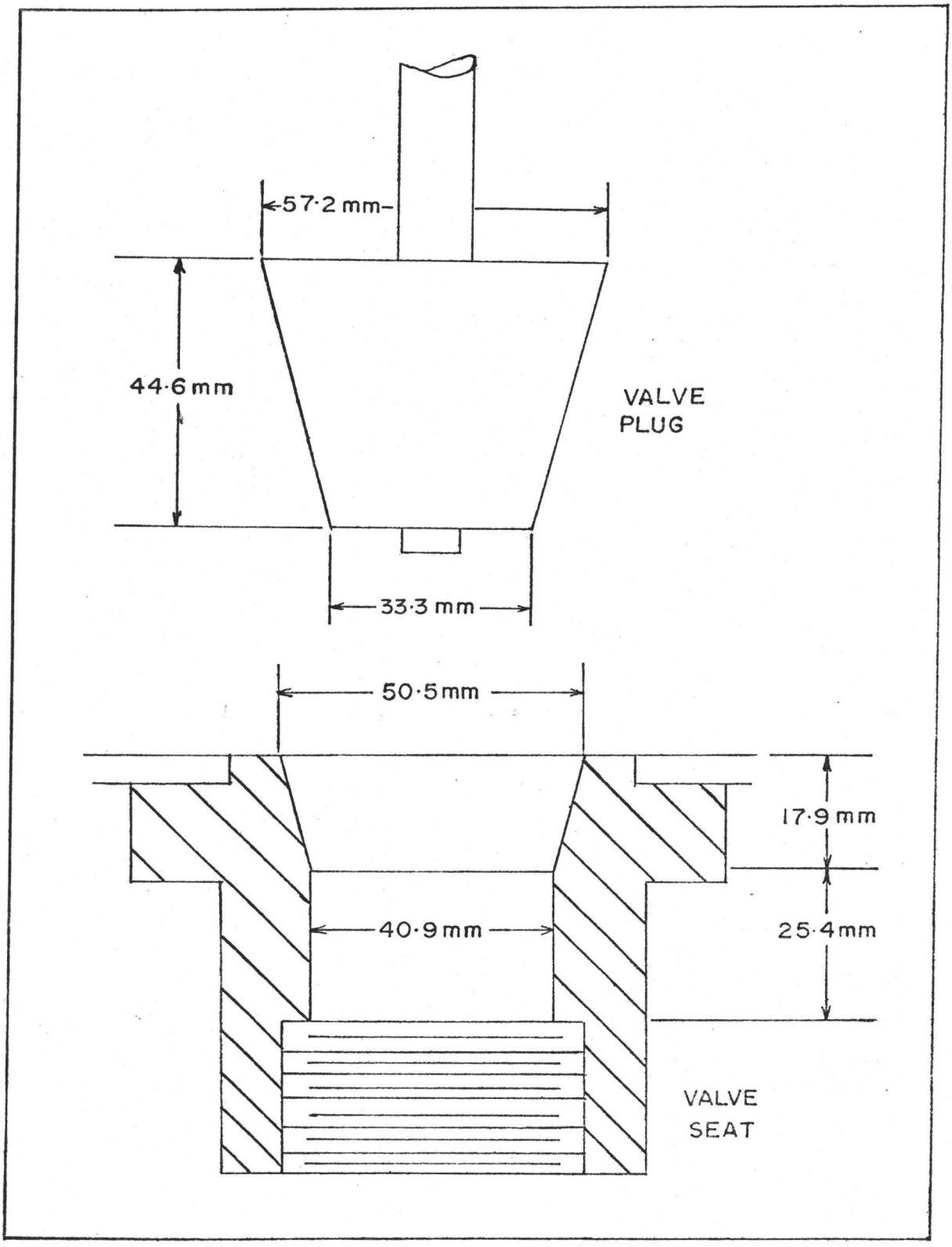

Figure 3.2 Valve plug and seat.

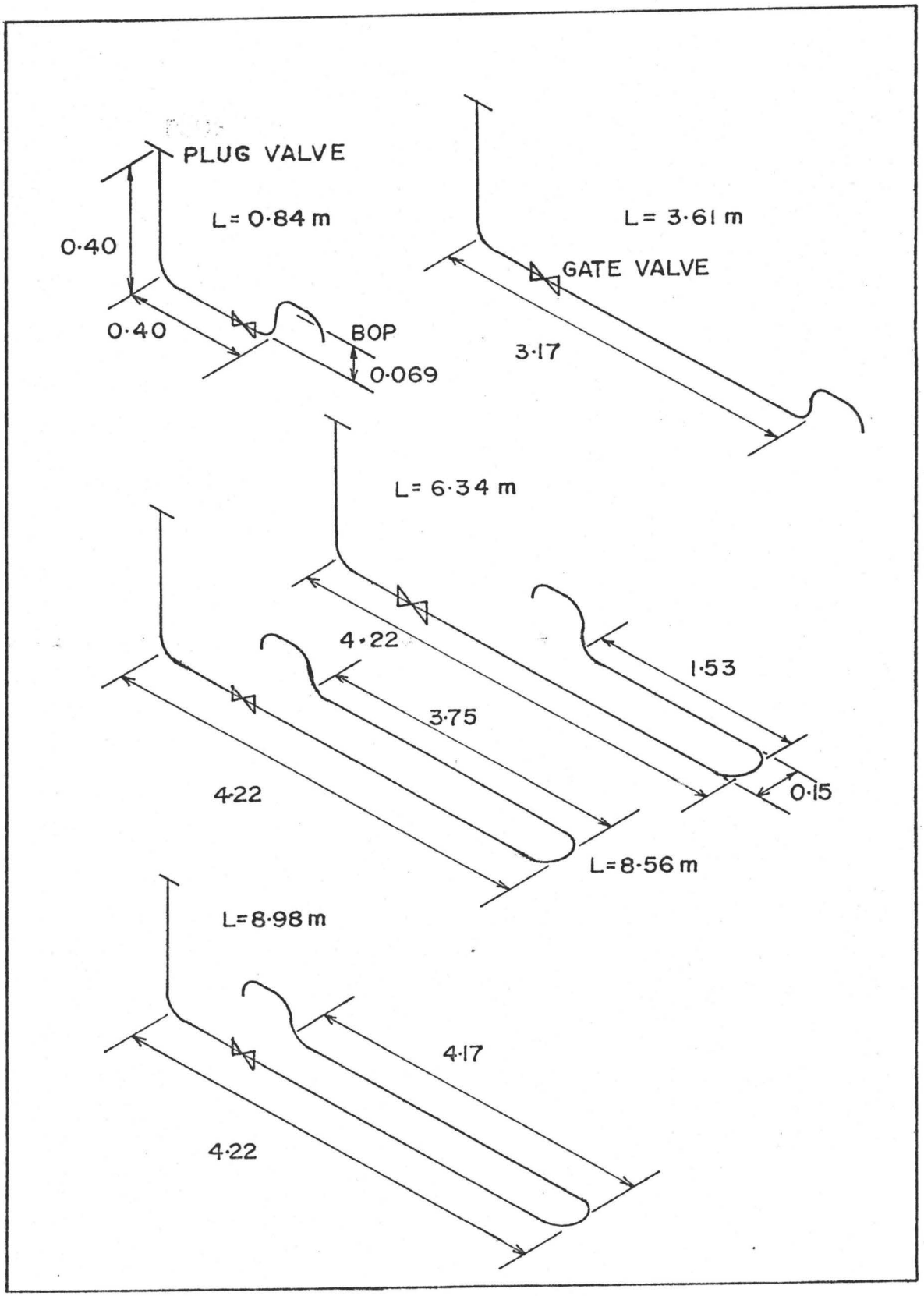

Figure 3.3 Downstream pipeline configurations.

the bolts.

The plug valve is mounted on a 12.7 mm outside diameter stainless steel shaft, which runs through two Thompson ball bushings. The shaft extends upwards to the springs which are mounted in a pair and preloaded against each other. At the top end of the shaft there is a 1-72 threaded hole into which the position transducer core is screwed. Two spring cups sit on the shaft, the upper one is held in place on the threaded section by a back-up nut, the lower one is clamped to the shaft by a set screw. The set of springs is shown in Figure 3.4. With each spring used there is a corresponding aluminum insert. Each insert clears the spring so that chafing does not occur and so that the spring remains properly centred. Hence lateral forces and mechanical damping on the shaft are minimized. To change the stiffness of the valve restraint requires disassembly of the support system shown in Figure 3.4, changing the appropriate springs and inserts followed by reassembly of the support system.

Table 3.1 gives the effective stiffness of spring combinations used in experimentation for this thesis. The method used to obtain the load-deflection lines for each spring is described in Appendix D. The effective spring stiffness in Table 3.1 is obtained by adding together the appropriate spring constants. The springs used were made from stock springs supplied by Hamilton Wire Products Ltd. The stock springs had twenty coils with open ends. These were

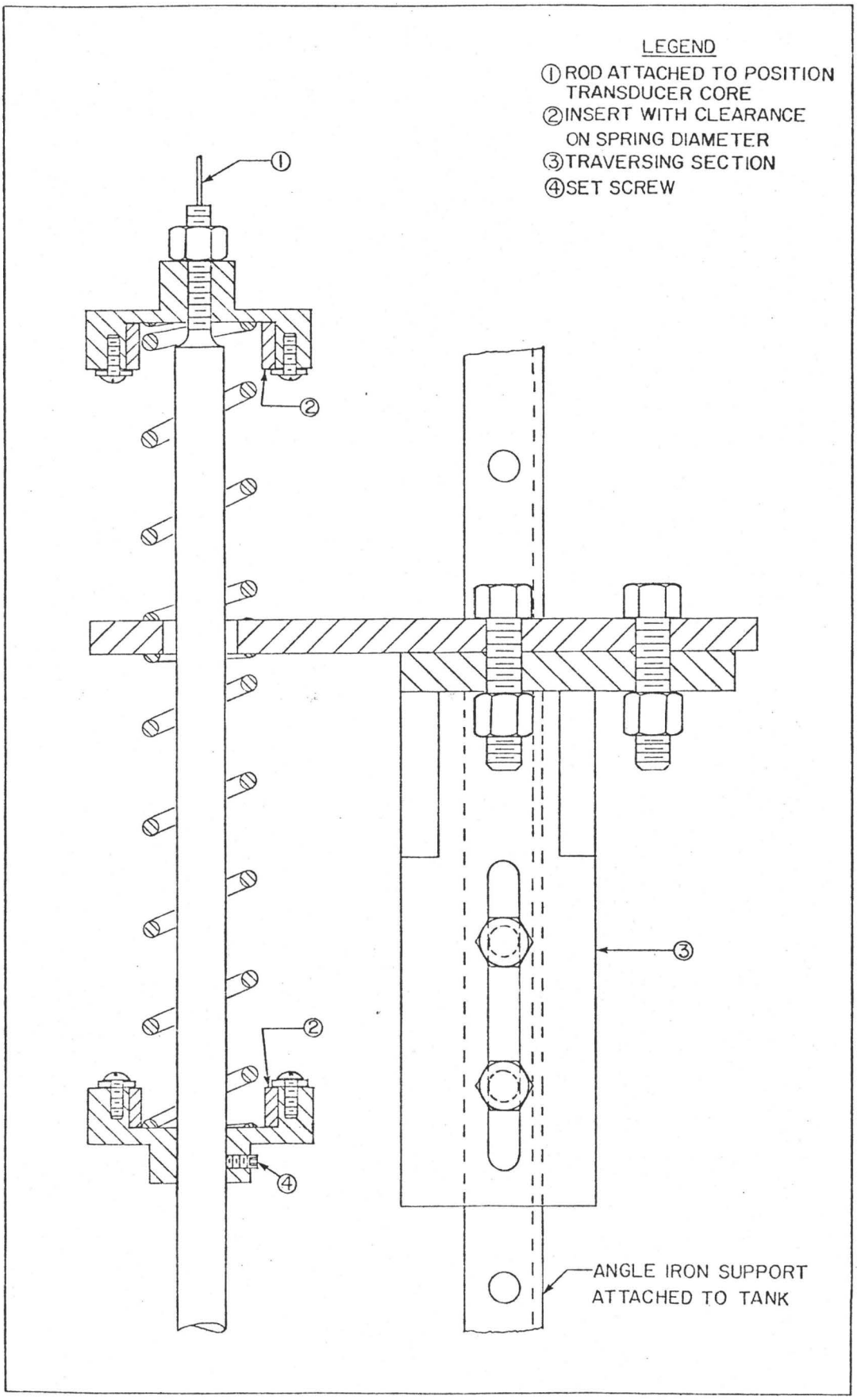

Figure 3.4 Vertical restraint system of shaft.

cut to various lengths, the ends were twisted so that closed ends were made and then ground flat. A photograph of the above hydraulic equipment is shown in Figure 3.6.

Table 3.1

Spring Combination	Stiffness K N/m
A	946
B	1386
C	2125
D	3017
E	3440

3.3 Instrumentation

The position transducer is located at the top end of the valve shaft and can be seen in Figure 3.6. This transducer is a Hewlett Packard Linear Induction Transducer Model 7DCDT-1000, which has a displacement range of 50 mm. The manufacturer specifies the frequency of response in terms of a 3 db amplitude attenuation which occurs at 135 Hz for this model. The calibration of this transducer is reported in Appendix E.

Figure 3.7 shows the Pace Model CP5IDR+20 pressure transducer mounted to its measuring position. This pressure transducer is a variable reluctance type with interchangeable diaphragms rated to a maximum pressure difference of 140 kPa (20 psi).

The low pressure port of the transducer was connected to the pressure tap downstream of the valve, the high pressure port was connected to a pressure tap in the bottom of the constant head tank far from the plug valve. The transducer was powered directly from the mains and gave an output DC voltage proportional to the pressure difference. The manufacturer of this pressure transducer indicates that the frequency response is flat to 1000 Hz and a linearity of 0.5% for this transducer. The calibration curve of this transducer is given in Appendix E.

During the course of experimentation the Pace transducer failed to give a signal and a replacement was sought. In Chapter 5, the results of Figures 5.11 and 5.12 were recorded using the Pace transducer.

A Schaevitz Engineering Model P2142-0025 pressure transducer was procured as a replacement. The manufacturer describes the pressure sensing element as a "twin cantilever sensor beam" and specifies a mechanical natural frequency of 3.5 kHz. The Schaevitz transducer had a range of 345 kPa (50 psi) differential pressure and required a regulated d.c. power supply. The calibration curve of this transducer is given in Appendix E.

Figures 3.5, 3.7 and 3.8 describe the essentials of the optical and electrical set-up of the Laser Doppler Anemometer. The Laser Doppler Anemometer was made by Thermo-Systems Inc. and consisted of a 15 mW Spectra-Physics Model

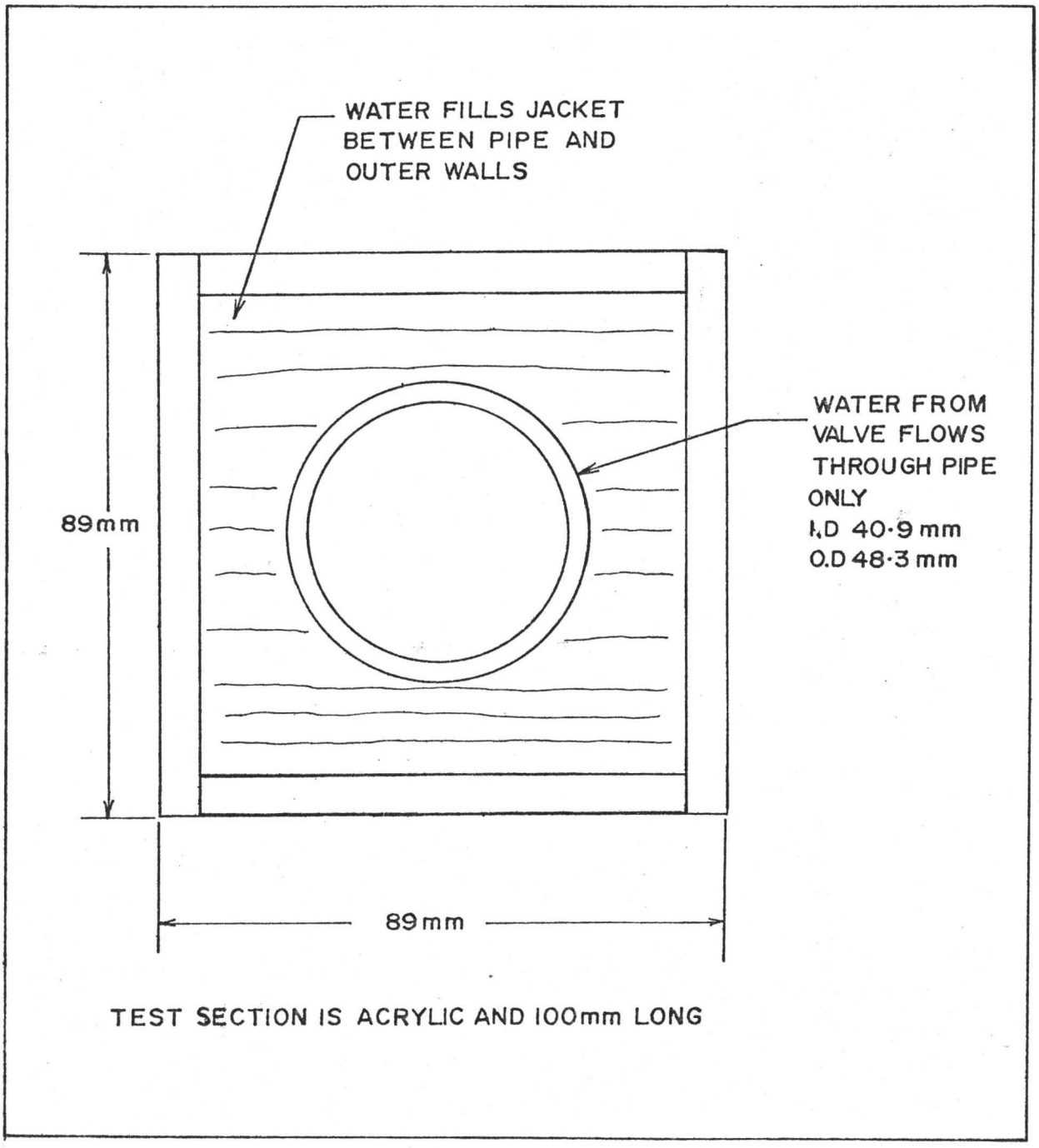

Figure 3.5 Flow measurement test section

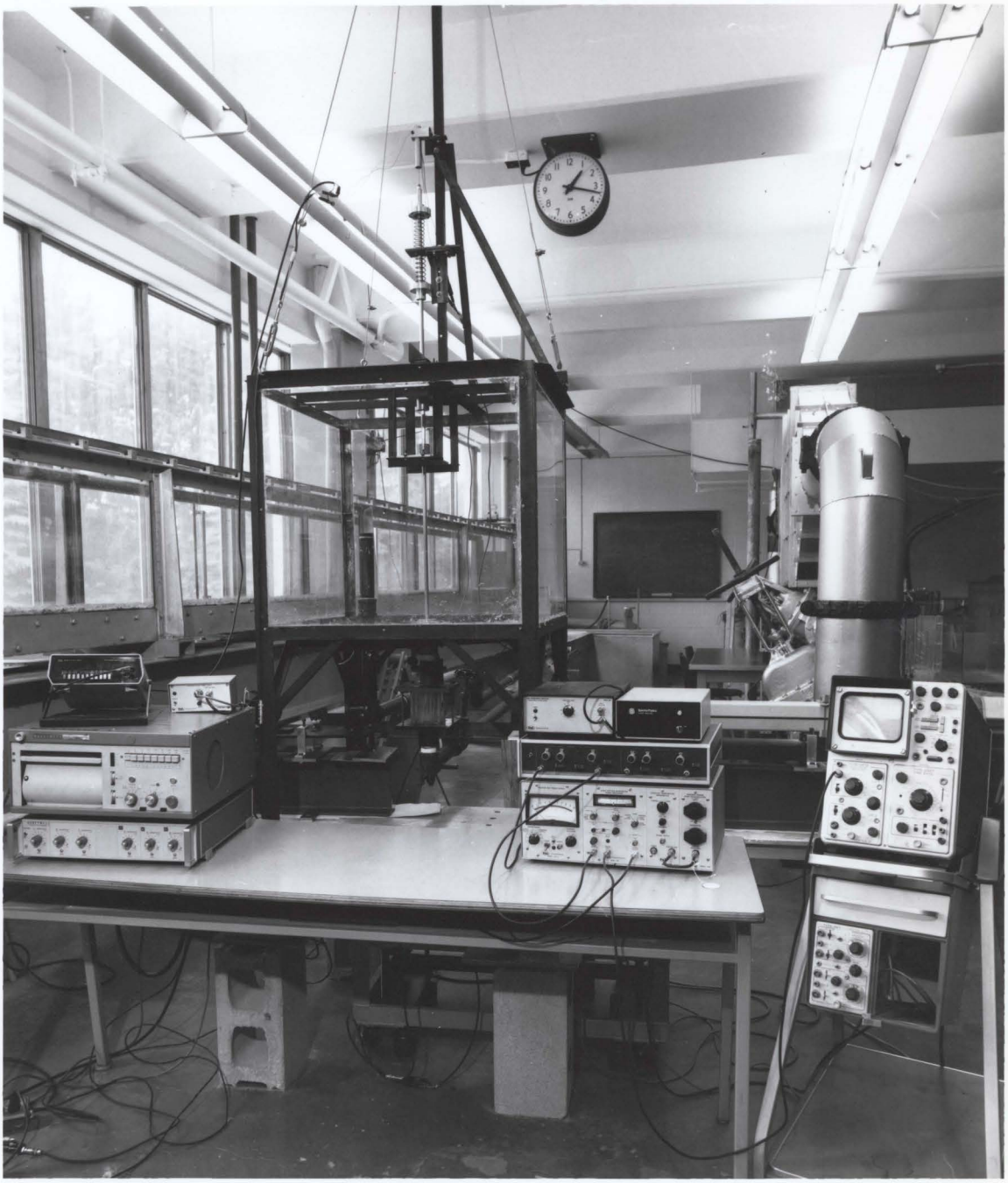

Figure 3.6 Overall view of test equipment.

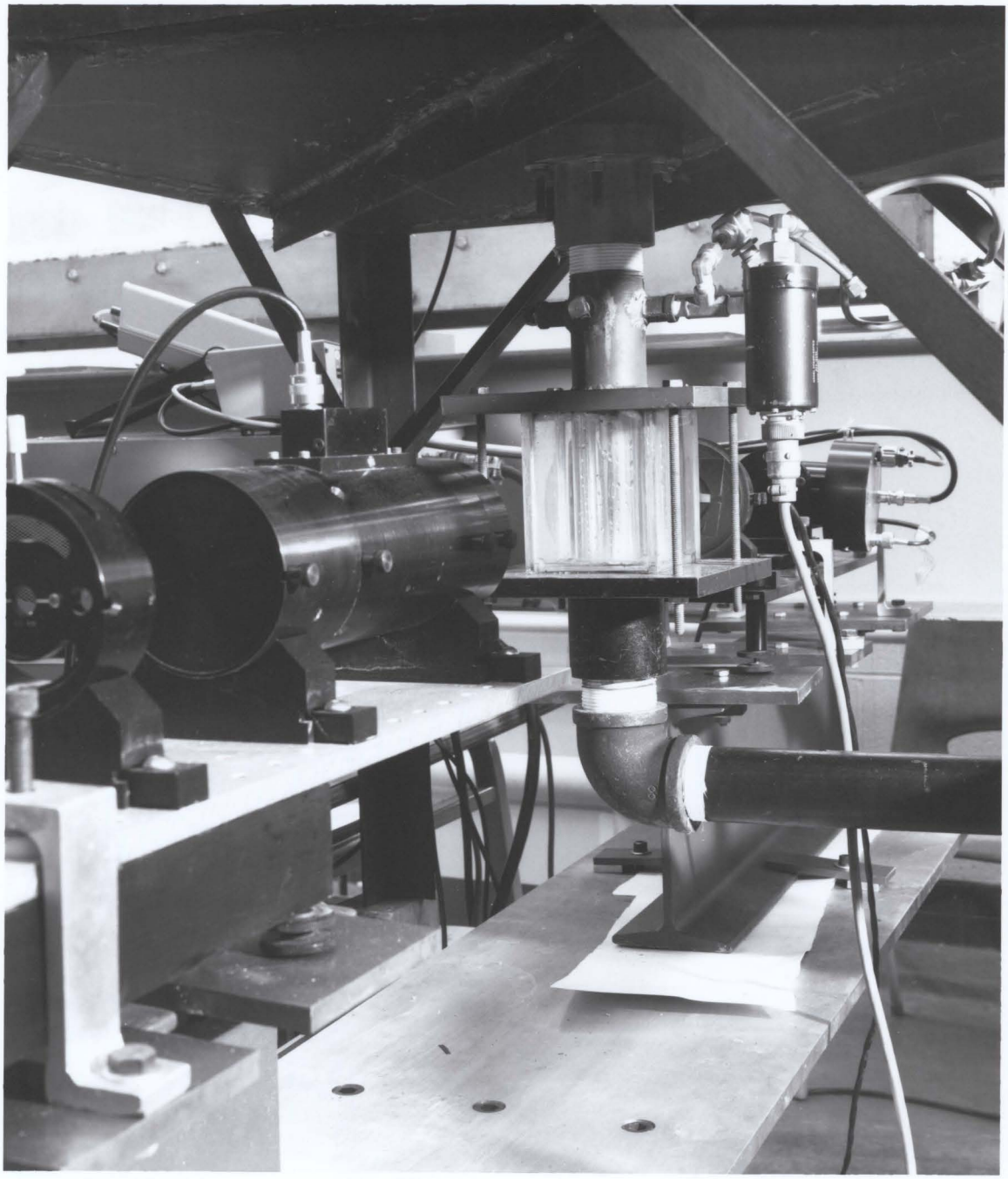

Figure 3.7 View of flow measurement test section.

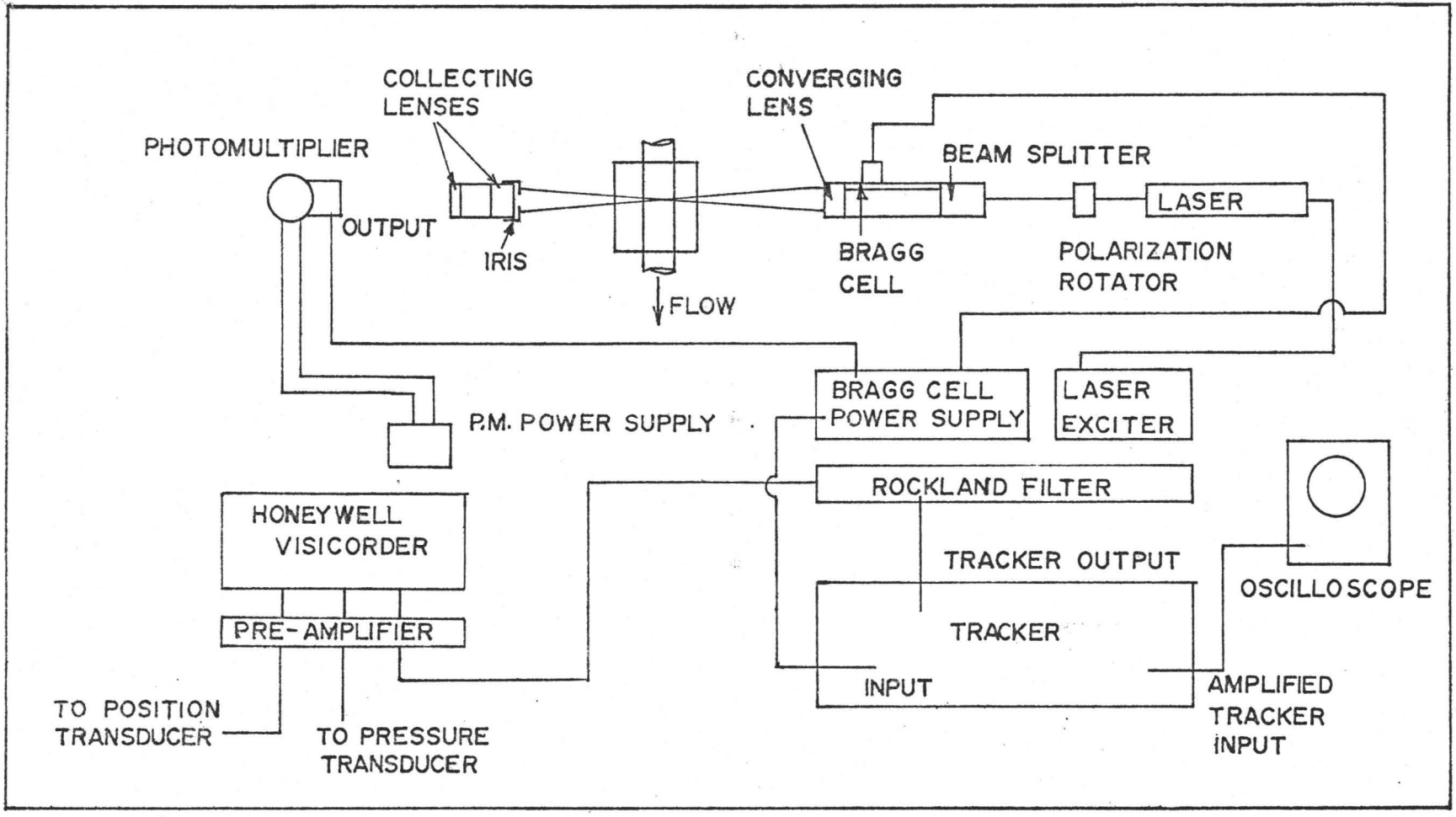

Figure 3.8 Electrical and optical set up of LDA and associated output equipment.

124 Helium Neon Laser and Thermo-Systems Inc. Series 900 Optics, Bragg Cell, photomultiplier, and a Model 1090 Tracker.

The optical set-up used is known as the dual beam mode [25]. The laser beam leaving the laser is vertically polarized. Referring to Figure 3.8 the beam next passes through a polarization rotator which is set such that the beam emerging from it is polarized in the plane perpendicular to the plane of the flow measurement direction. In this case this would be into or out of the page. The beam is then split and the upper beam is frequency shifted by the Bragg Cell. The two beams are then focussed by a lens, which in this case had a focal length of 248 mm, to the crossing point of the two beams. These beams crossing in the acrylic pipe contained in the flow measurement test section illustrated in Figures 3.5 and 3.7. The purpose of the acrylic box filled with water which surrounds the pipe is to reduce optical effects due to curvature of the pipe wall [26]. When the beams emerge from the test section they are not permitted to continue to the photomultiplier. Using the two collecting lenses, scattered light from the crossing point of the two beams is focussed on the photomultiplier aperture. The photomultiplier signal is then electronically processed and the tracker puts out a signal proportional to the particle velocity in the measuring volume created by the beam intersection point. This signal contains noise and the tracker manual [25] recommends the use of a low pass filter on the output signal. When operating in

the lowest tracker range the output was found to be sufficiently noise free that such a filter was not necessary. In the middle tracker range the signal to noise ratio was much lower so that the use of a filter became necessary. The filter used was a Rockland Model 432 with a rolloff of 24 dB/octave/channel. Only one channel was used with a cutoff frequency of 100 Hz, at the cutoff frequency the output is specified by the manufacturer to be down 3 dB.

The position, pressure and laser anemometer signals were recorded using a Honeywell 2106 Visicorder and a Honeywell Accudata 117 D.C. amplifier. The visicorder uses a light beam to record the data on ultraviolet light sensitive paper.

CHAPTER 4

PRELIMINARY EXPERIMENTS

4.1 Introduction

In order to model the self-excited vibrations of the valve properly, it is necessary to have some basic information, namely the free vibration characteristics of the valve and the static discharge characteristic.

Two quantities are sought for evaluation from the free vibration behaviour of the valve. The theoretical prediction of the valve frequency in water must be compared with the actual natural frequency. This gives an indication of the accuracy of the prediction of the added mass component of the total mass. It is also necessary to evaluate the damping of the valve since there seems to be no guide for estimating this.

Static discharge characteristics are evaluated to provide a datum against which dynamic discharge behaviour can be compared. They must also be examined to see if any rapid changes in discharge coefficient occur since this has been cited [15] as a major factor affecting valve stability.

4.2 Theoretical Formulation of Free Vibration

Figure 4.1(a) shows a schematic of the plug valve system.

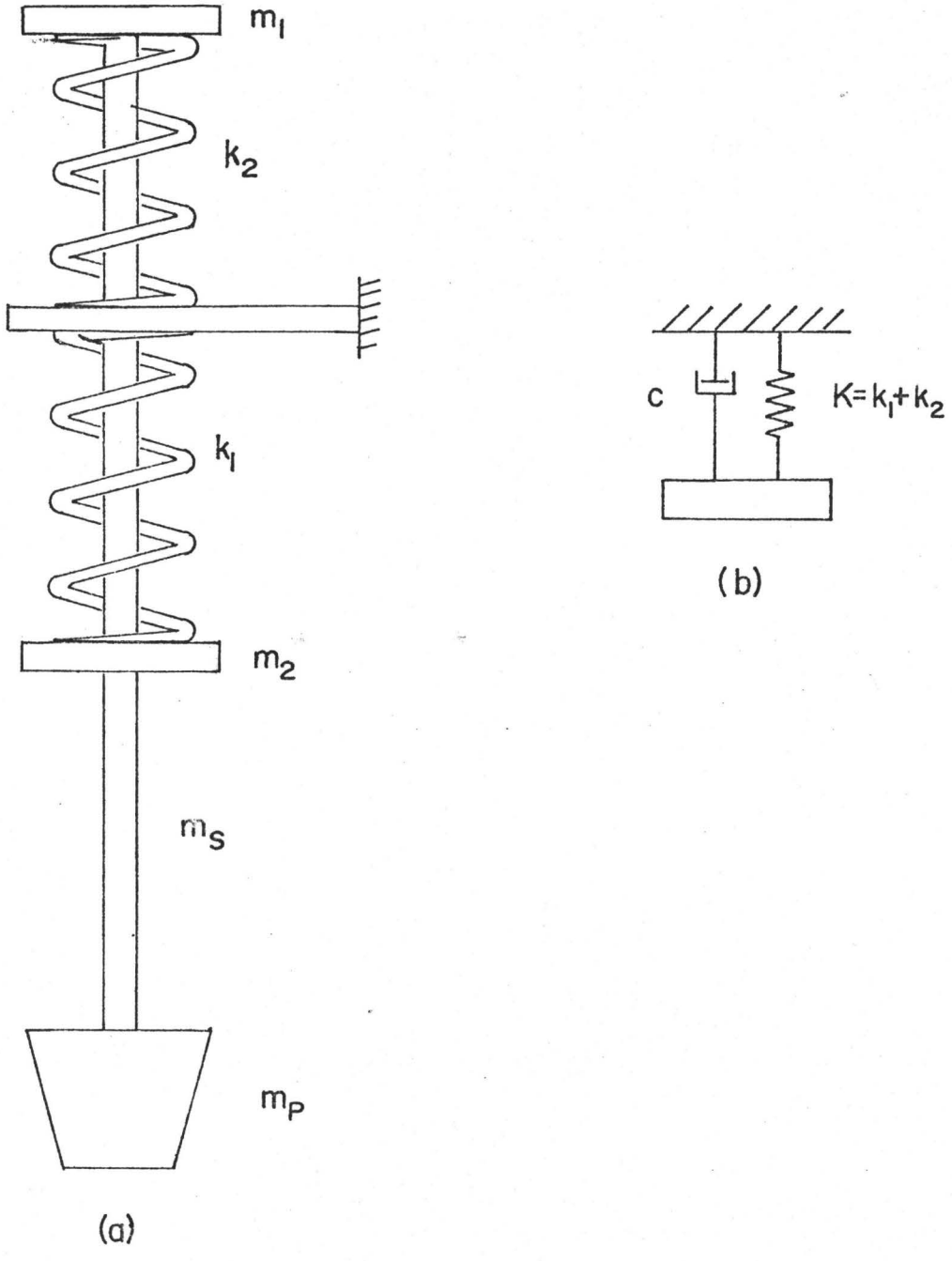

Fig. 4.1 Schematic of plug valve system and free vibration model

It's corresponding free vibration model is shown in Figure 4.1(b).

The mass of the system in air has been determined by weighing the shaft, cups and plug on a mass balance. The mass in air was found to be 946.5 gm. In the evaluation of the free vibration model in air, this is the mass that has been used.

Fritz [18] has tabulated formulas for the added masses of various bodies. For a disk of diameter D in quiescent fluid of density ρ, far from any rigid boundaries, the added mass, m' is given by,

$$m' = 0.637 \left(\frac{\pi}{6} \rho D^3\right) \tag{4.1}$$

Using the largest diameter of the plug (D = 57.2 mm) and for water as the fluid (ρ = 1000 kg/m^3) the added mass becomes,

$$m' = 62.4 \text{ gm} \tag{4.2}$$

Theoretical calculation of the natural frequency, f_n, of the mass-spring system is straightforward,

$$f_n = \frac{1}{2\pi}\sqrt{\frac{k}{M}} \tag{4.3}$$

where k is the spring stiffness and M is the virtual mass (mass in air + added mass). When f_n^2 is plotted against stiffness (k), the result is a straight line. Lines representing equation (4.3) are drawn in Figures 4.2 and 4.3. In Figure 4.2 the mass is that of the system weighed in air. In Figure 4.3 the line drawn represents the total mass in water

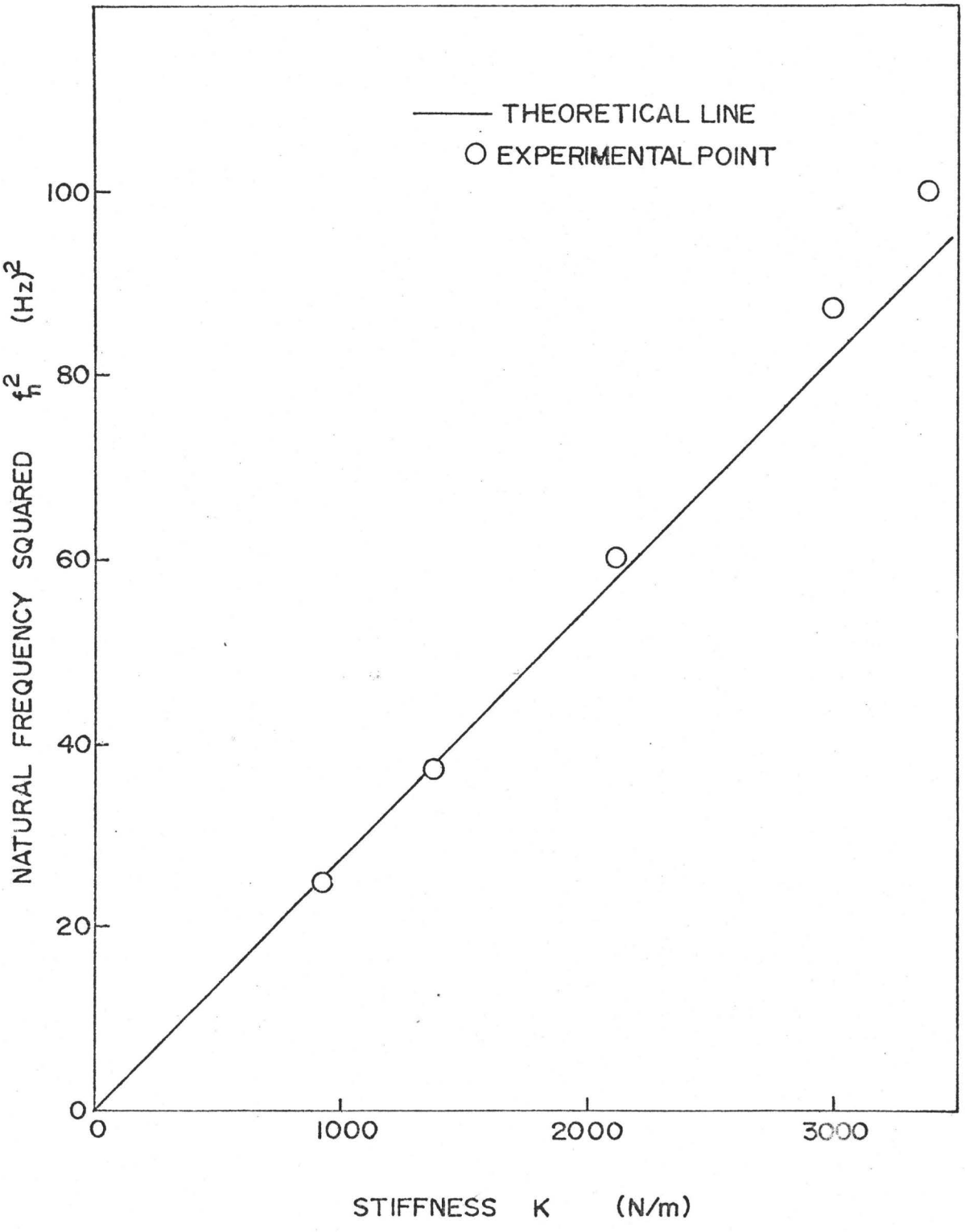

Fig. 4.2 Vibration frequency squared vs spring stiffness for plug valve in air

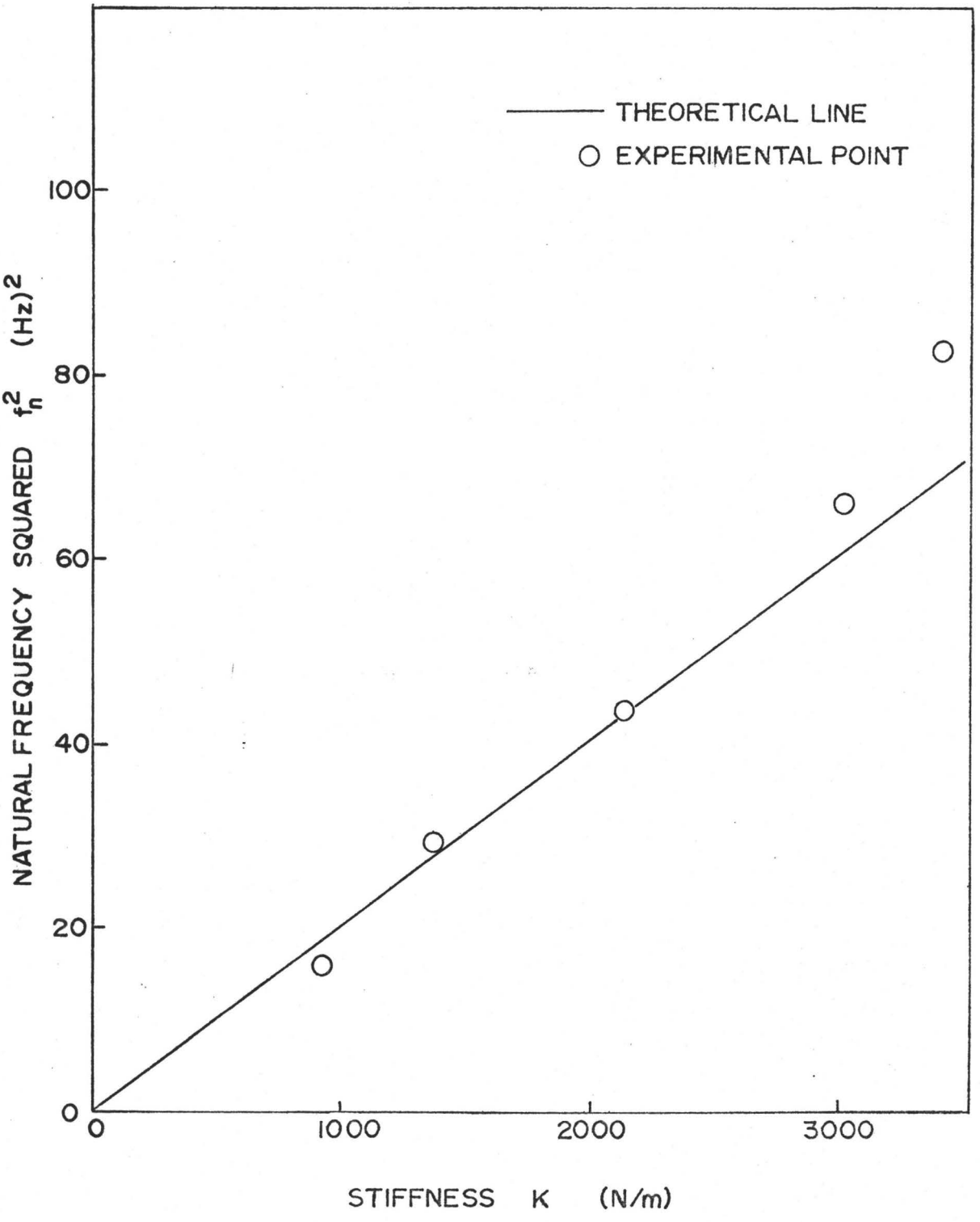

Fig. 4.3 Vibration frequency squared vs spring stiffness for plug valve in water

determined experimentally. How this was determined is described in the next section, Section 4.3.

4.3 Experimental Procedure and Results

This section outlines the method used to measure the natural frequency and damping of the plug valve system in air and water.

The procedures for determining the free vibration characteristics of the plug valve system are essentially the same in air and water. In water, it is necessary to measure the opening of the valve because the added mass and hence the vibration frequency is a function of relative proximity of the valve to the seat. For all measurements taken in water the opening was initially set to 7.62 mm as this was thought to be an opening at which the valve would be self-excited under flowing conditions.

The apparatus used in this set of experiments is the same as that described in Chapter 3. The Laser Doppler Anemometer and the pressure transducer are not necessary for this experiment and the downstream pipeline configuration is of no consequence because the downstream gate valve is kept shut during the experiment. For each spring combination used, the following procedure was adopted both in air and water with the position transducer connected to the visicorder. With the visicorder running, the valve was pushed to the seat, held there, and then released. Each experiment was repeated and

the average frequency is reported in Table 4.1. Uncertainties associated with these frequency measurements have been estimated to be: $\pm$ 0.1 Hz for measurements in air and $\pm$ 0.2 Hz for measurements in water.

Fluid	Air	Water
Stiffness k (N/m)	Natural Frequency	
	f_{n_a} (Hz)	f_{n_w} (Hz)
946	5.0	4.0
1386	6.1	5.4
2125	7.8	6.6
3017	9.35	8.15
3440	10.0	9.1

Table 4.1

These experimental results are plotted in Figures 4.2 and 4.3. It is seen in Figure 4.2 that for results in air agreement is good for the first three experimental points and that at higher stiffnesses higher frequencies than expected arise. In Figure 4.3 this nonlinearity is more marked. It is thought that end effects of the springs result in the nonlinearity by making springs stiffer. If this were the cause then the end effects should be more marked for shorter (stiffer) springs. This certainly seems to be the case. Given these observations, the total mass in water has been calculated on the least squares

fit of a straight line through the origin of the first three points plotted in Figure 4.3. The line drawn in Figure 4.3 corresponds to this experimental total mass, M_e, which has been found to be 1254 g. The experimental added mass m'_e is found to be,

$$m'_e = M_e - m_a \tag{4.4}$$
$$= 1254 - 946.5$$
$$= 307.5 \text{ g}$$

where m_a is the mass of the plug valve system in air. This compares to a theoretically calculated added mass of 62.4 g, which is about one fifth of the experimental added mass. This discrepancy arises from the proximity of boundaries, hence the effect of confinement is a large contributor to the added mass in water.

The damping of the valve system can be calculated from the decay traces of the free vibration tests. The logarithmic decrement of damping, δ, is given by (27):

$$\delta = \frac{1}{n} \ln \frac{x_o}{x_n} \tag{4.5}$$

where x_o is some datum amplitude and x_n is the amplitude of vibration measured after n cycles have elapsed. This calculation was carried out for two traces. In all cases the results obtained agreed within fifteen percent of each other and average values were used in reporting the values in Table 4.2. The damping ratio, ξ, is calculated using a linear approximation, valid for small damping.

$$\xi = \frac{\delta}{2\pi} \qquad (4.6)$$

Fluid	Air	Water
Stiffness k (N/m)	Damping Ratio ξ	Damping Ratio ξ
946	.074	.110
1386	.050	.135
2125	.051	.136
3017	.053	.164
3440	.050	.153

Table 4.2

Contributions to the damping come from three main sources. There is damping due to friction when the the transducer core is moving with respect to the fixed part of the position transducer. Damping is increased by friction from the ball bushings resting on the valve shaft. Third, damping is present when the valve is submerged. In air this is negligible, in water, however, fluid damping is significant as can be seen from Table 4.2.

4.4 Static Discharge Characteristics

To measure the discharge coefficient of a valve it is necessary to know the gap opening, the pressure difference and the volumetric flowrate of the fluid. The Schaevitz pressure transducer described in Chapter 3 was used to measure the static

pressure difference across the valve. The relation between the valve gap area g_2 and valve lift x has been derived in Appendix B. The effective gap width W is 31.32 mm such that,

$$g_2 = Wx \tag{4.7}$$

where x is the valve lift as recorded by the position transducer.

The flowrate was measured by timing the flow of water out of the downstream pipeline into a container. The volume of water in the container was subsequently determined using a measuring cylinder. For larger plug valve openings the gate valve was operated so that the flowrates varied from about 0.5 to 0.8 ℓ/s. At smaller openings this flowrate could not be achieved and so the gate valve was either fully open or nearly fully open for these measurements.

Figure 4.4 is a schematic of the plug valve and immediate downstream piping. Two possible pressure distributions in the system are shown. Initial calculations of the discharge coefficients were performed assuming pressure distribution A, i.e. negligible pressure recovery downstream of the plug valve. Calculations performed in this manner resulted in very high discharge coefficients, in fact, some turned out to be greater than one. Hence, it was concluded that pressure recovery was not negligible in this configuration.

To calculate pressure recovery the control volume in Figure 4.4 was used. It has been assumed that the pressure at the base of the plug is the same pressure P_2 at the gap.

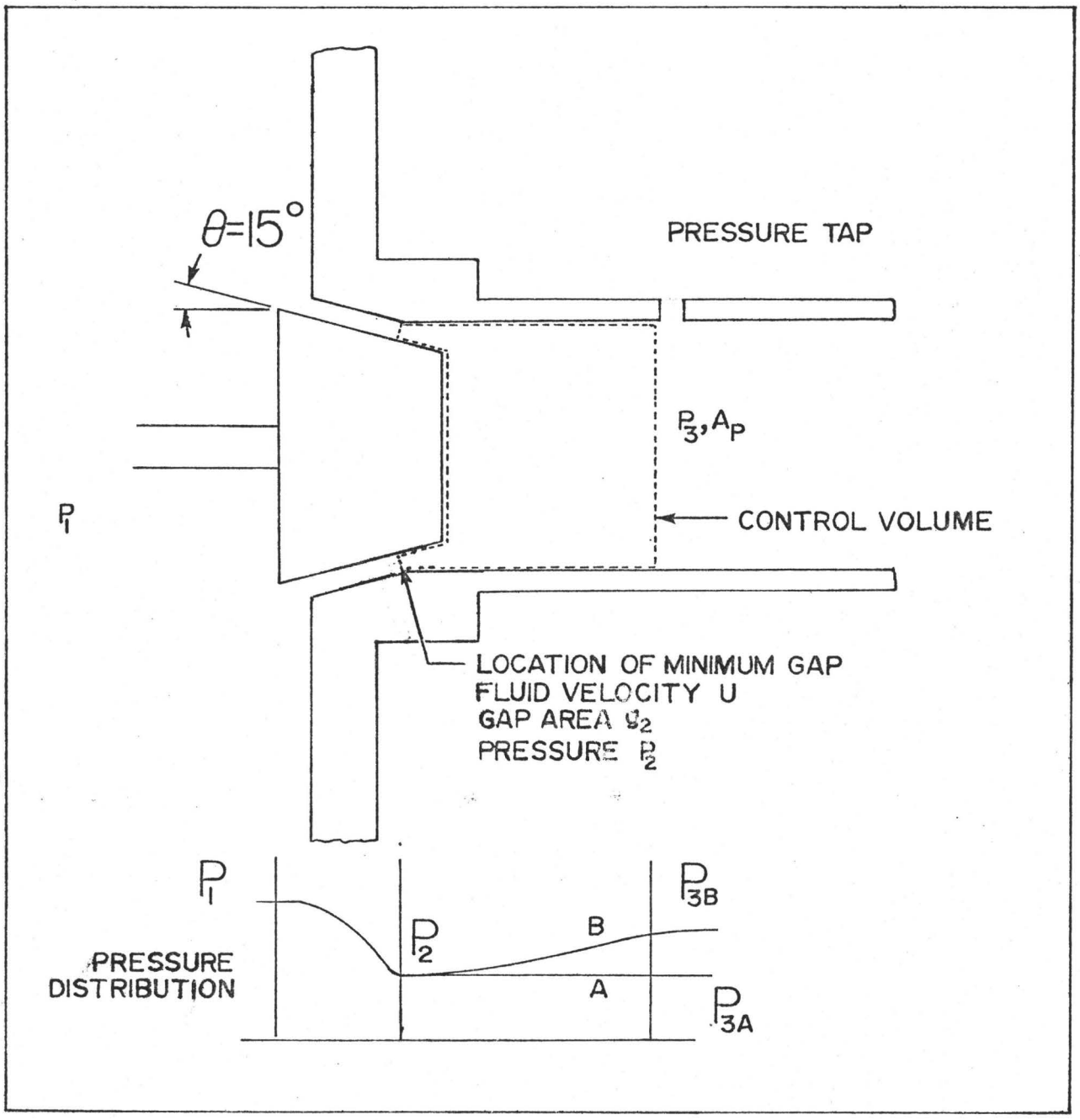

Fig. 4.4 Pressure distribution in valve and pipe immediately downstream

Applying the steady-state momentum equation,

$$P_2 A_p - P_3 A_p = \rho A_p V_3^2 - \rho U_2^2 g_2 \cos\theta \qquad (4.8)$$

The continuity equation gives,

$$Q = V_3 A_p = U_2 g_2 \qquad (4.9)$$

By combining equations (4.8) and (4.9) it can be shown that,

$$P_2 = P_3 + \frac{\rho Q^2}{A_p} \left(\frac{1}{A_p} - \frac{\cos\theta}{g_2}\right) \qquad (4.10)$$

Now the gap area $g_2 = Wx$, hence,

$$\Delta P_{23} = P_2 - P_3 = \frac{\rho Q^2}{A_p} \left(\frac{1}{A_p} - \frac{\cos\theta}{Wx}\right) \qquad (4.11)$$

The discharge coefficient is defined by,

$$Q = C_D Wx \sqrt{2(P_1 - P_2)/\rho}$$

$$= C_D Wx \sqrt{2\Delta P_{13} - \Delta P_{23})/\rho}$$

ΔP_{13} is the pressure difference measured by the pressure transducer. Table 4.3 summarizes the results obtained for the plug valve discharge characteristics. These results are plotted in Figure 4.5.

4.5 Discussion

The results of the free vibration tests reported in this chapter indicate the natural frequency of the plug valve system can be reasonably accurately predicted. The theoretical value

of added mass in unconfined water does not accurately reflect the actual added mass as expected. This is due to the proximity of the valve to the seat and hence a greater added mass results.

The discharge coefficient is plotted in Figure 4.5. It can be seen that it does not vary much between an opening of 2 mm and 20 mm. Hence if it were desired to model the plug valve using static discharge coefficients, C_D, one could probably use a constant value of $C_D = 0.87$ without incurring significant errors.

Scatter is present in the discharge coefficient data. Two sources of error are experimental uncertainty and calculation approximations. The largest experimental uncertainty lies with the measurement of flowrate. The total volume of water collected varied, but was in general around 4 ℓ. Hence timing errors of five percent may be present for the higher flowrates used. The flowrate is also used in calculating the pressure recovery so that this also has an uncertainty associated with it.

Pressure recovery may also be occurring along the valve plug from the gap to the plugs base. This pressure recovery will change with opening. There is no way of knowing how much pressure recovery actually occurs. Hence this adds further uncertainty to the discharge coefficient calculation.

Table 4.3

Static Discharge Characteristics of Plug Valve

x mm	Q dm^3/s	ΔP_{13} kPa	ΔP_{23} kPa	C_D
25.5	.5124	.200	-.090	.84
25.5	.5200	.324	-.092	.72
25.5	.4749	.210	-.077	.79
23.9	.4870	.222	-.096	.82
23.9	.7831	.530	-.247	.88
20.2	.7554	.654	-.332	.84
20.2	.5678	.358	-.188	.86
17.4	.6099	.593	-.286	.85
17.4	.7949	.876	-.486	.88
17.4	.7805	.924	-.469	.86
14.9	.5947	.765	-.352	.85
14.9	.7341	1.124	-.537	.86
14.9	.5128	.600	-.262	.83
12.5	.5801	.972	-.437	.88
12.5	.6897	1.407	-.618	.87
10.4	.5277	1.296	-.467	.87
10.4	.7658	2.406	-.984	.90
10.4	.4354	.779	-.318	.90
7.3	.3761	1.269	-.373	.91
7.3	.4233	1.724	-.473	.89
7.3	.5790	2.751	-.884	.94
5.1	.2537	1.358	-.259	.88
5.1	.2030	.938	-.166	.86
5.1	.2021	.924	-.164	.86
4.1	.2089	1.482	-.225	.89
4.1	.2411	2.034	-.299	.87
4.1	.2606	2.379	-.350	.87
2.4	.1475	2.489	-.200	.85
2.4	.2258	5.281	-.469	.88
1.3	.1052	5.599	-.194	.76
1.3	.1103	6.040	-.213	.77

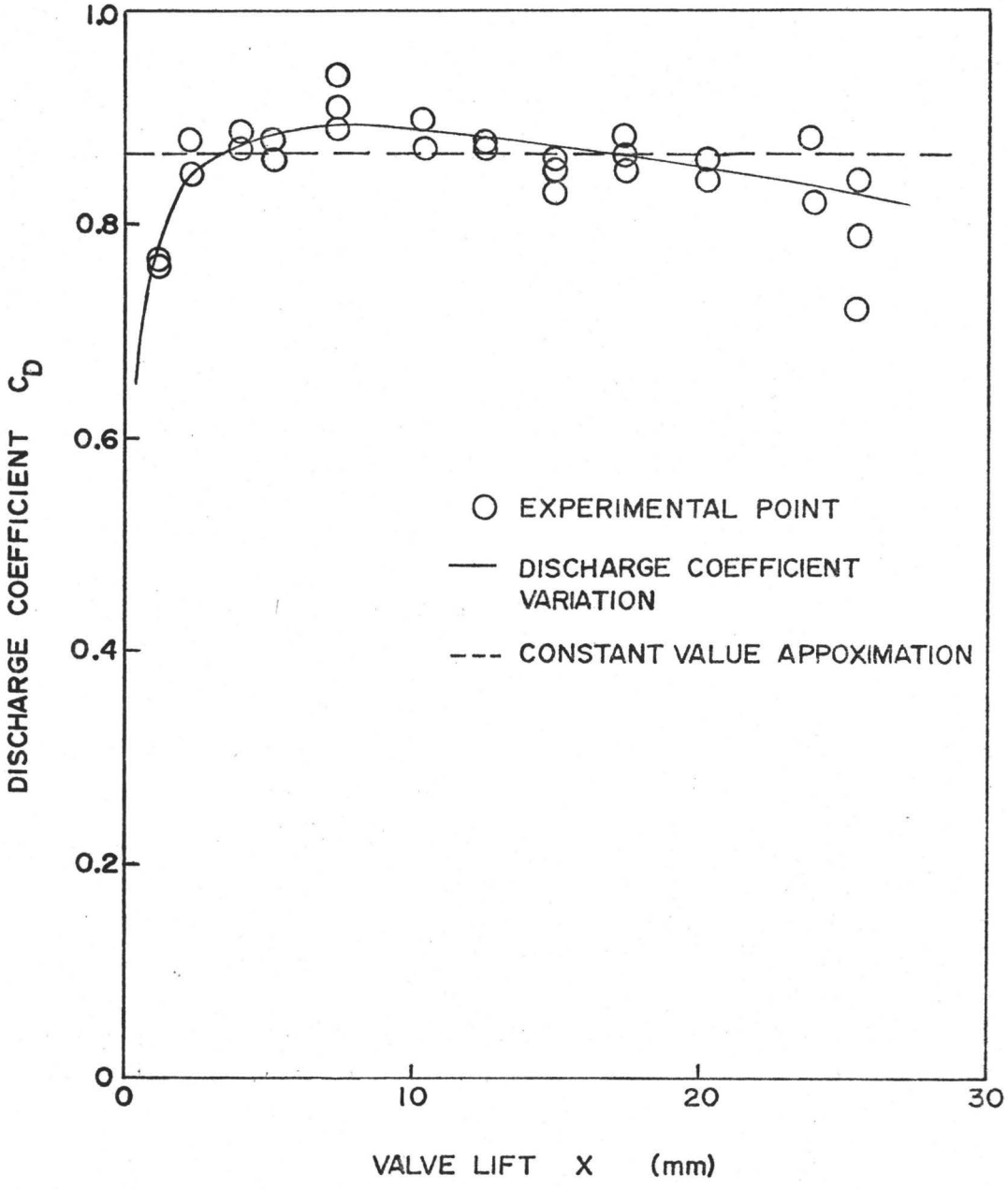

Fig. 4.5 Static discharge characteristic of plug valve

CHAPTER 5

SELF-EXCITED VIBRATIONS OF A PLUG VALVE

5.1 Introduction

In this Chapter, experiments are reported, which were conducted to improve our understanding of self-excited valve vibrations. The experiments are broken into three main sections: stability experiments, vibration characteristics within the region of instability and valve and fluid behaviour during vibration.

5.2 Static System Characteristics

Adubi [27] reports numerous stability charts similar to that presented in Figure 5.1. The region of instability in such a stability chart can be divided into two regions using the static valve characteristic [27]. This is defined by,

$$kx_o = \gamma \Delta H \, S \qquad (5.1)$$

where k is the stiffness, x_o the initial opening, γ the specific weight of the fluid and S is the effective area over which the hydrostatic head difference, ΔH, acts. kx_o represents the minimum force required to close the valve. $\gamma \Delta HS$ represents the closing force available from hydrostatic head. The region of instability develops around this characteristic. If there is sufficient hydrostatic head to close the valve, then a disturbance is required to initiate or continue

limit cycle oscillations. Such a disturbance could be provided by a reflected waterhammer wave or the valve bouncing off the seat. If, however, there is not sufficient hydrostatic head to close the valve, then hydrodynamic head is required to close the valve and no disturbance is needed to allow the valve to reopen after closure. Hence the static system characteristic divides the region of instability of Figure 5.1 into two regions; one in which disturbances are required to sustain the limit cycle oscillations and another in which no such disturbances are necessary but hydrodynamic head is required to cause valve closure.

5.3 Stability Tests

Tests were performed to determine the limits of the region of instability by varying two parameters out of stiffness, initial opening and fluid inertia at a time. With a large fluid inertia, as produced by a long downstream pipe, spring stiffness and initial opening were varied to give data summarized by Figure 5.1. Then the effect of fluid inertia on this instability region was investigated at constant stiffness.

5.3.1 Stability of Plug Valve - Pipe System with Large Fluid Inertia

Figure 5.1 shows an instability region similar to that reported for check valve vibration [15] with the region of instability extending from both sides of the static characteristic defined by equation (5.1). Below the lower stability threshold the valve is dynamically stable in the closed position.

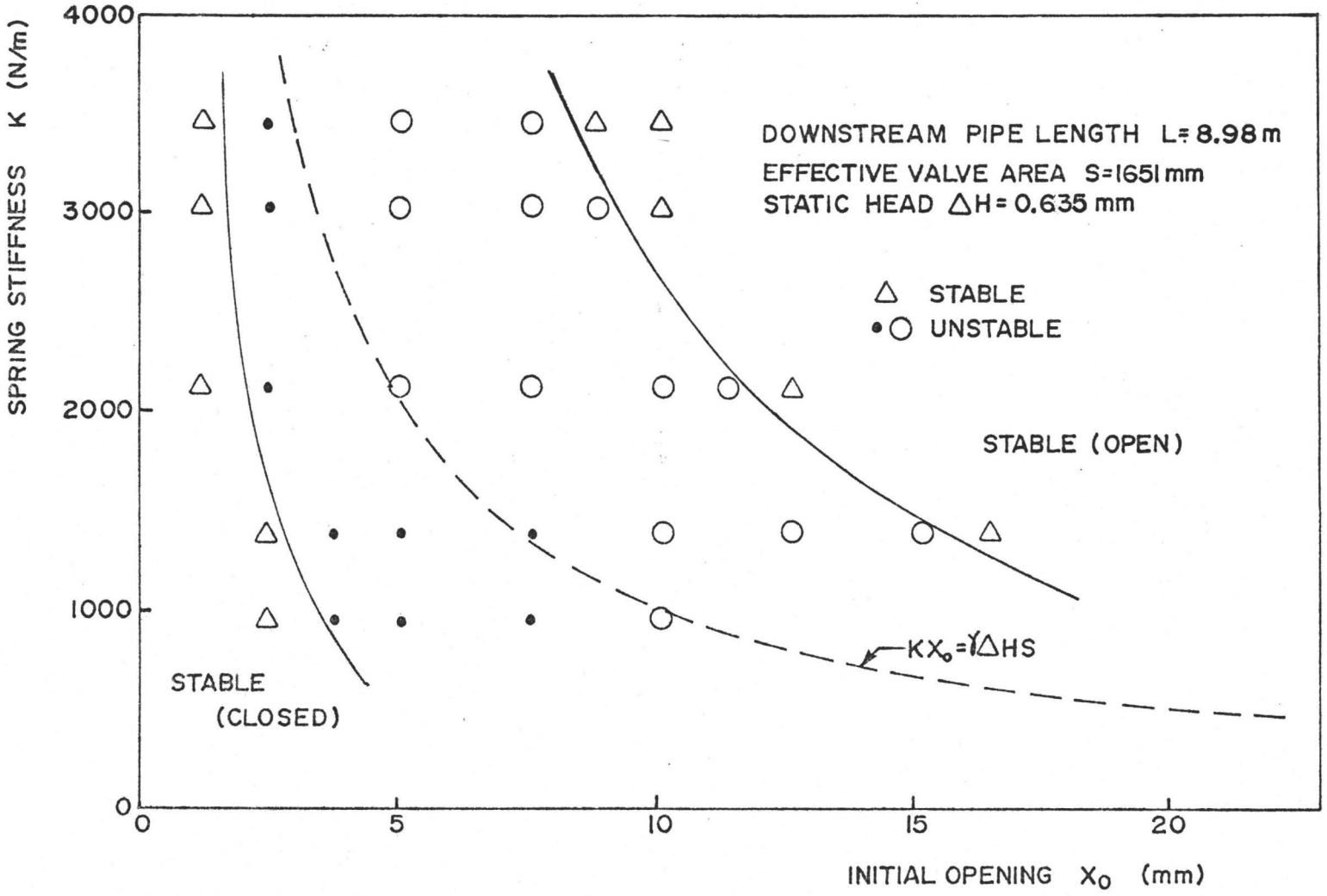

Fig. 5.1 Stability chart for plug valve

Disturbing the valve from the seat results in the valve bouncing and then coming to rest in the closed position. Between the lower stability limit and the static characteristic, disturbances are necessary to sustain limit cycle oscillations. If the valve is pushed to the seat and held there until all major disturbances such as waterhammer have died away and then released, the valve will in general remain seated. If a disturbance is introduced such as knocking the downstream pipe the valve will open and limit cycle oscillations will ensue. Between the static characteristic and the upper stability threshold the valve performs limit cycle oscillations regardless of initial conditions. For points above the upper stability threshold the valve settles to some equilibrium position with the valve open. When disturbed from this position, the valve performs typical damped harmonic oscillations, and hence is asymptotically stable.

The instability region for the plug valve appears to be larger than that reported for the check valve by Weaver et al. [15]. The check valve instability was attributed [15] to a region where a large drop in discharge occurred for a small change in valve opening. This resulted in a large hydrodynamic load on the valve. The region of instability is then limited on the upper side by where this drop in discharge decreases. The static discharge characteristic of the plug valve is similar to that of the check valve in the sense of having a sudden drop in discharge coefficient at small openings and a relative constant discharge coefficient at larger openings. The springs

chosen for the plug valve system, however, allow for instability to be developed in the region where the discharge coefficient is constant. As seen in Chapter 4 the discharge coefficient remains fairly constant for openings from about 2 to 20 mm. Thus the region of instability that develops about the static characteristic (equation (5.1)) is not limited by a sudden change in the discharge characteristic of the plug valve.

5.3.2 Effect of Changing Fluid Inertia on Stability

Figure 5.2 shows how fluid inertia affects the region of instability. Below the lower stability threshold the valve is dynamically stable in the closed position. Between the upper and lower stability thresholds the valve is dynamically unstable and will perform limit cycle oscillations. For points above the threshold the valve is asymptotically stable in the open position.

The lower stability threshold rises with decreasing fluid inertia. This rise can be explained in terms of work done on the valve due to pressure forces on the valve lagging the displacement of the valve. The hysteresis between these forces and displacement is a result of fluid inertia [1], [5], [6]. If fluid inertia is decreased, then the hysteresis between pressure forces and displacement decreases [6]. Reduced hysteresis means that less work is done on the valve, hence the lower stability threshold moves upwards as pipe length (and fluid inertia) reduces.

The upper stability boundary also rises as pipe length reduces. Kolkman [4] predicts such a trend in his analysis of

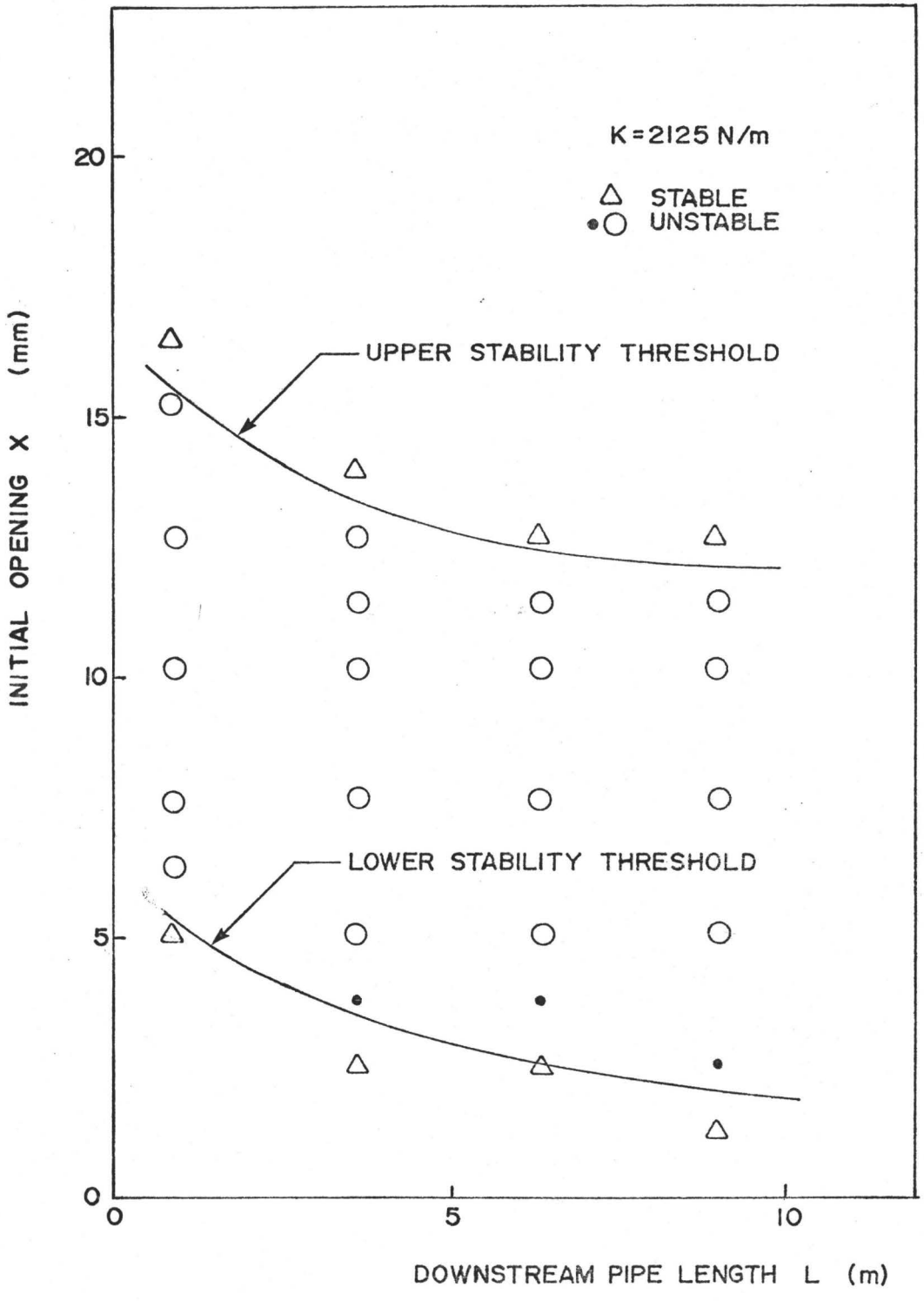

Fig. 5.2 Variation of stability threshold with downstream inertia

a simple plug valve. The reason for such a rise in the stability limit is not clear at this point, comparison of Kolkman's predictions and those from the nonlinear theory of Chapter 6 are compared with these experimental results in Chapter 7.

5.4 Parametric Tests

Results reported in this section, show the effects of changing initial opening, spring stiffness and fluid inertia on the characteristics of the plug valve limit cycle oscillations. These results are examined to see if any trends are obvious and, if so, to provide explanations where possible. Similar parametric tests have been reported previously [15], [20], and comparisons are made with these results.

5.4.1 Effect of Stiffness and Initial Opening on Limit Cycle Oscillations

Figures 5.3 and 5.4 show the effect of changing initial opening and stiffness on the frequency ratio. The frequency ratio reported in these figures is based on the ratio of the limit cycle oscillation frequency ω, to that of the natural frequency of the valve in water ω_n. In calculating the limit cycle frequency ω, the portion of the cycle for which the valve remains closed is not included. This is so that results can easily be compared to the theoretical results since the theory does not account for the time for which the valve is closed.

Clearly, the effect of increasing stiffness or initial opening can be seen from Figures 5.3 and 5.4, to be a decreasing

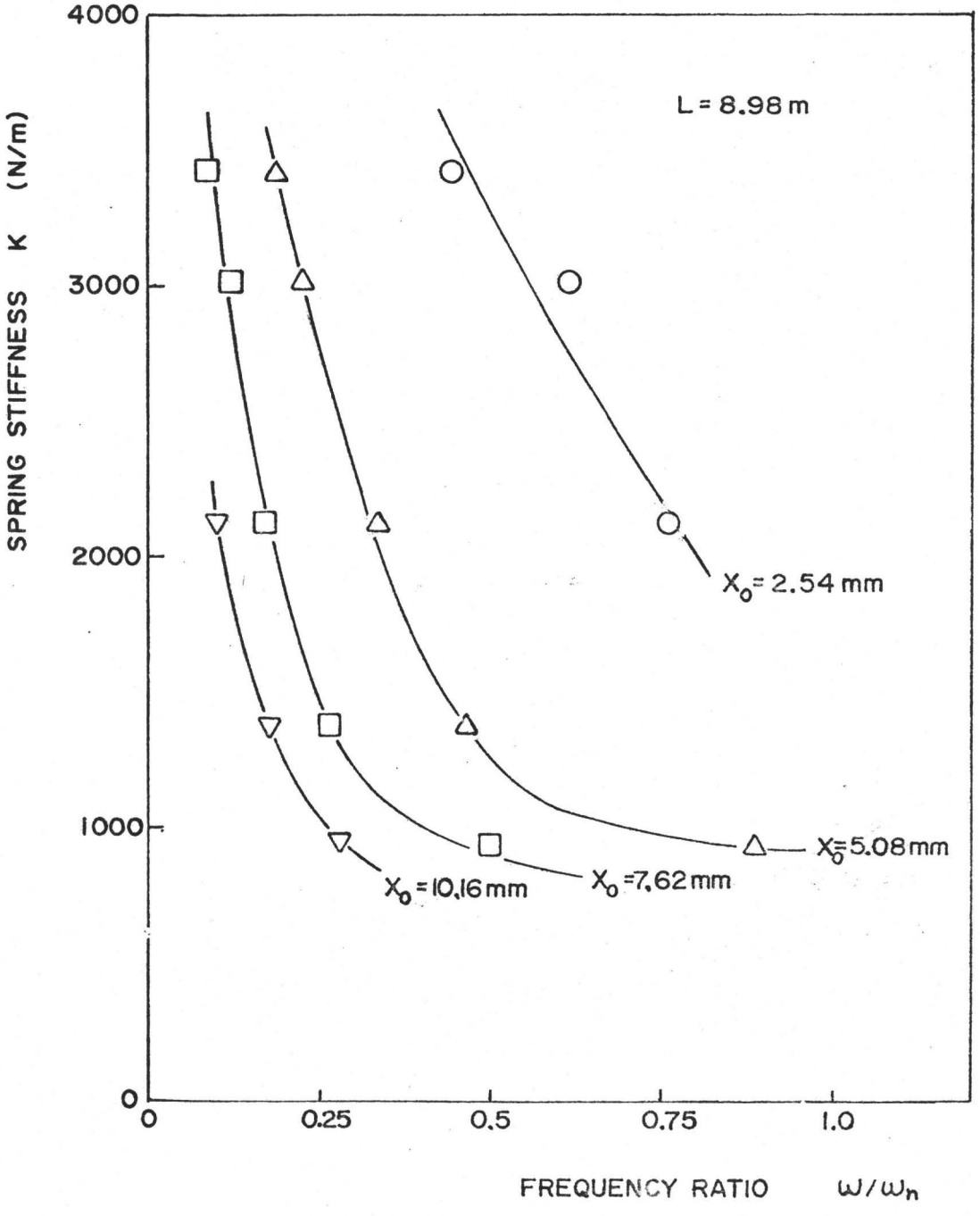

Fig. 5.3 Spring stiffness vs frequency ratio

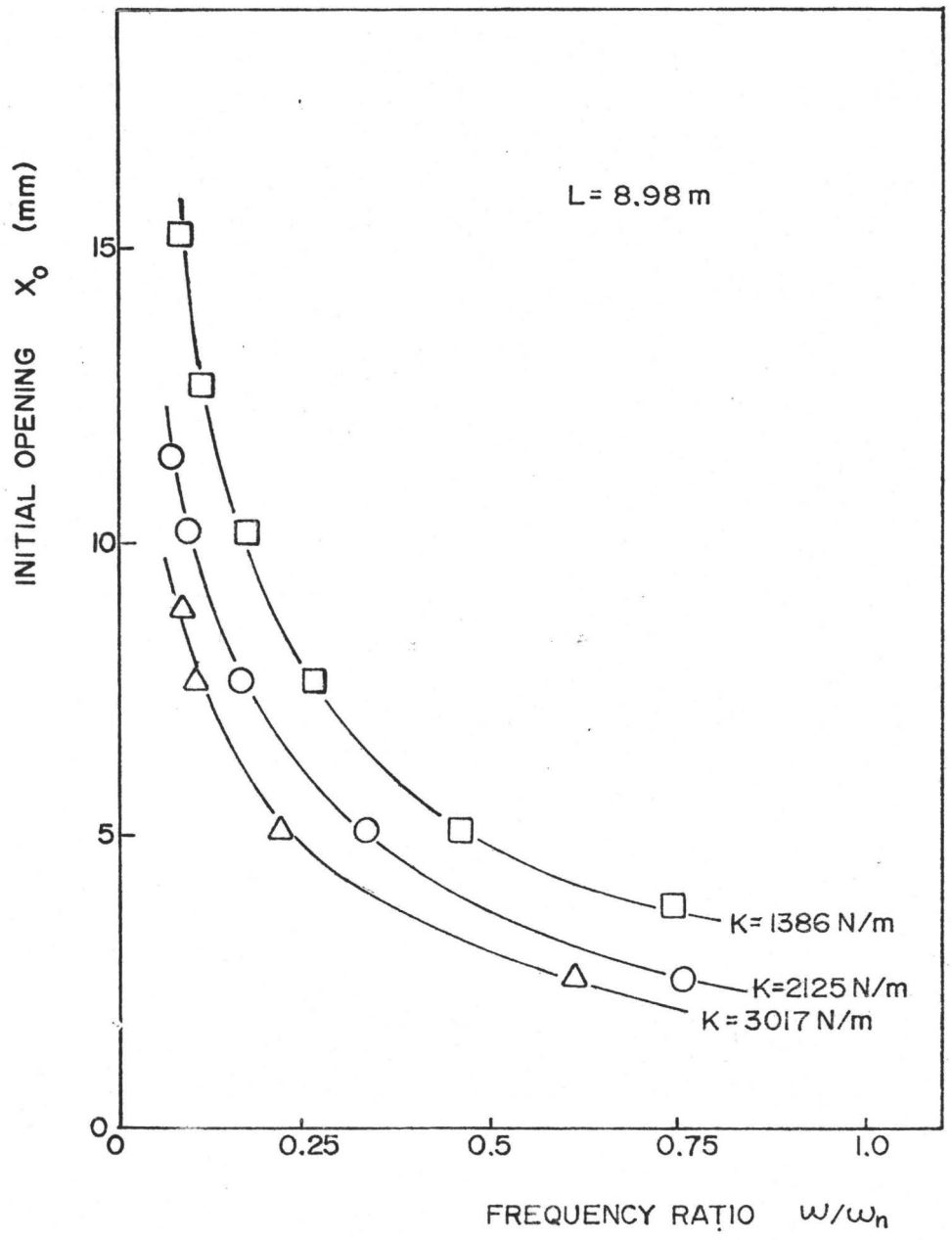

Fig. 5.4 Initial opening vs frequency ratio

frequency ratio. At low stiffnesses and openings the frequency ratio changes more rapidly with a change in either parameter.

In Figure 5.3, it appears that the points for an initial opening of 2.54 mm do not fit the curve drawn as well as at the other three openings. This discrepancy is explained below.

In Chapter 4, confinement has been discussed with respect to its effect on added mass. Confinement of the flow around the valve also results in increased fluid damping. This damping becomes larger as the initial opening of the valve is reduced. The initial opening was experimentally set using the position transducer. To determine whether the opening set was correct, the valve was displaced from its equilibrium position (in the no load position) and allowed to come to rest. When damping is small one can be reasonably certain that the valve will come to rest near its equilibrium position. However, when damping is large, due to the effects of friction the valve's initial opening is more difficult to determine precisely. This is the case for openings of 2.54 mm, in this particular case the initial opening may be in error by as much as ten percent. Furthermore, Figure 5.3 shows that at small initial valve openings that the frequency ratio is very sensitive to a change in initial opening. Hence there is a larger experimental uncertaintly associated with the anomalous points of the curve at an initial opening of 2.54 mm. For this reason the curve corresponding to this has been drawn with a similar

trend to those at larger openings, rather than a curve which might be suggested by taking these points in isolation.

Figures 5.5 and 5.6 show the effect of changing stiffness and initial opening on the amplitude of the limit cycle oscillations. Figure 5.5 shows that the amplitude of vibrations increase slowly as stiffness is increased. At low stiffness the amplitude drops off faster as stiffness reduces. There are two effects which cause such a trend.

The first effect is caused by considering the time required for the valve to reach its maximum displacement. This time will reduce as the natural frequency of the system increases. Such a reduction can be brought about at constant mass by increasing the stiffness of the system. The downward force on the valve due to flow past the valve increases with time, hence if the natural frequency of the system is higher then the downward force acting on the valve when it reaches its maximum displacement from the seat is reduced.

The second effect comes about by considering the direct effect of increasing stiffness. The static displacement of a system of stiffness k acted upon by a force F is given by

$$d = F/k$$

Hence systems with higher stiffness are less sensitive to a displacing force. Hence the force which is created by fluid pressure as the valve leaves the seat will reduce the amplitude of a less stiff system than that of a stiffer system.

Hence, the net result of the two mechanisms of

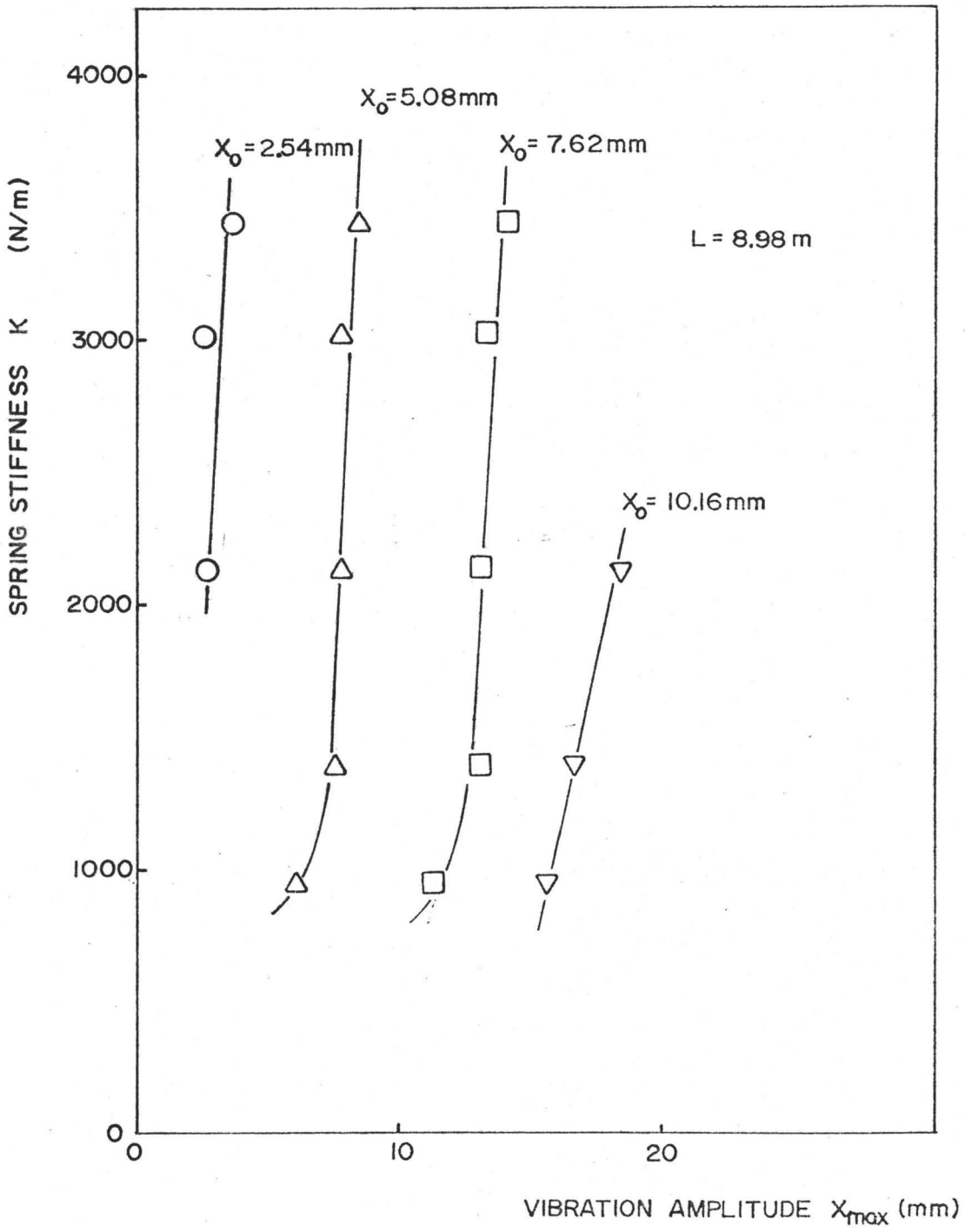

Fig. 5.5 Effect of spring stiffness on amplitude

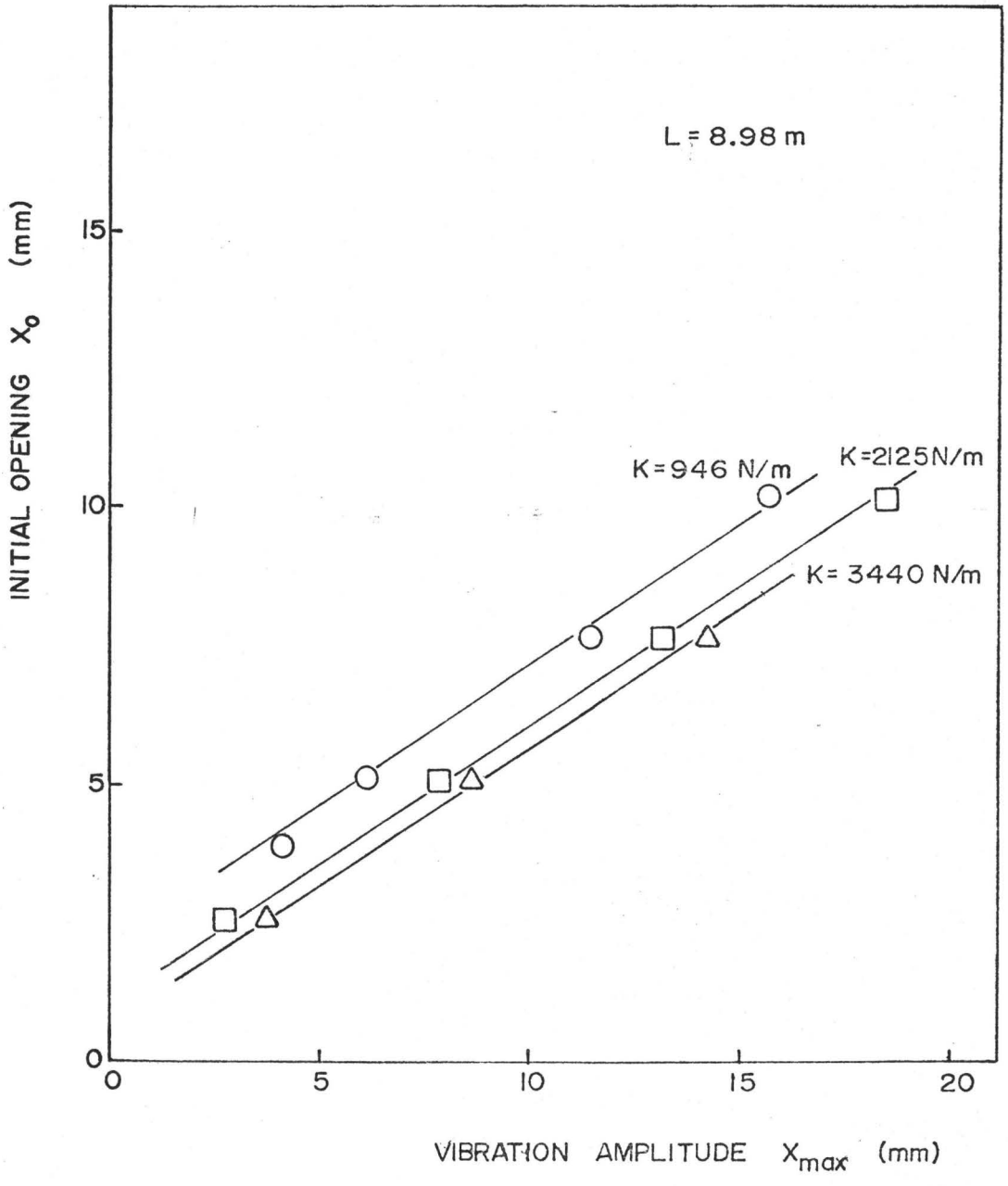

Fig. 5.6 Effect of initial opening on vibration amplitude

amplitude reduction, due to the pressure forces acting on the valve is to reduce the amplitude for a less stiff system more than that of a stiffer system.

Figure 5.6 shows that amplitude is proportional to initial opening. It is interesting to see that the slope of these lines is approximately equal to two. If flow re-establishment and damping were negligible when this system reaches a maximum, an amplitude of 2 x_o could be expected with the mass spring system just described. The lines in Figure 5.6 do not however go through the origin. Presumably this is because of flow re-establishment causing a drag force and damping causing a reduction in amplitude.

These experimental results show that increasing either stiffness or initial opening has qualitatively the same effect. The amplitude is however, more sensitive to initial opening than stiffness. Increasing either results in an increased amplitude and a decreased frequency ratio. These conclusions are the same as those drawn by Adubi [28] for check valve vibrations.

5.4.2 Effect of Fluid Inertia on Limit Cycle Oscillations

Figure 5.7 shows that the amplitude of oscillations generally increase with fluid inertia. There seems to be three regions where the amplitude varies at different rates.

At low fluid inertias the fluid may accelerate very quickly in the pipe, hence one would expect that, here,

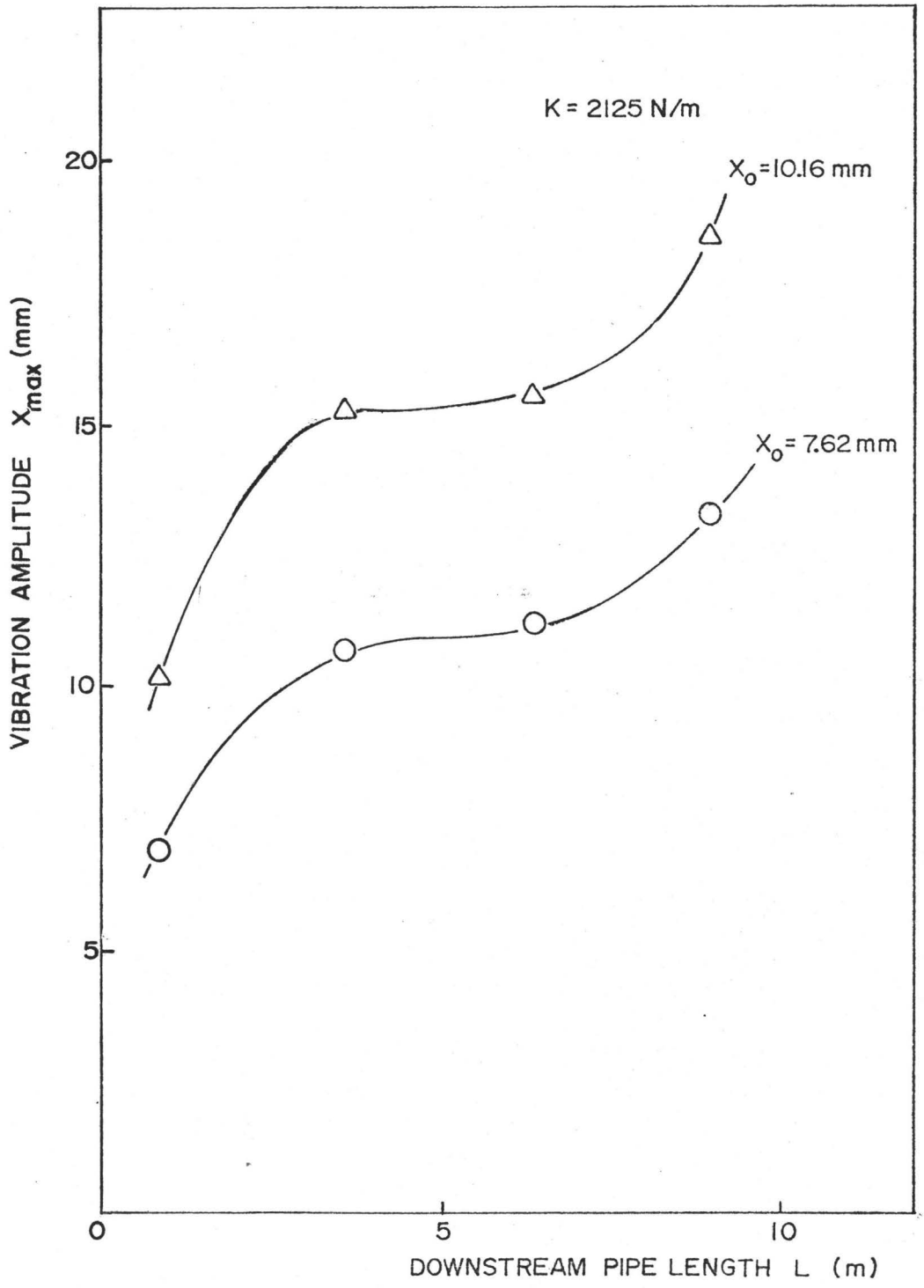

Fig. 5.7 Vibration amplitude vs fluid inertia

drag force on the plug valve affects the amplitude of the vibration. From the graph, this region seems to exist for pipe lengths less than about 4 m. Between 4 and 6 m pipe length the amplitude does not change significantly. Presumably this is because the drag force on the plug valve is now very small when the plug reaches its maximum height. At even higher fluid inertias (pipe length greater than 7 m) the amplitude of vibration rises again. Fluid inertia causes hysteresis between the pressure forces and displacement of the plug valve. Consequently, a larger change in flowrate at the end of the cycle (closure) is probable for higher fluid inertias. This results in a larger waterhammer. Hence we might expect larger waterhammer pressures to result and thus larger amplitudes.

Figure 5.8 shows a linear relation between the period of vibration and pipe length. This suggests the concept of a critical flowrate at which sudden closure starts and hydrodynamic pressures dominate. Figures 5.9 to 5.12 show that the flowrate increases more or less linearly with time, most of the pressure is being used to accelerate the fluid in the pipe. Thus if this critical flowrate were more or less independent of pipe length then one expects a linear variation of period with fluid inertia. Neither of the two lines drawn in Figure 5.8 intersect the origin. Two factors which may affect this are fluid inertia of the gap and the finite time required for the opening part of the cycle. Both of these effects would result in intersecting points at zero pipe length

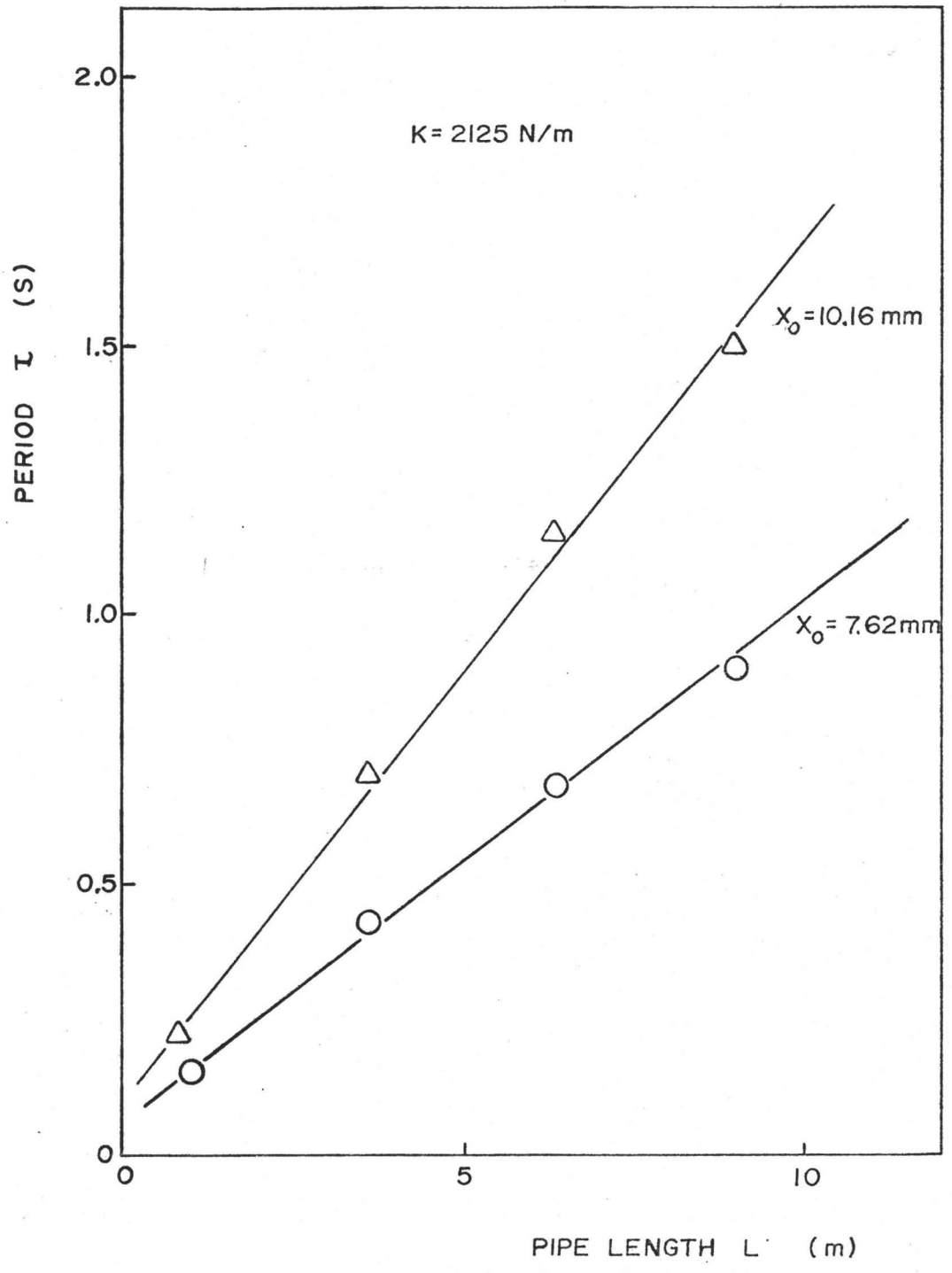

Fig. 5.8 Vibration period vs fluid inertia

on the positive period of vibration axis.

5.5 Closer Examination of the Self-Excited Oscillations

In this section self-excited plug valve vibrations at four parametric sets of valves are examined and the limit cycle is described in detail. In Section 5.4 it has been shown that increasing stiffness and initial opening have a similar effect. Hence a restoring force parameter kx_o can be used instead of separate stiffness and initial opening parameters in choosing measurement points. The four parametric sets of limit cycle oscillations are for large and small restoring forces and large and small fluid inertias. The limit cycles are described in the next section and Figures 5.9 to 5.12.

5.5.1 Typical Vibrations

Figures 5.9, 5.10, 5.11 and 5.12 show typical limit cycle oscillations performed by the plug valve examined in this thesis. The top trace in each of these diagrams represents the displacement of the plug valve from the seat. The middle trace shows the variation in pressure and the lower trace follows the fluid velocity measured at the centre of the pipe downstream of the valve, using the laser doppler anemometer.

The sequence of events which occurs in each cycle can be broken into three phases. There is an opening phase where the valve acts like a system in free vibration. This follows the pressure difference across the valve dropping to a value below ΔP^* $(=kx_o/S)$, which is the pressure difference required

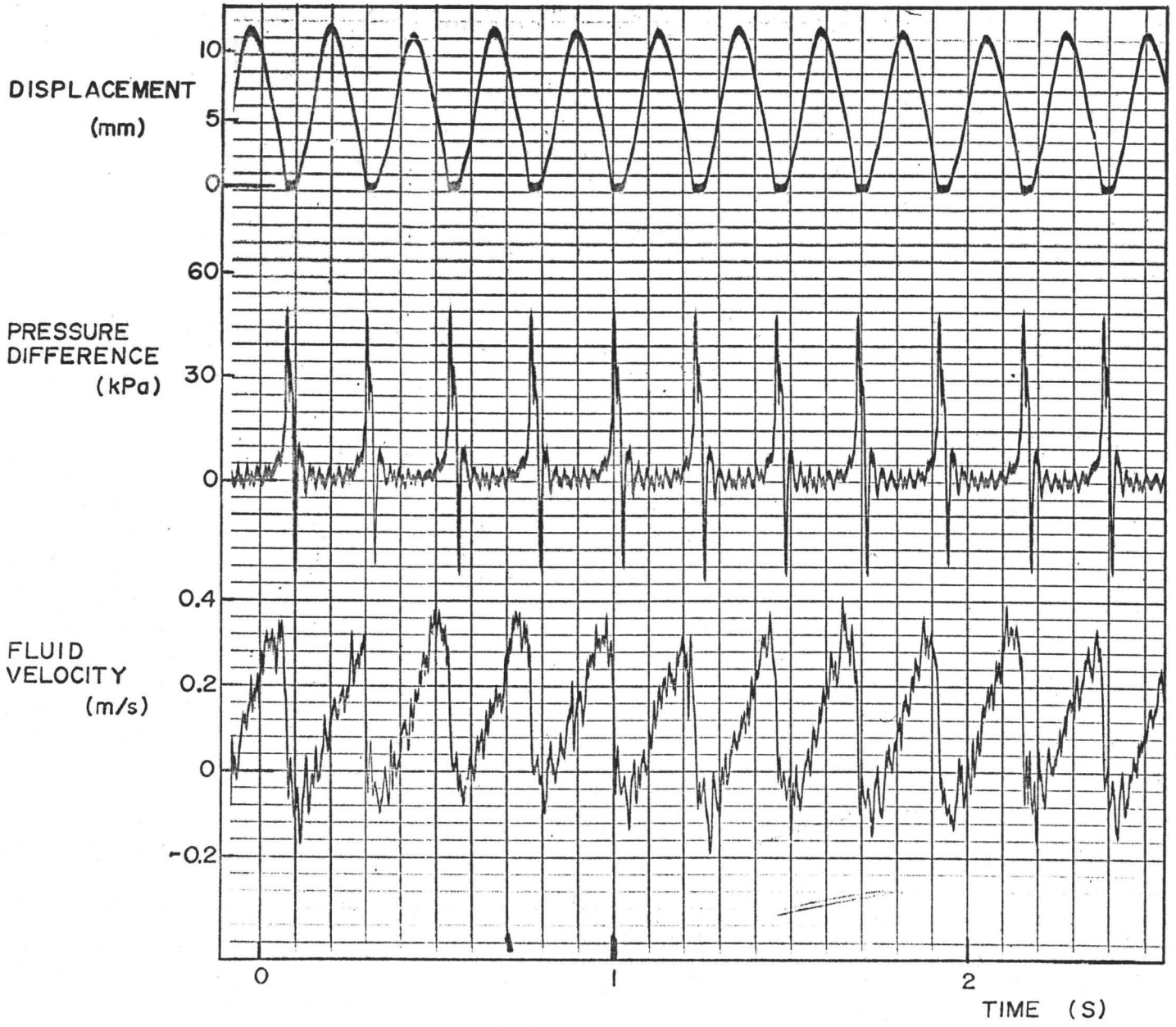

X_o = 8.0 mm K = 1386 N/m L = 0.84 m

Figure 5.9 Dynamic measurement

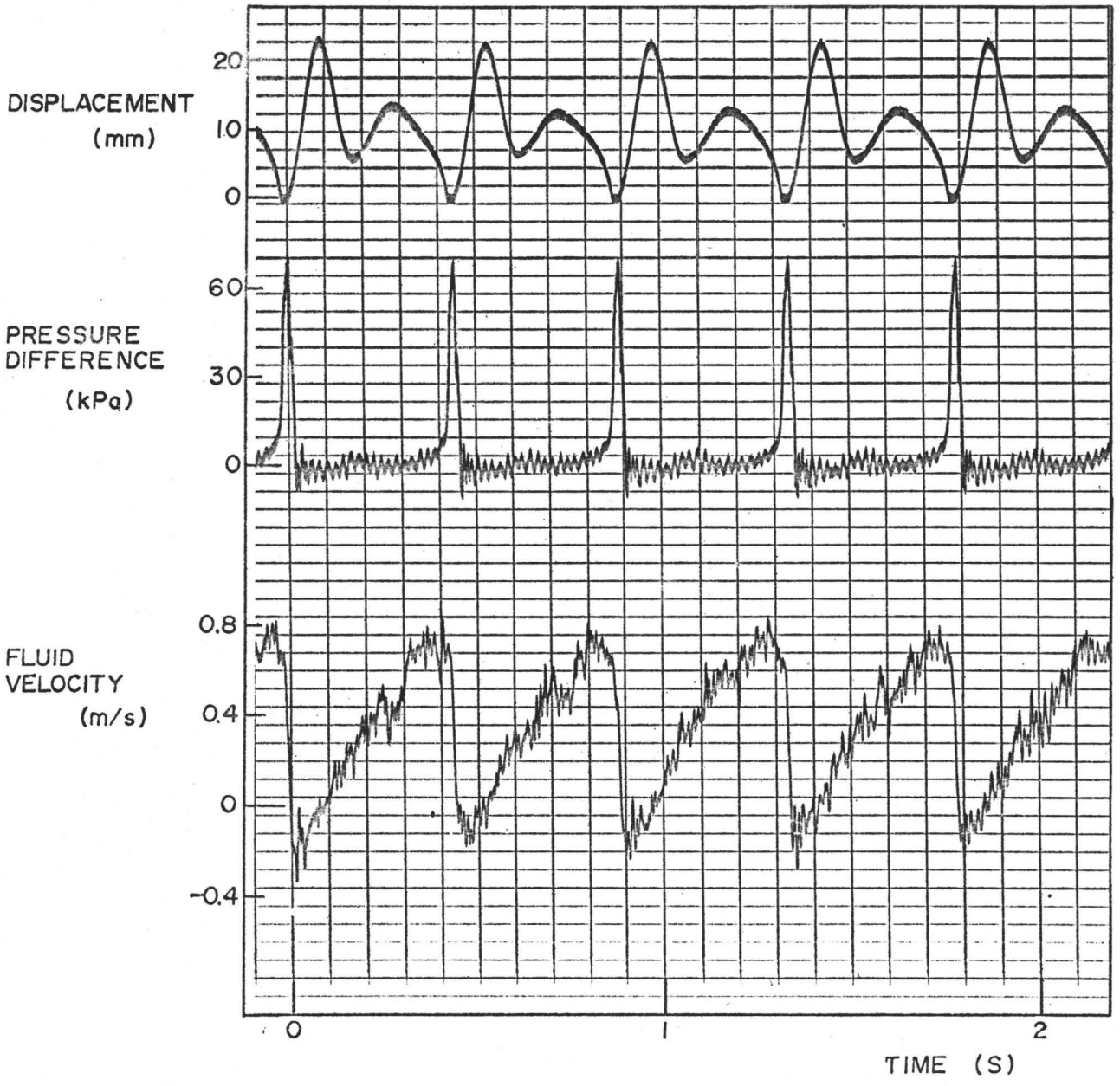

X_o = 12.7 mm K = 1386 N/m L = 0.84 m

Figure 5.10 Dynamic measurement

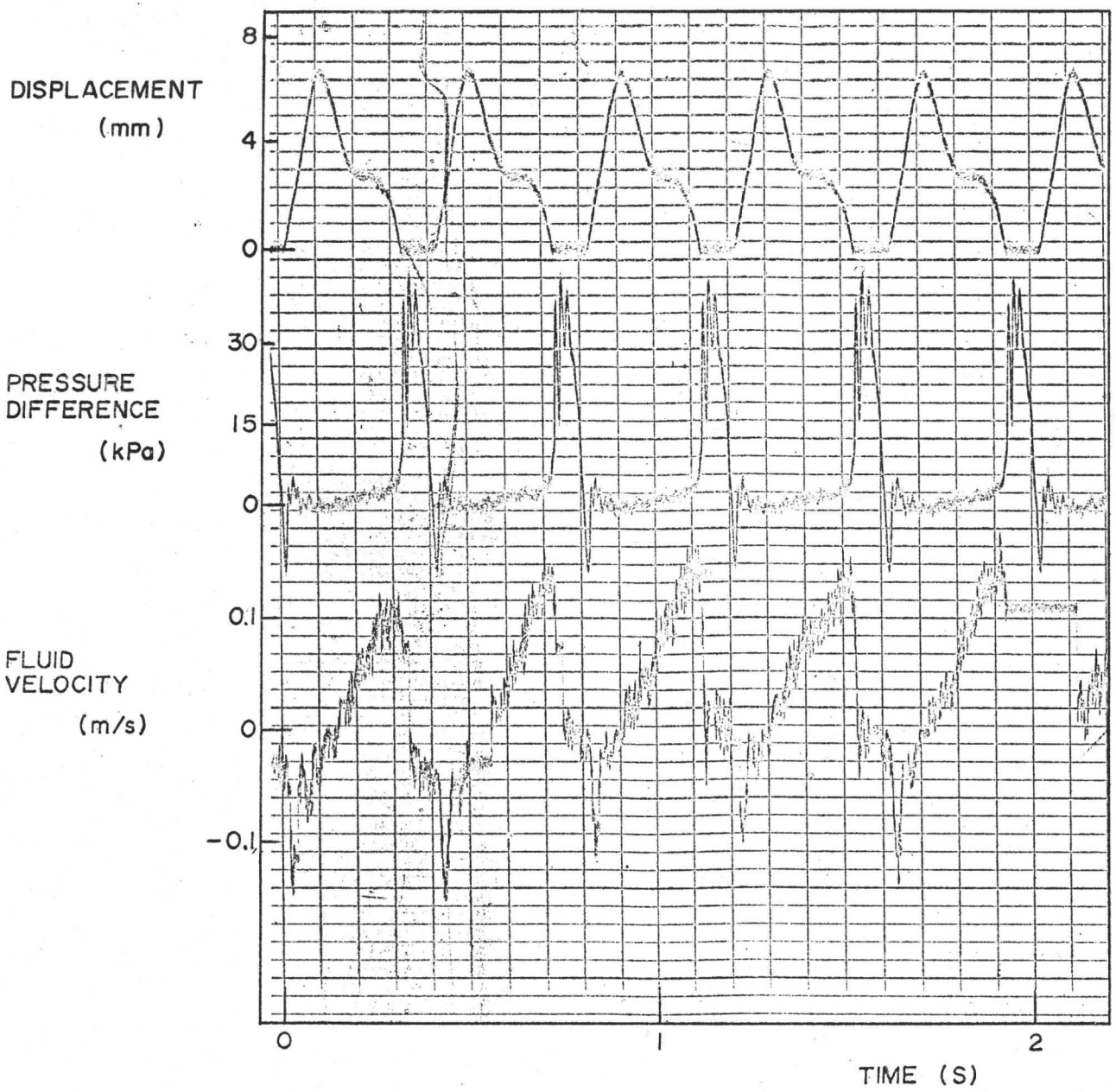

X_o= 4.3mm K = 1386 N/m L = 8.56 m

Figure 5.11 Dynamic measurement

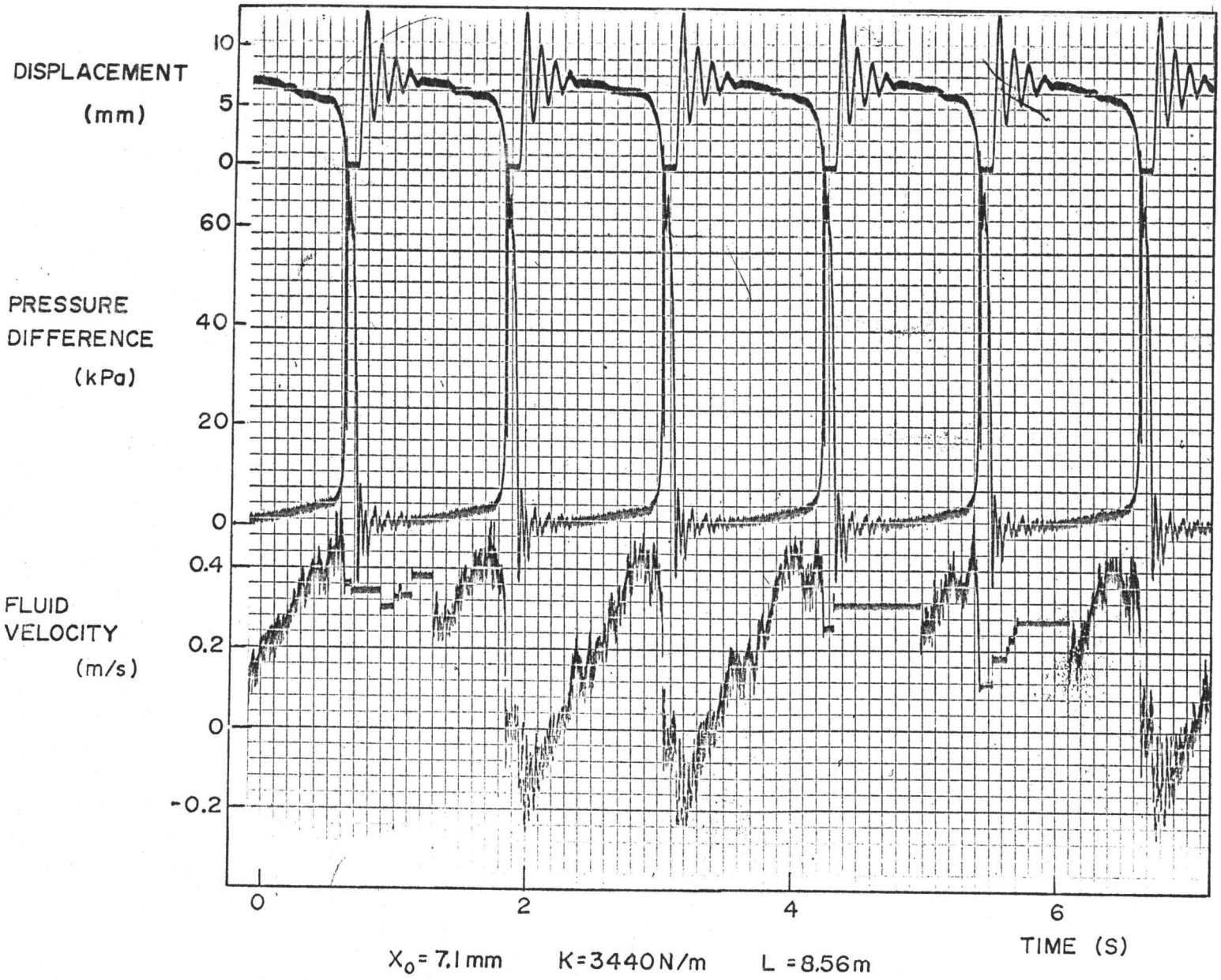

Figure 5.12 Dynamic measurement

to hold the valve at its seat. In all the reported cases opening is accompanied by reverse flow in the pipeline. Subsequently a middle phase arises where the pressure drop across the valve is minimal and the fluid in the pipe has an almost constant acceleration. Here most of the head drop goes into accelerating the fluid. The flow in the pipe reaches a maximum and rapid closure ensues. During the closing phase, the fluid undergoes rapid deceleration at the very end and the pressure difference across the valve rises rapidly. The valve then remains closed until the pressure difference drops, whence the valve reopens and repeats the cycle. The free oscillation portion is most obvious in Figure 5.12. In the other figures, the maximum flowrate is established more quickly. Hence the opportunity for many harmonic oscillation cycles does not exist. In Figure 5.9 the flow establishes so quickly that the frequency ratio is 0.95 and hence no free oscillations at the valves' natural frequency are apparent. In Figure 5.12 the frequency ratio is 0.11 and the free oscillations are damped out before closure occurs.

These limit cycle vibrations are clearly not simple harmonic in nature and hence nonlinear modelling of the vibrations as done by Weaver and Ziada [6] appears to be the only way to get a model which is capable of predicting the form of these vibrations. The basic breakdown of the cycle into free vibration, a dwell while the flowrate increases followed by sudden closure is the same as predicted by their nonlinear models. However, reverse flow in the pipeline at the beginning

of the cycle was not predicted.

Noise exists on the pressure traces in all four diagrams. To establish whether this was caused by vibration of the rig, a triaxial accelerometer was mounted in several key locations and the records obtained were compared to that of the pressure transducer. No matching of frequencies was obvious. Adubi's [28] experiments had similar spikes on the pressure signal while the check valve was closed. He explained that the noise was due to waterhammer causing movement of his rig and cavitation. Wood [29] has shown that if a pipeline is not perfectly rigid then spikes in the pressure variation can be expected. During the performance of experiments the pipeline did vibrate significantly, hence this cannot be ruled out as a source of noise. Furthermore, low pressures come about when the valve closes, hence cavitation and aeration are also possibilities. In fact bubbles were observed in the acrylic test section downstream of the valve. Air bubbles would also come out of solution on the acrylic pipe wall, hence air cavitation bubbles cannot be ruled out as a cause of noise. In fact, both of the sources mentioned are probably responsible for noise on the pressure signal.

Random phase fluctuations between particles entering and leaving the measuring volume of the Laser Doppler anemometer result in broad band noise on the output signal [30]. In Figures 5.11 and 5.12 the low range of the tracker was used and the signal-to-noise ratio of the output is good. In Figures 5.9 and 5.10 the middle range of the tracker was used.

This has two effects. Firstly the sensitivity of the system is decreased. Secondly, the dynamic response of tracking is greatly improved. In Figures 5.11 and 5.12 flat portions on the fluid velocity traces are present. This happens when the tracker does not follow the velocity of the particles in the fluid. This is termed "drop-out" and when this occurs the velocity output from the tracker is not a correct reading of the actual particle velocity. When this happens the output of the tracker is determined by the last validated velocity read and the output voltage of the tracker simply holds this value. In Figures 5.9 and 5.10 these periods of drop out are not present. This has been achieved by using the middle range of velocity on the tracker. In doing so the noise on the tracker output has increased substantially in comparison to the velocity variations through the valve cycle. The noise present on the output trace has been reduced by using a Rockland Filter at a cutoff frequency of 100 Hz on the fluid velocity signal. This does, of course, result in a slight phase lag in the higher frequency components of the signal, but the filtering frequency is sufficiently high that the general form of the output is not greatly distorted.

5.5.2 Discharge and Pressure Variations through Vibration Cycles

Figure 5.13 shows the pressure difference across the valve as a function of displacement. Just before the valve opens there is a sudden drop in pressure difference. Due to the rapidity of this drop it is difficult to determine

exactly at what pressure the valve opens. During the opening portion, the pressure difference drops slightly in Figure 5.13(a) and is more or less constant in Figures 5.13(b), (c) and (d). During the closing portion, the pressure difference across the valve increases the rate of this increase grows faster as the valve closes. In all cases the pressure difference is larger during the closing portion than the hydrostatic head difference . This indicates that hydrodynamic pressure differences, created by the rate of change of discharge, influences the closure of the valve.

The pressure ΔP^* marked on the graphs indicate the pressure difference where opening of the valve should occur. However, due to such a rapid drop in the pressure difference across the valve, it is difficult to tell whether the valve does open at that point. In no case, however, does it appear that the valve opens at a higher pressure difference. This behaviour is as expected.

In Figure 5.13(b) a negative pressure difference is seen to occur on opening. This means that the valve is being pushed from the seat by the downstream water column, rather than the spring pulling the valve open. If the latter were the case there would be a low pressure region just downstream of the valve and a higher pressure difference would result.

Figure 5.14 shows how the discharge in the pipeline varies through the valve cycle. In all cases upon opening there is a negative discharge in the pipeline, i.e., the flow

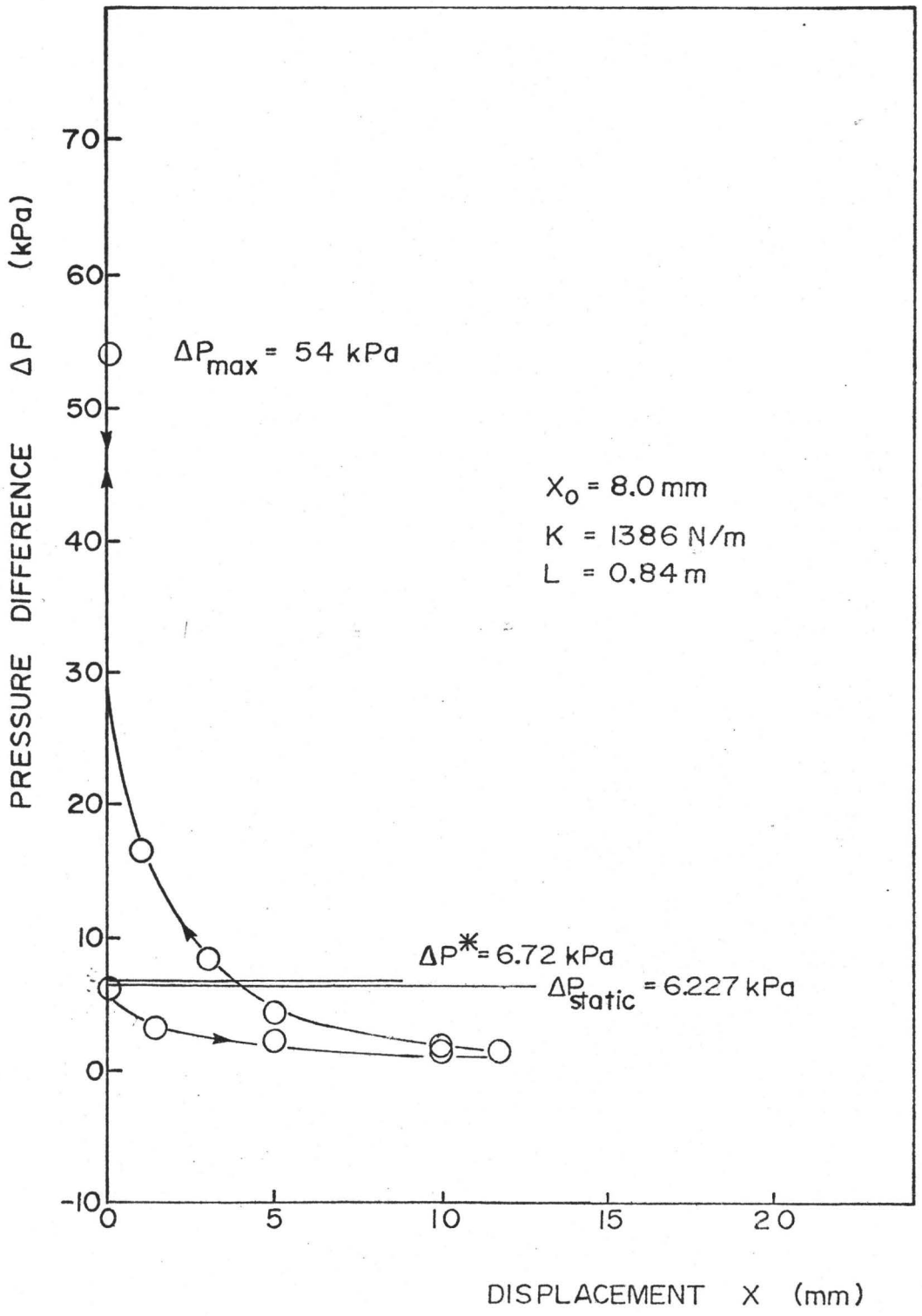

Figure 5.13(a) Pressure variation through cycle

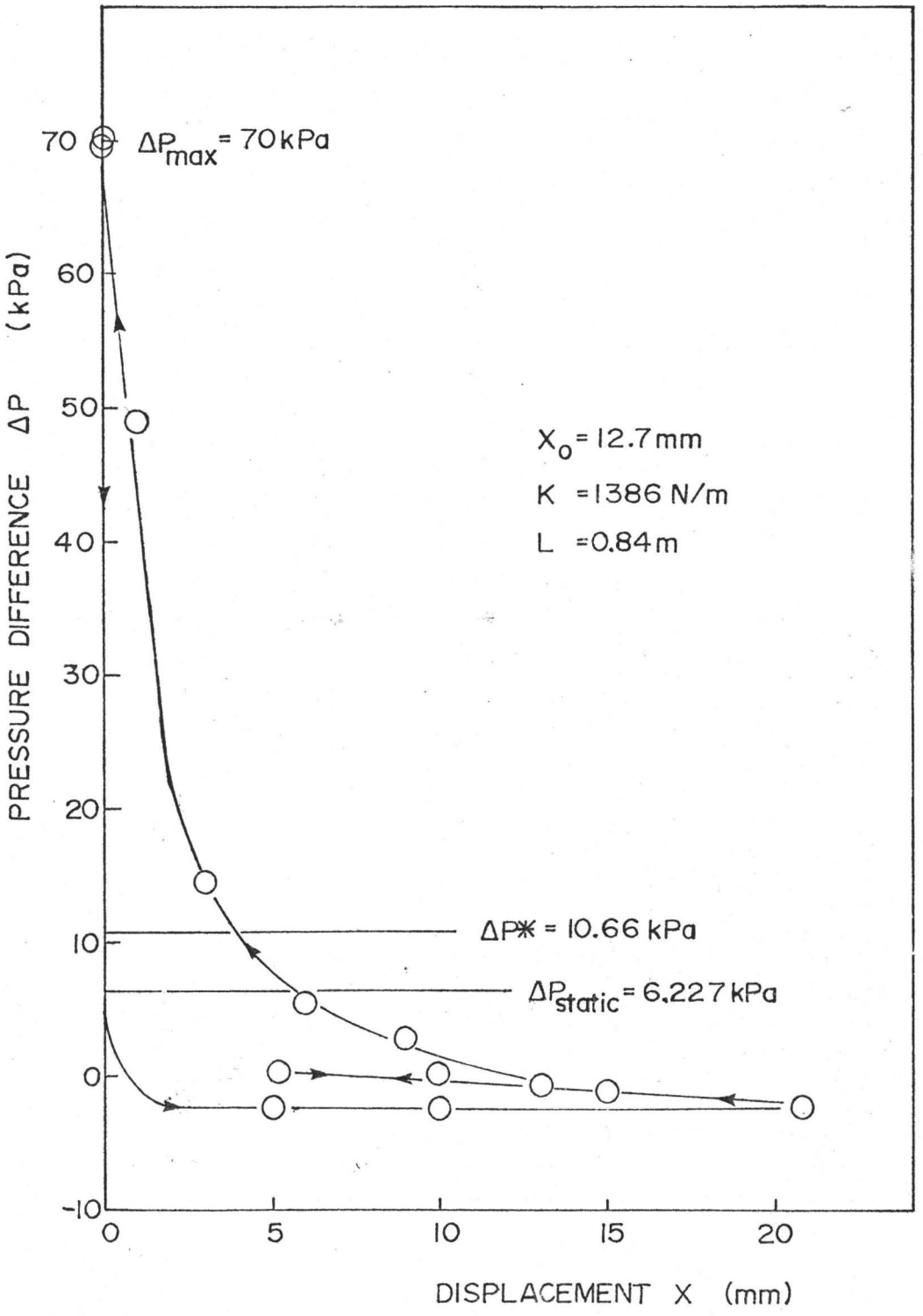

Figure 5.13(b) Pressure variation through cycle

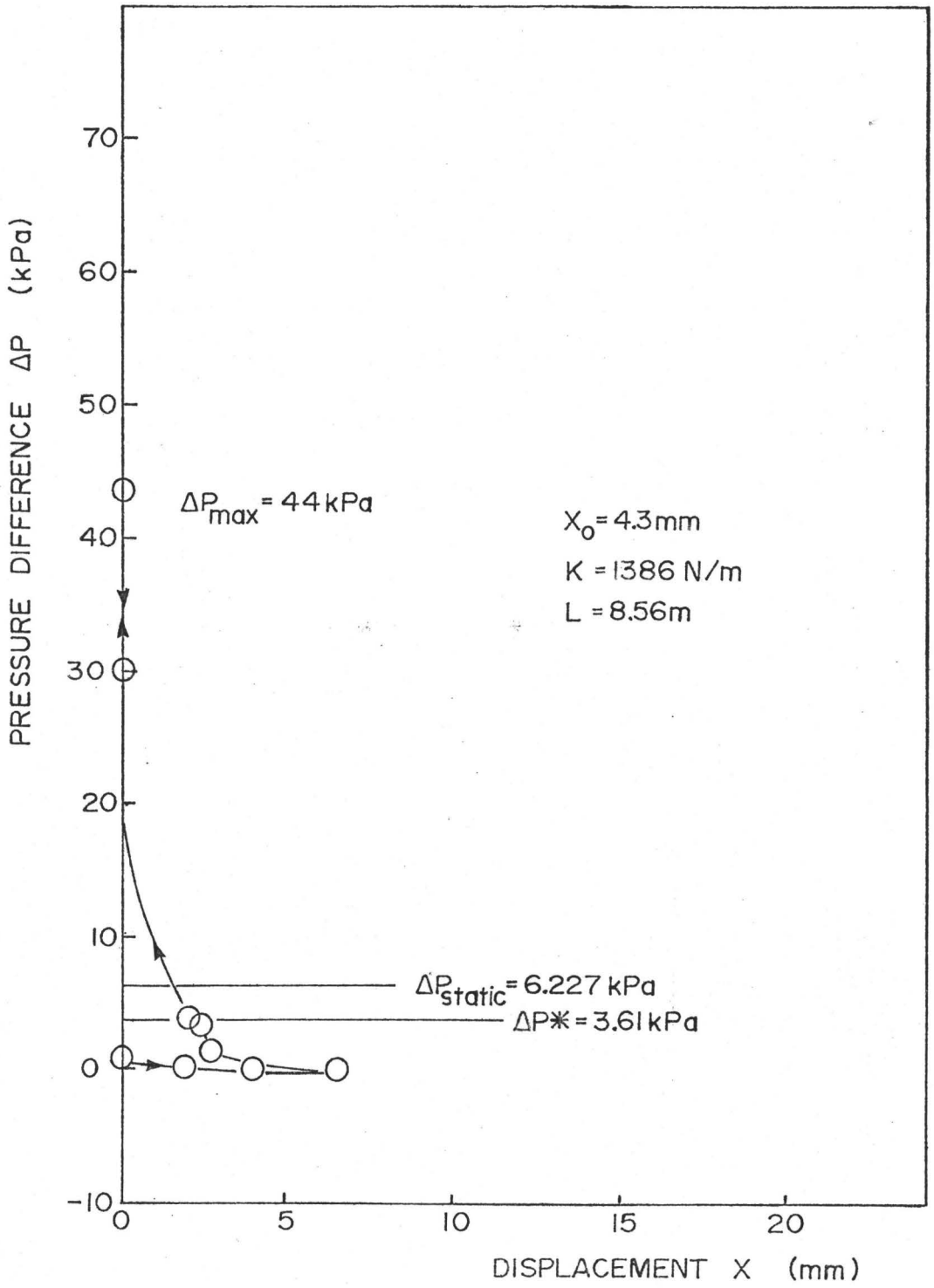

Figure 5.13(c) Pressure variation through cycle

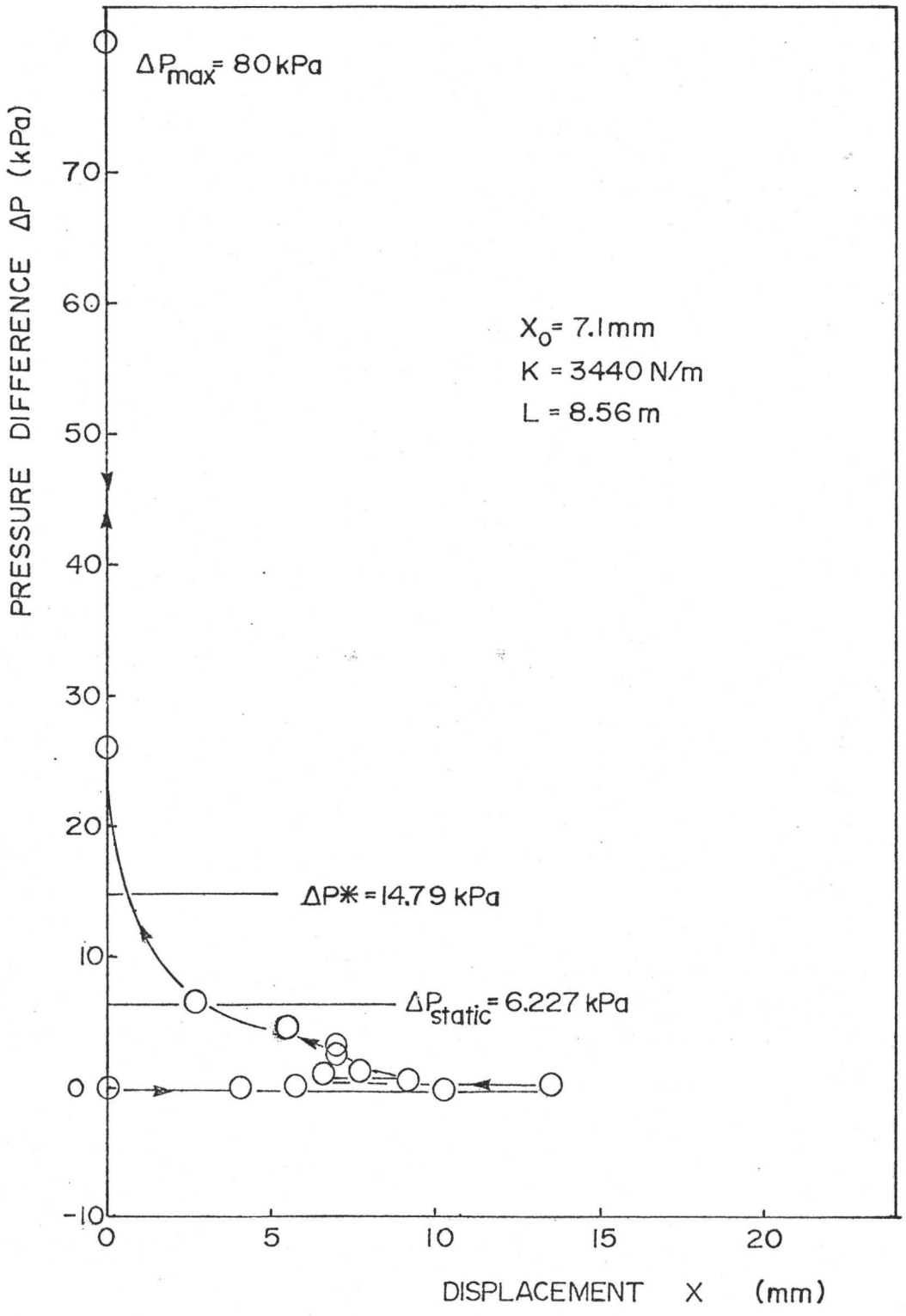

Figure 5.13(d) Pressure variation through cycle

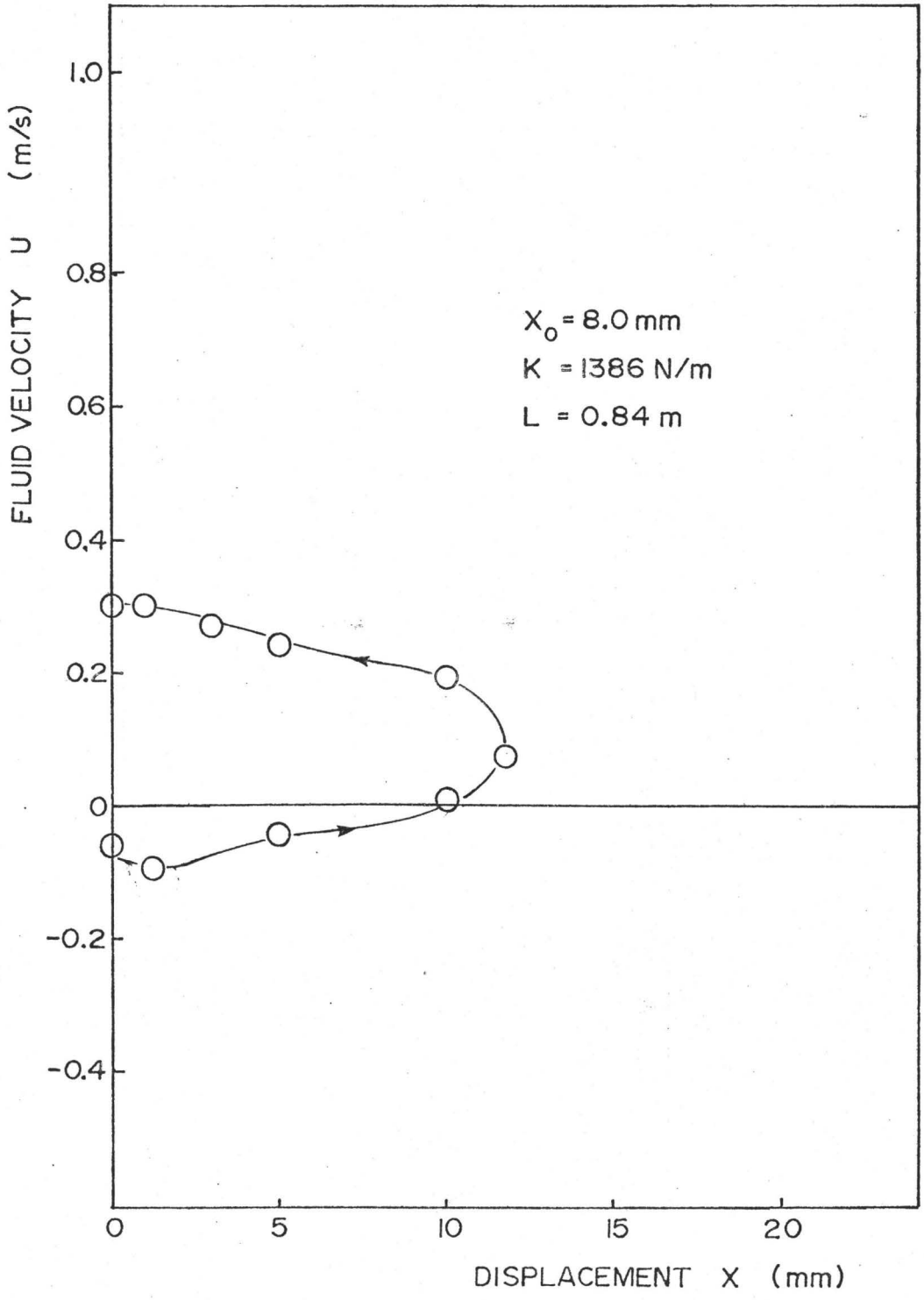

Figure 5.14(a) Discharge variation through cycle

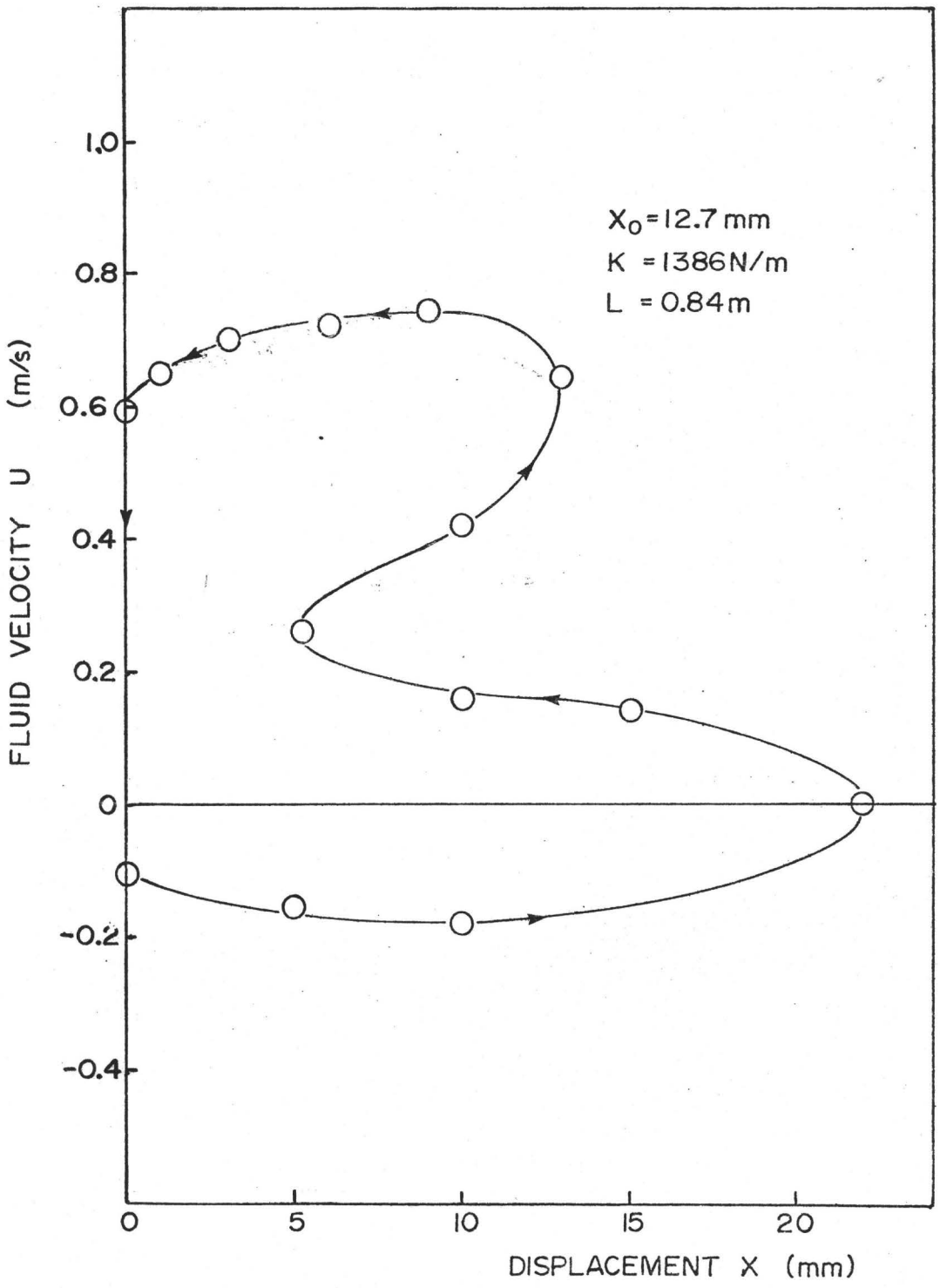

Figure 5.14(b) Discharge variation through cycle

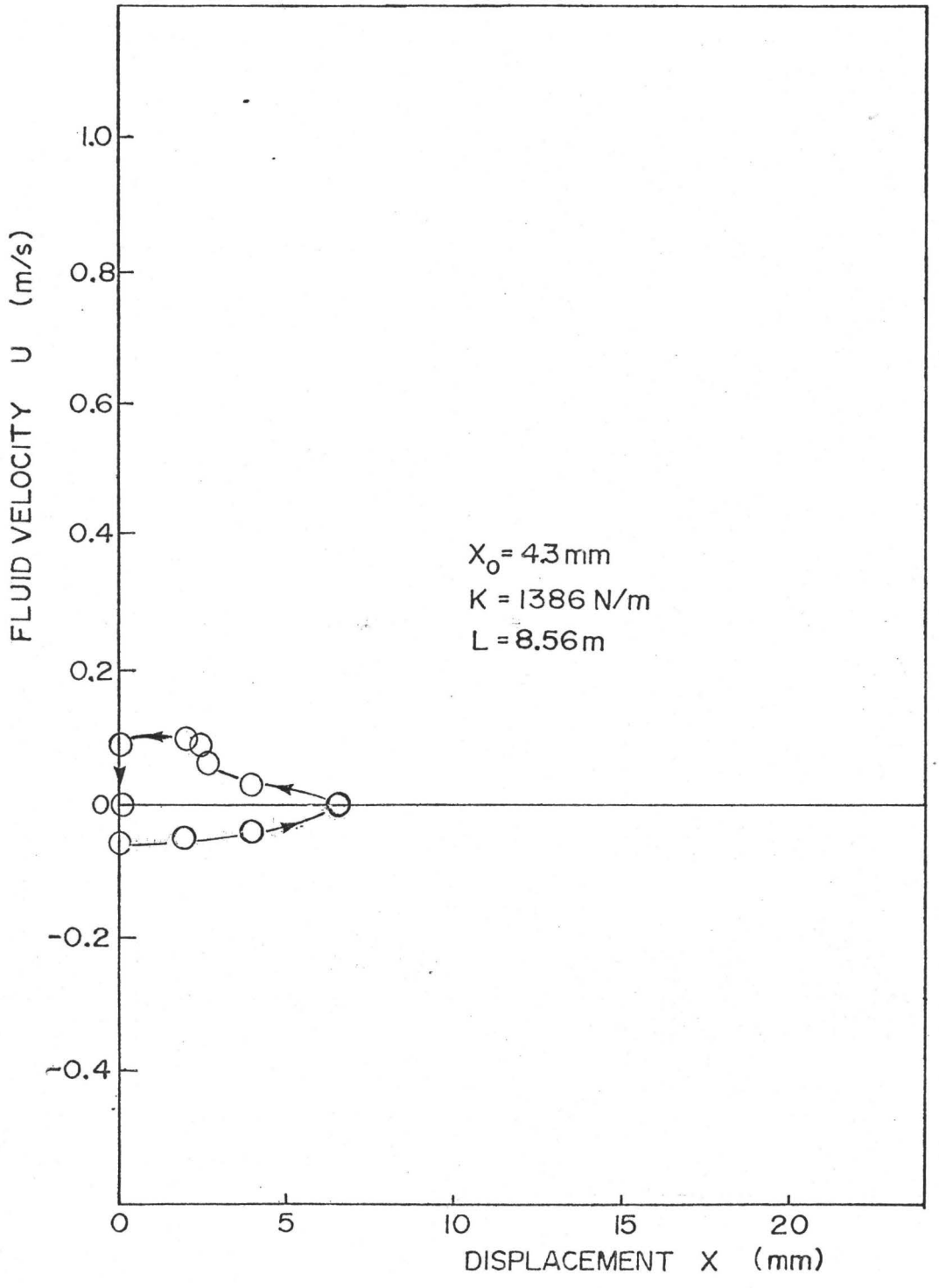

Figure 5.14(c) Discharge variation through cycle

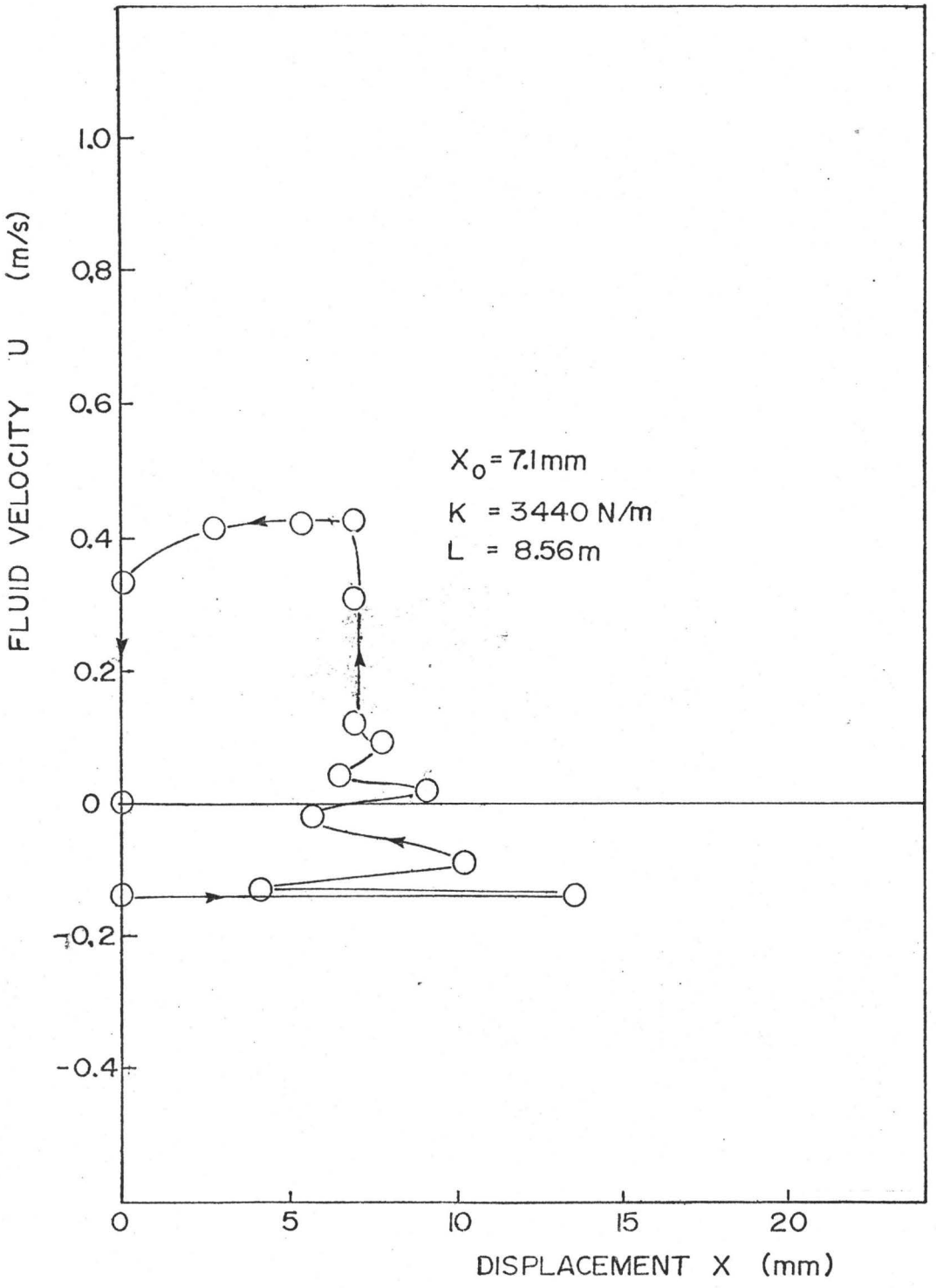

Figure 5.14(d) Discharge variation through cycle

is going backwards in the pipe. As the cycle proceeds the discharge becomes positive, the flowrate becomes a maximum and then closure results. These discharge curves are similar in nature to those obtained by Weaver and Ziada [6] in their nonlinear valve modelling. The displacement and flowrate maxima do not coincide and there is a definite hysteresis between flowrate and displacement. Weaver and Ziada [6] do not report results which indicate negative pipe flow. This is probably due to their neglect of pumping in their modelling. Pumping would also allow for a finite flow in the pipe at closing, proportional to the valve's velocity.

In Figure 5.14(a) it appears that the discharge is still increasing as the valve is closing. The pressure variation indicates however that at this point that the pressure difference across the valve is greater than that due to static head. Hence the flow should be decelerating. This abnormality in the curve is probably a result of phase delay due to the filter used on the output of the velocity signal.

5.5.3 Velocity Profile in the Pipe

The velocity profile in the pipe was obtained by repeating vibration measurements using the parameters shown in Figure 5.15. The measuring volume of the laser anemometer was translated with each repetition. The method used to locate the centre of the measuring volume is described in Appendix A. The Bragg cell was set so that an effective shift of 0.5 MHz was obtained and the middle tracker range was used

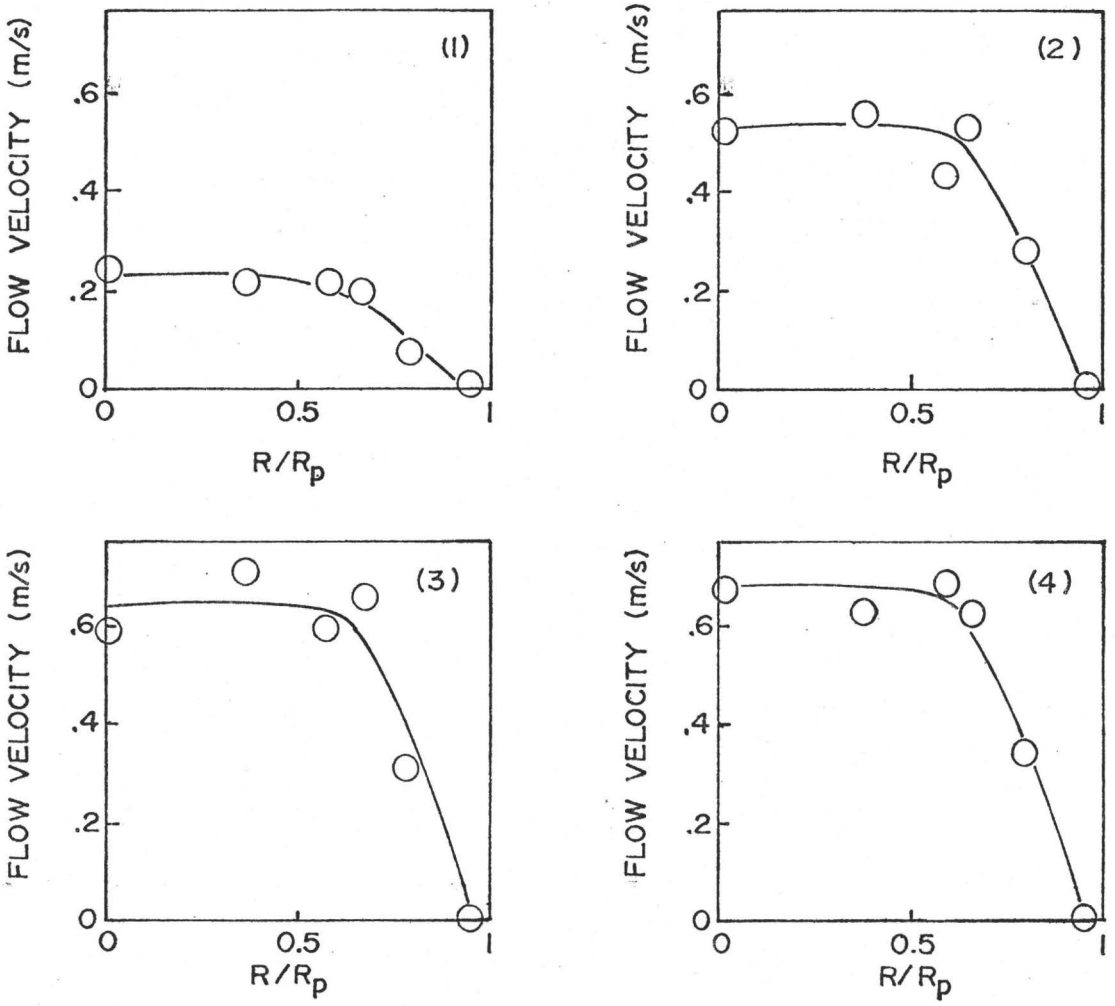

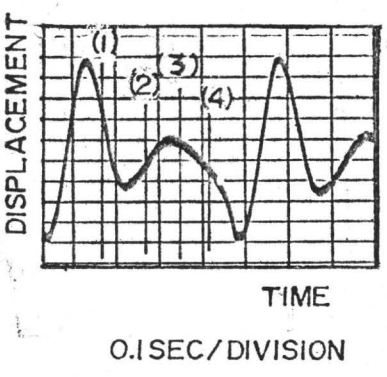

X = 12.7mm
K = 1386 N/m
L = 0.84 m

Figure 5.15 Measurement of velocity profile

with the output being filtered, low pass, at 100 Hz cutoff frequency.

The results of Figure 5.15 indicate that the velocities measured are in phase. To establish whether a flat velocity profile approximation based on the velocity at the centre of the section is justified requires some elaboration.

The drop of the velocity profile in the measurements is due to reflections of laser light off the acrylic pipe wall. Assuming a laser beam diameter of 0.5 mm and an intersection angle of the two beams of 7.72^{o} total included angle, then the length of the measuring volume is 7.4 mm. Details of performing this calculation can be found in [25]. The measuring volume extends approximately r/2 each side of the centre of the measuring volume where r is the pipe radius. Hence the outermost point in Figure 5.15 can be completely discounted and the measurements of the next point are also questionable. Observation of the percentage of time that the tracker signal was locked on support this view. For the outermost and next point, the percentage of time the tracker was "in-lock" was eighty and forty percent respectively. The four central points had only a twenty percent reading for in-lock time. Hence reflections off the acrylic wall caused errors in these readings.

Two theoretical considerations suggest that a flat velocity profile should be a good approximation. The measuring volume for the laser anemometer is about three diameters

downstream of a sudden expansion. Miller [31] states that by this point downstream fully developed turbulent flow should be established. The flow is accelerating through most of the cycle, therefore the central stream of fluid should move bodily and the velocity profile should steepen at the edges [22], [32]. Thus a flat velocity profile should prove to be a good approximation.

For the cycle shown in this Figure 5.15 water was collected in a container and measured. The results of this experiment are recorded in Table 5.1. Computations using the velocity of the fluid at the centreline of the pipe were performed using a flat velocity profile. $Q = A_p V_{cL}$ where Q is the instantaneous flowrate, A_p the pipe area and V_{cL} the centreline fluid velocity. By integrating the area under the flowrate versus time curve the average flowrate in the pipe during the vibration was computed. This was found to be 406 mℓ/s.

Time (s)	Volume of Water Collected (mℓ)	Flow Rate Q mℓ/s)
9.5	3800	400
7.8	3000	385
8.0	3250	406
10.0	4000	410

Table 5.1

Comparison of the average value using the LDA and those measured by collection of water show that these two values agree well. Since the phase of the velocities measured show little variation it seems appropriate to assume a flat velocity profile in calculating the dynamic discharge coefficient.

5.5.4 Estimates of Dynamic Discharge Coefficients

In estimating discharge coefficients, the relation between the total pressure upstream and the pressure and flowrate at the gap is investigated. Earlier work in this chapter has indicated that pumping may be significant in determining the dynamic discharge characteristic of the valve.

The dynamic discharge coefficients were initially calculated using the same method as used for the static coefficients in Chapter 4. Assumptions made in such a calculation include assuming the pressure at the base of the valve is the same as that at the gap, that unsteady inertial pressures are negligible, that the velocity profile of fluid in the pipe is flat and that the pumping action of the valve is negligible. A typical variation in dynamic discharge coefficient is shown in Figure 5.16. It can be seen that the discharge coefficients calculated neglecting pumping appear to be erroneously large in some cases.

Approximation to allow for pumping were made using the calculation method outlined in Appendix G. Figure 5.17 shows the volume swept as the valve moves upwards. This must

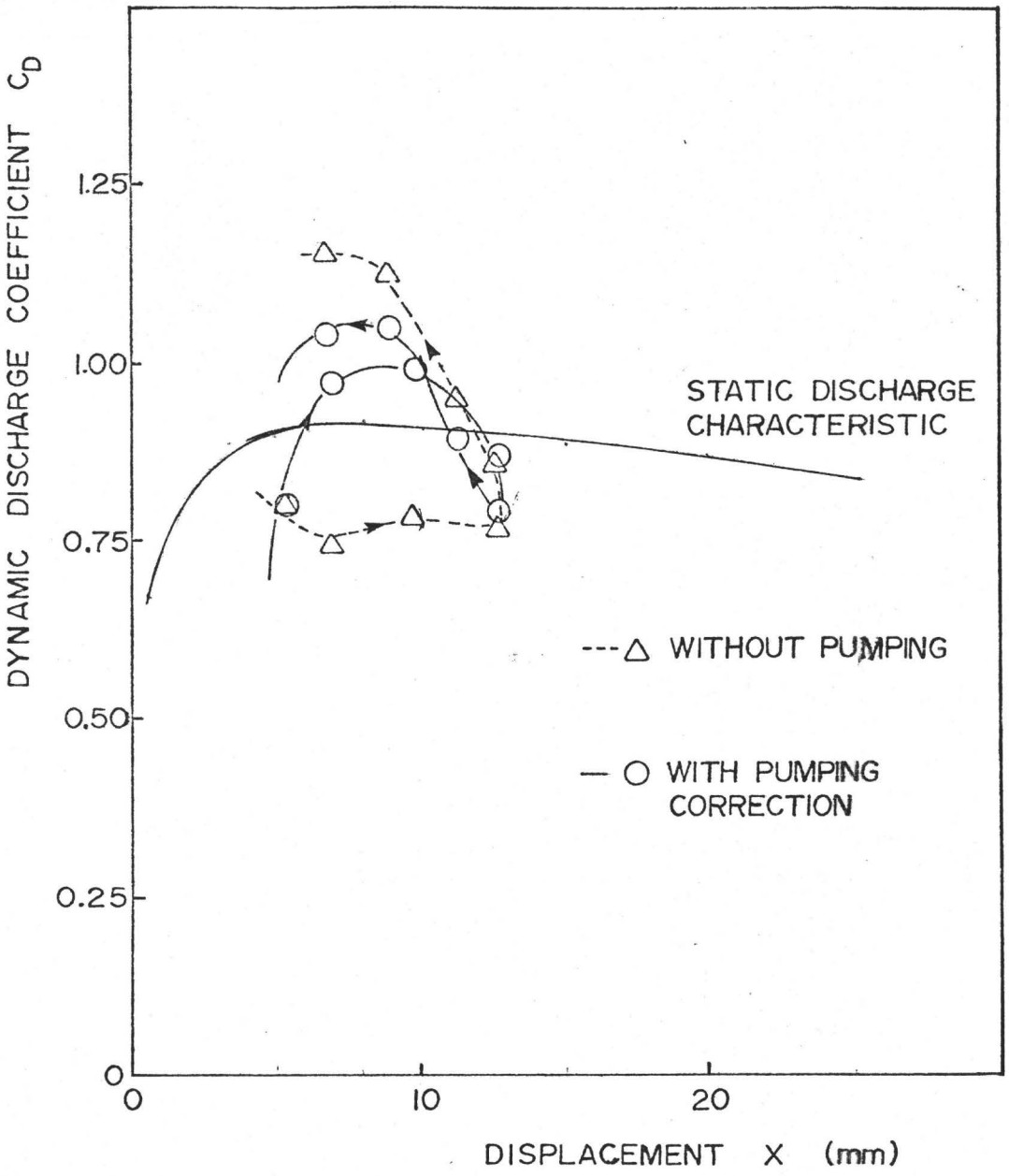

Figure 5.16 Dynamic discharge coefficient variation

be filled either from the downstream pipe or from the upstream tank. There is also a negatively swept area from where water had to be moved from to allow the valve to move. When the valve moves downwards, water must be pumped out of the regions 1, 2, and 3 in Figure 5.17 and water moves into region 4, which is the reverse of what happens when the valve moves upwards.

Assumptions made in calculating the dynamic discharge coefficients including the pumping are the same as those made for the calculations neglecting pumping. The pumping area has been taken to be the same as the pressure-force area of the valve, namely 1651mm^2. Typical variation of the dynamic discharge coefficient including pumping is shown in Figure 5.16.

There are several sources of error to be considered when evaluating the dynamic discharge coefficients in Figure 5.16. Noise has been recorded on both the pressure and velocity signals. Inertial pressures have been neglected and the pumping area chosen in the calculations is at best, just an approximation. Separation of flow has been assumed to fix the base pressure of the plug valve, and that pressure is assumed to be the same as that at the gap.

Flow is accelerating for most of the cycle, hence inertial pressures should have resulted in lower discharge coefficients being measured. Hence inertial pressures are not the cause of high discharge coefficients. Attempts to correlate dynamic discharge coefficients with acceleration

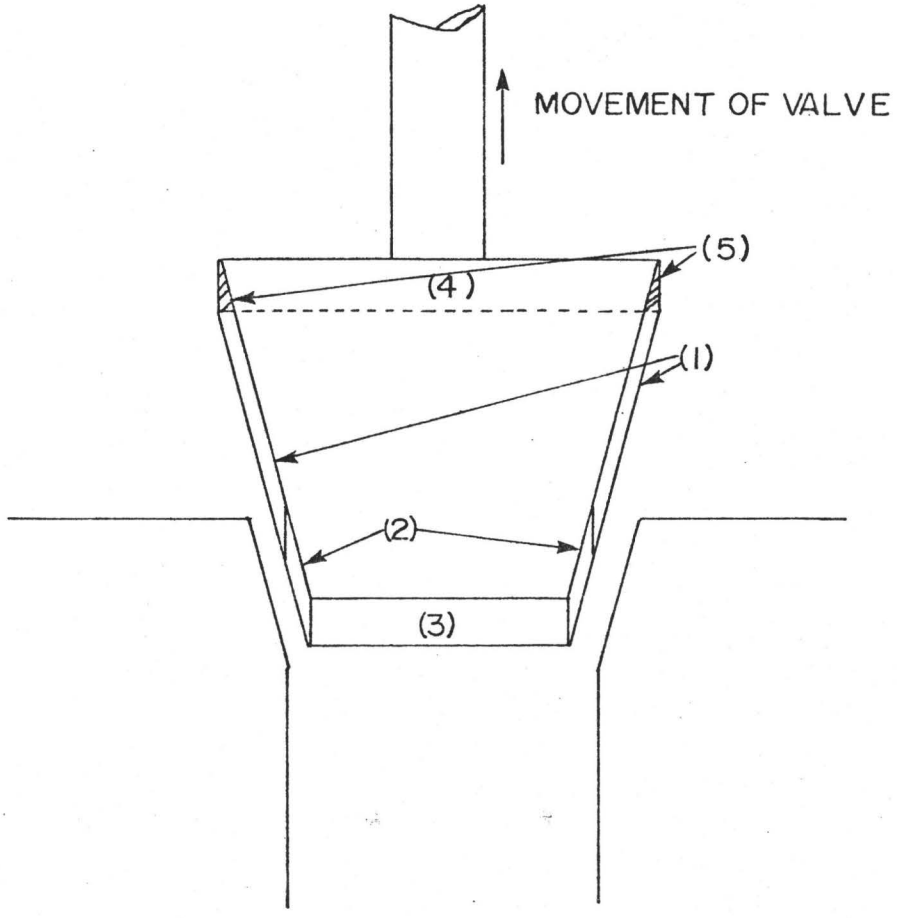

(1) UPSTREAM SWEPT VOLUME
(2) SWEPT VOLUME IN VALVE GAP
(3) SWEPT VOLUME IN PIPE
(4) NEGATIVE SWEPT VOLUME
(5) VOLUME INCLUDED IN BOTH (1) AND (4)

Fig. 5.17 Pumping area of plug valve.

as Daily et al. [22] have done proved fruitless. Dynamic discharge coefficients greater than one indicate the possibility of greater pressure recovery than anticipated. Hence it is possible that the plug valve base pressure is not equal to the gap pressure. There are obviously other flow changes that are going on during the vibrations and these need to be investigated. It would seem therefore that further experimental research is required to learn more about dynamic discharge characteristics of the plug valve. One possibility that deserves consideration is the idea of instrumenting the plug valve so that the actual pressure distribution in the valve could be found.

The present experiments do not reveal any clear method for predicting dynamic discharge coefficients and hence simulations performed in Chapter 7 use the static discharge characteristics.

5.6 Discussion of Results

In this chapter, the experimental results have been reported in three main sections: valve stability was studied and stability limits established, variation of frequency and amplitude as a function of stiffness, initial opening and inertia was examined, further work examining the dynamic discharge characteristics of the plug valve was then performed.

The study of stability showed that the region of instability was similar to that obtained by Weaver et al. [15].

In addition the region of instability was found to move upwards as fluid inertia was decreased.

Trends of frequency ratio and initial opening show the same trends as those reported for check valve vibrations [15], [28]. Closer examination of the vibrations showed similar pressure-displacement and flowrate-displacement curves. Reverse flow in the pipe was found to occur and pumping was found to affect the discharge coefficient significantly. No trends in the discharge coefficient measurements could be found and further possible experiments have been suggested. Meanwhile, the static discharge coefficients seem to be the only dependable values to use in simulating vibrations and predicting stability limits theoretically.

CHAPTER 6

THEORETICAL MODELLING

6.1 Introduction

In Chapter 5, the pumping action of the valve was found to make a significant difference in calculating the dynamic discharge coefficient. It is therefore prudent to determine what effect pumping has on the self-excited valve oscillations and stability. In this chapter, a theoretical model, similar to that derived by Weaver and Ziada [6] is derived. In fact, the model derived here is a refinement of their model, to include effects of pumping and pressure recovery. Integration of the differential equations of the model, the result of which are reported in Chapter 7, shows the effects pumping has on the self-excited vibrations.

Kolkman [4] has derived a stability threshold for a simple plug valve. His analysis reveals a fairly simple formulation of the upper stability threshold. A relatively uncomplicated formulation should also be expected using the nonlinear model, although some simplifications may have to be made to obtain this. The second half of Chapter 6 is devoted to this and a quasistatic stability analysis.

6.2 Derivation of General Model Including Pumping Term

6.2.1 Introduction

Ziada [3] has outlined the assumptions made for deriving

a general model in his thesis. The assumptons made here are similar.

The assumptions made in deriving the general model are as follows:

(a) The fluid in the system is incompressible.

(b) Aeration or cavitation does not occur.

(c) The velocity and pressure of the fluid are uniform over a transverse cross-section of the conduit, except immediately downstream of the valve which is analyzed separately.

(d) Water hammer pressure waves which occur in the system have no dominant effect on the stability [28].

(e) Pressure fluctuations due to vortex shedding are negligible compared with hydrostatic and fluid inertia pressures [3].

(f) Added mass is taken as a constant, even though confinement, frequency and amplitude of oscillation affect its value.

(g) Losses are assumed to be turbulent in nature.

6.2.2 Fluid Discharge Formulation

In this section, the discharge through the valve is expressed initially in terms of the pressure difference across the valve and valve motion. This pressure difference is then related to the hydrostatic head and the behaviour of the fluid in the pipe. This equation is used to compute the rate of

change of discharge, which can be integrated to give the discharge for the next point to be computed.

Referring to Figure 6.1, the Bernoulli equation under unsteady conditions can be written as,

$$\frac{P_2}{\gamma} + \frac{V_2^2}{2g} = \frac{P_3}{\gamma} + \frac{V_3^2}{2g} + h_{23} + I_{23}\frac{dQ_{23}}{dt} \qquad (6.1)$$

where P_2 and P_3 are the pressures at points 2 and 3 respectively, V_2 and V_3 are the corresponding velocities, and I_{23} is the fluid-inertance between points 2 and 3. Q_{23} is the flowrate between points 2 and 3 and h_{23} is the headloss between these points.

Referring to Figure 6.2 for the direction of valve movement, the continuity equation becomes,

$$V_2A_2 + A_v\dot{x} = V_3A_3 \qquad (6.2)$$

where A_i is the area of cross-section at point i, A_v is the effective pumping area of the valve.

Combining equations (6.1) and (6.2) to eliminate V_2, the velocity V_3 can be isolated as,

$$V_3 = \frac{-2B_1B_2\dot{x} \pm \sqrt{4B_1^2B_2^2\dot{x} + 4(2g(H_v-h_{23}) + B_2^2\dot{x}^2)(1-B_1^2)}}{2(1-B_1^2)} \qquad (6.3)$$

where

$$B_1 = A_3/A_2 \qquad (6.4a)$$

$$B_2 = A_v/A_2 \qquad (6.4b)$$

$$2gH_v = \frac{P_2-P_3}{\gamma} - I_{23}\frac{dQ_{23}}{dt} \qquad (6.4c)$$

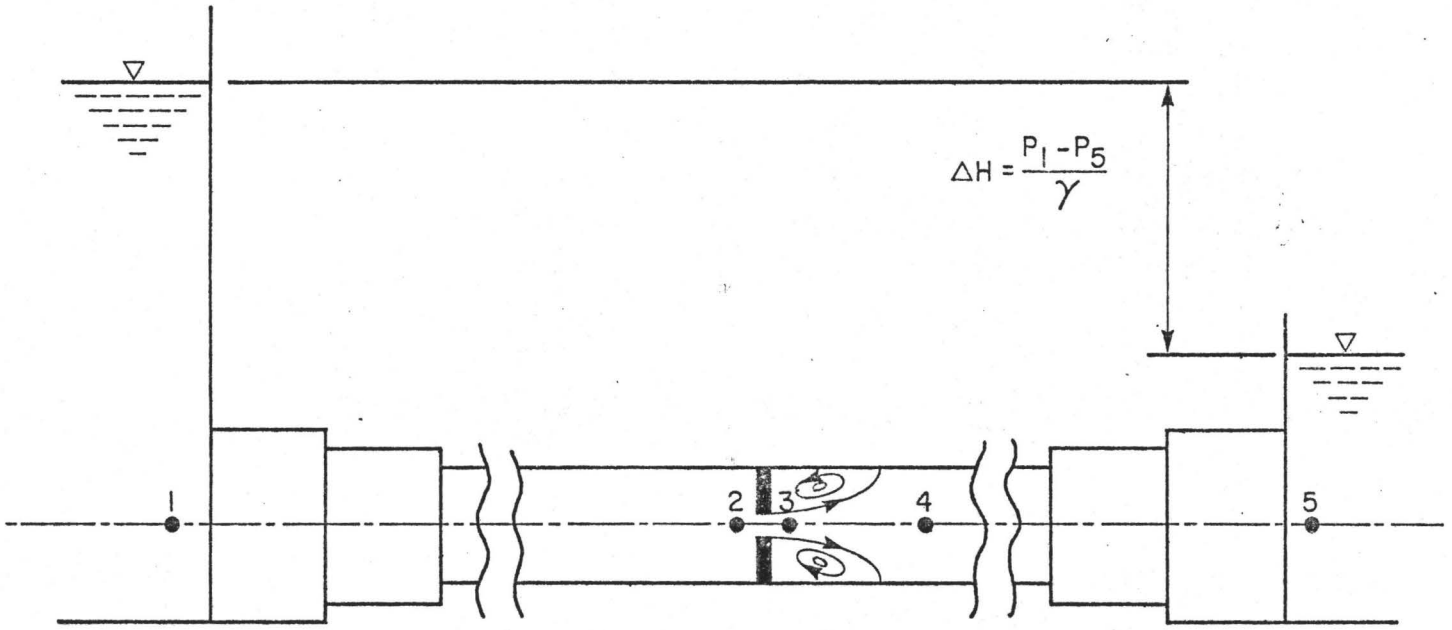

Fig. 6.1 General pipeline system with valve modelled as an orifice Ref. [6]

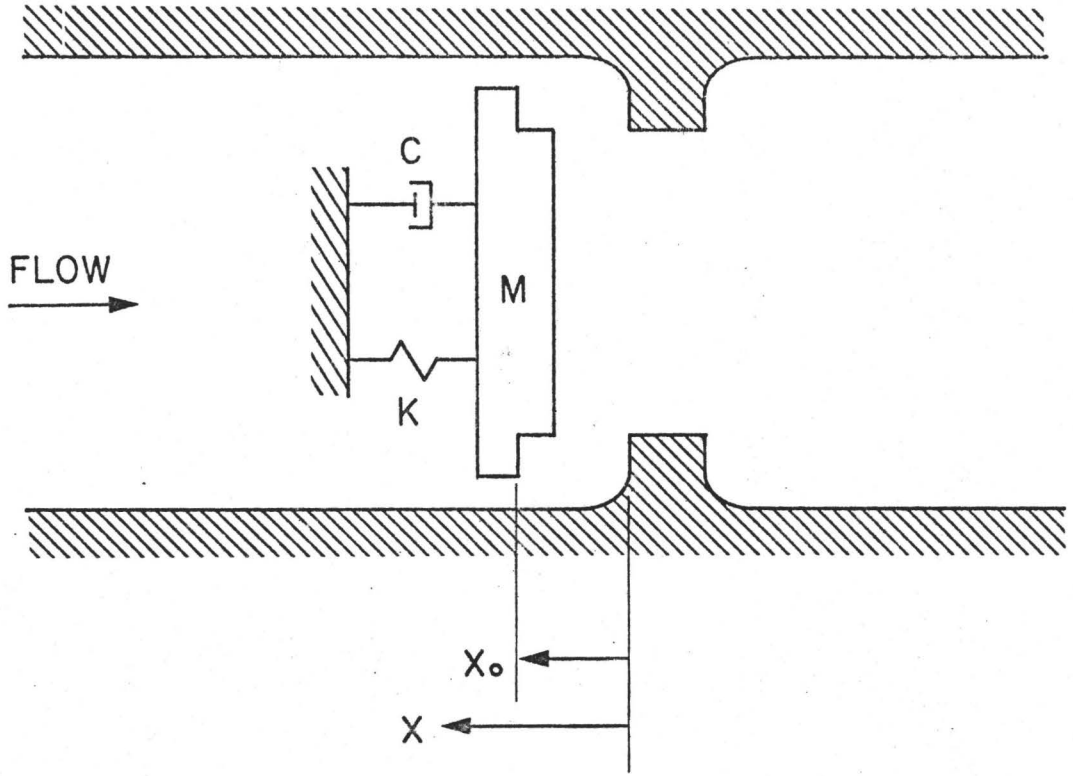

Fig. 6.2 Schematic of single degree of freedom flow control device Ref. [6]

The velocity coefficient, C_v, can be used to account for the head loss h_{23}, hence,

$$V_3 = C_v \frac{[-2B_1 B_2 \dot{x} \pm \sqrt{4B_1^2 B_2^2 \dot{x}^2 + 4(2gH_v + B_2^2 \dot{x}^2)(1-B_1^2)}]}{2(1-B_1^2)} \quad (6.5)$$

The discharge through the valve is:

$$Q_v = V_3 A_3 \quad (6.6)$$

Using equations (6.5) and (6.6) it can be shown that,

$$2g H_v = \frac{Q_v^2 (1-B_1^2)}{C_v^2 A_3^2} + \frac{2Q_v B_1 B_2 \dot{x}}{C_v A_3} - B_2^2 \dot{x}^2 \quad (6.7)$$

The unsteady Bernoulli equation,

$$\frac{P_i}{\gamma} + \frac{V_i^2}{2g} = \frac{P_j}{\gamma} + \frac{V_j^2}{2g} + h_{ij} + I_{ij} \frac{dQ_{ij}}{dt} \quad (6.8)$$

can be applied successively to (6.4c) to give,

$$2g H_v = \frac{P_1 - P_5}{\gamma} - \Sigma h_L - \Sigma I \frac{dQ}{dt} - \frac{V_2^2}{2g} + \frac{V_3^2}{2g} \quad (6.9)$$

where

$$\Sigma I \frac{dQ}{dt} = (I_{12} + I_{45}) \frac{dQ_p}{dt} + I_{23} \frac{dQ_{23}}{dt} + I_{34} \frac{dQ_{34}}{dt} \quad (6.10)$$

$$\Sigma h_L = h_{12} + h_{34} + h_{45} \quad (6.11)$$

where Q_p is the discharge in the pipeline and h_{ij} is the headloss between point i and point j.

As mentioned previously, this formulation is used to evaluate the rate of change of discharge. Hence, using equations

(6.7) and (6.9), the head available to accelerate fluid is,

$$\Sigma I \frac{dQ}{dt} = \frac{P_1 - P_5}{\gamma} - \Sigma h_L + \frac{1}{2g}\left[\frac{Q_v^2(B_1^2-1)}{C_v^2 A_3^2} - \frac{2Q_v B_1 B_2 \dot{x}}{C_v A_3} + B_2^2 \dot{x}^2 - \frac{Q_p^2}{A_2^2} + \frac{Q_v^2}{A_3^2}\right] \tag{6.12}$$

Headlosses h_{12} and h_{45} are assumed to be turbulent pipe losses, which according to Weaver and Ziada [6] can be written in the form:

$$\frac{\psi Q_p^2}{2gA_4^2} = h_{12} + h_{45} = \left[\frac{K_{12}}{A_{12}^2} + \frac{K_{45}}{A_{45}^2}\right] Q_p^2 \tag{6.13}$$

where K_{12} and K_{45} represent loss factors.

To evaluate h_{34}, closer examination of the system is required. The headloss calculation is performed for a steady-state condition, as shown in Fig. 6.3, the valve is assumed to move to the right with constant velocity - $\dot{x}$. The area of the orifice is treated as a constant for this calculation.

Applying the Momentum Equation,

$$P_3 A_4 - P_4 A_4 = - \rho A_3 V_3^2 + \rho A_4 V_4^2 - \rho A_v \dot{x}^2 \tag{6.14}$$

and the Bernoulli Equation for the jet,

$$\frac{P_3}{\gamma} + \frac{V_3^2}{2g} = \frac{P_4}{\gamma} + \frac{V_4^2}{2g} + h_{34} \tag{6.15}$$

The result of combining equations (6.14) and (6.15) is,

$$h_{34} = \frac{V_4^2}{2g} + \frac{V_3^2}{2g}\left(1 - \frac{2A_3}{A_4}\right) - \frac{A_v \dot{x}^2}{g A_4} \tag{6.16}$$

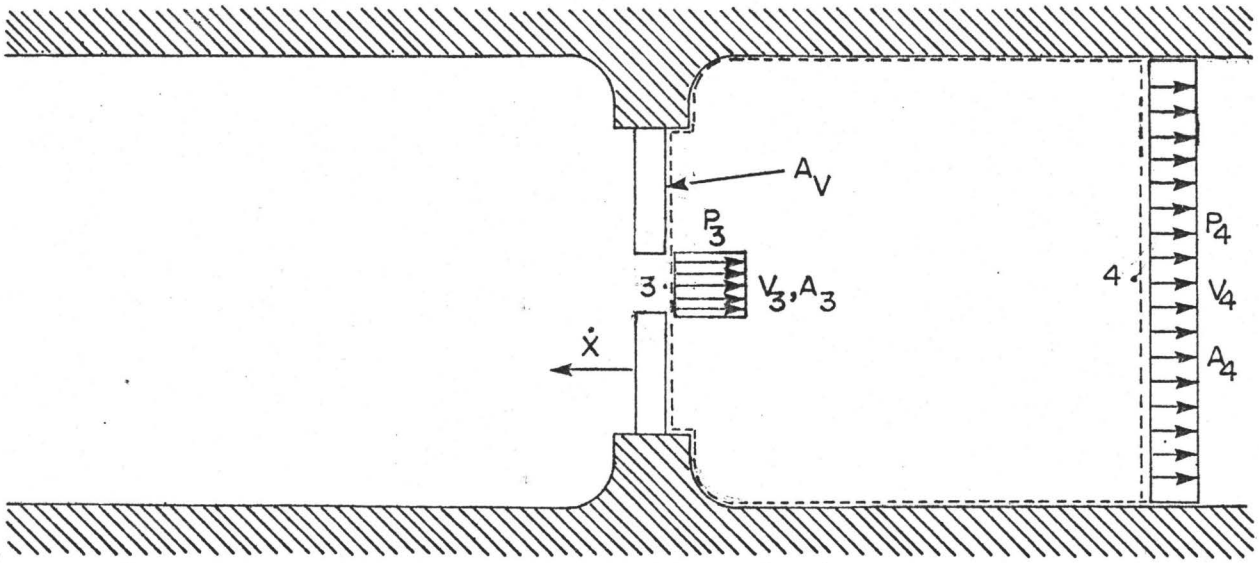

Fig. 6.3 Control volume for momentum analysis downstream of valve

or in terms of valve and pipe discharges,

$$h_{34} = \frac{Q_p^2}{2gA_4} + \frac{Q_v^2}{2g}\left(\frac{1}{A_3^2} - \frac{2}{A_3A_4}\right) - \frac{\dot{x}^2A_v}{g\ A_4} \tag{6.17}$$

where $\dot{x}$ is the velocity of the valve.

Using the headloss expressions of equations (6.13) and (6.17), equation (6.12) can be written as,

$$\Sigma I\ \frac{dQ}{dt} = \frac{P_1-P_5}{\gamma} - \frac{Q_p^2}{2gA_4^2}\left(\psi+1+\frac{A_4^2}{A_2^2}\right) + \frac{Q_v^2}{2g}\left(\frac{B_1^2}{C_v^2A_3^2} - \frac{1}{C_v^2A_3^2} + \frac{2}{A_3A_4}\right)$$

$$- \frac{\dot{x}}{2g}\left(\frac{2A_v}{A_4} - B_2^2\right) - \frac{Q_v\ B_1B_2\dot{x}}{g\ C_vA_3} \tag{6.18}$$

"A_3" in all of the foregoing equations represents the area of the vena contracta so that if a linear gap variation is assumed [6], then,

$$A_3 = C_c\ W\ x \tag{6.19}$$

where C_c is the contraction coefficient, W is the valve gap width and x is the valve displacement.

Combining equations (6.4), (6.18) and (6.19), it can be shown that,

$$\Sigma I\ \frac{dQ}{dt} = \frac{P_1-P_5}{\gamma} - \frac{Q_p^2}{2gA_4^2}\left(\psi+1+\frac{A_4^2}{A_2^2}\right) + \frac{Q_v^2}{2g}\left(\frac{1}{C_v^2C_c^2W^2x^2} + \frac{2}{C_cWxA_4}\right)$$

$$- \frac{\dot{x}^2}{2g}\left(\frac{2A_v}{A_4} - \left(\frac{A_v}{A_2}\right)^2\right) - \frac{2Q_v\dot{x}A_v}{A_2^2 2gC_v} \tag{6.20}$$

The fluid inertance, I, can be expressed in the form [6],

$$I_{ij} = L_{ij}/gA_{ij} \tag{6.21}$$

and by defining an equivalent pipe length of area A_4, having the same inertia effect as the combined system,

$$L_{eq} = A_4 \Sigma \cdot L_{ij}/A_{ij} \tag{6.22}$$

The jet inertia is defined by a length L_o based on a jet area of C_c Wx, then using equations (6.21), (6.22), and (6.20) gives,

$$\frac{L_o}{C_c Wx} \frac{dQ_v}{dt} + \frac{L_{eq}}{A_4} \frac{dQ_p}{dt} = \frac{g(P_1-P_5)}{\gamma} - \frac{Q_p^2}{2gA_4^2}(\psi+1+\frac{A_4^2}{A_2^2}) + \frac{Q_v^2}{2}(\frac{1}{C_v^2 A_2^2} - \frac{1}{(C_v C_c Wx)^2}$$

$$+ \frac{2}{C_c Wx A_4}) - \frac{\dot{x}^2}{2}(\frac{2A_v}{A_4} - (\frac{A_v}{A_2})^2) - \frac{Q_v \dot{x} A_v}{C_v A_2^2} \tag{6.23}$$

It is desired to isolate the rate of change of flow through the valve, $\frac{dQ_v}{dt}$. This can be done by first rewriting the continuity equation (6.2) in the form,

$$Q_p = Q_v - A_v \dot{x} \tag{6.24}$$

Differentiating,

$$\frac{dQ_p}{dt} = \frac{dQ_v}{dt} - A_v \ddot{x} \tag{6.25}$$

Applying this result to equation (6.23),

$$(\frac{L_o}{C_c Wx} + \frac{L_{eq}}{A_4}) \frac{dQ_v}{dt} = \frac{g(P_1-P_5)}{\gamma} - \frac{Q_p^2}{2A_4^2}(\psi+1+\frac{A_4^2}{A_2^2}) + \frac{Q_v^2}{2}(\frac{1}{C_v^2 A_2^2} - \frac{1}{(C_v C_c Wx)^2}$$

$$+ \frac{2}{C_c Wx A_4}) - \frac{\dot{x}^2}{2}(\frac{2A_v}{A_4} - (\frac{A_v}{A_2})^2) - \frac{Q_v \dot{x} A_v}{C_v A_2^2} + \frac{L_{eq}}{A_4} A_v \ddot{x}$$

(6.26)

Equation (6.26) is now defined in a way that can be integrated to give the flowrate.

6.2.3 Elastic Structure Modelling

To model the motion of the valve it is necessary to have information on mass, damping, stiffness and other forces which act on the valve. Assuming the valve can be represented by the single degree of freedom system shown in Figure 6.2, the forces on the valve can be represented in the following manner,

$$M\ddot{x} + c\dot{x} + K(x - x_o) + F = 0 \qquad (6.27)$$

where x_o is the no load valve opening, M is the total effective mass including added mass and K is the structural stiffness.

The external force, F, is given by the pressure difference across the valve in the following manner,

$$F = \kappa S (P_2 - P_3) \qquad (6.28)$$

where κ is an integration factor based on the valve geometry and S is the area of the valve [6].

By using equations (6.4c) and (6.7), it can be shown that,

$$\frac{P_2 - P_3}{\gamma} = \frac{Q_v^2(1-B_1^2)}{C_v^2 A_3^2} + \frac{2Q_v B_1 B_2 \dot{x}}{C_v A_3} - B_2^2 \dot{x}^2 + I_{23}\frac{dQ_{23}}{dt} \qquad (6.29)$$

Using (6.4a), (6.4b) and (6.19) to subsitute for B_1, B_2 and A_3 respectively, equation (6.29) becomes,

$$\frac{P_2-P_3}{\gamma} = \frac{Q_v^2}{C_v^2C_c^2W^2x^2} - \frac{Q_v^2}{C_v^2A_2^2} + \frac{2A_vQ_v\dot{x}}{C_vA_2^2} - \frac{A_v^2}{A_2^2}\dot{x}^2 + I_{23}\frac{dQ_{23}}{dt} \tag{6.30}$$

Recalling that jet inertia is given by its length and area, then,

$$\frac{P_2-P_3}{\gamma} = \frac{Q_v^2}{C_v^2C_c^2W^2x^2} - \frac{Q_v^2}{C_v^2A_L^2} + \frac{2A_vQ_v\dot{x}}{C_vA_2^2} - \frac{A_v^2}{A_2^2}\dot{x}^2 + \frac{L_o}{C_cWx}\frac{dQ_v}{dt} \tag{6.31}$$

Hence the valve motion is given using equations, (6.27), (6.28) (6.31),

$$M\ddot{x} + c\dot{x} + K(x-x_o) + \kappa S\gamma\left[\frac{Q_v^2}{(C_vC_cWx)2} - \frac{Q_v^2}{C_v^2A_2^2} + \frac{2Q_v\dot{x}A_v}{C_vA_2^2} + \frac{L_o}{C_cWx}\frac{dQ_v}{dt}\right] = 0 \tag{6.32}$$

This equation is used to integrate acceleration to give velocity, thus, the form required is,

$$M\ddot{x} = -c\dot{x} - K(x-x_o) - \kappa S\gamma\left[\frac{Q_v^2}{C_v^2C_c^2W^2x^2} - \frac{Q_v^2}{C_v^2A_2^2} + \frac{2Q_v\dot{x}A_v}{C_vA_2^2} - \frac{A_v^2\dot{x}}{A_2^2} + \frac{L_o}{C_cWx}\frac{dQ_v}{dt}\right] \tag{6.32a}$$

6.2.4 Non-Dimensional Analysis

Equations (6.26) and (6.32a) can be non-dimensionalized using the method of Weaver and Ziada [6]. There are a few changes made for convenience and one additional parameter. Two reference quantities are necessary, d a characteristic valve dimension and K_r a reference stiffness. Dimensionless parameters are defined as follows:

Frequency $\omega^2 = \frac{K_r}{M}$ Stiffness $\bar{k} = \frac{K}{K_r}$

Time $\tau = \omega t$ Displacement $\bar{x} = \frac{x}{d}$

Zero Load Opening $\beta = \frac{x_o}{d}$ Damping $\xi = \frac{c}{2M\omega}$

Pressure Difference

$\bar{\Delta P} = \frac{2(P_1 - P_5)}{\rho(\omega d)^2}$ Discharge $\bar{Q} = \frac{Q}{A_4 \omega d}$

Mass Ratio $\mu = \frac{\rho \kappa Sd}{M}$ Gap Width $\eta = \frac{A_4}{\omega d}$

Upstream Pipe Area

$\theta = A_2/A_4$ Pipe Fluid Inertia $\alpha = \frac{2 L_{eq}}{d}$

Jet Fluid Inertia

$\alpha_o = \frac{2 L_o}{d}$ Pumping Area $\varepsilon = A_v/A_4$

The equations governing integration of dQ_v, and $\ddot{\bar{x}}$ after introducing the discharge coefficient $C_D = C_v C_c$ are given by

$$\left(\frac{\eta \alpha_o}{C_c \bar{x}} + \alpha\right) \frac{d\bar{Q}_v}{d\tau} = \overline{\Delta P} - \bar{Q}_p^2 \left(\psi + 1 + \frac{1}{\theta^2}\right) + \bar{Q}_v^2 \left(\frac{1}{C_v^2 \theta^2} - \frac{\eta^2}{C_D^2 \bar{x}^2} + \frac{2\eta}{C_c \bar{x}}\right)$$

$$- \left(\frac{d\bar{x}}{d\tau}\right)^2 \left(\frac{\varepsilon^2}{\theta^2} - \varepsilon\right) - \frac{2\bar{Q}_v \left(\frac{d\bar{x}}{d\tau}\right)\varepsilon}{C_v \theta^2} + \varepsilon\alpha \frac{d^2\bar{x}}{d\tau^2} \qquad (6.33)$$

and

$$\frac{d^2\bar{x}}{d\tau^2} = -2\xi \frac{d\bar{x}}{d\tau} - \bar{k}(\bar{x} - \beta) - \frac{1}{2}\mu \left[\frac{\bar{Q}_v^2 \eta^2}{C_D^2 \bar{x}^2} - \frac{\bar{Q}_v^2 C_c^2}{C_D^2 \theta^2} + \frac{2\bar{Q}_v \left(\frac{d\bar{x}}{d\tau}\right)\varepsilon}{C_v \theta^2} - \left(\frac{\varepsilon}{\theta} \frac{d\bar{x}}{d\tau}\right)^2 + \frac{\eta \alpha_o}{\varepsilon \bar{x}} \frac{d\bar{Q}_v}{d\tau}\right] \qquad (6.34)$$

For long pipes, where the inertia of the fluid in the pipe dominates, the jet inertia can be neglected so that the following equations holds,

$$\frac{\alpha d\bar{Q}_v}{d\tau} = \overline{\Delta P} - Q_p^2 \left(\psi+1+\frac{1}{\theta^2}\right) + \bar{Q}_v^2 \left(\frac{1}{C_v^2\theta^2} - \frac{\eta^2}{C_D^2\bar{x}^2} + \frac{2\eta}{\varepsilon\bar{x}}\right) - \left(\frac{d\bar{x}}{d\tau}\right)^2\left(\frac{\varepsilon^2}{\theta^2} - 2\varepsilon\right) - \frac{2\bar{Q}_v\left(\frac{d\bar{x}}{d\tau}\right)\varepsilon}{\omega\theta^2} + \varepsilon\alpha\frac{d^2\bar{x}}{d\tau^2} \tag{6.35}$$

and

$$\frac{d^2\bar{x}}{d\tau^2} = -2\xi\frac{d\bar{x}}{d\tau} - \bar{k}(\bar{x}-\beta) - \frac{1}{2}\mu\left[\frac{\bar{Q}_v^2\eta^2}{C_D^2\bar{x}^2} - \frac{\bar{Q}_v^2C_c^2}{C_D^2\theta^2} + \frac{2\bar{Q}_v\left(\frac{d\bar{x}}{d\tau}\right)\varepsilon}{C_v\theta^2} - \left(\frac{\varepsilon}{\theta}\frac{d\bar{x}}{d\tau}\right)^2\right] \tag{6.36}$$

Equations (6.35) and (6.36) are used as the starting point in the Routh Hurwitz analysis in Section 6.3.

When there is a tank upstream, the θ parameter becomes large and the following equations result,

$$\left(\frac{\eta\alpha_o}{C_c\bar{x}}+\alpha\right)\frac{d\bar{Q}_v}{d\tau} = \bar{\Delta}p - \bar{Q}_p^2(\psi+1) - \bar{Q}_v^2\left(\frac{\eta^2}{C_D^2\bar{x}^2} - \frac{2\eta}{C_c\bar{x}}\right) + 2\varepsilon\left(\frac{d\bar{x}}{d\tau}\right)^2 + \varepsilon\alpha\frac{d^2\bar{x}}{d\tau^2} \tag{6.37}$$

and

$$\frac{d^2\bar{x}}{d\tau^2} = -2\xi\frac{d\bar{x}}{d\tau} - \bar{k}(\bar{x}-\beta) - \frac{1}{2}\mu\left[\frac{\bar{Q}_v^2\eta^2}{C_D^2\bar{x}^2} + \frac{\eta\alpha_o}{C_c\bar{x}}\frac{d\bar{Q}_v}{d\tau}\right] \tag{6.38}$$

Equations (6.37) and (6.38) are used for simulation of plug valve vibrations examined in this thesis. Further details on the application are in Appendix C.

6.3 Stability Analyses

Two stability criteria are reported in this section. The first is based on a Routh Hurwitz analysis of the nonlinear differential equations of motion just derived. The second is based on a quasistatic stability analysis. These predictions are compared to experimental results in Chapter 7.

6.3.1 Routh-Hurwitz Stability Analysis of Nonlinear Model

To be able to perform the Routh-Hurwitz [33] stability analysis it is first necessary to write the equations of motion in a slightly different form.

Defining $y_1 = \bar{Q}_v$, $y_2 = \bar{x}$, $y_3 = \frac{d\bar{x}}{d\tau}$, and then equations (6.35) and (6.36) can be used to write:

$$\frac{\alpha dy_1}{d\tau} = \bar{\Delta}P - (y_1-\varepsilon y_3)^2(\psi+1+\frac{1}{\theta^2}) + y_1^2\left(\frac{1}{C_v^2\theta^2} - (\frac{\eta}{C_D y_2})^2 + \frac{2\eta}{C_D y_2}\right)$$

$$-y_3^2\left(\frac{\varepsilon^2}{\theta^2} - 2\varepsilon\right) - \frac{2y_1y_3\varepsilon}{C_v\theta^2} + \frac{\varepsilon\alpha dy_3}{d\tau} \qquad (6.39)$$

$$\frac{dy_2}{d\tau} = y_3 \qquad (6.40)$$

$$\frac{dy_3}{d\tau} = -2\varepsilon y_3 - \bar{k}(y_2-\beta) - \frac{1}{2}\mu\left[\frac{y_1^2\eta^2}{C_D^2y_2^2} + \frac{y_1^2C_c^2}{C_D^2\theta^2} + \frac{2y_1y_3\varepsilon}{C_D\theta^2} - (\frac{\varepsilon}{\theta}y_3)^2\right]$$

(6.41)

The term $y_1-\varepsilon y_3$ enters through the nondimensional form of the continuity equation (6.24).

Let w_1, w_2, and w_3 be the equilibrium values of y_1, y_2 and y_3 respectively, then,

$$\bar{\Delta}P = w_1^2 \left(\psi+1+ \frac{1}{\theta^2}\right) - w_1^2 \left(\frac{1}{C_v^2\theta^2} - \frac{\eta^2}{C_D^2 w_2^2} + \frac{2\eta}{C_c w_2}\right) \tag{6.42}$$

$$w_3 = 0 \tag{6.43}$$

$$\bar{k}\,(\beta - w_2) = \frac{1}{2}\,\mu \left(\frac{w_1^2\eta^2}{C_D^2 w_2^2} - \frac{w_1^2 C_c^2}{C_D^2\theta^2}\right) \tag{6.44}$$

The coefficients $a_{ij} = \frac{d}{dy_i}\left(\frac{dy_i}{d\tau}\right)\Big|_{w_1,w_2,w_3}$ are found using equations (6.40) and (6.41).

$$a_{11} = -\frac{2w_1}{\alpha}\left(\psi+1+\frac{1}{\theta^2}\right) + \frac{2w_1}{\alpha}\left(\frac{1}{C_v^2\theta^2} - \left(\frac{\eta}{C_D w_2}\right)^2 + \frac{2\eta}{C_c w_2}\right) + \varepsilon a_{31}$$

Using equation (6.24) this becomes,

$$a_{11} = b_{11} + \varepsilon a_{31} \tag{6.45}$$

where

$$b_{11} = -\frac{2\bar{\Delta}P}{w_1\alpha} \tag{6.46}$$

$$a_{12} = b_{12} + \varepsilon a_{32} \tag{6.47}$$

where

$$b_{12} = \frac{2w_1^2}{w_2\alpha}\left(\left(\frac{\eta}{C_D w_2}\right)^2 - \frac{\eta}{C_c w_2}\right) \tag{6.48}$$

$$a_{13} = b_{13} + \varepsilon a_{33} \tag{6.49}$$

where

$$b_{13} = \frac{2\varepsilon w_1}{\alpha}\left(\psi+1+\frac{1}{\theta^2} - \frac{1}{C_v\theta^2}\right) \tag{6.50}$$

$$a_{21} = 0 \tag{6.51}$$

$$a_{22} = 0 \tag{6.52}$$

$$a_{23} = 1 \tag{6.53}$$

$$a_{31} = \mu w_1 \left(\left(\frac{\eta}{C_D w_2}\right)^2 - \frac{C_c^2}{C_D^2 \theta^2}\right) \tag{6.54}$$

$$a_{32} = -\bar{k} + \frac{\mu w_1^2 \eta^2}{w_2^3 C_D^2} \tag{6.55}$$

$$a_{33} = -2\xi - \frac{\mu w_1 \varepsilon}{C_v \theta^2} \tag{6.56}$$

Hayashi [33] defines the matrices necessary to determine the stability threshold for a third order system as

$$-\begin{vmatrix} a_{11} - \lambda & a_{12} & a_{13} \\ a_{21} & a_{22} - \lambda & a_{23} \\ a_{31} & a_{32} & a_{33} - \lambda \end{vmatrix} = 0 \tag{6.57}$$

This is expanded to,

$$a_o \lambda^3 + a_1 \lambda^2 + a_2 \lambda + a_3 = 0 \tag{6.58}$$

The Routh-Hurwitz stability criterion requires that all coefficients and principal determinants are greater than zero.

$$a_i > 0 \tag{6.59a}$$

$$D_i > 0 \tag{6.59b}$$

where

$$i = 1,2,3$$

$$D_1 = a_1 \tag{6.60a}$$

$$D_2 = a_1 a_2 - a_3 a_o \tag{6.60b}$$

$$D_3 = a_3 D_2 \tag{6.60c}$$

If all the inequalities in (6.59) are satisfied then the system is stable according to the Routh-Hurwitz stability criterion. If any of the above conditions are not satisfied then the system is unstable. These conditions can be simplified.

If a_3 and D_2 are greater than zero then D_3 is also greater than zero. If a_1, a_3, a_o and D_2 are greater than zero then a_2 must also be greater than zero. Hence the stability criteria reduces to,

$$a_o > 0 \tag{6.61a}$$

$$D_1 = a_1 > 0 \tag{6.61b}$$

$$a_3 > 0 \tag{6.61c}$$

$$D_2 > 0 \tag{6.61d}$$

Using equations (6.57) and (6.58) the condition (6.61a) can be seen to be satisfied at all times, since $a_o = 1$.

Equations (6.45), (6.47), (6.49) (6.57) and (6.58) lead to

$$a_1 = - a_{33} - b_{11} - \varepsilon a_{31} \tag{6.62}$$

$$a_2 = b_{11}\, a_{33} - a_{32} - a_{31}\, b_{13} \tag{6.63}$$

$$a_3 = b_{11}\, a_{32} - b_{13}\, a_{31} \tag{6.64}$$

Using equations (6.46), (6.54) and 6.56), equation (6.62) becomes,

$$a_1 = 2\xi + \frac{\mu w_1 \varepsilon}{C_v \theta^2} + \frac{2\bar{\Delta}P}{w_1 \alpha} + \varepsilon \mu w_1 \left(\left(\frac{\eta}{C_D w_2} \right)^2 - \frac{C_c^2}{C_D^2 \theta^2} \right) \qquad (6.65)$$

The first three terms in this equation are made up of positive coefficients only. The last term in brackets alone has the potential to be negative. This is positive provided,

$$1 > \frac{w_2 C_c}{\eta \theta}$$

This represents the ratio of the vena contracta area to the upstream pipe area, and hence is true in general. Thus, condition (6.61b) is satisfied in general.

Using equation (6.46), (6.50), (6.54) and (6.55) and substituting into equation (6.64), the expression for a_3 becomes,

$$a_3 = \frac{2\bar{\Delta}P}{w_1 \alpha} \left(\bar{k} - \frac{\mu w_1^2 \eta^2}{w_2^3 C_D^2} \right) + \frac{2\mu w_1^3}{w_2 \alpha} \left(\left(\frac{\eta}{C_D w_2} \right)^2 - \frac{\eta}{C_c w_2} \right) \left(\frac{\eta}{C_D w_2} \right)^2 - \frac{C_c^2}{C_D^2 \theta^2} \qquad (6.67)$$

This results in condition (6.61c) being only conditionally satisfied and needs to be examined with condition (6.61d). Since in general, both the upstream and downstream pipe areas will be greater than the valve gap area, the second term in equation (6.67) will be positive so that a_3 can only be negative if,

$$k < \frac{\mu w_1^2 \eta^2}{w_2^3 C_D^2} \qquad (6.68)$$

Combining equations (6.60b), (6.62), (6.63) and (6.64), an

expression for D_2 in the following form can be obtained:

$$D_2 = a_{31}(b_{11}b_{13} - \varepsilon b_{11}a_{33} + \varepsilon a_{31}b_{13} + \varepsilon a_{32} + a_{33}b_{13} + b_{12}) + a_{33}(-b_{11}^2 - b_{11}a_{33} + a_{32}) \tag{6.69}$$

Using expressions for b_{ij}, a_{ij} given by equations (6.45) to (6.56), the expression for D_2 becomes,

$$\begin{aligned} D_2 = \mu w_1 \Big(\Big(\frac{\eta}{C_D w_2}\Big)^2 - \Big(\frac{C_c}{C_D\theta}\Big)\Big)\Big[\frac{4\bar{\Delta}P\varepsilon}{\alpha^2}\Big(\psi+1+\frac{1}{\theta^2} - \frac{1}{C_v\theta^2}\Big) + \frac{2\bar{\Delta}P}{w_1\alpha}\Big(2\xi+\frac{\mu w_1\varepsilon}{C_v\theta^2}\Big) \\ + 2\varepsilon^2\,\frac{\mu w_1^2}{\alpha}\Big(\psi+1+\frac{1}{\theta^2} - \frac{1}{C_v^2\theta^2}\Big)\Big(\frac{\eta}{C_D w_2}\Big)^2 - \Big(\frac{C_c}{C_D\theta}\Big)^2\Big) + \varepsilon\Big(\bar{k} - \frac{\mu w_1^2\eta^2}{w_2^3 C_D^2}\Big) \\ + \frac{2\varepsilon w_1}{\alpha}\Big(2\xi + \frac{\mu w_1\varepsilon}{C_v\theta^2}\Big)\Big(\psi+1+\frac{1}{\theta^2} - \frac{1}{C_v\theta^2}\Big) - \frac{2w_2^2}{w_2\alpha}\Big(\Big(\frac{\eta}{C_D w_2}\Big)^2 - \frac{\eta}{C_c w_2}\Big)\Big] \\ + \Big(2\xi + \frac{\mu w_1\varepsilon}{C_v^2}\Big)\Big[\frac{4\bar{\Delta}P}{w_1^2\alpha^2} + \frac{2\bar{\Delta}P}{w_1\alpha}\Big(2\xi + \frac{\mu w_1\varepsilon}{C_v\theta^2}\Big) + \Big(\bar{k}_1 - \frac{\mu w_1\eta^2}{w_2^3 C_D^2}\Big)\Big] \end{aligned} \tag{6.70}$$

It can be seen at this stage that the stability criterion is very complicated. To simplify matters the inertia α is allowed to grow, so that as $\alpha \to \infty$ then equation (6.70) becomes,

$$D_2 = \mu w_1\Big(\Big(\frac{\eta}{C_D w_2}\Big)^2 - \Big(\frac{C_c}{C_D\theta}\Big)^2\Big)\Big(\varepsilon\Big(\bar{k} - \frac{\mu w_1^2\eta^2}{w_2^3 C_D^2}\Big)\Big) + \Big(2\xi + \frac{\mu w_1\varepsilon}{C_v\theta^2}\Big)\Big(\bar{k} - \frac{\mu w_1^2\eta^2}{w_2^3 C_D^2}\Big) \tag{6.71}$$

As pointed out earlier $\frac{\eta}{C_D w_2} > \frac{C_c\varepsilon}{C_D\theta}$ in general, and all the coefficients here are positive. Hence, D_2 is greater than zero if

$$\bar{k} > \frac{\mu w_1^2 \eta^2}{w_2^3 C_D^2} \tag{6.72}$$

a_3 which is given by equation (6.67) is only negative if condition (6.68) is satisfied, which is contrary to condition (6.72). Hence if condition (6.72) is satisfied $a_3 > 0$. This means that for large inertia α, conditions equation (6.61d), the stability criterion is satisfied provided,

$$\bar{k} > \frac{\mu w_1^2 \eta^2}{w_2^3 C_D^2} \tag{6.72}$$

The stability threshold, is defined by the equality,

$$\bar{k} = \frac{\mu w_1^2 \eta^2}{w_2^3 C_D^2} \tag{6.73}$$

By making a further simplification, the stability threshold can be expressed in terms of vibration parameters only, that is a condition where the equilibrium position (w_1, w_2, w_3) need not be calculated.

Let $\theta \to \infty$, that is let the upstream pipe area become large, so we now have a tank upstream of the valve. The equilibrium equations (6.42) and (6.44) then become,

$$\bar{\Delta P} = w_1^2 \left(\psi + 1 + \frac{\eta^2}{C_D^2 w_2^2} - \frac{2\eta}{C_c w_2}\right) \tag{6.74}$$

and

$$\bar{k}(\beta - w_2) = \frac{\varepsilon \mu w_1^2 \eta^2}{C_D^2 w_2^2} \tag{6.75}$$

Substitution of the stability threshold equation (6.73)

into equation (6.75) yields,

$$w_2 = \frac{2\beta}{3} \tag{6.76}$$

Now substituting for w_1^2 in equation (6.75) from equation (6.74) results in the stability threshold becoming

$$\bar{k}(\beta - w_2) = \frac{\mu \bar{\Delta} P \eta^2}{2C_D^2 w_2^2 (\psi + 1 + \frac{\eta^2}{C_D^2 w_2^2} - \frac{2\eta}{C_c w_2})} \tag{6.77}$$

substituting for w_2 from equation (6.76) into this expression yields,

$$\bar{k} = \frac{27 \mu \bar{\Delta} P \eta^2}{8C_D^2 \beta^3 (\psi + 1 + \frac{9\eta^2}{4C_D^2 \beta^2} - \frac{3\eta}{C_c \beta})} \tag{6.78}$$

Equation (6.78) represents the minimum stiffness required for stability, given a tank upstream of the valve and a long downstream pipe. The stability threshold defined by equations (6.75) and (6.78) contain only static terms. That is they are independent of the pumping term ε and the damping ξ. Hence when fluid inertia is large the instability phenomenon appears to be one of divergence. In order to confirm this a quasistatic stability analysis is described in the next section.

6.3.2 Quasistatic Stability Analysis of a Plug Valve Connected to a Long Pipeline

The assumptions made in deriving the quasistatic stability criterion are:

(a) Fluid in the system is incompressible

(b) Aeration or cavitation does not occur.

(c) The velocity and pressure of the fluid are uniform over a transverse cross section of the conduit, except immediately downstream of the valve.

(d) The instability mechanism is divergence and therefore only static forces need to be considered.

(e) The discharge coefficient, contraction coefficient and velocity coefficients are constant.

(f) The pipeline is long and hence fluid inertia is large.

(g) The area of the gap varies linearly with the displacement of the valve from the seat.

Definition of no load position: at $\Delta P = 0$, $Q = 0$, $\dot{Q} = 0$, $x = x_o$, where ΔP is the pressure difference across the valve, Q is the flowrate of fluid through the valve and x is the valve's displacement from the seat. Consider the valve in equilibrium with a flowrate Q_1 through the valve at an opening x_1, and a pressure drop ΔP_1. Then,

$$\Delta P_1 S = k(x_o - x_1) \tag{6.79}$$

Now consider a force F applied to the valve as shown in Figure 6.4. The force F necessary to hold the valve at any opening x under static conditions is given by:

$$F = \Delta PS - k(x_o - x) \tag{6.80}$$

Thus the restoring force in the system i.e., that force trying to bring the valve back to equilibrium is given by,

$$F_{REST} = k(x_o - x) - \Delta PS \tag{6.81}$$

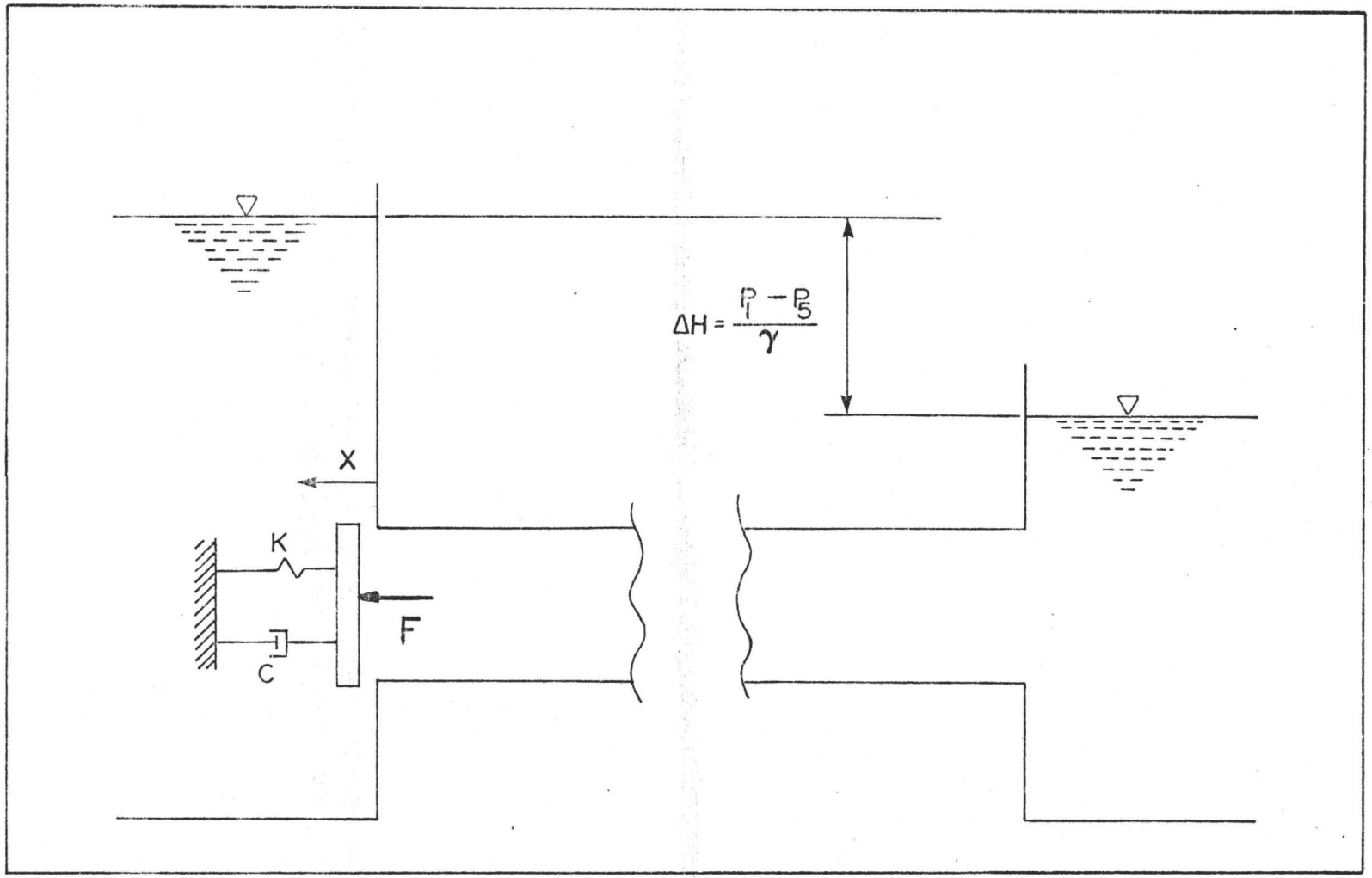

Fig. 6.4 Plug valve model with a large tank upstream

The restoring force F_{REST} is equal to zero at equilibrium. For stability F_{REST} should increase as x increases and decrease as x decreases around the equilibrium point if the system is statically stable. That is to say the condition for stability is:

$$\left.\frac{\partial F_{REST}}{\partial x}\right|_{x_1, \Delta P_1} > 0 \tag{6.82}$$

To evaluate $\frac{\partial F_{REST}}{\partial x}$ the discharge characteristic of the valve needs to be examined.

$$Q = C_D \, W \, x \, \sqrt{2\Delta P/\rho g_c} \tag{6.83}$$

where W is the gap width, C_D is the discharge coefficient, ΔP the pressure difference across the valve and ρ the fluid density.

Taking the partial derivatives with respect to x,

$$\frac{\partial Q}{\partial x} = C_D \, W \, \sqrt{2\Delta P/\rho g_c} + \frac{C_D W x}{2}\sqrt{\frac{2\rho g_c}{\Delta P}} \, \frac{\partial(\Delta P)}{\partial x} \tag{6.84}$$

If a small change in x is considered and a large downstream inertia is assumed such that $\frac{\partial Q}{\partial x}$ can be taken as zero, then,

$$\frac{\partial(\Delta P)}{\partial x} = -\frac{2\Delta P}{x} \tag{6.85}$$

Using equation (6.85) and taking the partial derivative of equation (6.81) with respect to x, it can be shown that,

$$\frac{\partial F_{REST}}{\partial x} = -k + \frac{2\Delta PS}{x} \tag{6.86}$$

Evaluating this at the equilibrium position,

$$\left.\frac{\partial F_{REST}}{\partial x}\right|_{x_1, \Delta P_1} = -k + \frac{2\Delta P_1 S}{x_1} \tag{6.87}$$

so that at the stability threshold,

$$kx_1 = 2\Delta P_1 S \tag{6.88}$$

Using the equilibrium equation (6.79), this can be rewritten as,

$$3x_1 = 2\, x_o \tag{6.89}$$

The nondimensional equivalent of this expression is equation (6.76). Since further substitutions used in the nondimensional analysis were based solely on the static equilibrium of the valve, then the same substitutions can be made here by nondimensionalizing equation (6.89)

$$w_2 = 2\beta/3 \tag{6.90}$$

Where $w_2 = x_1/d$, $\beta = x_o/d$ and d is a characteristic dimension of the valve. Thus the stability threshold obtained from the quasistatic stability analysis gives:

$$\bar{k} = \frac{27\mu\bar{\Delta}P\eta^2}{8\, C_D^2\, \beta^3 \left(\psi + 1 + \frac{9\eta^2}{4C_D^2\beta^2} - \frac{3\eta}{C_c\beta}\right)} \tag{6.91}$$

This stability criterion is the same as that obtained from the Routh Hurwitz analysis for large fluid inertia and

a large upstream pipe area. Hence the instability under these conditions is one of divergence.

6.4 Discussion

In this Chapter theory has been derived to include the effect of pumping and pressure recovery. The theory derived modifies slightly the form of equations obtained by Weaver and Ziada [6], the influence of these changes can be examined closely by integrating the nonlinear differential equations numerically. The results of such integrations are presented in Chapter 7 along with comparisons to the experimental results.

Derivation of the stability threshold for large fluid inertia has been made, quantities required to make these predictions are based solely on the static discharge characteristics of the valve and parameters which should be easy to determine, such as operating pressure difference, initial opening, valve stiffness etc. The instability phenomenon for a large fluid inertia has been found to be a divergence instability, and hence a static analysis is applicable.

Thus the theory derived in this chapter allows for determination of stability thresholds and vibration properties such as frequency and amplitude through numerical integration. A stability criteria which does not require use of a computer program has also been derived. The results of these are presented in Chapter 7 along with the corresponding experimental results.

CHAPTER 7

COMPARISON OF EXPERIMENTAL RESULTS AND THEORETICAL PREDICTIONS

7.1 Introduction

In this Chapter theoretical predictions of stability boundaries, frequencies and amplitudes are compared with experimentally obtained self-excited valve vibrations.

Stability predictions have been made by using the computer program in Appendix C to numerically integrate the nonlinear differential equations of valve motion. The stability threshold formula derived in Section 6.3.1 of this thesis as well as Kolkman's plug valve analysis [4] have been used to make stability predictions. The stability thresholds obtained in the above manner are compared in Section 7.2.

The equations of motion have been used to simulate the valve vibrations. Hence from their integration it is possible to determine the amplitude, frequency and form of the limit cycle oscillations. The principal oscillation characteristics are compared in Section 7.3.1 In Section 7.3.2 the general trends of frequency and amplitude are investigated as a function of system parameters.

Section 7.4 is devoted to analyzing the effect of pumping on the limit cycle oscillation predictions. Hence this will

provide a quantitative assessment of how this term affects the results.

In the last section of this Chapter, the performance of each of the theoretical predictions is discussed, discrepancies are analyzed and recommendations concerning further work are made.

7.2 Stability Thresholds

Figure 7.1 shows the regions where the valve is theoretically dynamically stable or unstable. The lower region labelled "stable closed" represents the region where the valve is predicted to come to rest in the closed position. In the region labelled "unstable", limit cycle oscillations of the valve are predicted by the theory. In the upper region, "stable open", the valve is stable in the open position.

Only integration of the full nonlinear equations is capable of predicting the lower stability threshold. Predictions of the upper stability threshold have been made in several ways: using the nonlinear theory numerically integrated, using the stability formula derived in Chapter 6 and using Kolkman's analysis [4]. The latter two formulations predict discrete points on the threshold through which a curve has been drawn. The nonlinear theory on the other hand arises from computations at specific intervals. Hence the exact location of the stability threshold could only be determined by successively reducing the increments of initial opening, β, and integrating

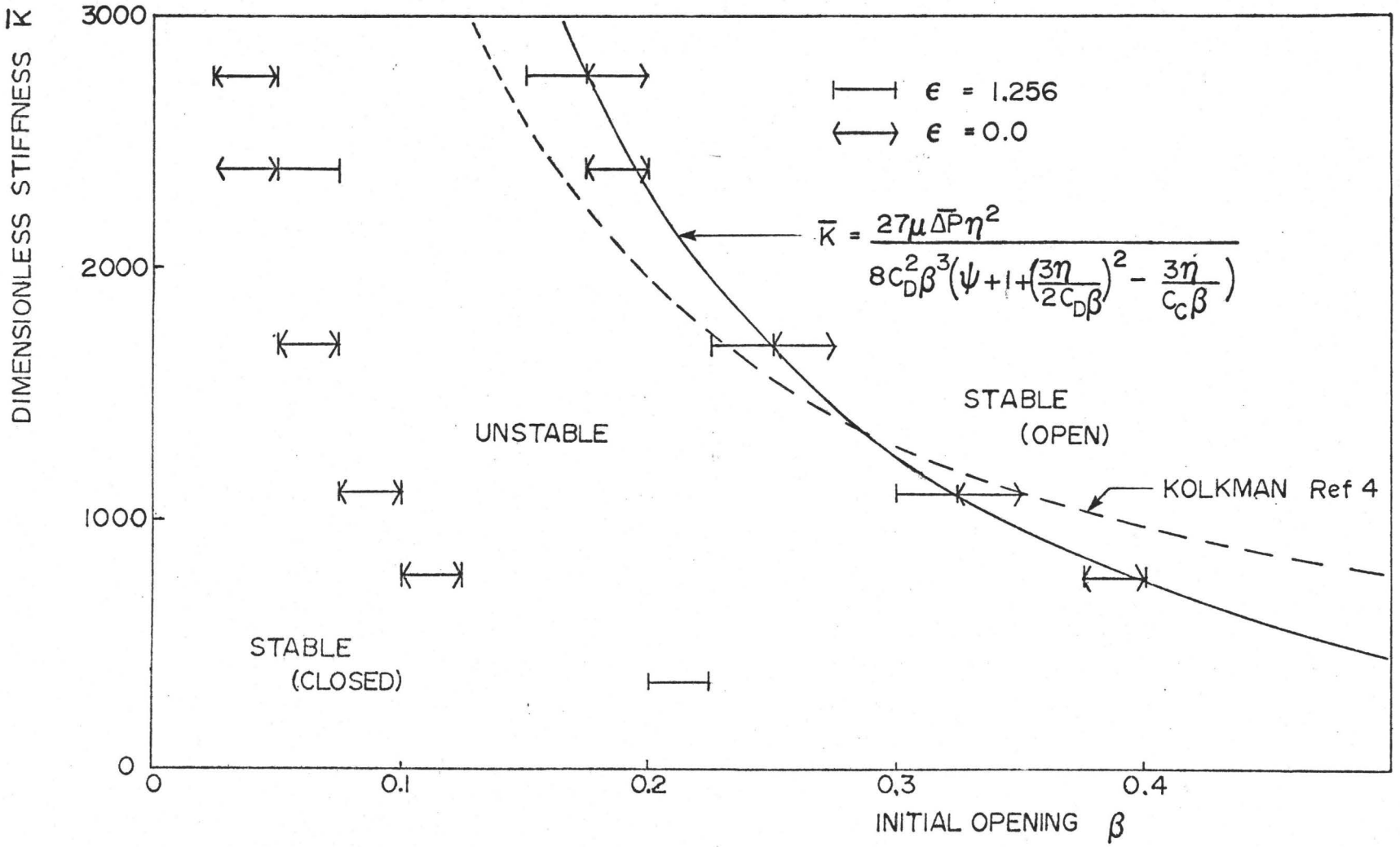

Fig. 7.1 Comparison of theoretical stability thresholds (α= 354)

the equations again. Bands have been drawn in Figure 7.1 to show the area in which the threshold lies. At one end of the band the valve is predicted to be stable whereas at the opposite side of the band the valve is predicted as being unstable.

In Chapter 6 the theoretical derivation of the long pipe stability threshold showed that the threshold is independent of the pumping parameter ε. As can be seen from Figure 7.1 this divergence formula agrees extremely well with the full nonlinear theoretical stability threshold. There is a minor discrepancy between the nonlinear theory with pumping and that without pumping. This is probably due to the fact that the computations were made for a pipe of finite length and hence the pumping parameter ε still has some small effect. Hence it can be concluded that the instability at this fluid inertia (α = 354) approaches divergence and the long pipe formula is valid.

The divergence formula derived from Kolkman's analysis (pipe length $\rightarrow \infty$) is represented by the dashed line in Figure 7.1. Several important effects are neglected by Kolkman. Firstly, he assumes the effective area over which the valve pressure differences acts is equal to that of the downstream pipe cross-sectional area. Secondly, he neglects pressure recovery downstream of the valve. Both of these effects would result in a lower stability prediction in the case of the plug valve examined. At larger openings flow losses in the pipe become more important, consequently there would be a reduced pressure difference across the valve. Kolkman also neglects

these losses. Hence at large openings his stability predictor should be high. Given these approximations made by Kolkman it is not surprising to find his stability predictor in Figure 7.1 deviate from the nonlinear predictor in the manner observed.

Figure 7.2 shows how the theoretical predictions compare with the experimental results. The upper stability threshold is predicted very well by the long pipe stability formula. Since these predictions are made for a constant discharge coefficient it appears that changes in discharge coefficient due to unsteadiness in the flow have a minor role in determining the upper stability threshold at large fluid inertias.

The lower theoretical stability threshold appears to agree better with experiments at higher stiffnesses. The reason for the discrepancy at lower stiffnesses is not clear. This may be due to rapid variations in the discharge coefficient, or more likely due to the high velocity at which the valve leaves the seat. A coefficient of restitution of 0.05 was used in all computations. In the vibrations shown in Chapter 5 the coefficient of restitution is obviously far greater than 0.05, hence this accounts for the discrepancy in the lower stability threshold.

Figure 7.3 shows how the stability thresholds change with fluid inertia. The theoretical line for the nonlinear model has been predicted by computing the behaviour of the valve at various openings. Error bounds due to computing the valve behaviour at discrete points are shown on this graph as they

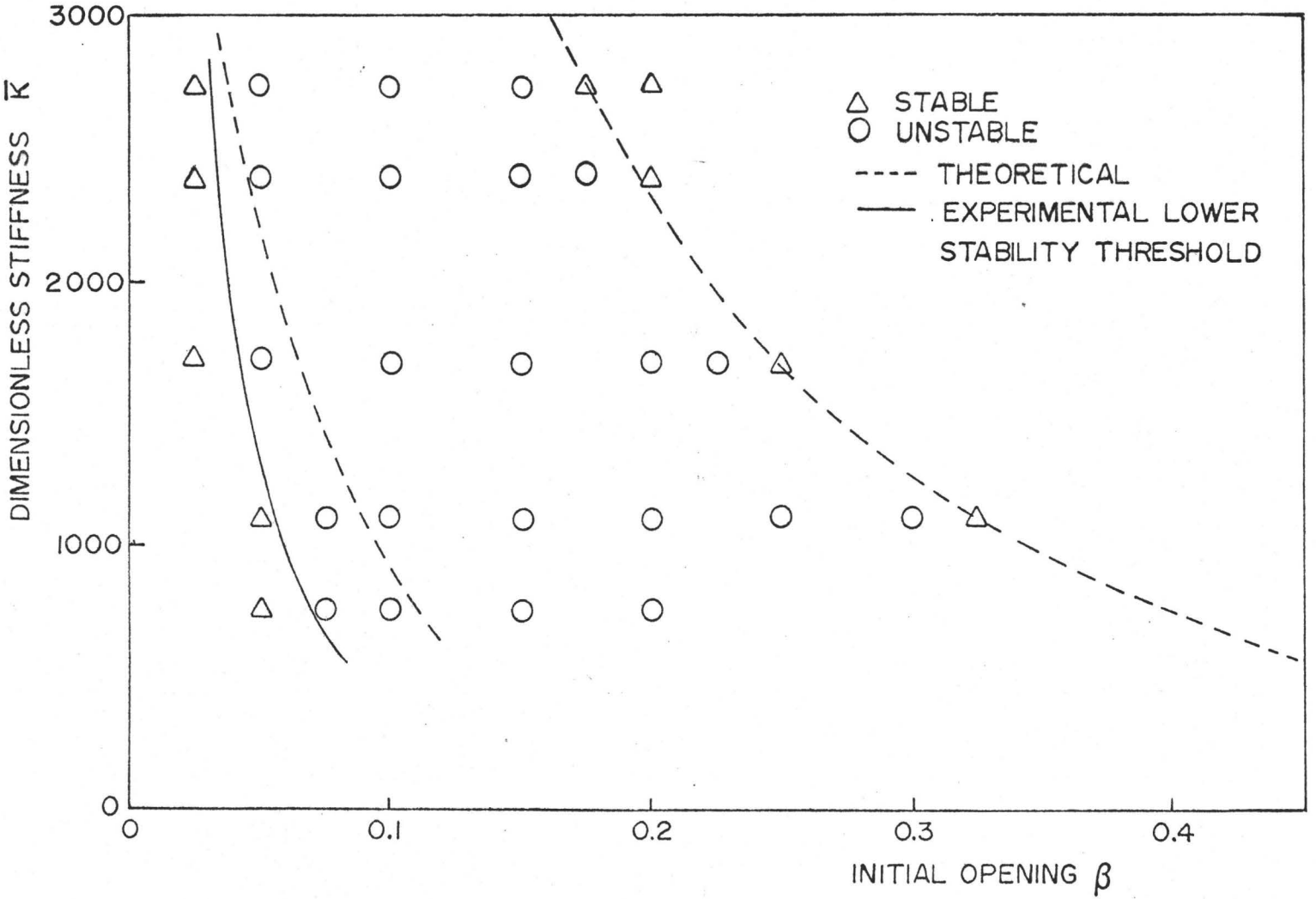

Fig. 7.2 Comparison of experimental and theoretical stability thresholds

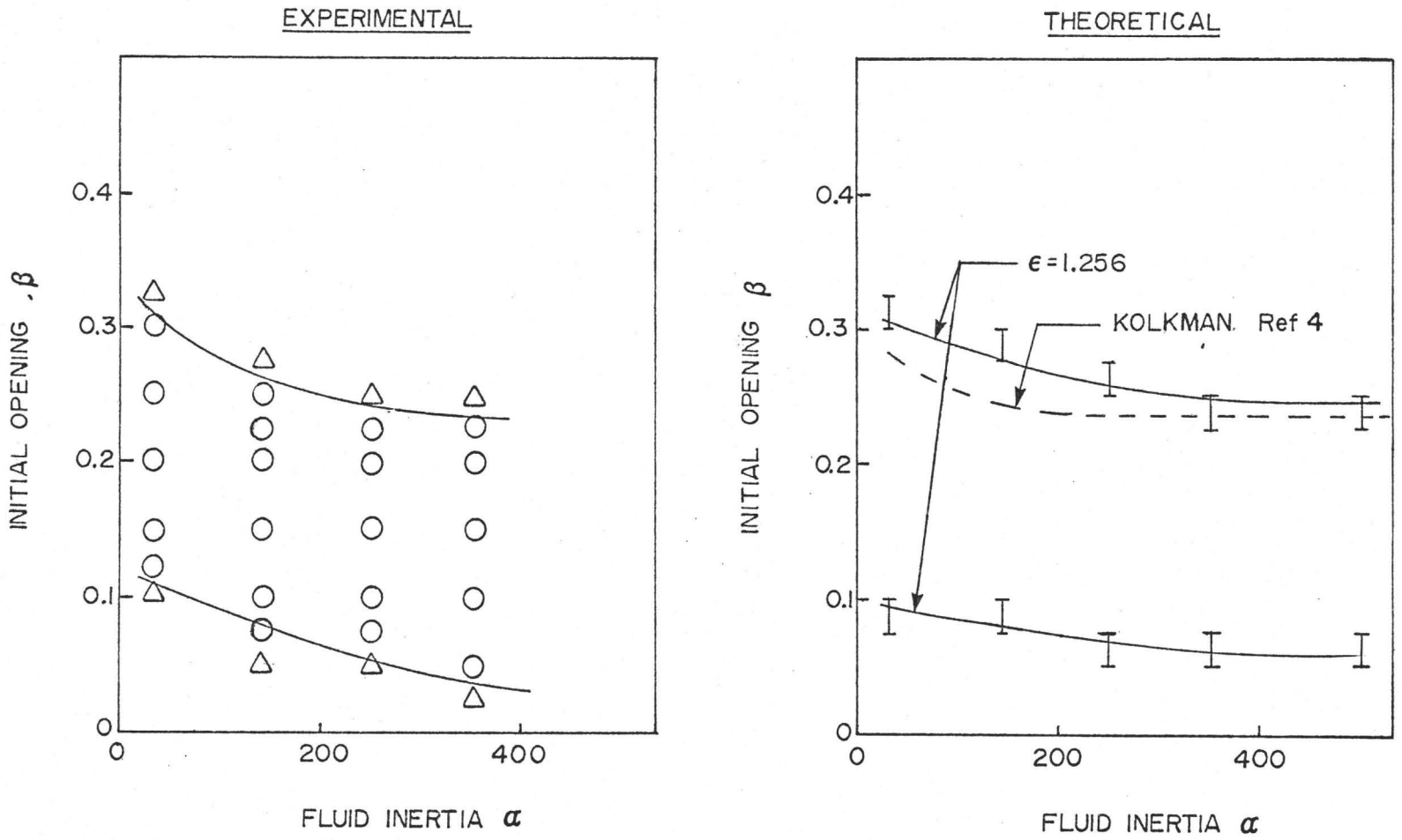

Fig. 7.3 Effect of fluid inertia on stability ($\bar{k}$=1695)

were in Figure 7.1 It can be seen that the trend for both the upper and lower stability thresholds is to rise as fluid inertia decreases.

The theoretical prediction for the lower stability threshold changes less rapidly than the experimental change. This suggests that the valve behaviour is not adequately modelled for small openings.

Kolkman's prediction for the rise in the upper stability threshold is not as large as the experimental change. The prediction of the nonlinear model appears to follow the experimental curve more closely. At the lowest inertia some computations predicted limit cycles in which valve closure was not predicted. These points were classified as dynamically unstable even though no counterpart was found experimentally. This phenomena may not have occurred in the experiments for various reasons. Changes in discharge coefficients may be a dominant effect. Large acceleration and deceleration of the flow combined with large static discharge coefficient variations at small openings could result in large dynamic discharge coefficient variations. Such variations could result in more rapid reduction of flow. Thus, the larger fluid pressures generated would cause closure which is not predicted for a constant discharge coefficient.

7.3 Comparison of Limit Cycle Oscillations

The discussion in this section is centred on the

comparison between the experimental and theoretical limit cycle oscillations. To this end, the theoretical time histories of vibrations corresponding to the experimental results presented in Figures 5.9 to 5.12 are presented. Comparisons are also made between limit cycle amplitudes and frequencies and how they are affected by changing initial opening, spring stiffness and fluid inertia.

7.3.1 Typical Limit Cycle Oscillations

Figure 7.4 shows limit cycle behaviour for four different sets of parameters as predicted by the computer integration of the nonlinear differential equations of motion. These diagrams correspond to the same set of openings, stiffnesses and fluid inertias recorded in Figures 5.9 to 5.12 except for Figure 7.4(c). The computer program predicted that at an opening of $\beta = 0.085$ ($x_o = 4.3$ mm) that the plug valve would not perform limit cycle oscillations but shut and remain shut. A value of $\beta = 0.100$ which is just inside the region of dynamic instability has been used for this computation. Thus Figure 5.11 and Figure 7.4(c) can only be compared qualitatively. The dimensionless displacement scale is related to the experimental displacement scale by equation (7.1).

$$\bar{x} = x/50.8 \qquad (7.1)$$

where $\bar{x}$ is the dimensionless displacement and x is the experimental displacement measured in millimetres. The pressure

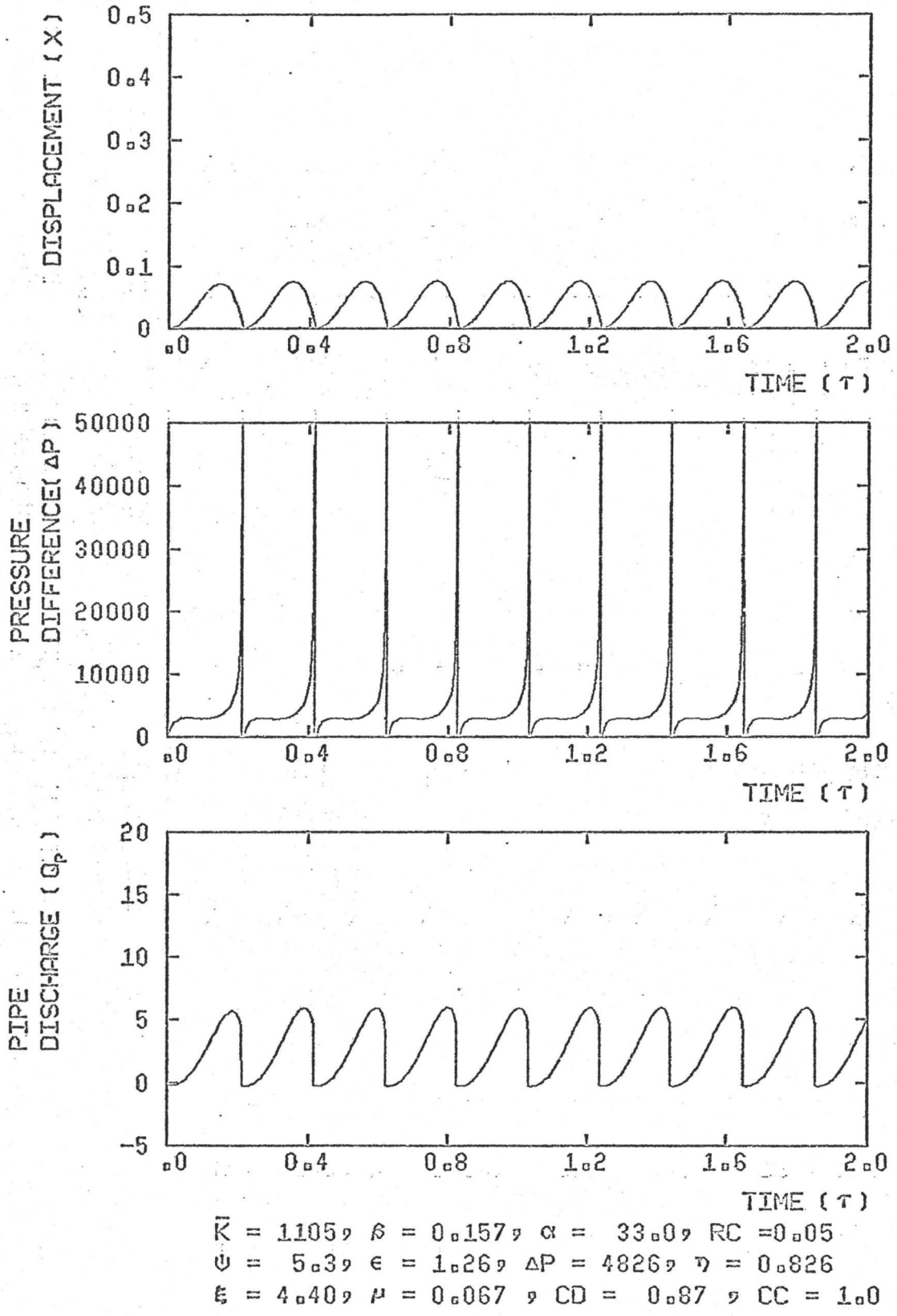

Fig. 7.4(a) Theoretical limit cycle oscillation as a function of time.

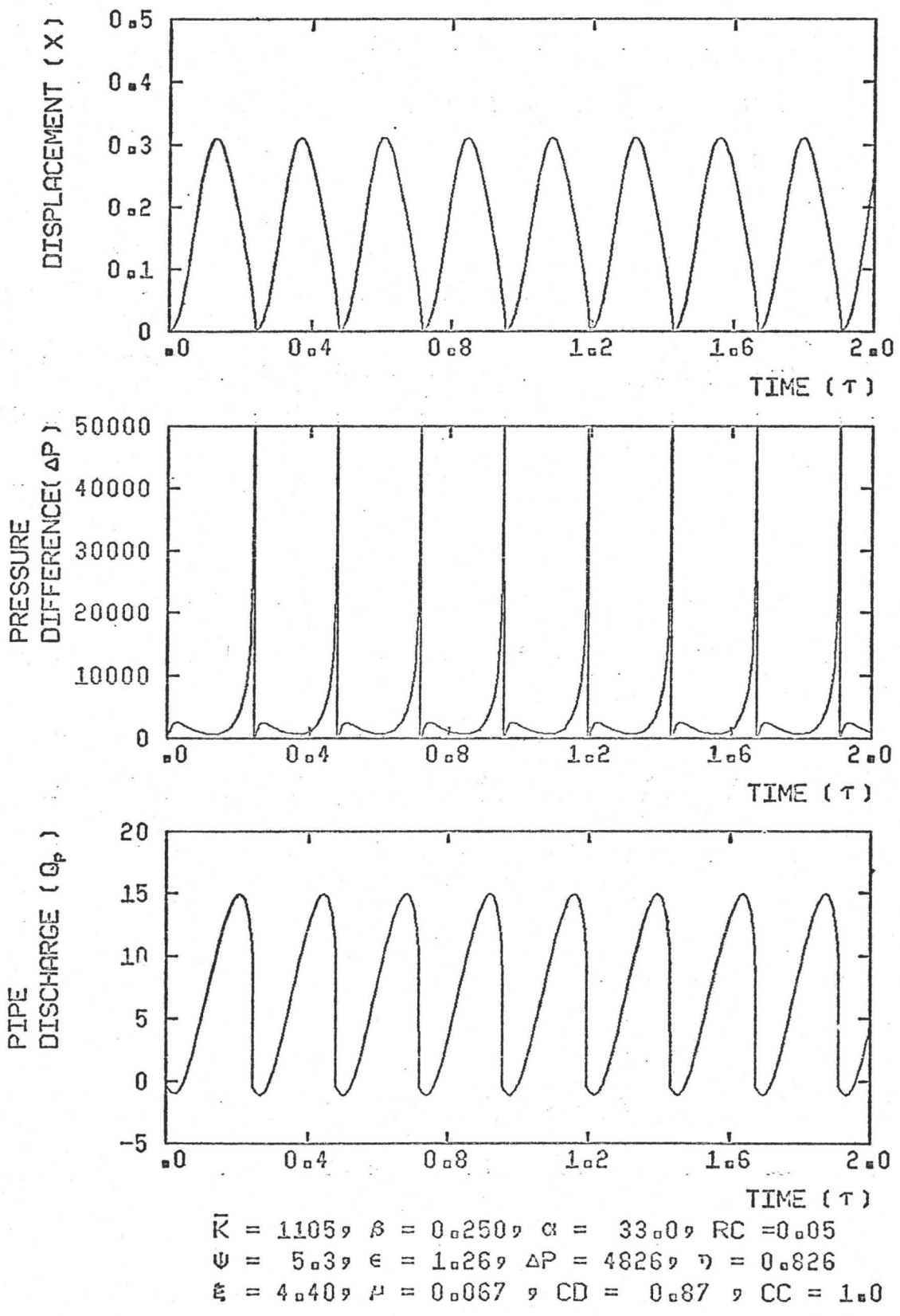

Fig. 7.4(b) Theoretical limit cycle oscillation as a function of time.

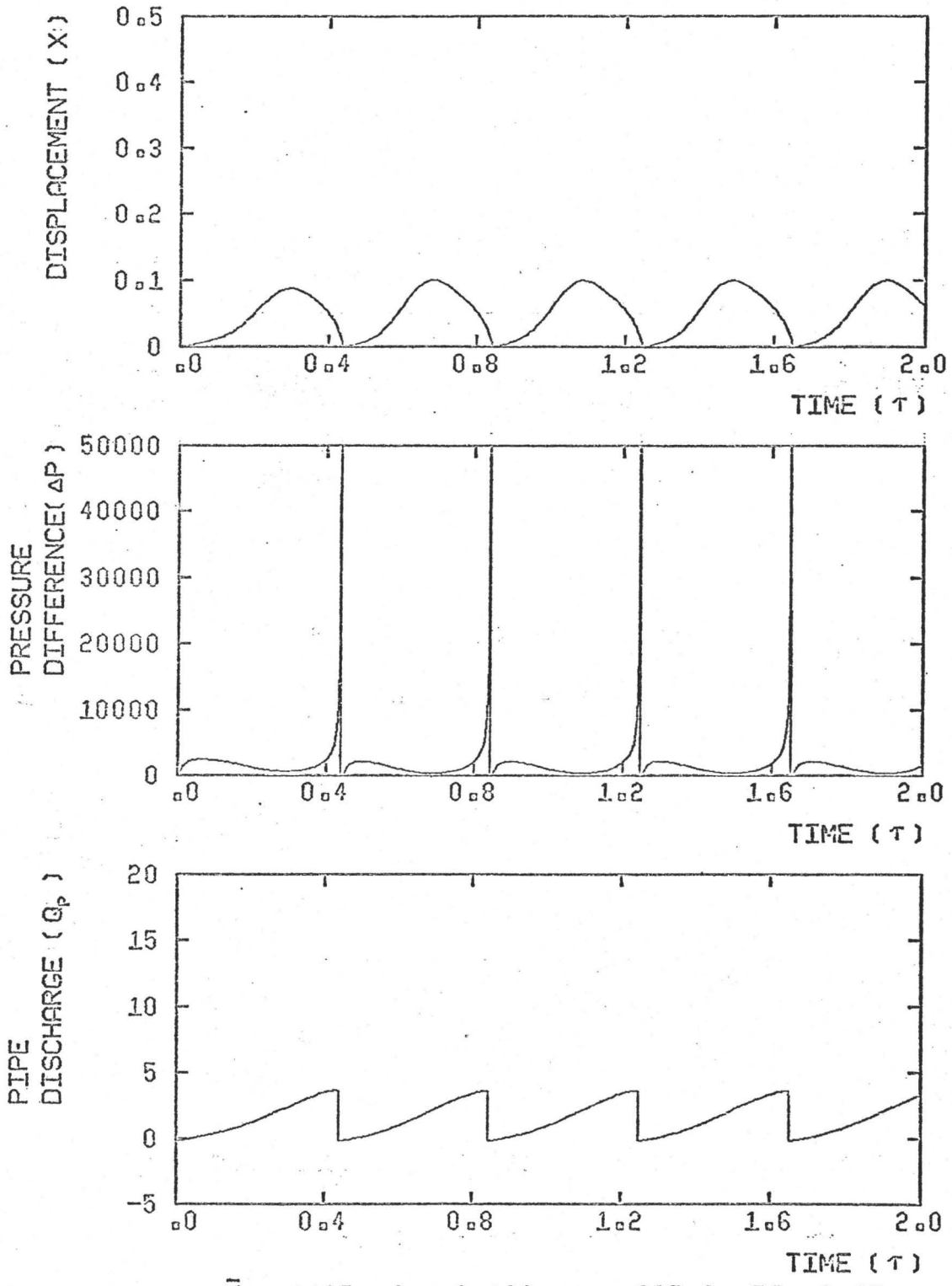

$\bar{K}$ = 1105, β = 0.100, α = 337.0, RC =0.05
Ψ = 13.2, ϵ = 1.26, ΔP = 4826, η = 0.826
ξ = 4.40, μ = 0.067 , CD = 0.87 , CC = 1.0

Fig. 7.4(c) Theoretical limit cycle oscillation as a function of time.

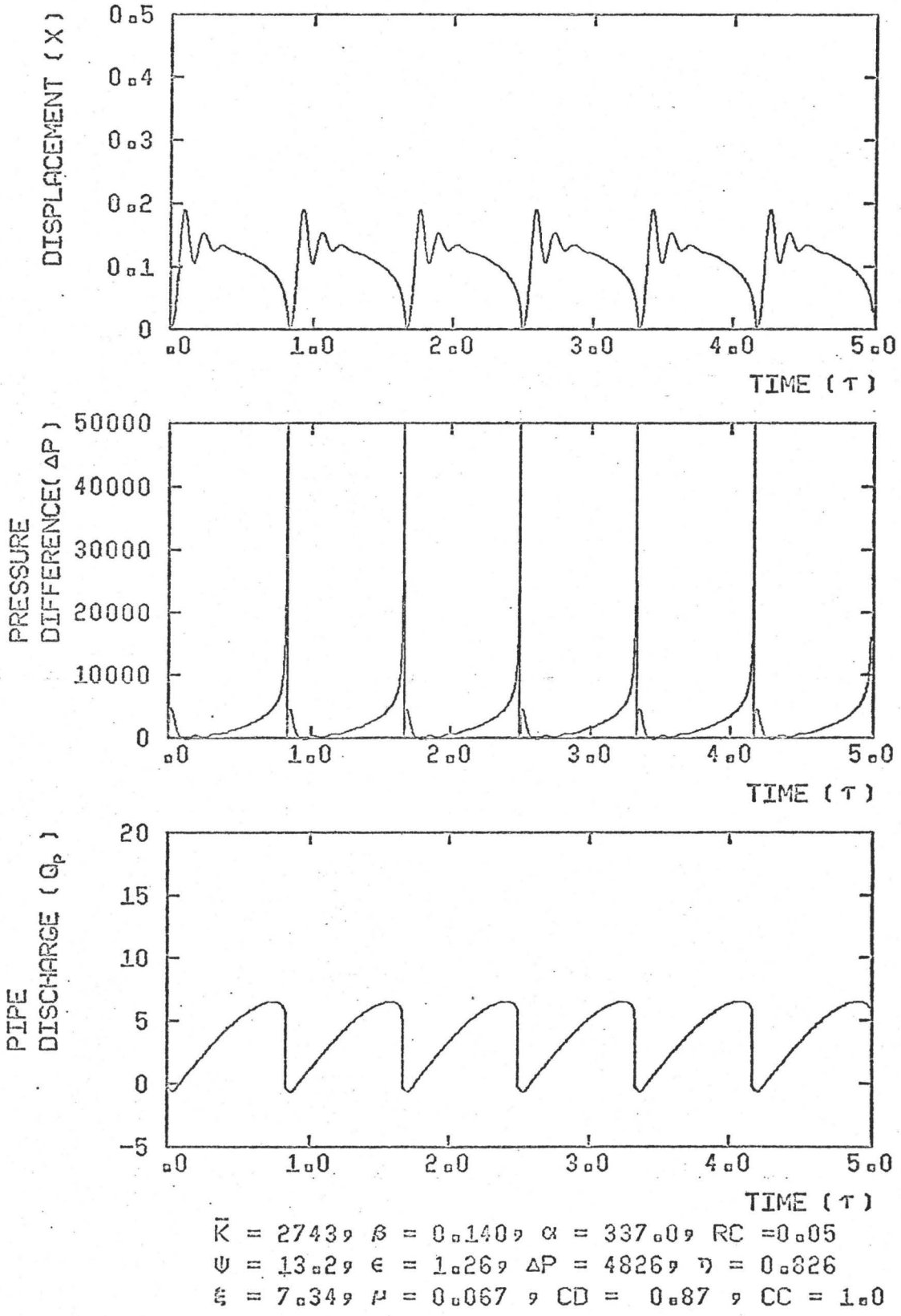

Fig. 7.4(d) Theoretical limit cycle oscillation as a function of time.

differences in Figures 7.4 are the pressure differences across the valve in contrast to the experimentally measured ones, where, the downstream pressure tap is located after the flow reattaches itself and some pressure recovery has occurred. The pressure difference ΔP in kPa is related to the dimensionless pressure difference $\overline{\Delta P}$ by equation (7.2).

$$\Delta P \text{ (kPa)} = .00129\ \overline{\Delta P} \tag{7.2}$$

The pipe discharge $\overline{Q}_p$ is the same discharge that would be measured by the laser doppler anemometer, in that this is the flowrate in the pipe at any instant. The velocity of flow for a flat profile in m/s is related to the dimensionless pipe discharge $\overline{Q}_p$ by,

$$V = 0.05080\ \overline{Q}_p \tag{7.3}$$

A value of $\omega = 1$ has been chosen so that the dimensionless time scale and the time in seconds are exactly equivalent.

In all the cases examined here one can show that the theoretically predicted amplitudes are lower than those obtained experimentally. In Figure 7.4(c) it is obvious that the opening part of the cycle is very different from the result shown for the experiment in Figure 5.11. Reversal of flow in the pipe for the experimental results is very much larger than that obtained theoretically for the opening portion of the cycle. Discrepancies in the opening part of the cycle are, however, not surprising since the valve is given a small initial velocity ($R_c = 0.05$). It is obvious from the experimental results that a much larger value of R_c would be more

realistic.

Similarities in the closures are hard to assess quantitatively because of the influence of the opening part of the cycle. However, comparison of the actual and theoretical maximum flowrates are possible. The reason for choosing to compare this value is that after this point hydrodynamic forces start to dominate the system and subsequent valve closure results. Table 7.1 gives this comparison, $\overline{Q}_{max}$ is the dimensionless maximum pipe flowrate observed.

For initial openings of 8.0 and 12.7 mm the theoretical and experimental maximum flowrates agree to within five percent. The experimental maximum flowrate for an initial opening of 7.1mm

Initial Opening x_o (mm)	β	Figure	$\overline{Q}_{max}$
8.0	.157	5.9	6.1
12.7	.250	5.10	14.8
4.3	.085	5.11	2.1
7.1	.140	5.12	8.5
8.0	.157	7.4(a)	5.8
12.7	.250	7.4(b)	15.5
5.1	.100	7.4(c)	3.8
7.1	.140	7.4(d)	6.5

Table 7.1

is higher than that theoretically predicted and the dwell portion of the displacement cycle is larger for the experiment. The

time histories of the displacement cycles are, however, similar. One possible cause could be a rise in the discharge coefficient during the phase when flow is accelerating, as suggested by Weaver and Ziada [6]. Another possible reason for the delay could lie in the nature of the damping. A significant portion of the effective damping can be attributed to friction (see Table 4.2). This retarding frictional force would also result in a higher flowrate required before the hydrodynamic force dominates the limit cycle.

At closure the experimental traces show that the valve remains closed until the pressure difference across the valve drops. The time during which the valve remains closed will depend on the water hammer wave reflections. The theoretical simulations do not have such an effect included but a coefficient of restitution of 0.05 is used to simulate initiation of valve opening. This has two important consequences. First, in calculating the frequency or period of oscillation, the portion during which the valve remains closed must not be included. Secondly, in the experiments the velocity at which the valve leaves the seat is very much higher than assumed. Hence, amplitude predictions using the model can be expected to be low. The differences in the mode shapes between Figures 5.10 and 5.11 and Figures 7.4(b) and 7.4(c) might also have arisen due to this discrepancy. Better simulations of the vibration are therefore possible by using a higher value of the coefficient of restitution.

Figures 7.5 show how pipe discharge, pressure difference

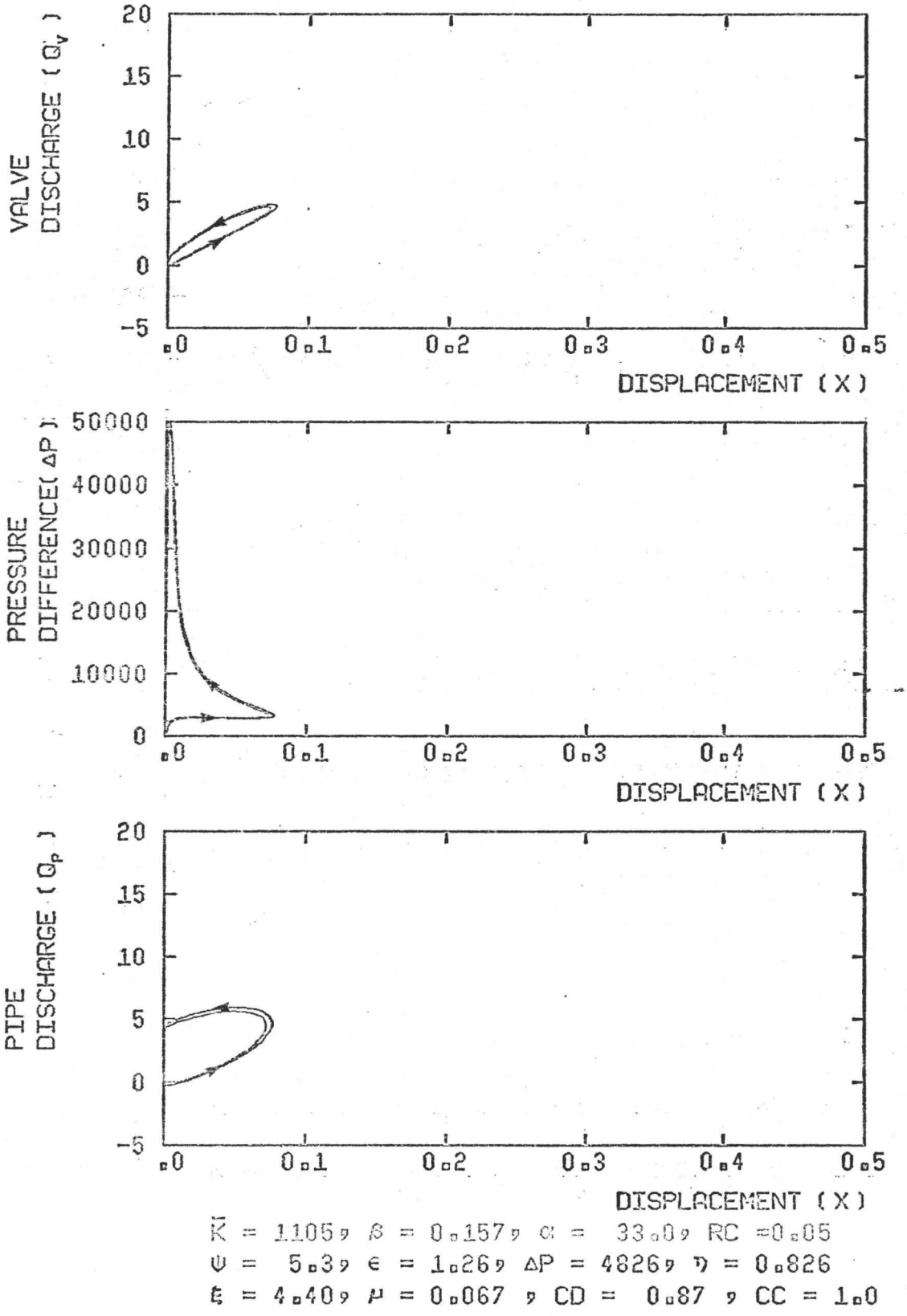

Fig. 7.5(a) Theoretical limit cycle oscillation as a function of displacement.

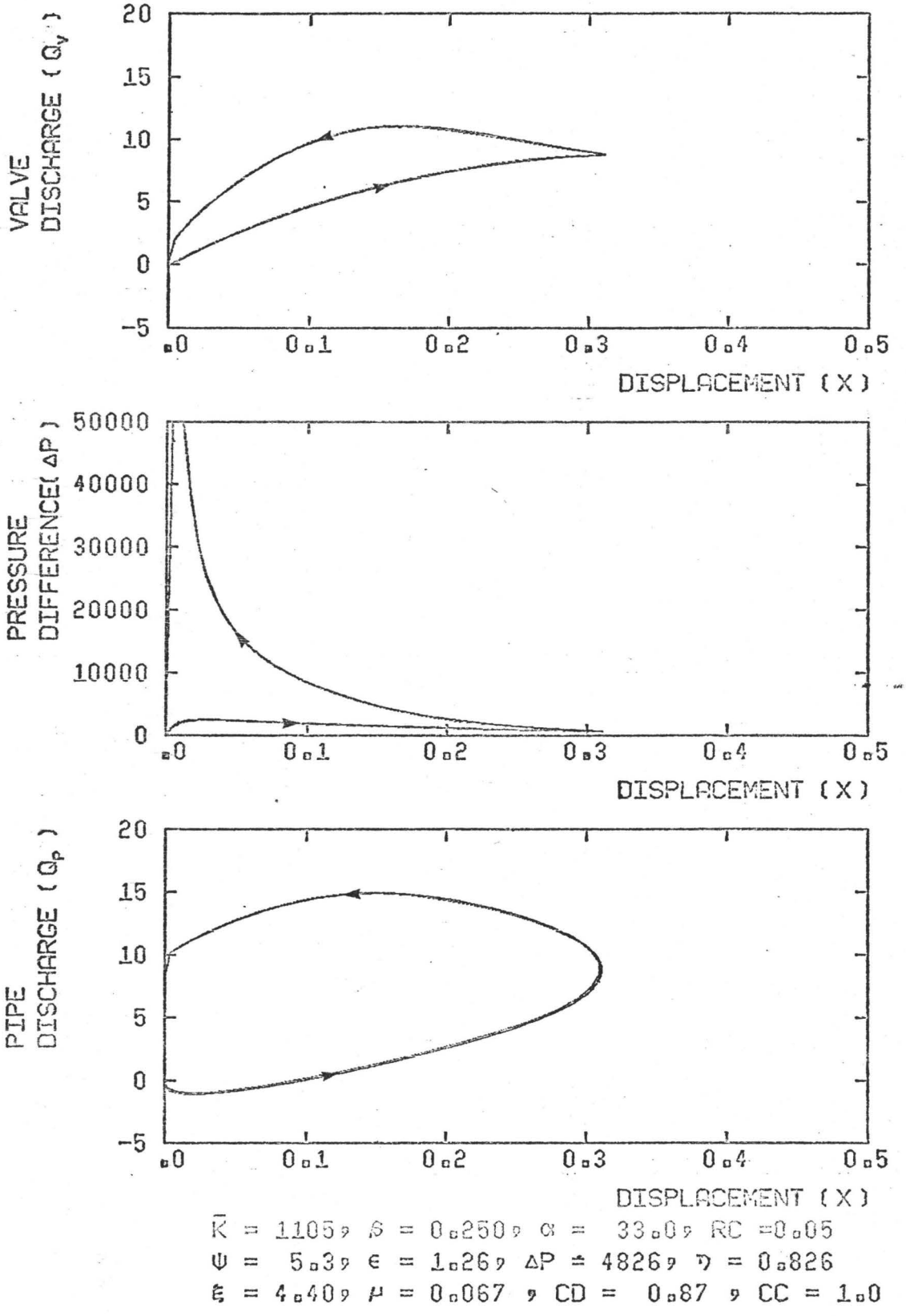

Fig. 7.5(b) Theoretical limit cycle oscillation as a function of displacement.

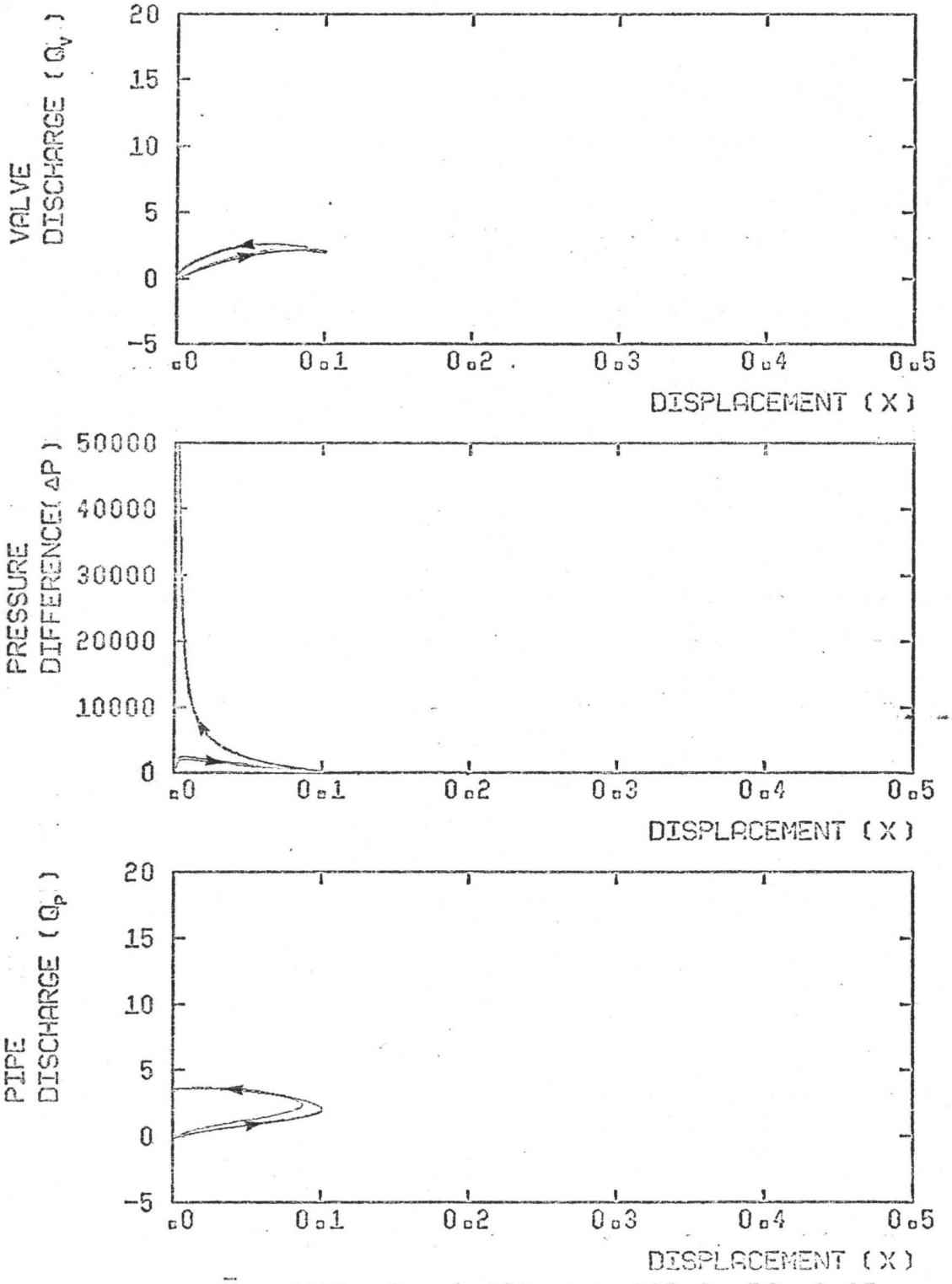

Fig. 7.5(c) Theoretical limit cycle oscillation as a function of displacement.

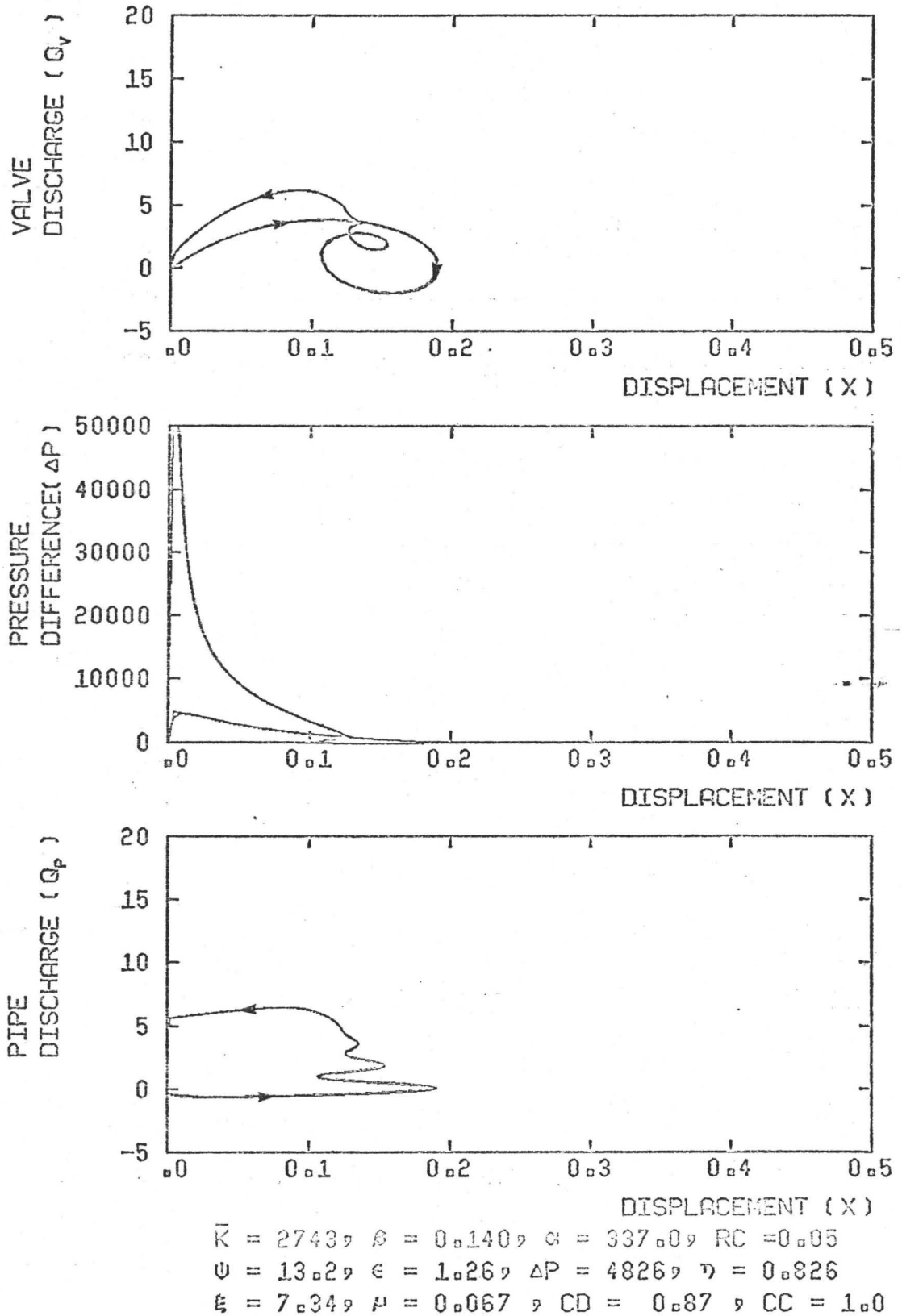

Fig. 7.5(d) Theoretical limit cycle oscillation as a function of displacement.

and valve discharge vary with valve displacement. The pipe discharge and pressure differences plotted correspond to those in Figure 7.4. Valve discharge represents flow through the gap of the valve at any instant.

Comparison of Figure 7.5 with Figure 5.13 reveals that the pressure changes during closure are essentially the same i.e., the pressure difference across the valve rises as the valve approaches its seat. The opening portions of the cycles are also similar in that the pressure difference across the valve does not change appreciably. For all of the opening parts of the cycle, with the exception of the very first part of Figures 5.13(a) and 7.5(a), the theoretical pressure differences are higher than the experimental ones. This is consistent with the observation that the valve opens faster experimentally than theoretically predicted.

The theoretical graphs of pipe discharge do not indicate large backward pipe flows, however some reverse flow is evident at larger openings. The valve discharge curve shows that reversal of flow in the pipe does not mean flow reversal in the valve gap. In fact, reverse flow through the gap is only observed in Figure 7.5(d) among the theoretical curves being examined. This occurs due to the valve overshooting and on the way back towards the seat, flow is pushed back through the gap, because, this provides the path of least resistance to the fluid.

The closing part of the cycle shows that the pipe flow changes slowly until the valve closes, when, it is abruptly

halted. In contrast, the valve discharge goes smoothly to zero. When one considers that the mass of fluid in the pipeline is very much larger than the mass of the valve plug, it is not surprising that the pipe flow undergoes such a sharp change, since a drop in pressure behind the valve affects the valve much more than the water in the pipeline. Hence the valve keeps closing until the discontinuity of the valve impacting on the seat occurs, when pipe flow suddenly is arrested.

As previously mentioned, discharge coefficient calculations in Chapter 5 were initially performed without accounting for the pumping action of the valve. It can however be seen from Figure 7.5 that the pipe and valve discharges are very different. Hence to make meaningful discharge coefficient calculations it is necessary to know the velocity of the valve and the effective pumping area of the valve accurately. This certainly has caused scatter in the discharge coefficients calculated in Chapter 5.

In conclusion, Figures 7.4 and 7.5 reveal that the closing portion of the valve cycle is predicted well by theory, however, the opening part of the limit cycle presents a limitation on how well the valve vibrations were predicted.

7.3.2 Large Inertia Vibrations

Figures 7.6 and 7.7 show the effect of changing initial opening and stiffness on the self-excited plug valve vibrations. The left hand diagrams present the experimental data whilst on the right the theoretical predictions corresponding to the

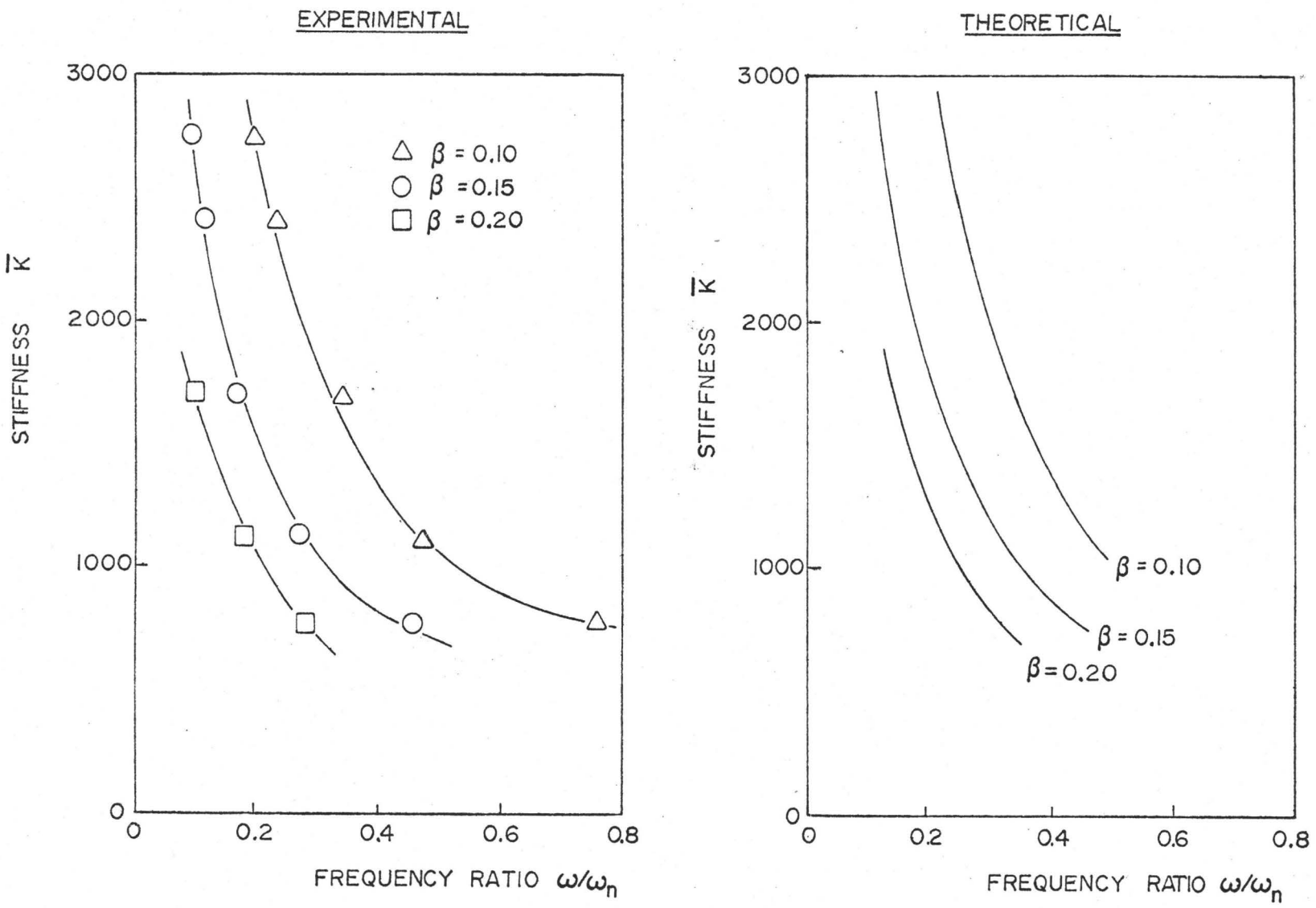

Fig. 7.6 Effect of stiffness on frequency ratio (α=354, ε=1.256)

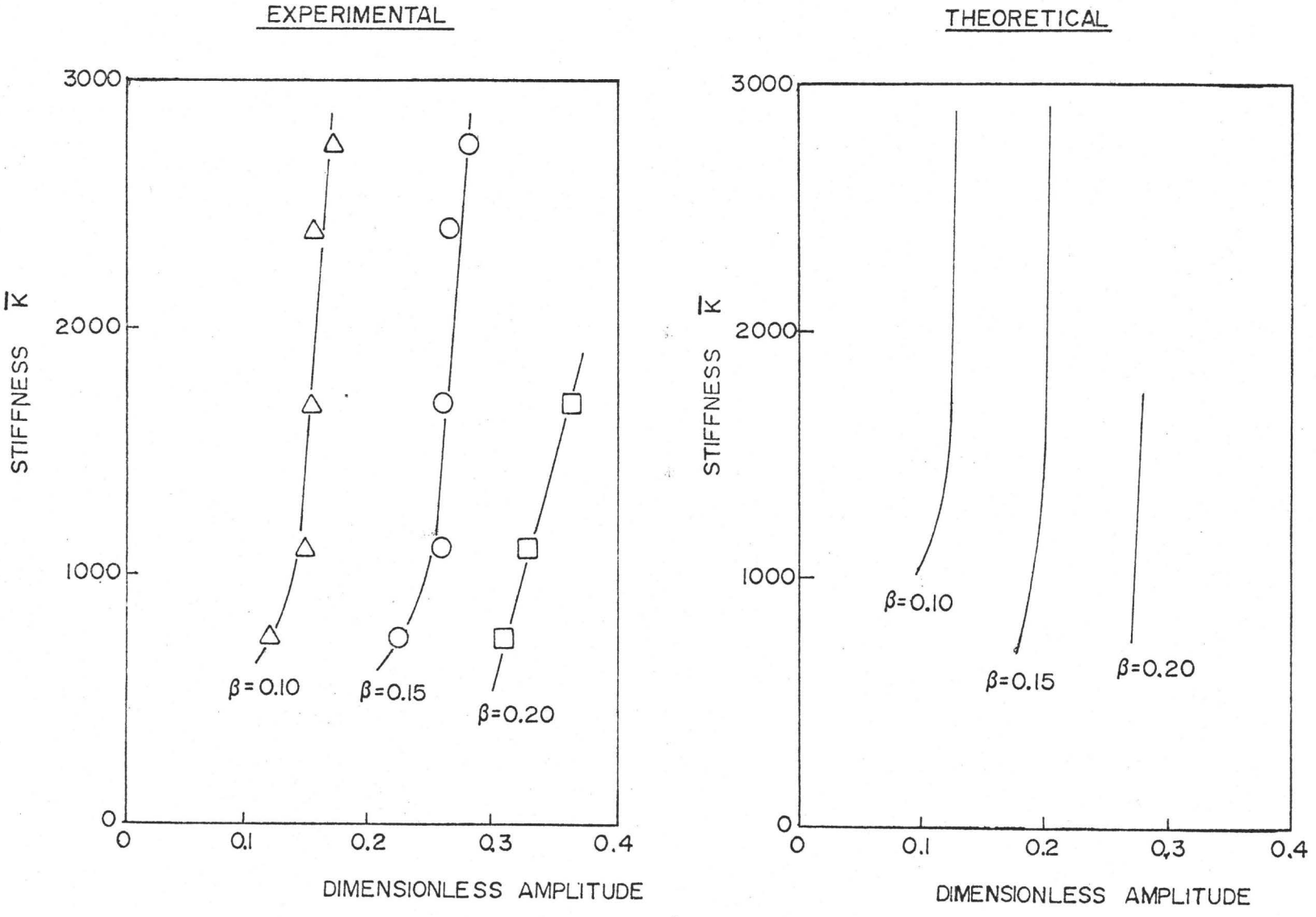

Fig. 7.7 Effect of stiffness on amplitude (α=354, ε=1.256)

experiments are presented.

Both of these diagrams show that the effect of changing stiffness or initial opening is the same for each set of curves. That is to say that the theoretical and experimental trends are the same. The theoretical frequency ratios are higher than the corresponding experimental ones. Weaver and Ziada [6] reported that their modelling of a swing check valve resulted in the same sort of deviation in frequency ratio. This discrepancy was thought to be due to the dynamic discharge characteristics of the valve being different from the static ones. Since dynamic discharge effects have not been compensated for in obtaining the theoretical results it is probable that this is a major contributor to the discrepancy in frequency ratio.

Amplitudes predicted theoretically are lower than those obtained experimentally. While it may have been a good approximation to take a coefficient of restitution of 0.05 for the check valve vibrations, it does not fit the opening characteristics of the plug valve. This is responsible for the substantial discrepancy in the magnitude of the amplitudes.

These results indicate that for large inertias that the mechanism of instability is fundamentally modelled correctly and some minor adjustments in the behaviour of the theoretical model on the opening portion and proper discharge coefficient estimations could result in improvements, particularly in the prediction of vibration amplitude.

7.3.3 Changes of Characteristics with Inertia

Figures 7.8 and 7.9 show the effect of fluid inertia on the period of vibration and the amplitude. The effect of increasing fluid inertia is to increase the period of vibration in such a fashion that the period is proportional to the inertia. The period predicted by the theory is generally about ten percent lower than the experimental results. This sort of discrepancy is to be expected in light of the fact that substantial reverse pipe flow at the beginning of the cycle is not predicted by the theory. Such a reverse initial flow in the theory would undoubtedly lead to a longer period of vibration.

The amplitude variation is separated into distinct regimes. At the lower fluid inertias the quick reestablishment of flow results in a large drag on the plug valve being rapidly established. The theoretical curve levels off after this and the fluid inertia has no effect on amplitude. The experimental curve on the other hand after levelling off starts to increase again. This has been attributed in Chapter 5 to be an effect of water hammer waves. The implicitly assumes that a longer pipe means a stronger water hammer wave bouncing the valve off its seat.

The drop at the lower end of the curves is much sharper for the experimental curves than for the theoretical curves. This may be due to the very rapid flow reestablishment and hence the variation in dynamic discharge coefficient at small openings may be an important factor. The discharge coefficient drops rapidly near the closed position. This lowering of the

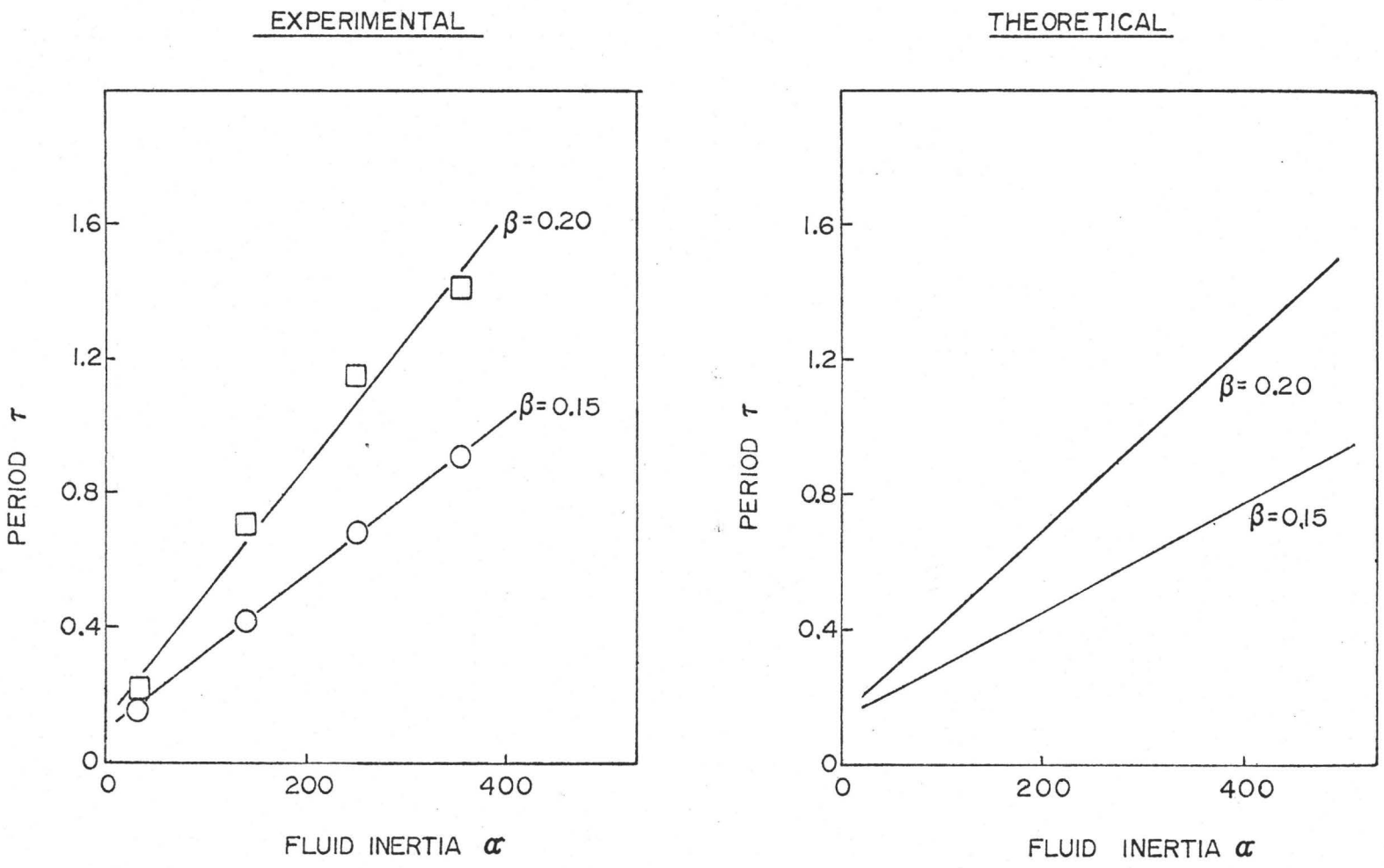

Fig. 7.8 Effect of fluid inertia on period of vibration ($\bar{k}$=1695)

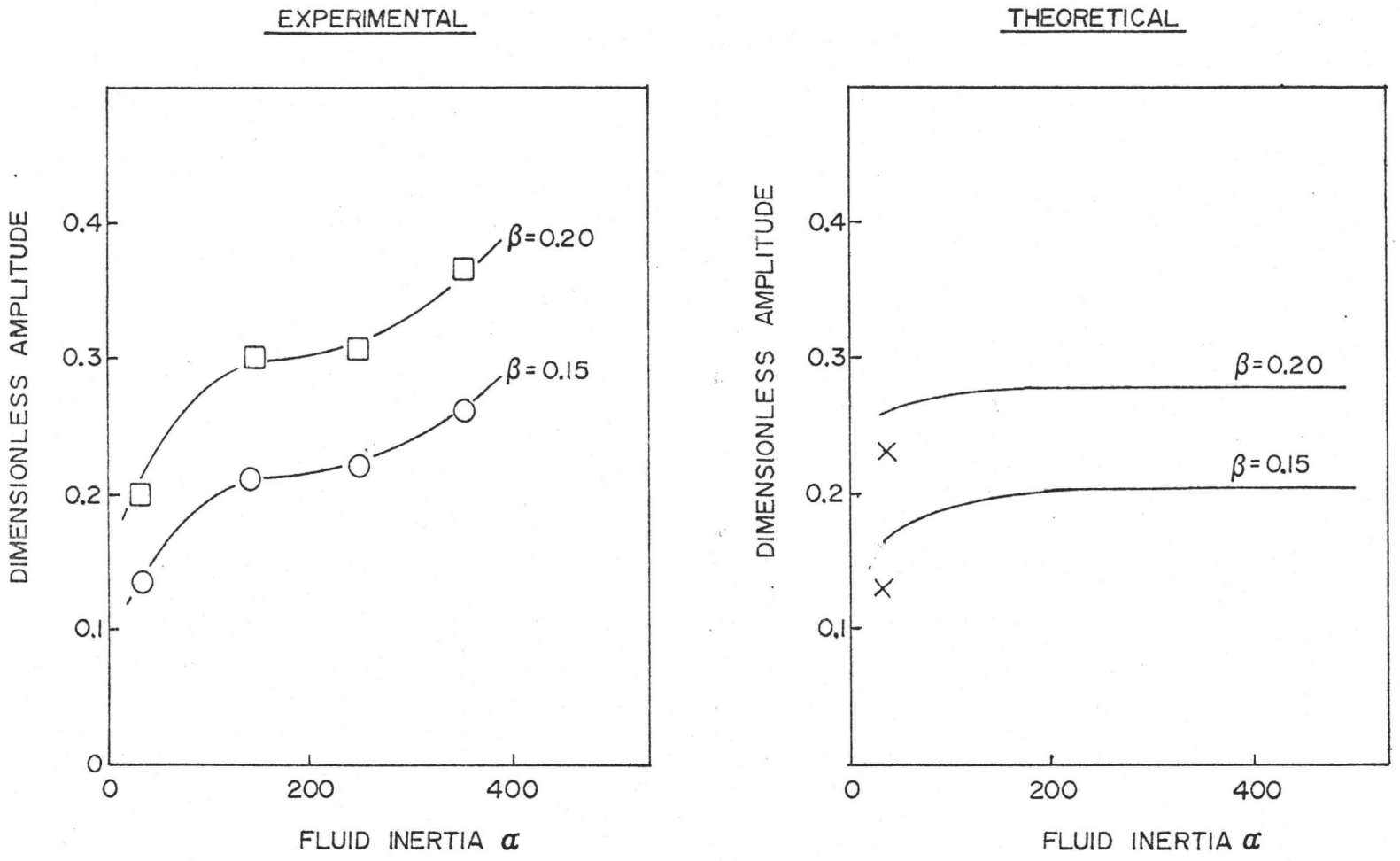

Fig. 7.9 Effect of fluid inertia on amplitude of vibration ($\bar{k}$=1695)

discharge coefficient would result in a lower amplitude. Weaver and Ziada [6] show that reducing the discharge coefficient at high fluid inertias results in a slight decrease in amplitude. At low fluid inertias this effect may become much more marked as the flow through the valve is much higher by the time the valve reaches its highest point. To test this hypothesis two further computer runs were done at a fluid inertia $\alpha = 33$ with a discharge coefficient of 0.4. The result obtained was that amplitudes of 0.23 and 0.13 were obtained for initial openings of $\beta = 0.20$ and $\beta = 0.15$ respectively as indicated by crosses in Figure 7.9. These computations also had about a ten percent shorter period of vibration. The computations show that discharge coefficient reduction does result in a decrease in amplitude at small fluid inertias.

7.4 Effect of Neglecting Pumping

The purpose of this section is to establish what effects neglecting the pumping term has on the theoretical predictions and to determine whether better results are obtained by its inclusion in the equations of motion.

The effect of pumping on stability has already been theoretically established. In Chapter 6 the derivation for a long pipe stability threshold showed that the pumping parameter ε was not important. Figure 7.1 showed that the exclusion of the pumping resulted in minor changes in the stability threshold.

Figure 7.10 shows how the frequency ratio and amplitude of vibration vary with stiffness. The frequency ratio predictions including pumping are better than the theory without pumping, however for the vibration amplitudes the reverse appears to be true. The amplitudes are, however dependent on the value chosen for the coefficient of restitution, and consequently is not as important in indicating the performance of the theory as the frequency is.

As stiffness is decreased, the inclusion of pumping results in a close match in frequency ratio, while omitting the pumping result in substantial deviation from the experimental curve. The experimental amplitude drops off as stiffness is decreased in Figure 7.10. This drop in amplitude occurs only when pumping is included, hence local flow around the valve is an important factor in determining the amplitude at low stiffnesses.

Figure 7.11 shows the effect of varying initial opening on the frequency ratio and amplitude. The effect of increasing initial opening and that of increasing stiffness on frequency ratio is identical, and the curves drawn in Figure 7.11 vary in the same manner as they do in Figure 7.10. At small openings the frequency ratio curve with $\varepsilon = 1.256$ (pumping included) falls below the experimental curve. The reason for this is that at small openings, the opening portion of the cycle tends to be elongated and dominate the period. This is exemplified by comparing Figure 7.4 (c) to Figure 5.11. Notice how slowly the displacement increases with time initially. Amplitude

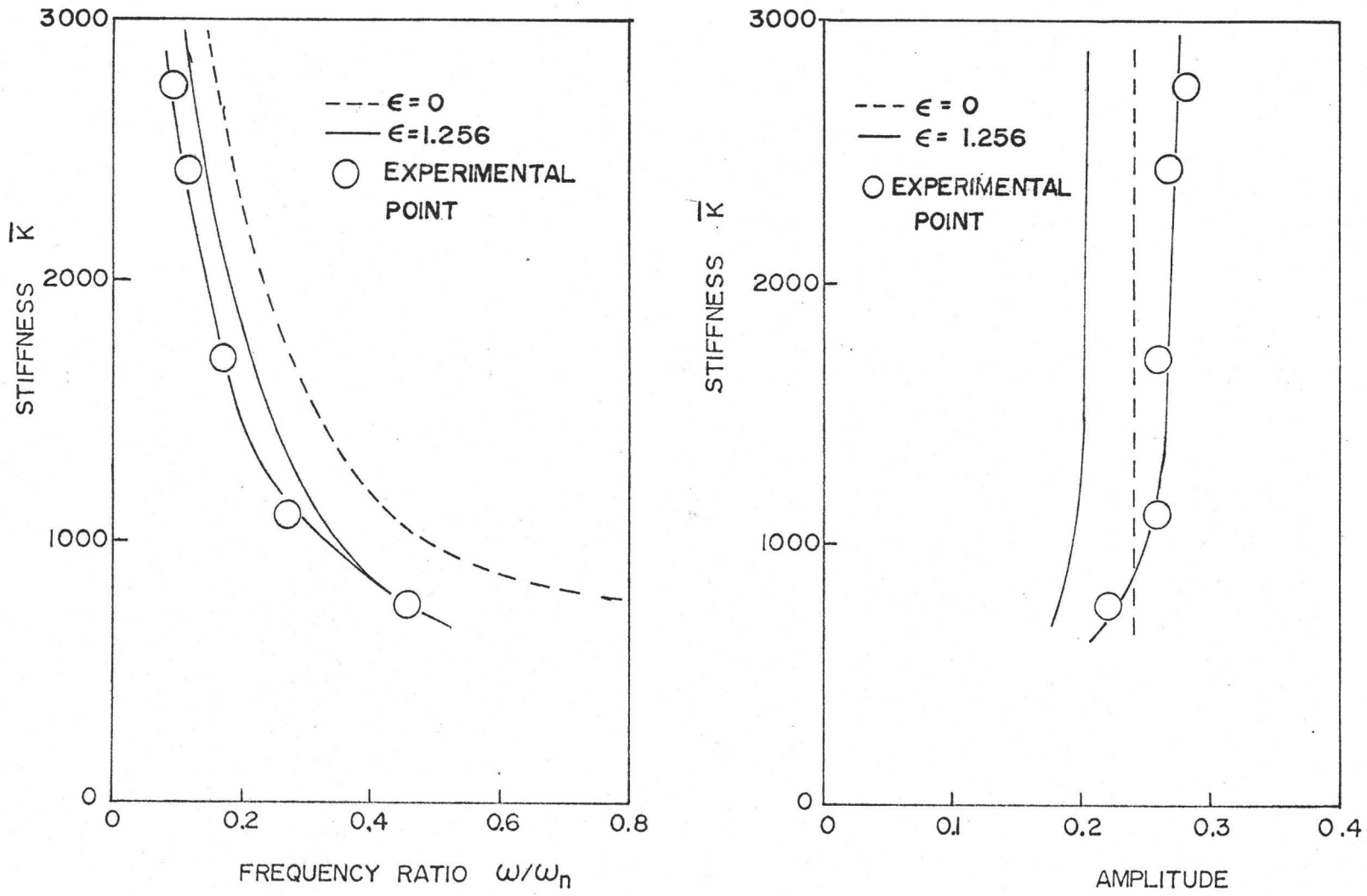

Fig. 7.10 Effect of neglecting pumping action, variation of frequency ratio and amplitude with stiffness (β=0.150, α=354)

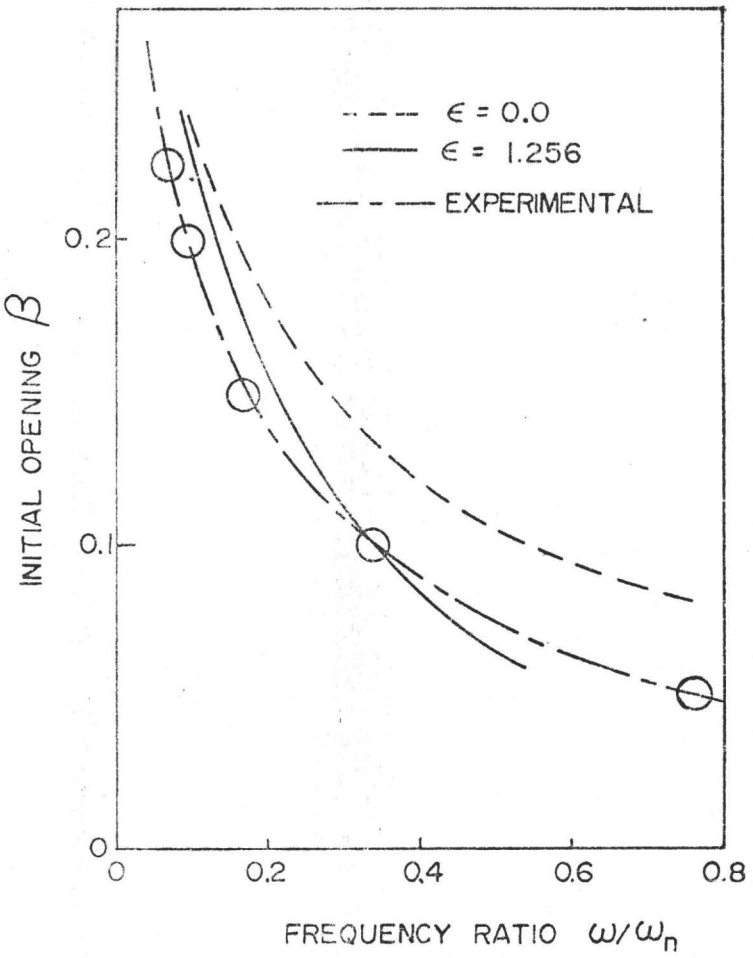

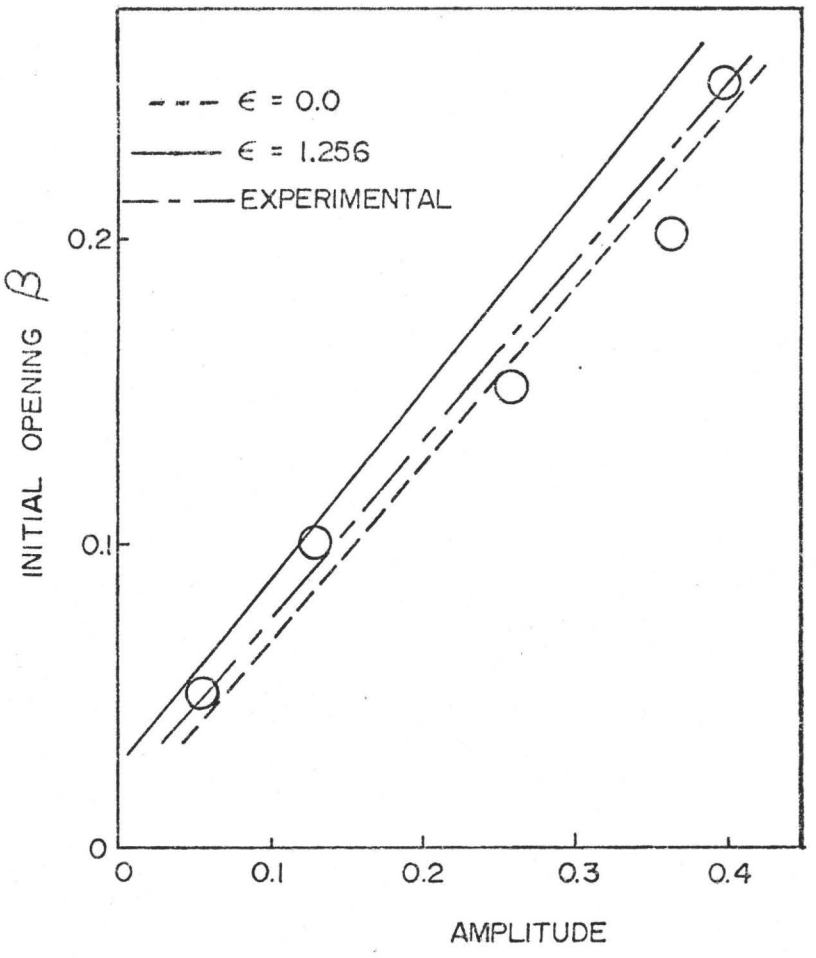

Fig. 7.11 Effect of neglecting pumping action, variation of frequency ratio and amplitude with initial opening ($\bar{k}$ = 1695, α=354)

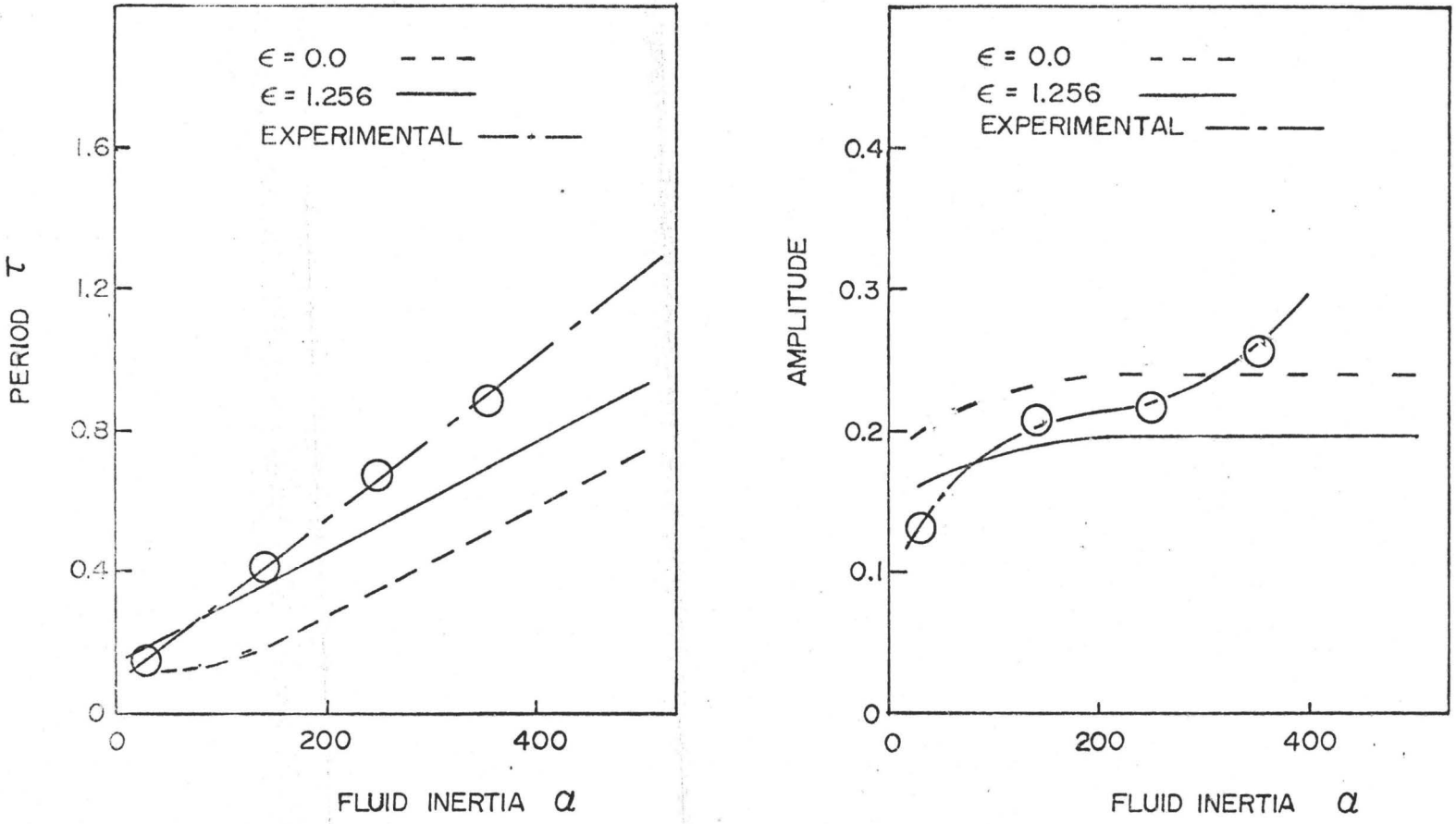

Fig. 7.12 Effect of neglecting pumping action, variation of vibration period and amplitude with fluid inertia ($\overline{K}$=1695, β=0.15)

predictions without pumping are better than those with pumping, both however predict the linear proportionality between amplitude and initial opening correctly.

Figure 7.12 shows that the period of vibration is directly proportional to inertia. The formulation of the valve model without pumping deviates from proportionality at small fluid inertias. It is clear, however, that the inclusion of pumping gives better predictions of the period of vibration.

Amplitude predictions, with and without pumping, follow the same trend, rising as low fluid inertias and flattening off at higher fluid inertias. The experimental amplitude rises more rapidly at low inertias. This difference between the experimental and theoretical amplitude trends predicted, is undoubtedly due to not having accurate knowledge of the actual fluid inertia when the fluid inertia is small. That is, because the inertia of the jet through the valve orifice is unknown, a discrepancy between theoretical predictions and experimental results arises. At higher fluid inertias, the experimental amplitude rises again. This is probably due to more violent waterhammer waves at longer pipe lengths. Such an effect is not accounted for by the theory.

The reasons why the pumping term was added to the theory initially are discussed at the end of Chapter 5. Such factors as discharge coefficient calculations and reverse flow in the pipe have made this addition necessary. The addition of pumping to the theory has resulted in amplitudes that are in general further from the experimental amplitudes. Periods of vibration

(and frequency ratios) are, however, predicted more accurately by the inclusion of pumping. Experimental evidence indicates that the initial phase of the vibrations are not predicted correctly. This is however, a strong function of the coefficient of restitution used in the theory, hence emphasis should be placed on the period predictions rather than amplitudes. Thus the inclusion of pumping improves the theory.

7.5 Discussion and Conclusions

Results in this Chapter indicate that the fundamental modelling of the valve vibration is essentially correct. Predictions of stability thresholds have been made. Predictions from the integration of the nonlinear equations of motion show excellent agreement with experimental results for the upper stability threshold. The inclusion of pumping does not appear to significantly affect this upper stability threshold.

Upper stability threshold predictions have been made using theoretical stability analysis at a point. The divergence formula derived in Chapter 6 from the nonlinear model (which is identical to the static analysis formula of Chapter 6) shows excellent agreement with both the nonlinear integration and the experimental results. The general trends of Kolkman's stability predictor agree with experimental observations, however, the theory developed in this thesis is superior.

Only the nonlinear theory is capable of predicting the lower stability threshold. These predictions have not been as accurate as the predictions for the upper threshold. Better

predictions of this threshold would be possible by changing the value of the coefficient of restitution. It should be noted however, that the valve's resting position below the static characteristic (see Figure 5.1) is the closed one. From a practical point of view, control of valve position has been lost in this case. Hence the prediction of the lower threshold is not as important as predicting the upper stability threshold.

Comparison of time histories, amplitudes and frequencies have shown that the nonlinear model performs well except in the opening portion of the valve vibration. This again is due to poor predictions of initial valve velocity as it moves off the seat. Thus, discrepancies arise due to a single point in the vibration being underestimated, rather than fundamental errors in the modelling of the valve motion or fluid mechanics.

Comparison of the nonlinear theories including and excluding the effect of pumping have shown that pumping does affect the amplitude and period of vibration. The general behaviour of the valve with and without pumping is similar. An opening portion occurs where the valve behaves more or less as a system undergoing free oscillations. A dwell portion may then occur if the fluid inertia is large, followed by sudden valve closure.

The upper stability threshold does not seem to be affected by pumping at large fluid inertias. This is in fact predicted by the divergence formula of Chapter 6. Pumping is associated with a time derivative and hence cannot enter the

static analysis which may be used to determine divergence phenomena. It is also interesting that the dynamic discharge coefficient variation does not affect the stability threshold, at large fluid inertias. This is probably due to the fact that when sufficient flow is reached for instability that the pressure rises across the valve so quickly that a change in discharge coefficient is only a second order effect.

The largest uncertainty in the present investigation seems to be related to the exact estimation of pumping. Certainly with the configuration used, the area of the piston is not clearly defined and approximations have had to be made. This clearly has effects on the local flow around the valve. Hence further work should be concentrated on local flow effects in the vicinity of the valve. The actual pressure distribution and flow around the valve would be of most interest.

In conclusion, the theory derived in this thesis has provided for an excellent prediction of the upper stability threshold of the plug valve and reasonably good predictions of the lower stability threshold, time histories, amplitudes and frequencies. The theory is fundamentally correct and further improvement could likely only be obtained by properly modelling water hammer and local flow effects.

CHAPTER 8

CONCLUSIONS

The first Chapter of this thesis stated that one of the objectives of this research was to further our knowledge of valve vibration mechanisms. Various works on the jet-flow inertia mechanism have been examined and these models have been classified as linear and nonlinear models. Of the linear models, those of Abelev and Dolnikov [13], and Lyssenko and Chepajkin [14] breakdown to negatively damped simple harmonic oscillators dependent on discharge coefficient variation as an excitation mechanism. The linear model of Kolkman [4] and the nonlinear model of Weaver and Ziada [6] do not require a variable discharge coefficient in their instability mechanisms. Hence the latter two models are superior and further examination of them was undertaken. In the case of Kolkman's theory, this has simply been applied to the plug valve configuration, whereas the model of Weaver and Ziada has been extended to account for pressure recovery and pumping. A Routh-Hurwitz analysis has also been applied to the nonlinear model. These theoretical additions to Weaver and Ziada's model have been presented in Chapter 6.

Experiments have been performed so that the theories could be evaluated. Quantitative measurements of limit cycle displacement, pressure variations and fluid discharge have

been made. These results are necessary for validation and evaluation of the theoretical model.

Analysis of the plug valve system started in Chapter 4, where the free vibrations and static discharge characteristics of the plug valve were considered. From these, two important characteristics were examined. Firstly, information on the free vibration of the plug valve was used to estimate added mass and damping in water. Secondly, the static discharge characteristic of the plug valve revealed that pressure recovery was important and that the static discharge coefficient was essentially constant over a wide range of openings. Hence at the outset, one of Weaver and Ziada's assumptions [6] was found to be questionable in this particular application, i.e. pressure recovery was not negligible.

Using the experimental results reported in Chapter 5, it has been possible to show how frequency, frequency ratio and amplitude are affected by changing spring stiffness, initial opening and fluid inertia. Further experiments showed how discharge varied throughout the valve cycle. The discharge variation obtained indicated the need for inclusion of pumping.

Weaver and Ziada [6] recommended that measurement of the dynamic discharge coefficient be the next step in refining their general model. The experiments have indicated that, in the plug valve configuration considered, two of their assumptions were not accurate. Hence the model was refined by allowing for pressure recovery and pumping. The theory

derived to allow for these two modifications is rather cumbersome. However, this is not a major difficulty since numerical integration of the differential equations of motion must be performed anyway. That is, the majority of the program is not devoted so much to the differential equations themselves as to: integration, input, output and plotting the theoretical vibration cycle.

Modifications to allow for variation in the dynamic discharge coefficient were not made in the computer program. This was found to be impossible because the dynamic discharge coefficient obtained in Chapter 5 had no obvious relation to acceleration and deceleration of the fluid or valve.

Even though the dynamic discharge coefficient variation through the cycle was not used in computation, the upper stability threshold prediction was very close to the experimental threshold. This is particularly true for large fluid inertia. The upper stability threshold was also predicted at large fluid inertias using a Routh Hurwitz stability analysis [33]. This prediction coincided with that of the nonlinear theory and agreed very well with the experimental results. These results gave better predictions than the theory of Kolkman [4], probably due to the theory presented here having accounted for local flow effects more thoroughly. The fact that the stability threshold predictions agree so well with the experiments indicate that the dynamic discharge coefficient does not play a significant role in determining the stability of this configuration.

The lower stability threshold predictions are not as good as the upper stability threshold predictions. One of the problems associated with predicting this threshold has been the opening of the valve. Waterhammer theory incorporated into the computer program could be used to supply a prediction for: the time for which the valve remains shut, the maximum pressure experienced as well possibly the initial velocity of the valve and fluid in the pipe upon the opening of the valve. Moreover, with such programming included, predictions for maximum waterhammer pressure experienced in a transient case, such as in a pump shutdown, could be predicted.

Experimental development is also possible. These experiments should be aimed at understanding the forces acting on the plug valve. This might be possible by instrumenting the plug valve and measuring the pressure distribution around it. Integrating this distribution would give the force acting on the valve. Any further developments using this course of action are expected to be minor however, due to the proven workability of the theory in its present state.

REFERENCES

1. Weaver, D. S. and Adubi, F. A., "Flow Visualization Studies of Check Valve Vibrations", Proceedings of the Symposium on Turbulence in Fluids, University of Missouri-Rolla, 1975, J. L. Zakin, G. K. Patterson Editors, Science Press, Princeton, N.J., 1977, pp 201-209.

2. Beard, C. S., "Final Control Elements: valves and actuators", Rimback Publications Division, Chilton, G., Philadelphia, PA, 1969.

3. Ziada, S. R., "A Mechanism for Self-Excitation in Hydraulic Control Devices", M.Eng. Thesis, McMaster University, Hamilton, Ontario, Canada, 1977.

4. Kolkman, P. A., "Flow-Induced Gate Vibrations: prevention of self-excitation computation of dynamic behaviour and the use of models", Doctoral Dissertation, publication no. 164, Delft University of Technology, Delft, Holland, 1976.

5. Weaver, D. S., "Flow Induced Vibrations in Valves Operating at Small Openings", IUTAM/IAHR Symposium on Practical Experiences with Flow Induced Vibrations, Karlsruhe, Germany, 1979, Springer Verlag, 1980, pp. 305-319.

6. Weaver, D. S. and Ziada, S., "A Theoretical Model for Self-Excited Vibrations in Hydraulic Gates, Valves and Seals", Trans. ASME, Jo. of Pressure Vessel Technology, Vol. 102, May 1980, pp. 146-151.

7. Fung, Y. C., "An Introduction to the Theory of Aeroelasticity", John Wiley & Sons, Inc., New York, N.Y., 1957.

8. Kasai, K., "On the Stability of a Poppet Valve with an Elastic Support 1st Report", Bulletin JSME, Vol. 11, No. 48, 1968, pp. 1068-1083. "2nd Report", Bulletin JSME, Vol. 12, No. 53, 1969, pp. 1091-1098.

9. Ainsworth, F. W., "The Effect of Oil Column Acoustic Resonance on Hydraulic Valve Squeal", Trans. ASME, Vol. 78, 1956, pp. 773-778.

10. Ezekiel, F. D., "The Effect of Conduit Dynamics on Control Valve Stability", Trans. ASME, Vol. 80, pp. 904-908, 1958.

11. Ito, T., Muto, T., Suzuki, K., and Isukahara, K., "Study of the Self-Sustained Oscillation of a Piston-Type Valving System 1st Report", Bulletin JSME, Vol. 10, No. 41, 1967, pp. 793-807, "2nd Report", Bulletin JSME, Vol. 11, No. 45, 1968, pp. 487-495.

12. Thomann, H., "Oscillations of a Simple Valve Connected to a Pipe", Jo. Applied Math. Phys. (ZAMP), Vol. 27, pp. 23-40, 1976 and "Part II Experiments", Jo. Applied Math. Phys. (ZAMP), Vol. 29, pp 75-85, 1978.

13. Abelev, A. S., and Dolnikov, L. L., "Experimental Investigations of Self-Excited Vibrations of Submerged Vertical-Lift Hydraulic Gates", IUTAM/IAHR Symposium on Flow Induced Structural Vibrations, Karlsruhe, Germany, 1972, Springer-Verlag, 1974, pp. 265-277.

14. Lyssenko, P. E. and Chepajkin, G. A., "On Self-Excited Oscillations of Seals Concerning the Gates of Hydrotechnical Structural Vibrations", IUTAM/IAHR Symposium on Flow-Induced Structural Vibrations, Karlsruhe, Germany, 1972, Springer-Verlag, New York, N.Y., 1974, pp. 278-296.

15. Weaver, D. S., Adubi, F. A. and Kouwen, N., "Flow Induced Vibrations of a Hydraulic Valve and their Elimination", Trans. ASME, J. Fluids Engineering, Vol. 100, June 1978, pp. 239-245.

16. Weaver, D. S., "On Flow Induced Vibrations in Hydraulic Structures and their Alleviation", Canadian Journal of Civil Engineering, Vol. 3, No. 1, 1976, pp. 126-137.

17. Lamb, H., "Hydrodynamics", 6th Edition, Dover Publications Inc., New York, N.Y. 1932.

18. Fritz, R. J., "The Effect of Liquids on the Dynamic Motions of Immersed Solids" ASME Design Engg. Vib. Conf., Toronto, Ontario, Canada, paper 71-Vibr.-100.

19. Logvinovich , G. V. and Savchenko, YU, N., "A Study of Hydrodynamic Forces Attending Sinusoidal Vibrations of a Disk", Fluid Mechanics Soviet Research, Vol. 2, No. 4, 1973, pp. 36-41.

20. Chandrasekaran, A. J., Saini, S. S. and Malhotra, M. M., "Virtual Mass of Submerged Structures", ASCE J. Hydraul. Div., Vol. 98, (HY5), 1972, pp. 887-896.

21. Mcloy, D., "Effects of Fluid Inertia and Compressibility on the Performance of Valves and Flow Meters Operating Under Unsteady Conditions", J. Mech. Eng. Sci., Vol. 8, No. 7, 1966, pp. 52-61.

22. Daily, J. W. Hankey, W. L., Olive, R. W. and Jordaan, J. M., "Resistance Coefficients for Accelerated and Decelerated Flows through Smooth Tubes and Orifices", Trans. ASME, July 1956, pp. 1071-1077.

23. McCloy, D. and McGuigan, R. H., "Some Static and Dynamic Characteristics of Poppet Valves", Proc. Convn. on Advances in Automatic Control, Proc. Instn. Mech. Eng., Vol. 179, pt. 3H, paper 23, 1964-5, pp. 199-213.

24. Alpay, S. A., "The Flow Coefficient of a Hydraulic Control Valve Under Dynamic Conditions", Flow; Its Measurement and Control in Science and Industry, Vol. 1, part 3, W. E. Vannah and, H. Wayland Editors, Instrument Society of America, Pittsburgh, PA, 1974, pp. 1227-1234.

25. Thermo System Inc., "Series 900 Optics", "Model 1090 Tracker Manual" TSI, St. Paul, Minnesota, U.S.A.

26. Drain, L. E., "The Laser Doppler Technique", John Wiley and Sons, New York, New York, 1980.

27. Thompson, W. T., "Theory of Vibration with Applications", Prentice-Hall, Englewood Cliffs, N.J., 1972.

28. Adubi, F. A., "The Hydroelastic Vibration of a Hydraulic Swing Check Valve", PhD Thesis, McMaster University, Hamilton, Ontario, Canada, 1974.

29. Wood, D. J., "Influence of Line Motion on Waterhammer Pressures", J. Hydraulics Division, Proc. ASCE, May 1969.

30. George, W. K. Jr., "Limitations to Measuring Accuracy Inherent in the Laser Doppler Signal", Proc. LDA - Symposium, Copenhagen, 1975. Hemisphere Publishing Corporation, Washington, D.C., 1976.

31. Miller, D. S., "Internal Flow Systems", BHRA Fluids Engineering, Cranfield, England, 1979.

32. Schonfeld, J. G., "Resistance and Inertia of the Flow of Liquids in a Tube or Open Canal", Applied Scientific Research, Vol. A1, 1949, pp. 169 - 197.

33. Hayashi, C., "Nonlinear Oscillations in Physical Systems", McGraw-Hill, New York, New York, 1964.

34. Streeter, V. L., "Fluid Mechanics", 6th edition, McGraw-Hill, New York, New York, 1975.

APPENDIX A

ADDITIONAL NOTES ON THE LASER DOPPLER ANEMOMETER

The basic method of setting up the Laser Doppler Anemometer is given in the Thermo-Systems Inc. manuals [25]. In this Appendix, the method of locating the beam crossing points is described and the relationship between velocity and tracker output is calculated.

Location of Measuring Volume (Beam Intersection Point)

As mentioned already in Chapter 3, the lens used to focus the laser beams was a Thermo-Systems Inc. Model 918 with a focal length of 248 mm. In such a lens the total included angle between the beams is 11.52^{o} for an initial beam separation of 50 mm. The optics were set up in such a manner that the plane of the beams intersected the pipe radially. This configuration limits beam freedom to the vertical plane. The anemometer was mounted on a table, which had two translational degrees of freedom in the horizontal plane, in such a way that the two translational axes were parallel and orthogonal to the plane of the laser beams. The table was moved using screws similar to those on a milling machine bed. The table axes were graduated to the nearest thousandth of an inch.

Using the table to move the anemometer the laser beam crossing point was located in the following way. A reference point was established where the laser beams intersected on the

front acrylic wall. The distance required to move the measuring volume to anywhere in the pipe was calculated using elementary optical formulae. Figure A1 shows a view of the optical path of a laser beam to the intersection point. Only the upper beam need be considered because of symmetry. Points X and Y represent the actual intersection point of the beams and the place where unrefracted beams would intersect respectively.

Using Snell's Law angles θ_2 and θ_3 can be calculated, given the refractive indices μ_1, μ_2, μ_3 and the incident light beam angle θ_1.

For this lens, $\theta_1 = 11.52/2 = 5.76^o$ and hence $\theta_2 = 3.86^o$ and $\theta_3 = 4.33^o$. Using elementary geometric calculations, one can show, as long as the beams intersect within the pipe, that

$$\ell = 32.58 + 0.75063\ a$$

or,

$$a = -43.40 + 1.332\ \ell$$

Both a and ℓ are in millimetres, ℓ is the distance the table moved forward from the reference point, a is the distance from the centreline of the pipe to the measuring volume.

Calculation of Velocity

The Thermo-Systems Inc. manual [25] gives the formula for the frequency of the signal,

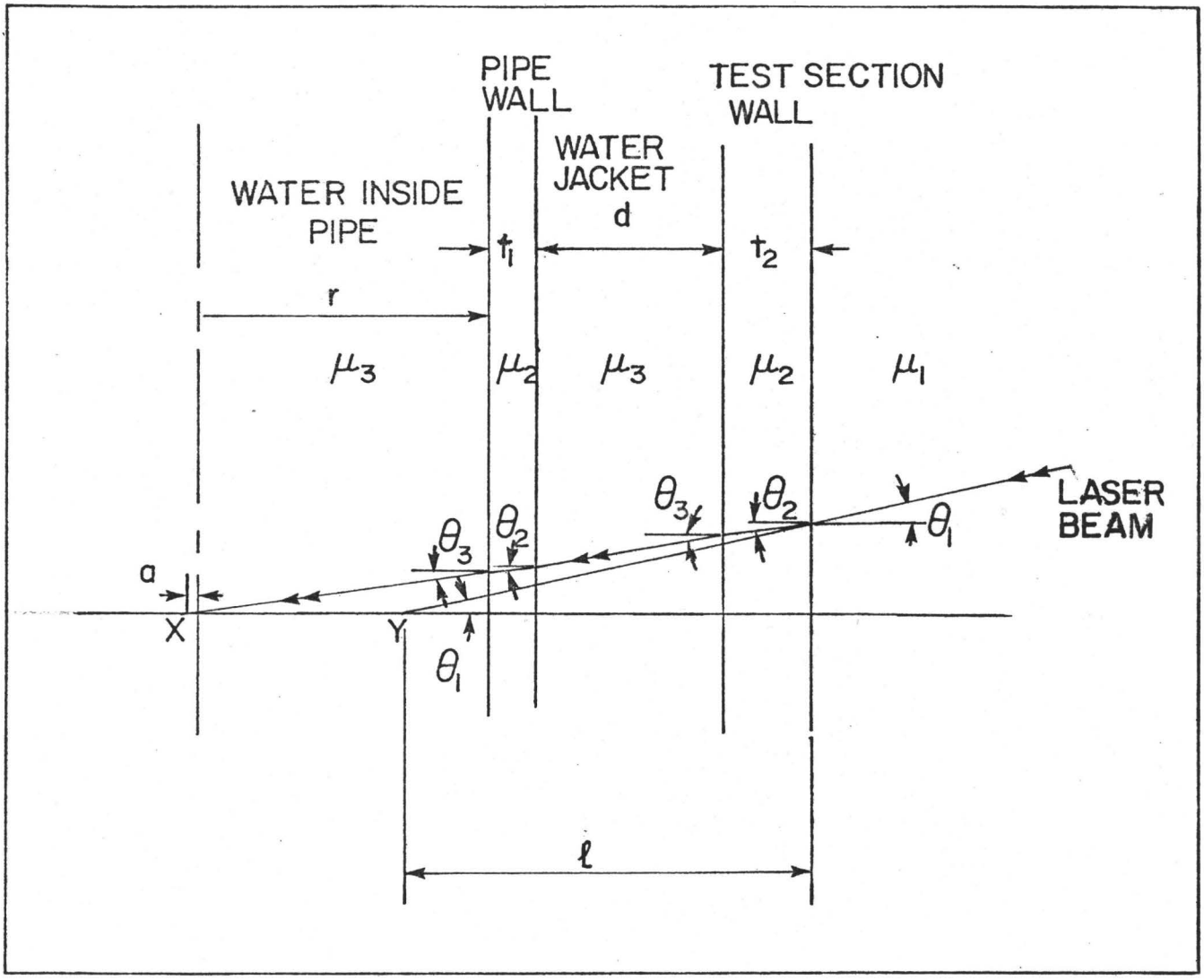

r = inside pipe diameter

t_1 = pipe wall thickness

t_2 = test section wall thickness

d = distance between pipe and test section wall

μ_1 = refractive index of air

μ_2 = refractive index of acrylic

μ_3 = refractive index of water

y = virtual beam intersection point

x = actual beam intersection point

Fig. A1 Optical path of laser beam through test section.

$$f = \frac{2\ U \sin\ (\phi/2)}{\lambda}$$

where U is the fluid velocity, ϕ is the total included angle between the intersecting laser beams, λ is the wavelength of the beam in air and f is the frequency of the doppler signal. From the Thermo-Systems Inc. manual λ = 632.8 nm and $\phi = 11.52/2 = 5.76^{o}$, then,

$$f = 3.172 \times 10^{5}\ U$$

where f is measured in Hertz and U is measured in metres/second. In experiments performed two tracker ranges were used, the lowest range where 0.01v of tracker output corresponds to 1 kHz and the middle range where 1 V of tracker output corresponds to 1 MHz. Hence the relationship between tracker output voltage and velocity becomes:

Lowest Range $\quad V = 3.172\ U + V_b$

Middle Range $\quad V = 0.3172 + V_b$

where V is in volts, U is in metres/second and V_b is the voltage measured when U = 0 due to the frequency shift of the Bragg Cell.

APPENDIX B

EVALUATION OF PLUG VALVE SYSTEM PARAMETERS

1.) The total mass of the plug, stem and spring cups in water has been determine experimentally in Chapter 4 and was found to be M = 1.254 kg.

2.) The area of the gap in Figure B.1 is given by

$$g = \pi(r_1+r_2)x \sin\theta \tag{B.1}$$

where g is the gap area. It can be shown that,

$$r_2 = r_1 - x \sin\theta \cos\theta \tag{B.2}$$

hence, combining equations (B.1) and (B.2),

$$g = \pi(2r_1 - x \sin\theta \cos\theta) \, x \sin\theta \tag{B.3}$$

This gap variation gives the gap area as a second order function of the value lift x, as shown in Figure 1.1.

Given that the radius at the bottom of the plug, r_3 = 16.7 mm, the maximum valve lift for which equation (B.3) holds can be found by substituting $r_2 = r_3$ in equation (B.2)

$$0 < x < 15.0 \text{ mm} \tag{B.4}$$

When choosing springs for experimentation, it was desired to keep the amplitudes of vibration fairly low so that large nonlinearities in the gap function did not occur. (The gap function being the variation of gap area with valve lift).

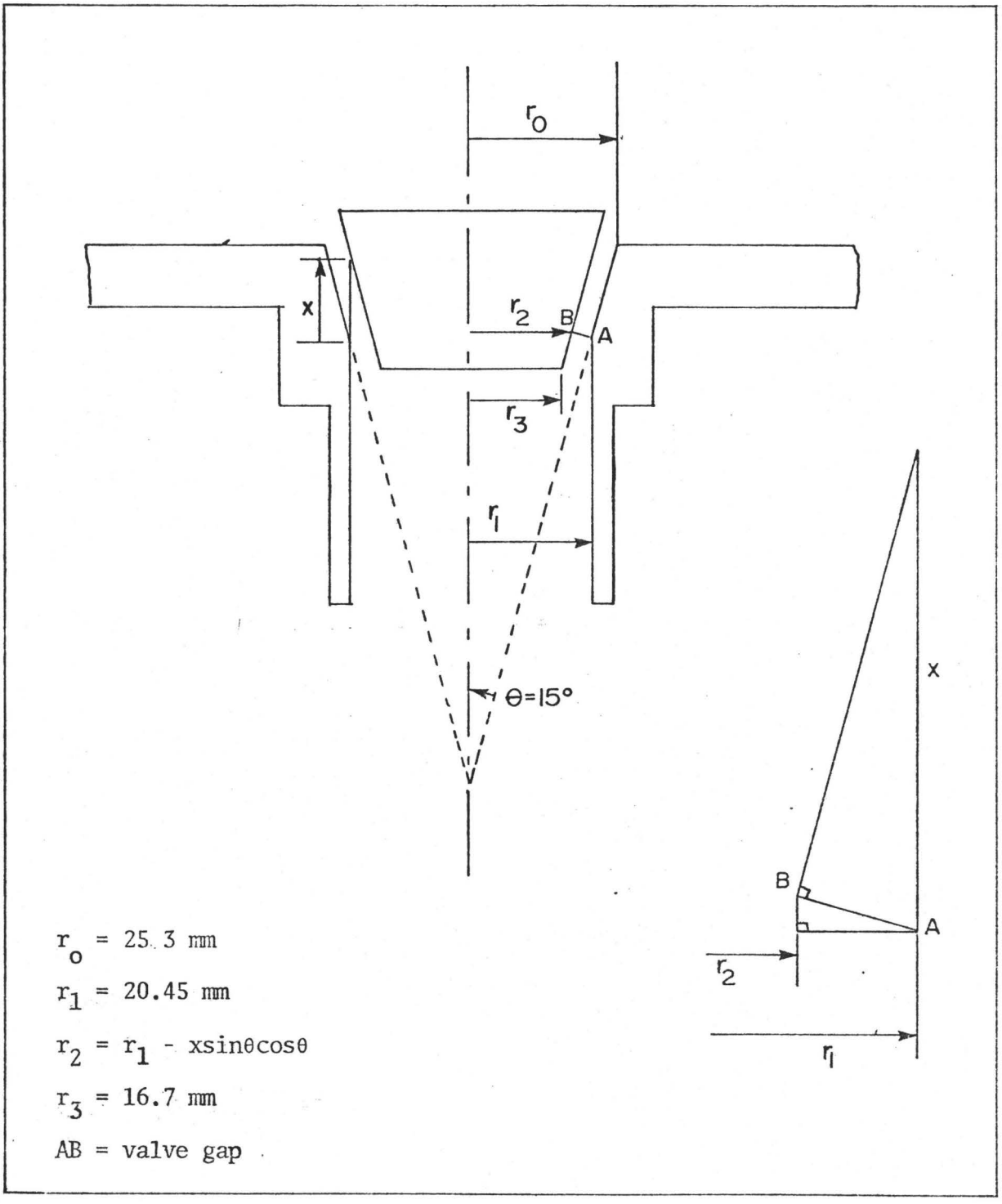

Fig. B1 Area of Valve Gap

12.7 mm (1/2") was thought to be a good upper bound on the openings through which the valve would perform excursions. The results in Appendix F show that amplitudes larger than this do occur. When this does occur, it is however, for very short periods of time at the beginning of the valve's limit cycle. It would not be wise therefore, to give the larger gap openings much weighting in evaluating the average gap width W. To this end, a least squares fit of the gap function to a linear gap function $g = Wx$ has been made. The gap function is a best fit between $x = 0$ and $x = 12.7$ mm. The value of W obtained by performing such a fit is:

$$W = 31.32 \text{ mm}$$

3.) The discharge coefficient used in modelling the valve is a constant value approximation worked out in Chapter 3, $C_D = 0.87$. The contraction coefficient for a long orifice, which is applicable to the plug valve is $C_c = 1$.

4.) The static pressure difference Δp is based on a head difference of 0.635 m of water,

$$\Delta p = 6.227 \text{ kPa}$$

5.) Two reference values are needed to fix the time and displacement scales. The characteristic dimension of the plug valve chosen was the seat diameter d = 50.8 mm. The time reference was chosen so that $\omega = 1$ rad/sec. This means that the reference stiffness k_r is chosen so that,

$$k_r = \omega^2 M = 1.254 \text{ N/m}$$

6.) The downstream pipe area A_4 is based on an inside pipe diameter of 40.9 mm, hence,

$$A_4 = 1314 \text{ mm}^2$$

7.) The effective valve area is chosen such that

$$S = A_v = 1651 \text{ mm}^2$$

Non Dimensional Parameters

Using the definitions of the dimensionless parameters in Section 6.24, the following are fixed for the plug valve used:

Frequency $\omega = 1$	Pressure Difference $\overline{\Delta p} = 4826$
Mass ratio $\mu = 0.0669$	Gap Width $\eta = 0.826$
Upstream Pipe Area $\frac{1}{\theta} = 0$	Pumping Area $\varepsilon = 1.256$

The values of dimensionless stiffness and damping can be found using data in Chapter 4 and are summarized in Table B1.

Stiffness k N/m	Stiffness $\bar{k}$	Damping ξ
946	754	3.30
1386	1105	4.40
2125	1695	5.56
3017	2406	7.71
3440	2743	7.34

TABLE B1

The dimensionless fluid inertia factors which correspond to experimental pipe length are given in Table B2.

Pipe Length L (m)	Inertia Factor α	Loss Factor ψ
0.84	33	5.27
3.61	142	7.47
6.34	250	11.44
8.56	337	13.21
8.98	354	13.54

TABLE B2

Each loss factor ψ is computed using the following data from Streeter [34]. For each elbow a loss factor of 0.9, a loss factor of 1 for the pipe discharge into the atmosphere and a loss factor 0.19 for the downstream gate valve fully open. The loss factor for friction has been assumed to be constant. A representative Reynolds number of 11100 was used with a pipe roughness of $\varepsilon/D = 0.00112$. The Moody Friction Chart gives a loss factor of $K_f = 0.795L$ where L is the length of the pipe in metres. Results calculated in this fashion are presented in Table B2.

APPENDIX C

APPLICATION OF COMPUTER PROGRAM TO DIFFERENTIAL EQUATIONS

Equations (6.37) and (6.38) are used as a starting point for numerical integration. These equations are repeated here:

$$\left(\frac{\eta\alpha_o}{C_c\bar{x}} + \alpha\right)\frac{d\bar{Q}_v}{d\tau} = \bar{\Delta}P - \bar{Q}_p^2(\psi+1) - \bar{Q}_v^2\left(\frac{\eta^2}{C_D^2\bar{x}^2} - \frac{2\eta}{C_c\bar{x}}\right) + 2\varepsilon\left(\frac{d\bar{x}}{d\tau}\right)^2 + \varepsilon\alpha\frac{d^2\bar{x}}{d\tau^2} \tag{C.1}$$

$$\frac{d^2\bar{x}}{d\tau^2} = -2\xi\frac{d\bar{x}}{d\tau} - \bar{k}(\bar{x} - \beta) - \frac{1}{2}\mu\left[\frac{\bar{Q}_v^2\eta^2}{C_D^2\bar{x}^2} + \frac{\eta\alpha_o}{C_c\bar{x}}\frac{d\bar{Q}_v}{d\tau}\right] \tag{C.2}$$

The equation (C.2) can be rewritten as two terms,

$$\frac{d^2\bar{x}}{d\tau^2} = G - \frac{\mu\eta\alpha_o}{2C_c\bar{x}}\frac{d\bar{Q}_v}{d\tau} \tag{C.3}$$

where

$$G = \bar{k}\,(\beta-\bar{x}) - \frac{1}{2}\mu\,\frac{\bar{Q}_v^2\eta^2}{C_D^2\bar{x}^2} - 2\xi\,\frac{d\bar{x}}{d\tau} \tag{C.4}$$

Note that G contains no time derivatives except for velocity which is treated as a separate variable for the integration.

Substituting for $\frac{d^2\bar{x}}{d\tau^2}$ from equation (C.3) into equation (C.1) results in:

$$\left(\frac{\eta\alpha_o}{C_c\bar{x}} + \alpha + \frac{\alpha\alpha_o\mu\varepsilon\eta}{2C_c\bar{x}}\right)\frac{d\bar{Q}_v}{d\tau} = \bar{\Delta P} - \bar{Q}_p^2(\psi+1) - \bar{Q}_v^2\left(\frac{\eta^2}{C_D^2\bar{x}^2} - \frac{2\eta}{C_c\bar{x}}\right)$$

$$+ 2\varepsilon\left(\frac{d\bar{x}}{d\tau}\right) + \varepsilon\alpha G \qquad \text{(C.5)}$$

A lower bound on α_o can be found by integrating the equivalent inertia of an elemental section of the gap from the beginning to the end of the gap. The appropriate expressions can be obtained by examining the gap area calculation in Appendix B. Using this method the equivalent jet length in the gap using the minimum gap area at the reference area was $L_o = 16.23$ mm. Hence $\alpha_o = 0.654$. This value of α_o is used in computing the derivatives of the system.

Letting $y_1 = \bar{Q}_v$, $y_2 = \bar{x}$, $y_3 = \frac{d\bar{x}}{d\tau}$ the formulation for integration becomes:

$$y_1' = \frac{1}{\left(\frac{\eta\alpha_o}{C_c y_2} + \alpha + \frac{\alpha\alpha_o\mu\varepsilon\eta}{2C_c y_2}\right)}\left(\bar{\Delta P} - (y_1 - y_3\varepsilon)^2(\psi+1) - y_1^2\left(\frac{\eta^2}{C_D^2 y_2^2} - \frac{2\eta}{C_c y_2}\right)\right.$$

$$\left. + 2\varepsilon y_3 + \varepsilon\alpha G\right) \qquad \text{(C.6)}$$

where $G = \bar{K}(\beta - y_2) - \frac{1}{2}\frac{y_1^2\eta^2}{C_D^2 y_2^2} - 2\xi\, y_3$

$$y_2' = y_3 \qquad \text{(C.7)}$$

$$y_3' = G - \frac{\eta\alpha_o}{2C_c y_2}\, y_1' \qquad \text{(C.8)}$$

```
      PROGRAM TST ( INPUT,OUTPUT,TAPE5= INPUT,TAPE6=OUTPUT)                  MAI  10
                                                                             MAI  20
                                                                             MAI  30
CXXXXXXXXXXXXXXXXXXXXXXXXXXXXXXXXXXXXXXXXXXXXXXXXXXXXXXXXXXXXXXXXXXXXXXXX MAI  40
CXXXXXXXXXXXXXXXXXXXXXXXXXXXXXXXXXXXXXXXXXXXXXXXXXXXXXXXXXXXXXXXXXXXXXXXX MAI  50
CX                                                                           MAI  60
CX                                                                           MAI  70
CX                                                                           MAI  80
CX                                                                           MAI  90
C                          A MECHANISM FOR SELF EXCITATION                   MAI 100
C                            IN HYDRAULIC CONTROL DEVICES                    MAI 110
CX                                                                           MAI 120
CXXXXXXXXXXXXXXXXXXXXXXXXXXXXXXXXXXXXXXXXXXXXXXXXXXXXXXXXXXXXXXXXXXXXXXXX MAI 130
CXXXXXXXXXXXXXXXXXXXXXXXXXXXXXXXXXXXXXXXXXXXXXXXXXXXXXXXXXXXXXXXXXXXXXXXX MAI 140
                                                                             MAI 150
C     (A)  DESCRIPTION OF SUBROUTINE RKGS                                    MAI 160
C                                                                            MAI 170
C          ==============================                                    MAI 180
C     THIS SUBROUTINE CAN BE USED TO SOLVE A SYSTEM OF FIRST ORDER           MAI 190
C     ORDINARY DIFFERENTIAL EQUATIONS WITH GIVEN INITIAL VALUES              MAI 200
C                                                                            MAI 210
C                                                                            MAI 220
C     DEFINITION OF PARAMETERS                                               MAI 230
C                                                                            MAI 240
C     -------------------------                                              MAI 250
C     PRMT  - AN INPUT AND OUTPUT VECTOR WITH DIMENSION GREATER THAN OR      MAI 260
C     EQUAL TO 5, WHICH SPECIFIES THE PARAMETERS OF THE INTERVAL AND         MAI 270
C     THE ACCURACY THIS SERVES FOR COMMUNICATION BETWEEN THE OUTPUT          MAI 280
C     SUBROUTINE AND SUBROUTINE RKGS                                         MAI 290
C     ONLY PRMT(5) IS DESTROYED BY RKGS                                      MAI 300
C                                                                            MAI 310
C   THE COMPONENTS ARE -                                                     MAI 320
C     PRMT(1)    LOWER BOUND OF THE INTERVAL (INPUT),                        MAI 330
C     PRMT(2)    UPPER BOUND OF THE INTERVAL (INPUT),                        MAI 340
C     PRMT(3)    INITIAL INCREMENT OF THE INDEPENDENT VARIABLE (INPUT),      MAI 350
C     PRMT(4)    UPPER ERROR BOUND (INPUT) .   IF THE ABSOLUTE ERROR IS      MAI 360
C     GREATER THAN PRMT(4) INCREMENTS GET HALVED. IF INCREMENT IS            MAI 370
C     LESS THAN PRMT(3) AND ABSOLUTE ERROR IS LESS THAN PRMT(4)/50           MAI 380
C     THE INCREMENT GETS DOUBLED.PRMT(4) MAYBE CHANGED BY MEANS OF           MAI 390
C                SUBROUTINE OUTPUT.                                          MAI 400
                                                                             MAI 410
                                                                             MAI 420
C   Y             INPUT VECTOR OF THE INITIAL VALUES (DESTROYED)             MAI 430
C                 LATER ON Y IS THE RESULTING VECTOR OF DEPENDENT VARIABLE    MAI 440
C                 COMPUTED AT INTERMEDIATE POINTS X                          MAI 450
                                                                             MAI 460
                                                                             MAI 470
C     DERY        INPUT VECTOR OF ERROR WEIGHTS (DESTROYED)                  MAI 480
C                 THE SUM OF IT"S COMPONENTS MUST BE EQUAL TO 1   LATER ON    MAI 490
C                 DERY IS THE VECTOR OF DERIVATIVES WHICH BELONG TO          MAI 500
C                 FUNCTION VALUES Y AT A POINT X                             MAI 510
C                 VALUES Y AT A POINT X                                      MAI 520
                                                                             MAI 530
C     NDIM        AN INPUT VALUE WHICH SPECIFIES THE NUMBER OF EQUATIONS     MAI 540
C                 IN THE SYSTEM                                              MAI 550
C     IHLF        AN OUTPUT VALUE WHICH SPECIFIES THE NUMBER OF INCREMENT    MAI 560
C                 BISECTIONS IF IHLF GETS GREATER THAN 10, RKGS RETURNS      MAI 570
C                 WITH THE ERROR MESSAGE IHLF = 11 INTO THE MAIN PROGRAM.    MAI 580
C                 MESSAGE IHLF = 12 OR IHLF = 13 APIF PRMT(3) = 0            MAI 590
C                 SIGN(PRMT(2)-PRMT(1)) RESPECTIVELY                         MAI 600
                                                                             MAI 610
C     FCT         THE NAME OF AN EXTERNAL SUBROUTINE THIS COMPUTES           MAI 620
C                 THE RIGHT HAND SIDES DERY OF THE SYSTEM TO GIVEN VALUES    MAI 630
C                 OF X AND Y. ITS PARAMETER LIST MUST BE X,Y,DERY            MAI 640
                                                                             MAI 650
C     OUTP        THE NAME OF AN EXTERNAL OUTPUT SUBROUTINE. ITS PARAMETER   MAI 660
C                 LIST MUST BE IHLF,NDIM,PRMT. IF PRMT(5) IS CHANGED TO      MAI 670
C                 NON-ZERO THEN SUBROUTINE RKGS IS TERMINATED                MAI 680
                                                                             MAI 690
C     AUX         AN AUXILIARY STORAGE ARRAY WITH 8 ROWS AND NDIM COLUMNS    MAI 700
                                                                             MAI 710
C     REMARKS                                                                MAI 720
                                                                             MAI 730
C     -------                                                                MAI 740
```

```
C     THE PROCEDURE TERMINATES AND RETURNS TO CALLING PROGRAM , IF
C     (1) MORE THAN 10 BISECTIONS OF THE INITIAL INCREMENT ARE NECESSARY
C     TO GET SATISFACTORY ACCURACY ( IHLF=11)
C     (2) INITIAL INCREMENT IS EQUAL TO 0 OR HAS THE WRONG SIGN
C     ( IHLF = 12 OR 13 ),
C     (3) THE WHOLE INTEGRATION INTERVAL IS WORKED THROUGH,
C     (4) SUBROUTINE OUTP HAS CHANGED PRMT(5) TO NON-ZERO

C     (B) PHYSICAL DIMENSIONS OF THE SYSTEM

C         ================================

C     S           IS THE CONTROL ELEMENT AREA WHICH IS SUBJECTED TO THE
C                 PRESSURE DIFFERENCE
C     A           IS THE CROSS-SECTIONAL AREA OF THE CONDIUT JUST
C                 DOWNSTREAM OF THE CONTROL DEVICE
C     CJ          IS THE REDUCED MASS OF THE MOVING PARTS
C     G           IS THE ACCELERATION DUE TO GRAVITY
C     GAMA        IS THE SPECIFIC WEIGHT OF THE FLOWING FLUID
C     ROW         IS THE FLIUD DENSITY
C     STL         IS THE EQUIVALENT LENGTH OF THE SYSTEM

C     (C) REFERENCE QUANTITIES

          ====================
C     D           REFERENCE DIMENSION
C     SKR         REFERENCE STIFFNESS
C     WR          REFERENCE FREQUENCY
C     DPR         REFERENCE PRESSURE DIFFERENCE

C     (D)   DESIGN PARAMETERS
C           =================
C     ZEATA       DAMPING FACTOR
C     SKB         DIMENSIONLESS STIFFNESS
C     BEATA       INITIAL SETTING PARAMETER
C     RM          MASS RATIO
C     DPB         DIMENSIONLESS PRESSURE DIFFERENCE
C     PSI         LOSS FACTOR
C     ALFA        INERTIA FACTOR
C     CC          DYNAMIC DISCHARGE COEFFICIENT

C     ESP         RATIO OF PUMPING AREA TO DOWNSTREAM PIPE AREA
C     RC          IS THE COEFFICIENT OF RESTITUTION
C                 AT AN INSTANT OF OPENING , IF THE HYROSTATIC PRESSURE FOR
C                 IS GREATER THAN THE SPRING FORCE TAKE RC = 0.05
C                 IF THE SPRING FORCE IS GREATER THAN THE HYDROSTATIC PRES
C                 FORCE PUT RC = 0.0
      COMMON/A/ ZEATA,DPB,SKB,BEATA,EATA,ALFA,RM,PSI,CD,CC,
     1YY1,YY2,YY3,XX,HH,YMAX,XC,RC,KKK,DERY1,DDER,D,ESP,ALFAZ,XREF
      COMMON/B/T(700),S(700),V(700),U(700),Z(700)
      COMMON/C/ FAC5,PR1,PR2
      COMMON/GG/X,Y,DERY,AUX

      DIMENSION Y(3),DERY(3),PRMT(5),HY(2),HZ(2),AUX(8,3),HW(2)
      DIMENSION AB(2),BC(2),CD1(2),DE(2)
      DIMENSION HP(3),FG(2)




C        DESIGN PARAMETERS

C        =================
      D = 2.
      HH = 0.088
      PRMT(2) = 2.0
      XC = 0.0
       Y(1) = -0.01
      Y(3)  =    0.01
      SKB = 2977.  $ DPB = 4828.  $ RM = 0.0822 $ ALFA = 353.5
```

```
      ALFAZ = 0.75  $ EATA = 0.8255 $ ZEATA = 8.95  $ PSI = 12.0 $          MAI1490
      ESP = 2.53/2.036  $ CC = 1.0 $ CD = 0.83                              MAI1500
      Y(2) = 0.003                                                          MAI1510
      XX = 0.0                                                              MAI1520
      YY1 = Y(1)                                                            MAI1530
      YY2 = Y(2)                                                            MAI1540
      YY3 = Y(3)                                                            MAI1550
      DERY1  = 0.0                                                          MAI1560
C     DERY(1) + DERY(2) + DERY(3) = 1                                       MAI1570
      DERY(1)  = 0.4                                                        MAI1580
      DERY(2) = 0.5                                                         MAI1590
      DERY(3)  = 0.1                                                        MAI1600
      NDIM = 3                                                              MAI1610
      PRMT(1) = 0.0                                                         MAI1620
      PRMT(3) = HH/10.0                                                     MAI1630
      PRMT(4) =  0.5E-4                                                     MAI1640
      PR1 = PRMT(4)                                                         MAI1650
      PR2 = 50.*PRMT(4)                                                     MAI1660
      ALFA = 33.   $  PSI = 5.27  $ ALFAZ =   1.5                           MAI1670
      BEATA = 0.25  $ SKB = 1403.  $ ZEATA = 5.49                           MAI1680
      RC = 0.05                                                             MAI1690
      KKK = 1                                                               MAI1700
                                                                            MAI1710
                                                                            MAI1720
                                                                            MAI1730
      FAC5  = 0.5*RM*DPB                                                    MAI1740
      T(1) = PRMT(1)                                                        MAI1750
      S(1) = YY1                                                            MAI1760
      V(1) = YY2                                                            MAI1770
      U(1) = YY3                                                            MAI1780
      Z(1) =  FAC5                                                          MAI1790
                                                                            MAI1800
                                                                            MAI1810
      DATA HX/8HTIME ( )/                                                   MAI1820
      DATA HY/10HDISPLACEME,6HNT (X)/                                       MAI1830
      DATA HZ/10HVELOCITY (,2HX)/                                           MAI1840
      WRITE(6,20)                                                           MAI1850
   20 FORMAT(1H1,3X,6HPT.NO.,T12,4HTIME,T32,9HDISCHARGE,T51,12HDISPLACEM    MAI1860
     1ENT,T63,8HPRESSURE,T80,5HDQ/DT/,T28,2HQV,T41,2HQP,T62,10HDIFFERENC    MAI1870
     2E////)                                                                MAI1880
                                                                            MAI1890
                                                                            MAI1900
      SKB = 2165.  $ ZEATA = 6.98  $  BEATA = 0.075                         MAI1910
      ALFA = 354.                                                           MAI1920
      ALFAZ = .654                                                          MAI1930
      XREF = .15                                                            MAI1940
      CALL RKGS (PRMT,NDIM,IHLF)                                            MAI1950
      KKK = KKK-1                                                           MAI1960
  300 WRITE(6,310) IHLF                                                     MAI1970
  310 FORMAT(1H1,5X,I4)                                                     MAI1980
                                                                            MAI1990
                                                                            MAI2000
                                                                            MAI2010
      CALL CMAP(KKK)                                                        MAI2020
      CALL PLOT (0.0,0.0,999)                                               MAI2030
      STOP                                                                  MAI2040
      END                                                                   MAI2050
```

```
      SUBROUTINE FCT (X, Y, DERY)
                                                                        FCT  10
C     ==========================
      COMMON/A/ ZEATA,DPB,SKB,BEATA,EATA,ALFA,RM,PSI,CD,CC,             FCT  20
     1YY1,YY2,YY3,XX,HH,YMAX,XC,RC,KKK,DERY1,DDER,D,ESP,ALFAZ,XREF      FCT  30
      COMMON/C/ FAC5                                                    FCT  40
      DIMENSION Y(3),DERY(3)                                            FCT  50
C  COMPUTE THE EASIEST DERIVATIVE FIRST                                 FCT  60
C  VELOCITY = THE DERIVZTIVE OF DISPLACEMENT                           FCT  70
      DERY(2) = Y(3)                                                    FCT  80
C  NOW COMPUTE SOME AUXILARY VARIABLES REQUIRED LATER ON               FCT  90
      QP = Y(1)-ESP*Y(3)                                                FCT 100
C   DTERMINE WHETHER THIS IS A SINGULARITY OR LARGE OPENING COMPUTATION FCT 110
      DC = 0.0005                                                       FCT 120
C     Y(2) AND Y(1) = ZERO AT THE SINGULAR POINT                        FCT 130
      IF(Y(2).EQ.0.0) GOTO10                                            FCT 140
      IF(Y(2).LT.DC.AND.Y(3).GT.0.0) GOTO30                             FCT 150
C  THIS PART FOR THE LARGER OPENINGS                                    FCT 160
C   COMPUTE THE ACCERATION OF THE PLUG VALVE                            FCT 170
      FAC5 = 0.5*RM*ABS(Y(1))*Y(1)*(EATA/(CD*Y(2)))**2                  FCT 180
      DERY(3)  = SKB*(BEATA-Y(2))-2.*ZEATA*Y(3)-FAC5                    FCT 190
C  NOW CALCULATE HEAD LOSS AT VALVE EXIT                                FCT 200
      H341 = QP**2                                                      FCT 210
      H342 = Y(1)*Y(1)*((EATA/(CC*Y(2)))**2-2.*EATA/(CC*Y(2)))          FCT 220
      H343 = 2.*ESP *Y(3)*Y(3)                                          FCT 230
      H34 = H341+H342+H343                                              FCT 240
      CON1=ALFA*(1.+EATA*ALFAZ*(1./ALFA+0.5*RM*ESP)/(CC*Y(2)))          FCT 250
      CON3 = (Y(1)*EATA/Y(2))**2                                        FCT 260
      CON2 = DPB-PSI*ABS(QP)*QP+SIGN(CON3,Y(1))*(1./CC**2-1./CD**2)     FCT 270
     1+ALFA*ESP*DERY(3)                                                 FCT 280
      IF(Y(1).LT.0.0)  H34 = -(Y(1)*EATA/CC*Y(2))**2                    FCT 290
      CON2 = CON2-H34                                                   FCT 300
      DERY(1) = CON2/CON1                                               FCT 310
      DERY(3) = DERY(3)-EATA*RM*ALFAZ*DERY(1)/(2.*CC*XREF)              FCT 320
C   CALCULATION FOR LARGE COMPLETE , RETURN                             FCT 330
      RETURN                                                            FCT 340
   10 DERY(1) = 0.0                                                     FCT 350
      GOTO 20                                                           FCT 360
   30 DERY(1) = 0.01                                                    FCT 370
   20 CONTINUE                                                          FCT 380
      FAC1 = 0.0                                                        FCT 390
      IF(Y(2).NE.0.0) FAC1 = DERY(1)*(ALFA+ALFAZ*EATA/(CC*Y(2)))        FCT 400
      IF(FAC1.GT.80000.) FAC1 = 80000.                                  FCT 410
      CON3 = 1.+0.5*RM*ALFA*ESP                                         FCT 420
      FAC2 = SKB*(BEATA-Y(2))-2.*ZEATA*Y(3)                             FCT 430
      FAC3 = 0.5*RM*(DPB-(PSI+1.)*QP*ABS(QP)-2.*ESP*Y(3)**2-FAC1)       FCT 440
      DERY(3) = (FAC2-FAC3)/CON3                                        FCT 450
      RETURN                                                            FCT 460
      END                                                               FCT 470
```

```
      SUBROUTINE OUTP (IHLF, NDIM, PRMT)
                                                                        OUT  10
C     ================================                                  OUT  20
      COMMON/A/ ZEATA,DPB,SKB,BEATA,EATA,ALFA,RM,PSI,CD,CC,             OUT  30
     1YY1,YY2,YY3,XX,HH,YMAX,XC,RC,KKK,DERY1,DDER,D,ESP,ALFAZ,XREF      OUT  40
      COMMON/B/T(700),S(700),V(700),U(700),Z(700)                       OUT  50
      COMMON/C/ FAC5,PR1,PR2                                            OUT  60
      COMMON/CC/X,Y,DERY,AUX                                            OUT  70
      DIMENSION DERY(3),Y(3),AUX(8,3),PRMT(5)                           OUT  80
C     REDUCE ACCURACY REQUIREMENT NEAR THE SINGULARITY                  OUT  90
      PRMT(4) = PR1                                                     OUT 100
      IF(Y(2).LT.8.E-3) PRMT(4) = PR2                                   OUT 110
      IF(IHLF.GT.20) GOTO300                                            OUT 120
      IF(Y(2).LT.0.0) GOTO40                                            OUT 130
C     DEFINE IMMINENT CLOSURE                                           OUT 140
      TLEFT = 500.                                                      OUT 150
      IF(Y(3).EQ.0.0) GOTO100                                           OUT 160
      IF(Y(3).LT.0.0) TLEFT = -Y(2)/Y(3)                                OUT 170
      IF(Y(2).LT.0.005.AND.TLEFT.LT.0.0008) GOTO4                       OUT 180
      GOTO 100                                                          OUT 190
    4 CONTINUE                                                          OUT 200
C     HERE IF CLOSURE IS IMMINENT                                       OUT 210
C     RECORD POINT PRIOR TO CLOSURE                                     OUT 220
      T(KKK) = X                                                        OUT 230
      S(KKK) = Y(1)                                                     OUT 240
      V(KKK) = Y(2)                                                     OUT 250
      U(KKK) = ABS(Y(1))*Y(1)*(EATA/(CD*Y(2)))**2                       OUT 260
      Z(KKK) = Y(1)-ESP*Y(3)                                            OUT 270
      WRITE(6,200) KKK,X,Y(1),Z(KKK),Y(2),U(KKK),DERY(1),IHLF           OUT 280
      KKK = KKK+1                                                       OUT 290
C     NOW SIMULATE THE CLOSURE                                          OUT 300
    5 T(KKK) = X+TLEFT                                                  OUT 310
      DERY(1) = 0.0                                                     OUT 320
      ICLOS = 25                                                        OUT 330
      S(KKK) = 0.0                                                      OUT 340
      V(KKK) = 0.0                                                      OUT 350
      U(KKK) = 0.0                                                      OUT 360
      Z(KKK) = -ESP*Y(3)                                                OUT 370
      X = T(KKK)                                                        OUT 380
      WRITE(6,200) KKK,T(KKK),S(KKK),Z(KKK),V(KKK),U(KKK),DERY(1),ICLOS OUT 390
      KKK = KKK+1                                                       OUT 400
C     NOW SIMULATE OPENING OF THE CYCLE                                 OUT 410
C     REBOUND SPEED = IMPACT VELOCITY *COEFFICIENT OF RESTITUTION       OUT 420
      Y(3) = -RC*Y(3)                                                   OUT 430
      T(KKK) = X+TLEFT                                                  OUT 440
      S(KKK) = 0.0                                                      OUT 450
      V(KKK) = RC*Y(2)                                                  OUT 460
      Y(2) = V(KKK)                                                     OUT 470
      U(KKK) = 0.0                                                      OUT 480
      Z(KKK) = -ESP*Y(3)                                                OUT 490
      Y(1) = 0.0                                                        OUT 500
      X= T(KKK)                                                         OUT 510
      WRITE(6,200) KKK,X,Y(1),Z(KKK),Y(2),U(KKK),DERY(1),IHLF           OUT 520
      KKK = KKK +1                                                      OUT 530
      CALL FCT(X,Y,DERY)                                                OUT 540
C     PREPARE AUXILARY ARRAYS FOR RKGS                                  OUT 550
      DO 3 I = 1,NDIM                                                   OUT 560
      AUX (1,I) = Y(I)                                                  OUT 570
      AUX(2,I) = DERY(I)                                                OUT 580
      AUX(3,I) = 0.0                                                    OUT 590
    3 AUX(6,I) = 0.0                                                    OUT 600
C     NOW RKGS CAN COMPUTE THE NEXT POINT                               OUT 610
      GOTO110                                                           OUT 620
C     HERE THE POINT COMPUTED HAS GONE PAST THE POINT OF CLOSURE        OUT 630
C     COMPUTE THE ACTUAL CLOSURE TIME                                   OUT 640
   40 X = XX + YY2*(X-XX)/(YY2-Y(2))                                    OUT 650
      Y(3) = YY3+ YY2*(Y(3)-YY3)/(YY2-Y(2))                             OUT 660
      TLEFT = X-XX                                                      OUT 670
      Y(2) = YY2                                                        OUT 680
      GOTO5                                                             OUT 690
C     COMPUTATION FAR FROM SINGULAR POINT                               OUT 700
  100 CONTINUE                                                          OUT 710
      T(KKK) = X                                                        OUT 720
      S(KKK) = Y(1)                                                     OUT 730
      V(KKK) = Y(2)                                                     OUT 740
```

```
      U(KKK) = 0.0                                                          OUT 740
      IF(Y(2).NE.0.0) U(KKK) = ABS(Y(1))*Y(1)*(EATA/(CD*Y(2)))**2*Y         OUT 750
      Z(KKK) = Y(1) -ESP*Y(3)                                               OUT 760
      WRITE(6,200) KKK,X,Y(1),Z(KKK),Y(2),U(KKK),DERY(1),IHLF               OUT 770
200   FORMAT (3X,I4,6(3X,1PE10.3),I10)                                      OUT 780
      IF(KKK.GE.700) GOTO300                                                OUT 790
      KKK = KKK + 1                                                         OUT 800
 110  YY1 = Y(1)                                                            OUT 810
      YY2 = Y(2)                                                            OUT 820
      YY3 = Y(3)                                                            OUT 830
      XX = X                                                                OUT 840
      RETURN                                                                OUT 850
300   PRMT(5) = 5.0                                                         OUT 860
      KKK = KKK-1                                                           OUT 870
      RETURN                                                                OUT 880
      END                                                                   OUT 890
```

```
      SUBROUTINE RKGS (PRMT, NDIM, IHLF)
                                                                        RKG  10
C     ================================
      COMMON/GG/X,Y,DERY,AUX                                            RKG  20
      DIMENSION Y(3),DERY(3),AUX(8,3),A(4),B(4),C(4),PRMT(5)            RKG  30
      DO 1  I = 1,NDIM                                                  RKG  40
    1 AUX(8,I) = .06666667*DERY(I)                                      RKG  50
      X = PRMT(1)                                                       RKG  60
      XEND = PRMT(2)                                                    RKG  70
      H = PRMT(3)                                                       RKG  80
      PRMT(5) = 0.0                                                     RKG  90
      CALL FCT(X,Y,DERY)                                                RKG 100
C     ERROR TEST                                                        RKG 110
      IF(H*(XEND-X)) 38,37,2                                            RKG 120
                                                                        RKG 130
C   PREPARATIONS FOR RUNGE-KUTTA METHOD                                 RKG 140
    2 A(1)  = .5                                                        RKG 150
      A(2) = .2928932                                                   RKG 160
      A(3) = 1.707107                                                   RKG 170
      A(4) = .1666667                                                   RKG 180
      B(1) = 2.                                                         RKG 190
      B(2) = 1.                                                         RKG 200
      B(3) = 1.                                                         RKG 210
      B(4) = 2.                                                         RKG 220
      C(1) = 0.5                                                        RKG 230
      C(2) = .2928932                                                   RKG 240
      C(3) = 1.707107                                                   RKG 250
      C(4) = 0.5                                                        RKG 260
C                                                                       RKG 270
C     PREPARATIONS FOR THE FIRST STEP OF THE RUNGE-KUTTA                RKG 280
      DO 3 I = 1,NDIM                                                   RKG 290
      AUX(1,I) = Y(I)                                                   RKG 300
      AUX(2,I) = DERY(I)                                                RKG 310
      AUX(3,I) = 0.0                                                    RKG 320
    3 AUX(6,I) = 0.0                                                    RKG 330
      IREC = 0                                                          RKG 340
      H = H+H                                                           RKG 350
      IHLF = -1                                                         RKG 360
      ISTEP = 0                                                         RKG 370
      IEND = 0                                                          RKG 380
                                                                        RKG 390
C                                                                       RKG 400
C                                                                       RKG 410
C     START OF RUNGE-KUTTA STEP                                         RKG 420
    4 IF((X+H-XEND)*H) 7,6,5                                            RKG 430
    5 H = XEND-X                                                        RKG 440
    6 IEND = 1                                                          RKG 450
C                                                                       RKG 460
C     RECORDING OF THE INITIAL VALUES                                   RKG 470
    7 CALL OUTP(IREC,NDIM,PRMT)                                         RKG 480
      IF(PRMT(5)) 40,8,40                                               RKG 490
    8 ITEST = 0                                                         RKG 500
    9 ISTEP = ISTEP + 1                                                 RKG 510
C                                                                       RKG 520
C     START OF THE INNERMOST RUNGE-KUTTA LOOP                           RKG 530
          J = 1                                                         RKG 540
   10     AJ = A(J)                                                     RKG 550
          BJ = B(J)                                                     RKG 560
          CJ = C(J)                                                     RKG 570
               DO 11 I = 1,NDIM                                         RKG 580
               R1 = H*DERY(I)                                           RKG 590
               R2 = AJ*(R1-BJ*AUX(6,I))                                 RKG 600
               Y(I) = Y(I) + R2                                         RKG 610
               R2 = R2+R2+R2                                            RKG 620
   11          AUX(6,I) = AUX(6,I) + R2 -CJ*R1                          RKG 630
          IF(J-4) 12,15,15                                              RKG 640
   12     J = J+1                                                       RKG 650
          IF(J-3) 13,14,13                                              RKG 660
   13     X = X+0.5*H                                                   RKG 670
    14    CALL FCT (X,Y,DERY)                                           RKG 680
          GOTO10                                                        RKG 690
C     END OF THE INNER MOST LOOP OF THE RUNGE KUTTA                     RKG 700
C                                                                       RKG 710
C                                                                       RKG 720
C                                                                       RKG 730
```

```
C                                                                       RKG 740
C     TEST THE ACCURACY                                                 RKG 750
  15  IF(ITEST) 16,16,20                                                RKG 760
C                                                                       RKG 770
C     IN CASE ITEST= 0 THERE IS NO POSSIBILITY FOR TESTING OF ACCURACY  RKG 780
   16     DO 17 I = 1,NDIM                                              RKG 790
   17     AUX(4,I) = Y(I)                                               RKG 800
      ITEST = 1                                                         RKG 810
      ISTEP = ISTEP+ ISTEP -2                                           RKG 820
   18 IHLF = IHLF +1                                                    RKG 830
      X = X-H                                                           RKG 840
      H = H*0.5                                                         RKG 850
          DO 19 I = 1,NDIM                                              RKG 860
      Y(I) = AUX(1,I)                                                   RKG 870
      DERY(I) = AUX(2,I)                                                RKG 880
   19 AUX(6,I) = AUX(3,I)                                               RKG 890
      GOTO9                                                             RKG 900
C                                                                       RKG 910
C     IN CASE ITEST = 1 TESTING OF ACCURACY IS POSSIBLE                 RKG 920
  20  IMOD = ISTEP /2                                                   RKG 930
      IF(ISTEP-IMOD-IMOD) 21,23,21                                      RKG 940
  21  CALL FCT(X,Y,DERY)                                                RKG 950
          DO 22 I = 1,NDIM                                              RKG 960
          AUX(5,I)  = Y(I)                                              RKG 970
 22       AUX(7,I) = DERY(I)                                            RKG 980
      GOTO9                                                             RKG 990
C                                                                       RKG1000
C     COMPUTATION OF TEST VALUE DELT                                    RKG1010
  23  DELT = 0.0                                                        RKG1020
          DO 24 I = 1,NDIM                                              RKG1030
   24     DELT = DELT+AUX(8,I)*ABS(AUX(4,I)-Y(I))                       RKG1040
      IF(DELT -PRMT(4))  28,28,25                                       RKG1050
C                                                                       RKG1060
C     ERROR IS TOO GREAT                                                RKG1070
  25  IF(IHLF-20) 26,36,36                                              RKG1080
   26     DO 27 I = 1,NDIM                                              RKG1090
   27     AUX(4,I)  = AUX(5,I)                                          RKG1100
      ISTEP = ISTEP+ISTEP-4                                             RKG1110
      X = X-H                                                           RKG1120
      IEND = 0                                                          RKG1130
      GOTO18                                                            RKG1140
C                                                                       RKG1150
C     RESULT VALUES ARE GOOD                                            RKG1160
   28 CALL FCT(X,Y,DERY)                                                RKG1170
      DO 29 I = 1,NDIM                                                  RKG1180
      AUX(1,I)  = Y(I)                                                  RKG1190
      AUX(2,I) = DERY(I)                                                RKG1200
      AUX(3,I)  = AUX(6,I)                                              RKG1210
      Y(I) = AUX(5,I)                                                   RKG1220
   29 DERY(I) = AUX(7,I)                                                RKG1230
      X = X-H                                                           RKG1240
      CALL OUTP(IHLF,NDIM,PRMT)                                         RKG1250
      X = X+H                                                           RKG1260
      IF(PRMT(5)) 40,30,40                                              RKG1270
   30     DO 31 I = 1,NDIM                                              RKG1280
          Y(I) = AUX(1,I)                                               RKG1290
   31     DERY(I)  = AUX(2,I)                                           RKG1300
      IREC = IHLF                                                       RKG1310
      IF(IEND) 32,32,39                                                 RKG1320
C                                                                       RKG1330
C     INCREMENT GETS DOUBLED                                            RKG1340
   32 IHLF = IHLF -1                                                    RKG1350
      ISTEP = ISTEP/2                                                   RKG1360
      H = H+H                                                           RKG1370
      IF(IHLF) 4,33,33                                                  RKG1380
   33 IMOD = ISTEP/2                                                    RKG1390
      IF(ISTEP-IMOD-IMOD) 4,34,4                                        RKG1400
   34 IF(DELT-.02*PRMT(4)) 35,35,4                                      RKG1410
   35 IHLF = IHLF-1                                                     RKG1420
      ISTEP = ISTEP/2                                                   RKG1430
      H = H+H                                                           RKG1440
      GOTO4                                                             RKG1450
C                                                                       RKG1460
C                                                                       RKG1470
```

```
C     RETURNS TO CALLING PROGRAM                                    RKG1480
  36  IHLF = 21                                                     RKG1490
      CALL FCT(X,Y,DERY)                                            RKG1500
      GOTO39                                                        RKG1510
  37  IHLF = 22                                                     RKG1520
      GOTO39                                                        RKG1530
  38  IHLF = 23                                                     RKG1540
  39  CALL OUTP (IHLF,NDIM,PRMT)                                    RKG1550
  40  RETURN                                                        RKG1560
      END                                                           RKG1570
```

```
      SUBROUTINE CMAP (KKK)
C     ====================                                              CMA  10
      COMMON /B/ T(700),S(700),V(700),U(700),Z(700)                     CMA  20
      COMMON /LOC/ LX,LY                                                CMA  30
      DIMENSION HS(3),HV(3),HZ(3),HU(3) ,YLIM(2),XLIM(2)                CMA  40
      DIMENSION     HT(3)                                               CMA  50
C     ARRAY VARIABLES                                                   CMA  60
C    T    TIME                                                         CMA  70
C     S     VALVE DISCHARGE                                           CMA  80
C     V    DISPLACEMENT                                               CMA  90
C     U   VALVE PRESSURE DIFFERRENCE                                  CMA 100
C     Z     PIPE DISCHARGE                                            CMA 110
C                                                                     CMA 120
C     INITIALIZE THE AXIES LABLES                                       CMA 130
      LX = 30                                                           CMA 140
      DATA HT/10H          ,10H          ,10H  TIME ( )/              CMA 150
      DATA HS/10HVALVE     ,10HDISCHARGE ,10H(Q )     /               CMA 160
      DATA HV/10H          ,10HDISPLACEME,10HNT (X)   /               CMA 170
      DATA HU/10HPRESSURE  ,10HDIFFERENCE,10H( P)     /               CMA 180
      DATA HZ/10HPIPE      ,10HDISCHARGE ,10H(Q )     /               CMA 190
C      QUANTITIES VS TIME                                             CMA 200
      XLIM(1) = 0.0                                                     CMA 210
      XLIM(2) = 2.0                                                     CMA 220
C    DISPLACEMENT VS TIME                                             CMA 230
      IMAP = 1                                                          CMA 240
      YLIM(1) = 0.0                                                     CMA 250
      YLIM(2) =     0.50                                                CMA 260
      LY = 16                                                           CMA 270
      CALL MAP(XLIM,YLIM,2,HT,HV,IMAP)                                  CMA 280
      CALL PLTMPL(T,V,KKK)                                              CMA 290
C    PLOT  PRESSURE DIFF VS TIME                                      CMA 300
      IMAP = 2                                                          CMA 310
      YLIM(1) = 0.0                                                     CMA 320
      YLIM(2) = 50000.                                                  CMA 330
      LY = 14                                                           CMA 340
      CALL MAP(XLIM,YLIM,2,HT,HU,IMAP)                                  CMA 350
      CALL PLTMPL(T,U,KKK)                                              CMA 360
C     PLOT  PIPE DISCHARGE VS TIME                                      CMA 370
      YLIM(1) =   -4.                                                   CMA 380
      YLIM(2) =  16.0                                                   CMA 390
      IMAP = 3                                                          CMA 400
      CALL MAP (XLIM,YLIM,2,HT,HZ,IMAP)                                 CMA 410
      CALL PLTMPL(T,Z,KKK)                                              CMA 420
      CALL LABEL(2)                                                     CMA 430
C    NEXT   PLOTS OVER TO THE RIGHT                                   CMA 440
      CALL PLOT(9.,1.,-3)                                               CMA 450
      LX = 26                                                           CMA 460
C     PLOTS VS DISPLACEMENT                                             CMA 470
      XLIM(1) = 0.0                                                     CMA 480
      XLIM(2) = 0.5                                                     CMA 490
C      PLOT VALVE DISCHARGE VS X                                        CMA 500
      IMAP = 1                                                          CMA 510
      CALL MAP(XLIM,YLIM,2,HV,HS,IMAP)                                  CMA 520
      CALL PLTMPL(V,S,KKK)                                              CMA 530
C   PLOT  QP VS X IN BOTTOM LOCATION                                    CMA 540
      IMAP = 3                                                          CMA 550
      CALL MAP(XLIM,YLIM,2,HV,HZ,IMAP)                                  CMA 560
      CALL PLTMPL(V,Z,KKK)                                              CMA 570
C   PLOT PRESSURE DIFFERENCE  VS DISPLACEMENT                           CMA 580
      IMAP = 2                                                          CMA 590
      YLIM(1) = 0.0                                                     CMA 600
      YLIM(2) = 50000.                                                  CMA 610
      CALL MAP(XLIM,YLIM,2,HV,HU,IMAP)                                  CMA 620
      CALL PLTMPL(V,U,KKK)                                              CMA 630
      CALL LABEL(2)                                                     CMA 640
      CALL PLOT( 9.,1.,-3)                                              CMA 650
      RETURN                                                            CMA 660
      END                                                               CMA 670
```

```
      SUBROUTINE AXE (YP, YD, NA)
                                                                      AXE  10
C     ========================
      AYP = ABS(YP)                                                   AXE  20
      IF(AYP.GT.1E-6.AND.AYP.LT.0.95)    GOTO50                       AXE  30
C    IF YP IS A WHOLE NUMBER IT CAN BE CONVERTED TO AN INTEGER        AXE  40
C     NOTE  THIS REQUIRES INTELLIGENT USE OF SCALES                   AXE  50
      YP = YP+1.E-6                                                   AXE  60
      IF(YP.LE.0.0) YP = YP-2.E-6                                     AXE  70
      IYP = INT(YP)                                                   AXE  80
      ENCODE(10,42,YD) IYP                                            AXE  90
   42 FORMAT(1X,I6,3X)                                                AXE 100
      IF(NA.EQ.2) ENCODE(10,45,YD) IYP                                AXE 110
   45 FORMAT (3X,I6,1X)                                               AXE 120
C  CHECK TO ENSURE YP WAS A WHOLE NUMBER                              AXE 130
      IIYP = INT(YP+0.95)                                             AXE 140
      IF(YP.LT.0.0) IIYP = INT(YP-0.95)                               AXE 150
      IF(IIYP.NE.IYP)  ENCODE (10,43,YD)YP                            AXE 160
      IF(NA.EQ.1)  ENCODE(10,43,YD) YP                                AXE 170
   43 FORMAT(2X,F7.1,1X)                                              AXE 180
      RETURN                                                          AXE 190
   50 CONTINUE                                                        AXE 200
C    USE 1 PLACE FORMAT AND A WRITTEN 0 BEFORE THE POINT              AXE 210
      ENCODE(10,44,YD ) YP                                            AXE 220
   44 FORMAT(6X,1H0,F2.1,1X)                                          AXE 230
      RETURN                                                          AXE 240
      END                                                             AXE 250
```

```
      SUBROUTINE MAP (X, Y, M, HX, HY, IMAP)
                                                                      MAP  10
C     ================================
      DIMENSION X(1),Y(1),HX(1),HY(1)                                 MAP  20
      DIMENSION H2(2)                                                 MAP  30
      COMMON /LOC/ LX,LY                                              MAP  40
      H1 = HY(1)                                                      MAP  50
      H2(1) = HY(2)                                                   MAP  60
      H2(2) = HY(3)                                                   MAP  70
      NHX = 30                                                        MAP  80
      NHY1 = 10                                                       MAP  90
      NHY  = 20                                                       MAP 100
      CALL NEWPEN (3)                                                 MAP 110
      XM = 2.                                                         MAP 120
      YM = 10. -2.6*FLOAT (IMAP)                                      MAP 130
      NX = 5                                                          MAP 140
      NY = 5                                                          MAP 150
      XL = XM + 5.                                                    MAP 160
      YL = YM+ 2.0                                                    MAP 170
      XX = XL - FLOAT( LX)*0.1                                        MAP 180
      YY =  YL  -FLOAT( LY)*0.1                                       MAP 190
      CALL LETTER(NHX,0.1,0.0,XX,YM-.4,HX)                           MAP 200
      CALL LETTER(NHY,0.1,90.,XM-.7,YY,H2)                           MAP 210
      CALL LETTER(NHY1,0.1,90.,XM-.9,YY,H1)                          MAP 220
      CALL FACTOR(M,X,Y,XL,YL,XM,YM)                                  MAP 230
      CALL PLOT (XM,YM,3)                                             MAP 240
      CALL PLOT (XL,YM,2)                                             MAP 250
      CALL PLOT (XL,YL,1)                                             MAP 260
      CALL PLOT (XM,YL,1)                                             MAP 270
      CALL PLOT (XM,YM,1)                                             MAP 280
      YS = (YL-YM)/FLOAT(NY)                                          MAP 290
      XH = XM                                                         MAP 300
      YH = YM                                                         MAP 310
   20 CALL PLOT(XH,YH,3)                                              MAP 320
      CALL PLOT(XH+.07,YH,2)                                          MAP 330
      CALL PLOT(XL-.07,YH,3)                                          MAP 340
      CALL PLOT(XL,YH,2)                                              MAP 350
      CALL INCHTO(XM,YH,XP,YP)                                        MAP 360
      CALL AXE (YP,YD,2)                                              MAP 370
      CALL LETTER (10,0.1,0.0,1.0,YH-.05,YD)                          MAP 380
      YH = YH + YS                                                    MAP 390
      IF(YH.LE.YL)  GOTO20                                            MAP 400
      XS = (XL-XM)/FLOAT(NX)                                          MAP 410
   22 CALL PLOT (XH,YM,3)                                             MAP 420
      CALL PLOT (XH,YM+.07,2)                                         MAP 430
      CALL PLOT (XH,YL-.07,3)                                         MAP 440
      CALL PLOT (XH,YL,2)                                             MAP 450
      CALL INCHTO (XH,YM,XW,YW)                                       MAP 460
      CALL AXE(XW,XD,1)                                               MAP 470
      CALL LETTER (10,0.1,0.0,XH-.75,YM-.15,XD)                       MAP 480
      XH = XH + XS                                                    MAP 490
      IF(XH.LE.XL) GOTO 22                                            MAP 500
      IF(H2(2).NE.4H( P)) GOTO10                                      MAP 510
      YDEL = YY+1.1                                                   MAP 520
      CALL MATH (XM-.7,YDEL,0.1,90.,18)                               MAP 530
   10 CONTINUE                                                        MAP 540
      IF(H1.NE.5HVALVE) GOTO11                                        MAP 550
      YDEL = YY + 1.2                                                 MAP 560
      CALL LETTER (1,0.06,90.,XM-.65,YDEL,1HV)                        MAP 570
   11 CONTINUE                                                        MAP 580
      IF(H1.NE.4HPIPE) GOTO12                                         MAP 590
      YDEL = YY + 1.2                                                 MAP 600
      CALL LETTER (1,0.06,90.,XM-.65,YDEL,1HP)                        MAP 610
   12 CONTINUE                                                        MAP 620
      IF(HX(3).NE.10H  TIME ( )) GOTO 13                              MAP 630
      CALL GREEK (XL-.2,YM-.4,.1,0.0,19)                              MAP 640
   13 CONTINUE                                                        MAP 650
      CALL NEWPEN(2)                                                  MAP 660
      RETURN                                                          MAP 670
      END                                                             MAP 680
```

```
      SUBROUTINE LABEL (NP)
                                                                      LAB  10
C     ====================
      COMMON/A/ ZEATA,DPB,SKB,BEATA,EATA,ALFA,RM,PSI,CD,CC,           LAB  20
     1YY1,YY2,YY3,XX,HH,YMAX,XC,RC,KKK,DERY1,DDER,D,ESP,ALFAZ,XREF    LAB  30
C     IF  NP = 0  DO NOT PRINT PARAMETERS                            LAB  40
C     IF NP = 1  PRINT  MAIN PARAMETERS ONLY                         LAB  50
C      OTHERWISE  ALL THE PARAMETERS ARE PRINTED ON THE VERSATEC     LAB  60
C     THE FOLLOWING FORMATS ARE USED                                 LAB  70
   1   FORMAT(I10)                                                   LAB  80
   2   FORMAT(5X,1H0,F4.3)                                           LAB  90
   3   FORMAT(F10.1)                                                 LAB 100
   4   FORMAT(6X,1H0,F3.2)                                           LAB 110
       IF(NP.EQ.0) RETURN                                            LAB 120
       CALL NEWPEN (3)                                               LAB 130
C      PRINT MAIN PARAMETERS                                         LAB 140
       IDUM = INT(SKB+0.5)                                           LAB 150
       ENCODE(10,1,HV) IDUM                                          LAB 160
       CALL LETTER (3,.1,0.0,2.3,1.6,3HK =)                          LAB 170
       CALL LETTER (1,.1,0.0,2.3,1.69 ,1H-)                          LAB 180
       CALL LETTER (10,.1,0.0,2.1,1.6,HV)                            LAB 190
       ENCODE(10,2,HV)BEATA                                          LAB 200
       CALL LETTER (5,.1,0.0,3.1,1.6,5H,    =)                       LAB 210
       CALL LETTER(10,.1,0.0,3.2,1.6,HV)                             LAB 220
       CALL GREEK(3.3,1.6,0.1,0.0,2)                                 LAB 230
       ENCODE(10,3,HV) ALFA                                          LAB 240
       CALL LETTER (5,.1,0.0,4.2,1.6,5H,    =)                       LAB 250
       CALL GREEK (4.4,1.6,0.1,0.0,1)                                LAB 260
       CALL LETTER (10,.1,0.0,4.3,1.6,HV)                            LAB 270
       ENCODE(10,4,HV)  RC                                           LAB 280
       CALL LETTER (6,.1,0.0,5.3,1.6,6H, RC =)                       LAB 290
       CALL LETTER (10,.1,0.0,5.3,1.6,HV)                            LAB 300
C      PRINT AUXILLARY PARAMETERS OR RETURN                          LAB 310
       CALL NEWPEN (2)                                               LAB 320
       IF(NP.EQ.1) RETURN                                            LAB 330
   5   FORMAT(F10.1)                                                 LAB 340
       CALL NEWPEN(3)                                                LAB 350
       ENCODE(10,5,HV) PSI                                           LAB 360
       CALL GREEK(2.3,1.4,0.1,0.0,23)                                LAB 370
       CALL LETTER(1,.1,0.0,2.5,1.4,1H=)                             LAB 380
       CALL LETTER(10,.1,0.0,2.1,1.4,HV)                             LAB 390
       ENCODE(10,6,HV) ESP                                           LAB 400
   6   FORMAT(F10.2)                                                 LAB 410
       CALL GREEK(3.3,1.4,.1,0.0,5)                                  LAB 420
       CALL LETTER(5,.1,0.0,3.1,1.4,5H,    =)                        LAB 430
       CALL LETTER(10,.1,0.0,3.1,1.4,HV)                             LAB 440
       IDUM = INT(DPB+0.5)                                           LAB 450
       ENCODE(10,1,HV) IDUM                                          LAB 460
       CALL MATH(4.3,1.4,0.1,0.0,18)                                 LAB 470
       CALL LETTER (6,.1,0.0,4.1,1.4,6H,  P =)                       LAB 480
       CALL LETTER (10,.1,0.0,4.2,1.4,HV)                            LAB 490
       ENCODE(10,2,HV) EATA                                          LAB 500
       CALL LETTER(5,.1,0.0,5.2,1.4,5H,    =)                        LAB 510
       CALL GREEK (5.4,1.4,0.1,0.0,7)                                LAB 520
       CALL LETTER (10,.1,0.0,5.3,1.4,HV)                            LAB 530
C      LIST NEXT GROUP OF PARAMETERS ON THE NEXT LINE                LAB 540
       ENCODE(10,6,HV) ZEATA                                         LAB 550
       CALL GREEK (2.3,1.2,0.1,0.0,14)                               LAB 560
       CALL LETTER (1,.1,0.0,2.5,1.2,1H=)                            LAB 570
       CALL LETTER (10,.1,0.0,2.1,1.2,HV)                            LAB 580
       ENCODE(10,2,HV) RM                                            LAB 590
       CALL GREEK (3.3,1.2,0.1,0.0,12)                               LAB 600
       CALL LETTER(5,.1,0.0,3.1,1.2,5H,    =)                        LAB 610
       CALL LETTER(10,.1,0.0,3.2,1.2,HV)                             LAB 620
       ENCODE(10,4,HV) CD                                            LAB 630
       CALL LETTER(6,.1,.0,4.3,1.2,6H, CD =)                         LAB 640
       CALL LETTER(10,.1,0.0,4.5,1.2,HV)                             LAB 650
       ENCODE(10,3,HV) CC                                            LAB 660
       CALL LETTER(6,.1,0.0,5.6,1.2,6H, CC =)                        LAB 670
       CALL LETTER(10,.1,0.0,5.6,1.2,HV)                             LAB 680
       CALL NEWPEN (2)                                               LAB 690
       RETURN                                                        LAB 700
       END                                                           LAB 710
```

APPENDIX D

CALIBRATION OF SPRINGS

Figure D1 shows a schematic of the apparatus used to measure the spring constants. At the top is the Hewlett Packard 7DCDT-1000 position transducer used throughout the course of experimentation reported in this thesis. Below that is a spring cup with an insert matching the spring diameter as described in Chapter 3. A threaded rod extends downward through the spring. There is a hole located at the bottom for changing weights. The spring is compressed between the spring cup and a plate with a hole to allow the threaded rod through. Each spring was loaded for 0 to 1500 gms and the results obtained are presented in Tables D1 and D2 and Figure D2. The spring constants were calculated using a least squares fit of the load deflection data and these values are recorded in Table D3. The spring combinations used in experiments with the valve are identified in Table D4 with the corresponding combined stiffnesses.

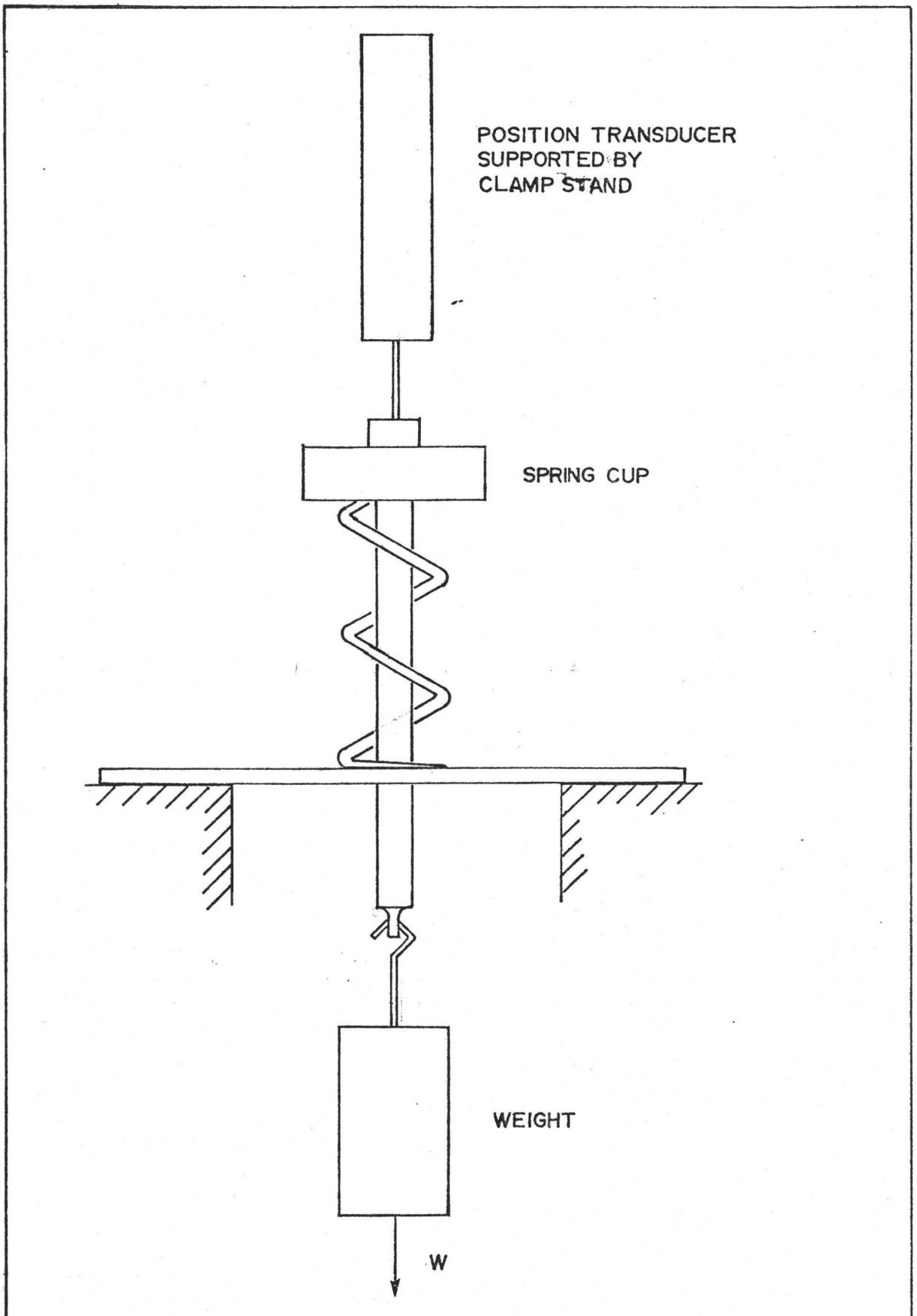

Fig. D1 Apparatus for measuring spring constant.

Spring / Load (W) gms	G8	C6	C7	G6.5
	Deflection δ (mm)	Deflection δ (mm)	Deflection δ (mm)	Deflection δ (mm)
0	0	0	0	0
200	2.57	.89	1.30	2.06
400	5.05	2.01	2.49	4.24
600	7.85	3.15	3.73	6.50
800	10.39	4.22	4.90	8.51
1000	13.23	5.41	6.12	10.26
1200	16.00	6.38	7.34	12.65
1500	19.66	7.90	9.14	15.82

Table D1

Spring / Load (W) gms	G5	G10	G13(1)	G13(2)
	Deflection (mm)	Deflection (mm)	Deflection (mm)	Deflection (mm)
0	0	0	0	0
200	1.70	3.23	4.29	4.14
400	3.40	6.17	8.46	8.13
600	4.95	8.94	12.80	11.91
800	6.55	12.01	17.35	16.03
1000	8.20	15.14	22.00	20.12
1200	9.86	18.29	25.78	24.26
1500	12.45	22.89	31.75	30.14

Table D2

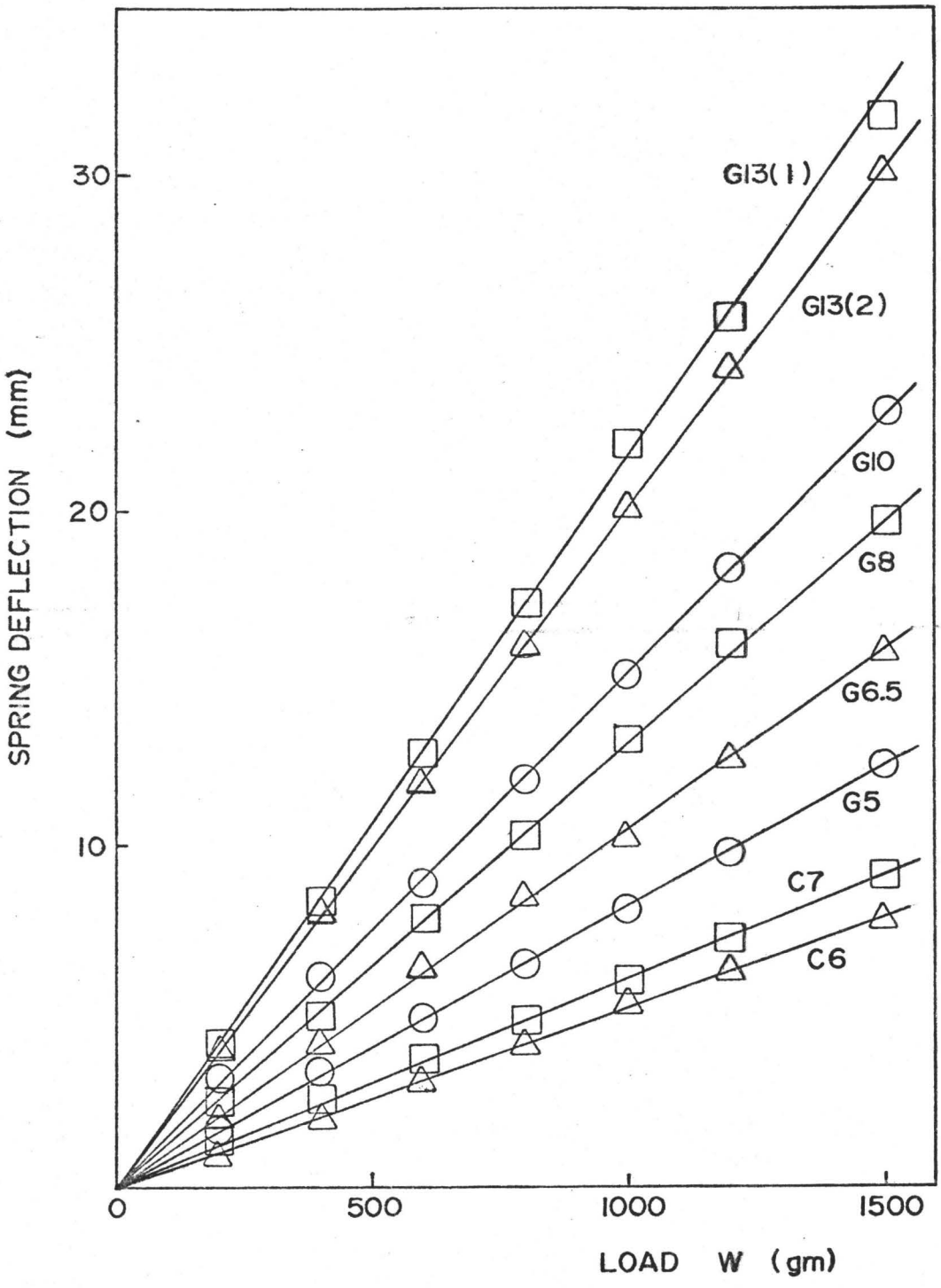

Fig. D2 Spring load-deflection lines.

Spring	Stiffness gm/mm	Stiffness N/m
C6	186.1	1825
C7	164.7	1615
G5	121.5	1192
G6.5	95.16	933
G8	75.49	740
G10	65.87	646
G13(1)	46.70	458
G13(2)	49.76	488

Table D3

Spring Combination	Spring 1	Spring 2	Combined Stiffness N/m
A	G13(1)	G13(2)	946
B	G10	G8	1386
C	G6.5	G5	2125
D	G5	C6	3017
E	C6	C7	3440

Table D4

APPENDIX E

CALIBRATION OF INSTRUMENTATION

Figure E1 shows the calibration curve of the position transducer. The relation between the output voltage of the transducer and displacement is reasonably linear. The transducer was powered using a 6V dry cell battery. Variation in the constant of proportionality between displacement and output voltage due to battery rundown were sufficient to justify calibration with performance of each set of experiments. This involved a two point measurement before and after each set of experiments.

The calibration in Figure E1 was performed using a graduated scale, whilst the daily calibrations check were performed using blocks of known thickness.

Calibration of each of the pressure transducers was performed using a dead weight tester. Results of these calibrations is shown in Figures E2 and E3. The Schaevitz pressure transducer was calibrated at an excitation voltage of 9.825 volts. During experimentation this excitation voltage was repeatable to within 15 mV. The Pace transducer was powered directly from the mains.

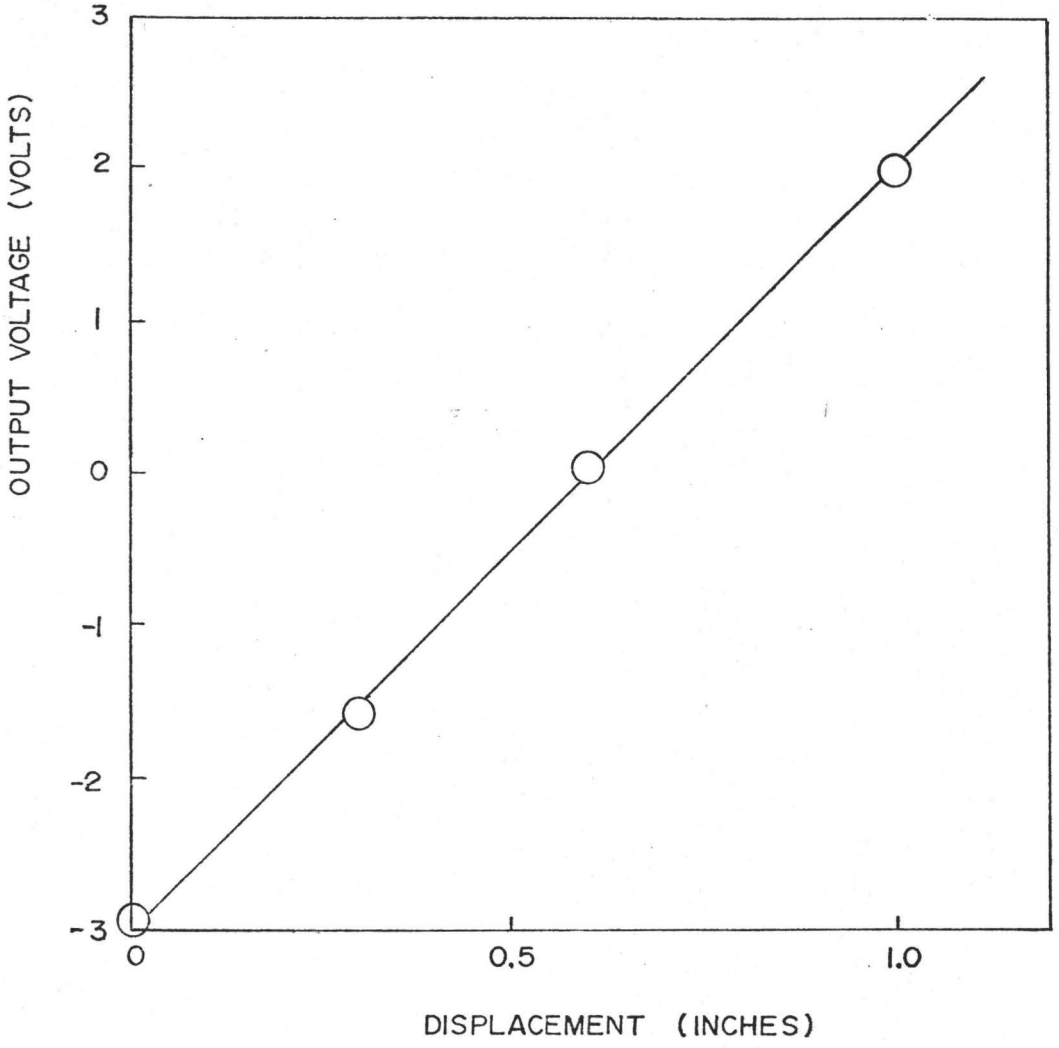

Fig. E1 Output voltage vs displacement of position transducer.

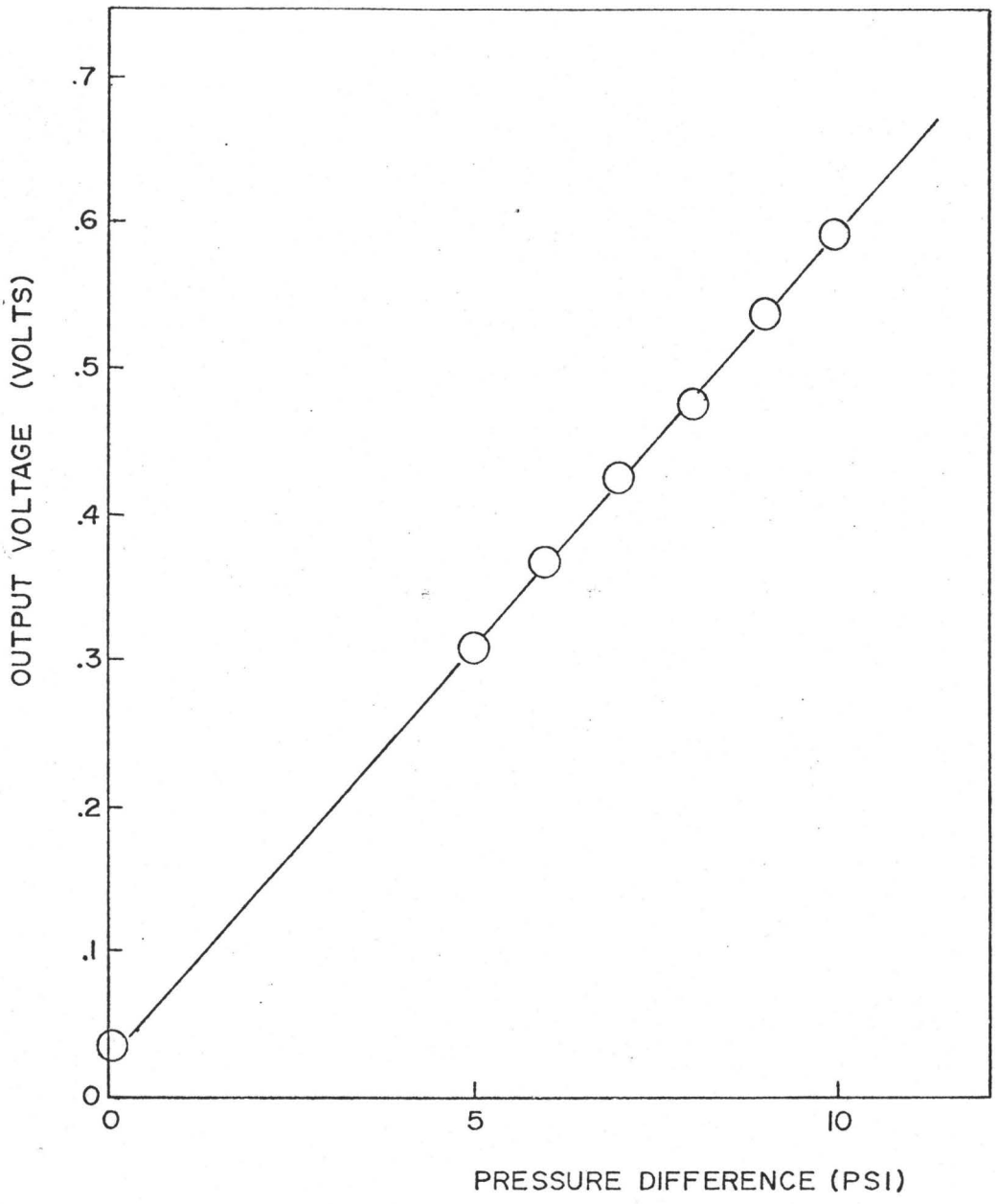

Fig. E2 Calibration of Schaevitz pressure transducer.

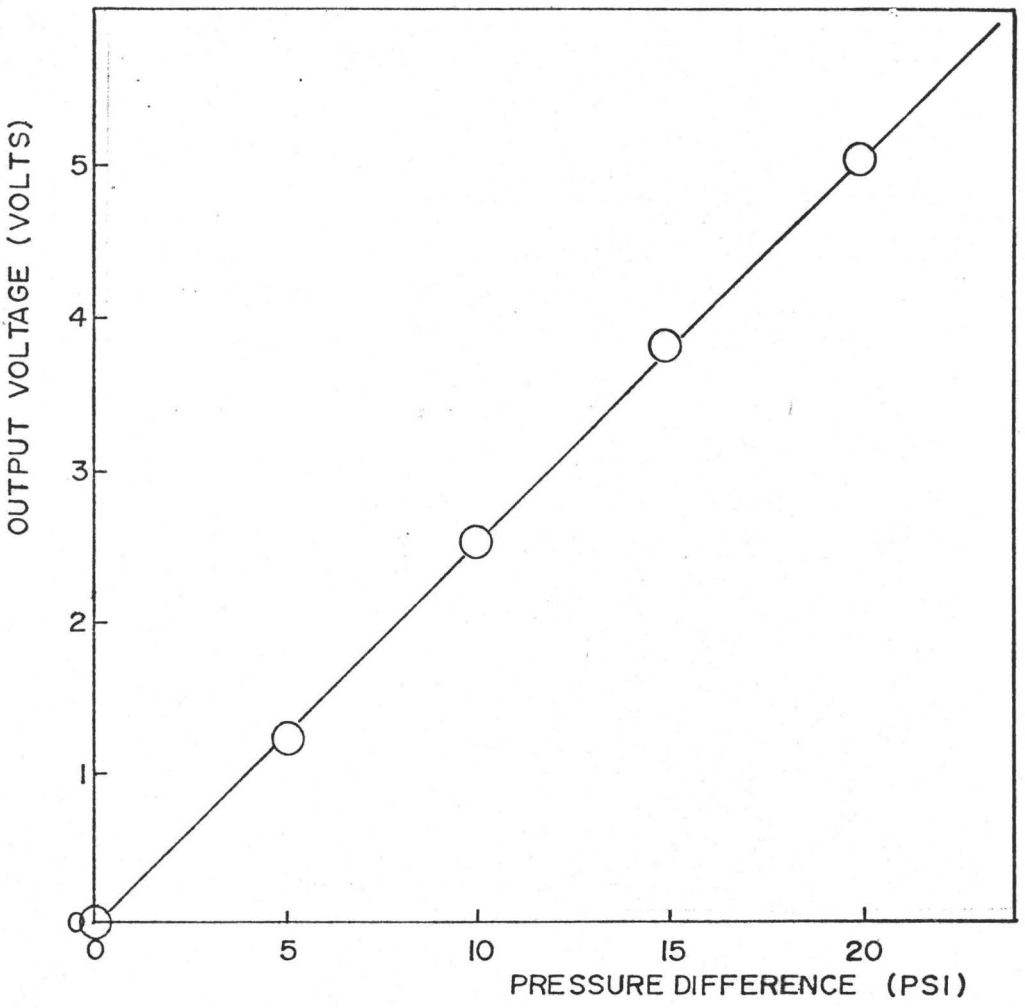

Fig. E3 Calibration of Pace pressure transducer.

APPENDIX F

SUMMARY OF EXPERIMENTAL RESULTS

PIPE LENGTH L = 8.98 m

TABLE F1

Spring Stiffness N/m	Initial Opening (inches)	Stability	Period of Cycle (seconds)	Amplitude (inches)
3440	.05	S	-	-
	.10	U*	.25	.15
	.20	U	.60	.34
	.30	U	1.3	.56
	.35	S		
	.40	S		
3017	.05	S	-	-
	.10	U*	.20	.11
	.20	U	.55	.31
	.30	U	1.1	.53
	.35	U	1.4	.61
	.40	S	-	-
2125	.05	S	-	-
	.10	U*	.20	.11
	.20	U	.45	.31
	.30	U	.90	.52
	.40	U	1.5	.73
	.45	U	2.0	.80
	.50	S	-	-
1386	.10	S	-	-
	.15	U*	.25	.18
	.20	U*	.40	.30
	.30	U*	.70	.52
	.40	U	1.05	.66
	.50	U	1.6	0.84
	.60	U	2.2	1.00
	.65	S	-	-

Table F1 (continued)

Spring Stiffness N/m	Initial Opening (inches)	Stability	Period of Cycle (seconds)	Amplitude (inches)
946	.10	S	-	-
	.15	U*	.25	.16
	.20	U*	.30	.24
	.30	U*	.50	.45
	.40	U	.90	.62

The results presented in Table F1 show data recorded from the self-excited oscillations of the plug valve. The interpretation of the stability symbols is as follows:

S - valve will not perform limit cycle oscillations. The valve is dynamically stable.

U - valve performs limit cycle oscillations independent of initial conditions.

U* - valve is capable of performing limit cycle oscillations. If the valve starts in the closed position and is not disturbed then the valve remains closed. A disturbance may initiate limit cycle oscillations.

The amplitude of the cycle is measured as the largest lift experienced by the valve in its limit cycle oscillations. The period record in this table does not include the time for which the valve is closed (See Chapter 5 for typical limit

TABLE F2

k = 2125 N/m

Pipe Length L (m)	Initial Opening x_o	Stability	Period of Cycle (seconds)	Amplitude (inches)
6.34	.10	S	-	-
	.15	U*	.25	.13
	.20	U	.40	.23
	.30	U	.68	.44
	.40	U	1.15	.61
	.45	U	1.38	.70
	.50	S	-	-
3.61	.10	S	-	-
	.15	U*	.18	.17
	.20	U	.28	.25
	.30	U	.42	.42
	.40	U	.70	.60
	.45	U	.80	.68
	.50	U	.90	.78
	.55	S	-	-
.84	.20	S	-	-
	.25	U	.15	.13
	.30	U	.15	.27
	.40	U	.22	.40
	.50	U***	.44/.22	.63/.63
	.60	U**	.41	.80
	.65	S	-	-

cycle oscillation time histories).

The results in Table F2 indicate the self-excited behaviour of the plug valve at constant stiffness and varying inertia. The following definitions of stability apply in addition to those for Table F1:

U** valve was stable in open position. When disturbed significantly the valve performed limit cycle oscillations.

U*** same as U** but two time histories were observed, hence two amplitudes and frequencies are recorded.

APPENDIX G

CALCULATION OF THE DYNAMIC DISCHARGE COEFFICIENT

In Chapter 5, initial discharge coefficient calculations were made ignoring the pumping effect of the valve as suggested by Weaver and Ziada (6). Results from this yielded some discharge coefficients greater than one. This observation and examination of results in Chapter 5 suggest that pumping is important in the dynamic discharge coefficient calculation.

To calculate the instantaneous dynamic discharge coefficient certain assumptions about the character of the flow have been made. It has been assumed that inertial pressures are negligible and that the effective pumping area of the valve A_v, is the same area of the valve as that used to give the total force on the valve S. In addition, the assumptions regarding pressure and velocity distribution made in Section 4.5 apply.

The steady state momentum equation applied to the control volume in Figure G1 is given by,

$$P_2A_p - P_3A_p = \rho A_p V_3^2 - \rho u_2^2 g_2 \cos\theta + \rho V_p^2 A_v \qquad (G.1)$$

and the continuity equation is given by:

$$u_2 g_2 = V_3 A_p + A_v V_p \qquad (G.2)$$

where V_p is the plug velocity and other symbols apply as in equation (4.8). The unknowns in equation (G.1) and (G.2) are P_2 and u_2.

The discharge coefficient C_D is given by,

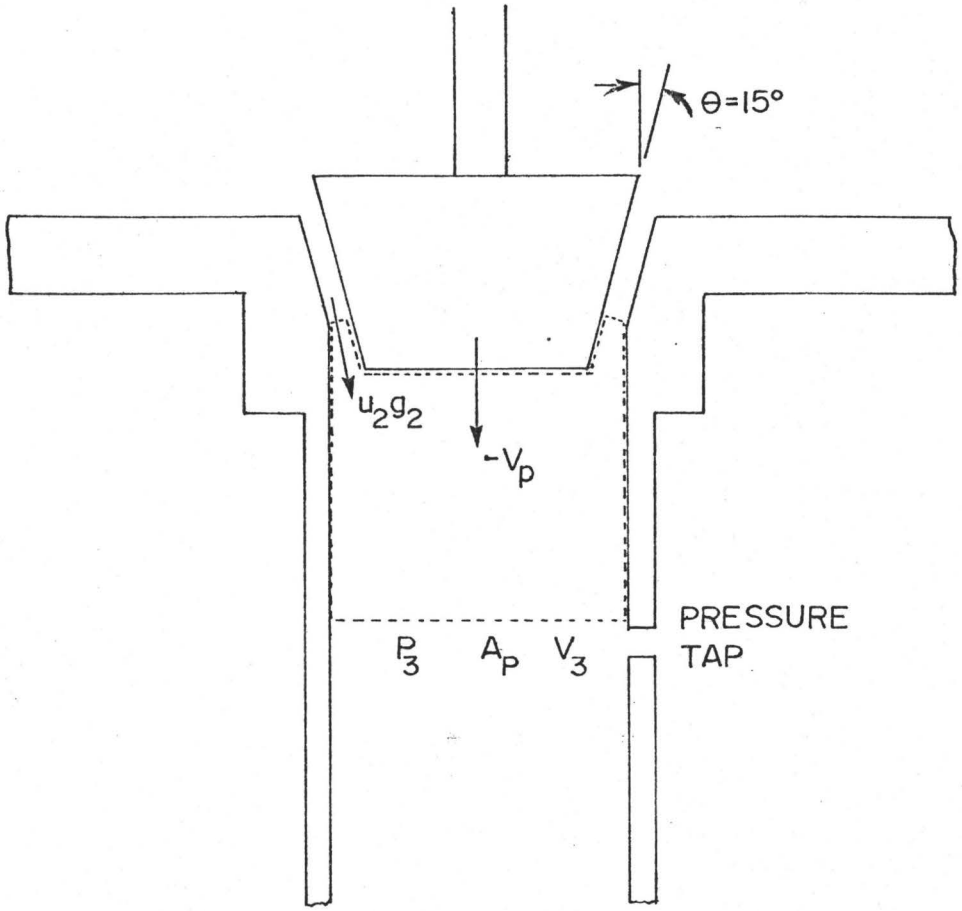

A_p area of pipe

V_p velocity of valve plug

A_v pumping area of valve

V_3 uniform flow velocity across pipe

P_3 pressure measured at tap

u_2 fluid velocity at gap

g_2 gap area

Fig. G1 Control volume for calculating dynamic discharge coefficient.

$$C_D = \frac{Q_v}{Wx\sqrt{\frac{2(\Delta P_{13} - \Delta P_{23})}{\rho}}} \qquad (G.3)$$

where Q_v is the flow through the valve, and $\Delta P_{ij} = P_i - P_j$. ΔP_{13} was measured using the pressure transducer and ΔP_{23} comes from equations (G.1) and (G.2)

$$\Delta P_{23} = P_2 - P_3 = \rho V_3^2 - \frac{\rho(V_3 A_p + A_v V_p)^2}{A_p g_2} \cos\theta + \rho V_p^2 \frac{A_v}{A_p} \qquad (G.4)$$

For the plug valve used in experimentation

$\theta = 15^o$, $A_p = 1313.2\ mm^2$, $A_v = 1651\ mm^2$ and $W = 31.32$ mm.

APPENDIX H

KOLKMAN'S ANALYSIS

This appendix provides an analysis of Kolkman's [4] stability criterion for the plug valve. The stability limit for a damped plug valve according to Kolkman is given by:

$$C_k = \left(1 + Cm + \frac{C\,A_{go}}{\rho A_c^2 \sqrt{2g\Delta H_o}}\right) \frac{1 - \dfrac{C}{\rho L\sqrt{2g\,H_o}\,(dA_g/dy)}}{1 + \dfrac{CA_{go}}{\rho A_c^2 \sqrt{2g\,H_o}}} \qquad (H.1)$$

where:
$$C_k = \frac{kA_{go}}{A_c(2g\Delta H_o)(dA_g/dy)} \qquad (H.2)$$

$$C_m = \frac{m}{\rho A_c L} \qquad (H.3)$$

and k is the spring stiffness, in the total mass of the plug valve, C the damping coefficient, ρ the fluid density, $A_{go} = C_D\, Wy_o$ for a linear variation in gap area, ΔH_o the static head, A_c the pipe crosssectional area which Kolkman also assumes to be the effective force area of the plug valve, L the length of the downstream pipe and y_o is the equilibrium position of the plug valve under the hydrostatic head effective force area of the plug valve, L the length of downstream pipe and y_o is the equilibrium position of the plug valve under the action of the hydrostatic head ΔH_o.

Equation (H.1) can be rewritten as:

$$\frac{ky_o}{2\Delta PA_c} = \left(1 - \frac{C}{C_D WL\sqrt{2\Delta p/\rho}}\right)\left(1 + \frac{m}{\left(\rho A_c + \frac{CWC_D y_o}{A_c\sqrt{2\Delta p/\rho}}\right)}\right) \qquad (H.4)$$

Kolkman also assumes that no pipe losses take place and that pressure recovery after the plug valve is negligible, hence,

$$x_o = y_o + \frac{\Delta PA_c}{k} \qquad (H.5)$$

where x_o is the no load opening of the valve.

In Appendix B the method for nondimensionalizing the no load opening and pipe length are already reported and the points on the stability threshold given in Table H1 can be determined using the following parametric values:

$k = 2125$ N/m, $\rho = 1000$ kg/m^3, $\Delta P = 6227$ Pu, $C = 14.04$ N/(m/s), $W = 31.32$ mm, $m = 1.254$ kg, $C_D = 0.87$ and $A_c = 1314$ mm^2.

One can see that for pipe lengths longer than about 7.5 m that the no load opening at which instability occurs is within five percent of the final value for a long pipe. Simplified calculations for L = 8.98 m are performed using the long pipe stability formula which can be obtained by setting $\frac{1}{L} \to 0$. Combining equations (H.4) and (H.5) the following formulation of the no load opening is arrived at.

$$k x_o = 3\Delta P A_c \qquad (H.6)$$

Solving equation (H.6) at various points allows for plotting of the long pipe stability criterion in Chapter 7.

Table H1

Pipe Length L (m)	Equilibrium Point y_o (mm)	No Load Opening β	Fluid Inertia α
0.84	10.69	.286	33
2.50	9.02	.253	98
5.0	8.41	.241	197
7.5	8.19	.237	295
10.0	8.07	.235	394
14.0	7.97	.233	552
∞	7.70	.227	∞

Table H2

k N/m	x_o mm	$\bar{k}$	β
946	25.95	754	.571
1386	17.71	1105	.349
2125	11.551	1695	.227
3017	8.136	2406	.160
3440	7.136	2743	.140